AD-A070 644 PMB SYSTEMS ENGINEERING INC SAN FRANCISCO CA F/G 11/2
FAILURE CRITERIA FOR REINFORCED CONCRETE STRUCTURES. VOLUME II.--ETC(U)
MAY 79 R W LITTON, J M GIDWANI F29601-76-C-0135
UNCLASSIFIED AFWL-TR-77-239-VOL-2 NL

1 OF 3
AD A070644

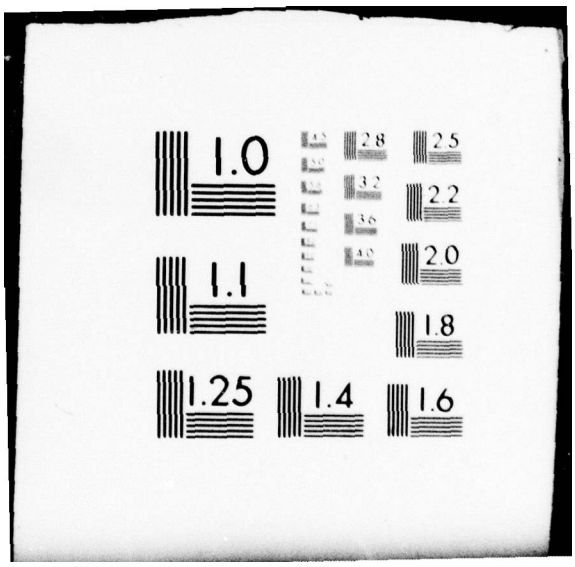
1.0
1.1
1.25
1.4
1.6
1.8
2.0
2.2
2.5
2.8
3.2
3.6
4.0

AFWL-TR-77-239, Vol. II

LEVEL III

12

B.S.

AFWL-TR-77-239 Vol. II

AD A070644

DDC FILE COPY

FAILURE CRITERIA OF REINFORCED CONCRETE STRUCTURES

Volume II
Analytical Model and Response Data

Richard W. Litton
Jawahar M. Gidwani

PMB Systems Engineering, Inc.
San Francisco, CA 94104

May 1979

Final Report

Approved for public release; distribution unlimited

This research was funded by the Defense Nuclear Agency under Subtask Y99AQXSC157, work unit 08, work unit title, "Dynamic Response of Buried Structural Systems and Contents."

Prepared for
Director
DEFENSE NUCLEAR AGENCY
Washington, DC 20305

AIR FORCE WEAPONS LABORATORY
Air Force Systems Command
Kirtland Air Force Base, NM 87117

This final report was prepared by the PMB Systems Engineering, San Francisco, California, under Contract F29601-76-C-0135, Job Order WDNS3428 with the Air Force Weapons Laboratory, Kirtland Air Force Base, New Mexico. Rodney G. Galloway (DES) was the Laboratory Project Officer-in-Charge.

This technical report has been reviewed and is approved for publication.

Rodney G. Galloway

RODNEY G. GALLOWAY
Project Officer

FOR THE COMMANDER

Gary P. Ganong

GARY P. GANONG
Major, USAF
Chief, Technology and Applications Branch

Stewart W. Johnson

STEWART W. JOHNSON
LtColonel, USAF
Chief, Civil Engineering Research Division

DO NOT RETURN THIS COPY. RETAIN OR DESTROY.

UNCLASSIFIED

SECURITY CLASSIFICATION OF THIS PAGE (When Data Entered)

REPORT DOCUMENTATION PAGE

READ INSTRUCTIONS BEFORE COMPLETING FORM

1. REPORT NUMBER: AFWL-TR-77-239-Vol-II	2. GOVT ACCESSION NO.
3. RECIPIENT'S CATALOG NUMBER	
4. TITLE (and Subtitle): FAILURE CRITERIA FOR REINFORCED CONCRETE Structures. Volume II. Analytical Model and Response Data. AD70643	5. TYPE OF REPORT & PERIOD COVERED: Final Report
	6. PERFORMING ORG. REPORT NUMBER
7. AUTHOR(s): Richard W. Litton, Jawahar M. Gidwani	8. CONTRACT OR GRANT NUMBER(s): F29601-76-C-0135
9. PERFORMING ORGANIZATION NAME AND ADDRESS: PMB Systems Engineering, 500 Sansome Street, San Francisco, CA 94104	10. PROGRAM ELEMENT, PROJECT, TASK AREA & WORK UNIT NUMBERS: 62704H, WDNS3428
11. CONTROLLING OFFICE NAME AND ADDRESS: Director, Defense Nuclear Agency, Washington, DC 20305	12. REPORT DATE: May 1979
	13. NUMBER OF PAGES: 266
14. MONITORING AGENCY NAME & ADDRESS (if different from Controlling Office): Air Force Weapons Laboratory (DES), Kirtland Air Force Base, NM 87117	15. SECURITY CLASS. (of this report): UNCLASSIFIED
	15a. DECLASSIFICATION/DOWNGRADING SCHEDULE

16. DISTRIBUTION STATEMENT (of this Report)

Approved for public release; distribution unlimited

17. DISTRIBUTION STATEMENT (of the abstract entered in Block 20, if different from Report)

WDNS, Y99QAXS

18. SUPPLEMENTARY NOTES

This research was funded by the Defense Nuclear Agency under Subtask Y99QAXSC157, work unit 08, work unit title "Dynamic Response of Buried Structural Systems and Contents."

19. KEY WORDS (Continue on reverse side if necessary and identify by block number)

Reinforced Concrete
Failure Criteria
Structural Analysis

20. ABSTRACT (Continue on reverse side if necessary and identify by block number)

Failure criteria defining complete loss of section strength for reinforced concrete sections are defined in this Volume II of the report. Failure envelopes obtained from a three-dimensional finite element analysis with a three dimensional nonlinear constitutive material model are presented in terms of deformations for various rectangular and cylindrical sections. Applications and examples of the use of these failure envelopes are also presented.

DD FORM 1 JAN 73 1473 EDITION OF 1 NOV 65 IS OBSOLETE

UNCLASSIFIED

SECURITY CLASSIFICATION OF THIS PAGE (When Data Entered)

TABLE OF CONTENTS

ILLUSTRATIONS

TABLES

SECTION I

INTRODUCTION

1. GENERAL

In the past decades, extensive attempts have been made to analyze and predict response of reinforced concrete members and structural systems.

A complete understanding or ability to predict this response has yet to be achieved. The heterogeneous nonlinear constitution of reinforced concrete challenges the analyst to predict micro behavior.

The finite element method provides the most promising means for detailed modeling of reinforced concrete. Some encouraging results have been obtained using 2-D finite element modeling, but the assumptions required are dissatisfying.

The constitutive behavior of plane concrete and the effect of confining steel are highly dependent on 3-dimensional concrete material behavior and steel-concrete interaction. The significance of this study is to attack the problem with three-dimensional nonlinear modeling.

A detailed statement of the specific purpose and scope of this study is given in this section, along with an extensive definition of terms and a summary of the contents of this volume.

2. PURPOSE AND SCOPE

As work progressed on the first task of this study, Literature Review (Volume I), the objectives were redefined to a more realistic work scope under the existing time and budget constraints. The initial purpose and scope are reviewed below followed by the final definition of work scope established for this study.

The purpose of this investigation was to more accurately define the response of reinforced concrete structures under complex dynamic (blast type) loads to the point of collapse. The intent was to develop yield and failure criteria for general structural shapes based on a consideration of the three-dimensional state of internal loading and strain. (Significant terms such as failure and yield are defined in detail in subsection 3.0, but briefly, failure defines the inability of a section to develop or maintain appreciable resistance to further deformation; yield is the onset of inelastic behavior.)

Proposed alternatives for failure criteria were to be evaluated by numerically analyzing beam-column, plate, and shell elements subjected to dynamic loads. Comparison with actual experimental data was to be used to aid the selection of the final criteria. Once the criteria were selected, they were to be used to develop simplified design aids which in turn were intended to be used as an improvement over the design aids currently presented in the Air Force Manual for Design and Analysis of Hardened Structures (AFWL-TR-74-102).

Through joint discussion and concurrence with AFWL personnel, PMB Systems Engineering (PMB) and Professor A. C. Scordelis (PMB consultant), the final work purpose and scope were defined as follows:

The overall objective to more accurately define the response of reinforced concrete members and structures under complex dynamic (blast type) loads to the point of collapse remained as the central purpose. In view of the very large loads associated with blast load effects, allowance for inelastic or plastic behavior is, of course, essential to maintain practical structural proportions. Additionally, consideration of three-dimensional interaction of deformation seems vital to improving existing work.

Thus, it was felt that the most important contribution in advancing the understanding of reinforced concrete behavior when subjected to the very large deformation strains anticipated in dynamic blast loads was to employ a consistent 3-dimensional analytical constitutive model for studying various structural sections of interest. The effect of confining steel on response and the yield and failure of plain concrete are highly dependent on 3-dimensional stress-strain relationships. The objective then was to establish a state-of-the-art 3-D finite element model accounting for these important nonlinear effects. Using this analytical tool, perform parametric studies on two selected structural sections: (1) rectangular, and (2) cylindrical.

These parameter studies were then used to evaluate failure strength of various reinforced concrete sections using a three-dimensional finite element analysis (3-D FEA) technique along with a 3-D nonlinear Constitutive Material Model. Each section was subjected to a fixed ratio of imposed displacement and rotation which was monotonically increased till the failure strength of the section was reached. Each section was subjected to seven such deformation ratios which yielded seven different failure strengths. These failure strengths were then plotted in terms of failure displacement and failure

rotation to give a section failure envelope. This failure envelope was then normalized to dimensionless form of strain and curvature.

Once a series of such failure envelopes were obtained for various sections, they were reduced to design failure envelopes. For example, a rectangular section, having a longitudinal reinforcement of 2 percent in the tension and compression zones and a certain area of transverse reinforcement, the ultimate strength in uniaxial compression of concrete was varied to 5 ksi, 6 ksi, 9 ksi and 9.3 ksi. Thus for this rectangular section, four design failure envelopes were obtained corresponding to the four strengths of concrete in uniaxial compression.

The failure strength of the sections obtained from a 3-D FEA was then compared to the ultimate strength as obtained from one-dimensional fiber analysis (1-D FA). The increase in strength using a 3-D FEA is quite obvious. Ductility of the section using a 1-D FA was also compared to the ductility of the section using 3D FEA.

To evaluate the failure capacity of complete structural systems, analytical techniques will have to be developed to extend the failure strengths of the sections to predict failure strength of complete structural systems. This is beyond the scope of this report. However, a limited application technique of the failure design curves is addressed in Section IV.

3. DEFINITION OF TERMS

It will be most useful to define the important terminology used in the study in the context of two different analysis techniques: (1) fiber analysis (FA) and (2) 3-D Finite Element Analysis.

a. Fiber Analysis (FA)

Ultimate strength of a reinforced concrete section can be evaluated in terms of its moment and axial force carrying capacities using a one-dimensional analysis defined herein as the fiber analysis (Figure 1.1). In such an approach, the section is subjected to an imposed assumed strain distribution through its depth which is resisted by internal compressive and tensile forces. Ultimate strength is determined by the strains in the section.

The compressive forces are due to the concrete block in compression, and the longitudinal steel in compression if it is a doubly reinforced section. These compressive forces in a doubly reinforced section can be evaluated from the stress distribution using uniaxial stress-strain relationships of concrete and steel. The tensile internal resisting forces are due to the straining of steel in the tension zone. The ability of the concrete to resist tensile forces may or may not be considered. In case of a singly reinforced concrete section ultimate strength of the section can be reached in three different ways:

(1) Tension Failure

This type of failure occurs when the strain distribution through the section is such that the compressive strain in the outermost concrete fiber reaches ultimate strain of the uniaxial stress-strain relationship of concrete (point 7 in Figure 1.1) and the steel tensile strain exceeds yield (point 8, Figure 1.1). Such a condition occurs in an under-reinforced section.

(2) Balanced Failure

This type of failure occurs when the compressive strain in the outermost concrete fiber reaches ultimate value (point 7, Figure 1.1)

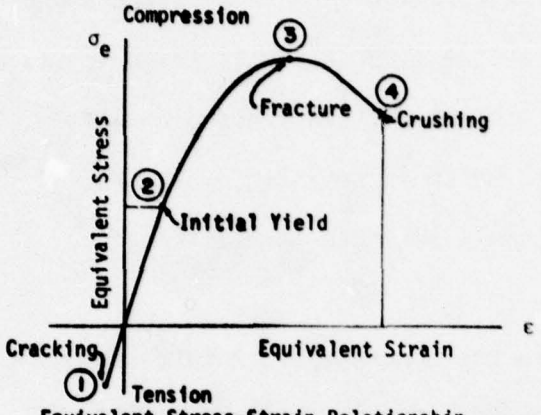

Equivalent Stress-Strain Relationship
3-D Constitutive Model

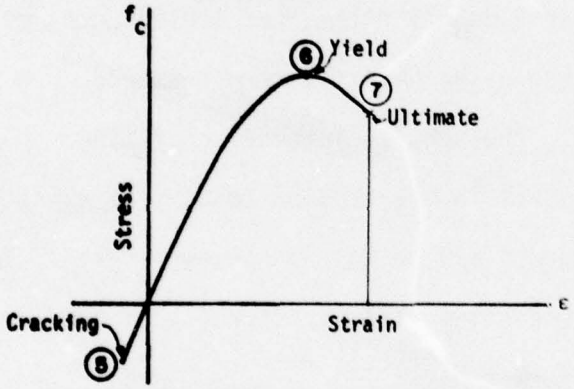

Uniaxial Compressive Stress-Strain
Relation for Concrete

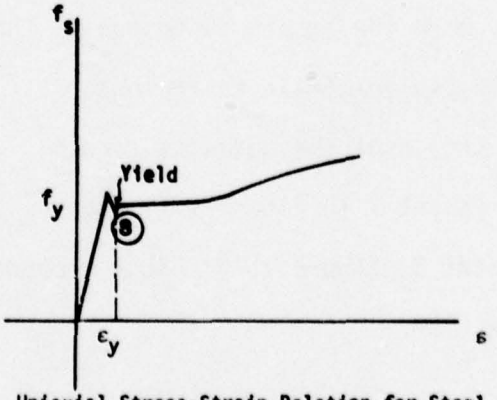

Uniaxial Stress-Strain Relation for Steel

3-D Finite Element Analysis

Failure strength of a section is reached when every element loaded in compression crushes.

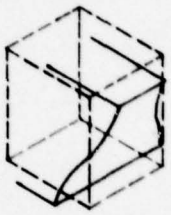

Fiber Analysis

Ultimate strength of a section is reached when the extreme concrete fiber in compression reaches a value ε ultimate strain.

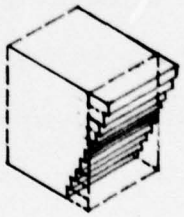

Figure 1.1 Definition of Terms. 3-D Finite Element Analysis and Fiber Analysis

and the tensile steel strain reaches yield simultaneously (point 8, Figure 1.1). Such an ultimate strength condition is reached in a balanced section.

(3) Compression Failure

This type of failure occurs when the tensile steel strain is less than yield (i.e., the steel remains elastic), while the outermost fiber of concrete in compression reaches an ultimate strain value (point 7, Figure 1.1). Such condition occurs in over-reinforced sections.

In all three failure modes mentioned above, ultimate strength occurs when the outermost concrete fiber in compression reaches its ultimate strain value obtained from uniaxial compressive stress-strain relationship of concrete (point 7, Figure 1.1). This value is usually assumed to be 0.003 in/in. The resulting internal resisting forces form a couple which can then be transferred into an equivalent resisting moment and axial force at the centroid of the section. The resisting moment and axial forces associated with the strain distribution that causes the ultimate strength of the section, is called the ultimate moment and the ultimate axial force carrying capacities. These quantities, along with the corresponding centroidal rotation and axial deformations, are classified as the section response quantities.

The history of these response quantities can be traced from zero strain to a strain distribution when ultimate strength of the section is reached. The response quantities can be graphically represented in terms of the moment-rotation and axial force deformation curves. Several points on these response curves can now be defined:

(1) Linear Behavior

A section is defined as linear when the steel and the concrete are elastic. Steel in the section is considered elastic if the strain in the reinforcing steel is less than its uniaxial yield strain. Assuming that concrete does not resist any tensile strain, the concrete section is considered linear until the compressive strain in the outermost fiber reaches the value of strain at maximum stress of the uniaxial compressive stress-strain curve of concrete.

(2) Cracking Point

This point in the M-θ and P-δ response curves is defined when the strain distribution in the section is such that the concrete in the tension zone has reached its cracking strength (point 5, Figure 1.1). This cracking strength may be reached when the stress in the extreme concrete fiber in tension reaches a value of approximately 10% of the ultimate compressive strength.

(3) Yield Point

Yield point on the M-θ, P-δ response curves are defined when the strain distribution is such that the tension zone steel reaches its yield strain value or the outermost fiber concrete strain in compression reaches a value of strain at maximum uniaxial compressive stress (point 6, Figure 1.1). Thus, if one has an under-reinforced section, yield strength is determined by tension zone steel, and for balanced and over-reinforced sections, yield strengths are defined by the strain in the outermost fiber of concrete in compression.

(3) Ultimate Strength

Ultimate strength of the section is defined when the strain in the outermost fiber of concrete in compression reaches an ultimate value of uniaxial strain (point 7, Figure 1.1). Three different common types of ultimate strengths have already been defined in preceeding paragraphs.

To summarize the ultimate strength obtained from a fiber analysis:

1. The ultimate strength of the section is reached when the outermost fiber of concrete in compression reaches an ultimate value of uniaxial compressive strain, usually 0.003 in/in. Once such a condition is reached the moment-carrying capacity of the section is considered to be zero on the assumption that this failure propagates through the depth of the concrete section instantaneously.
2. The position of the neutral axis of the section constantly changes through the depth of the section along the M-θ and P-δ curves from zero to the ultimate strength of the section.
3. Confinement effects are not considered. The member or the section is considered as a one-dimensional element.

b. Three-Dimensional Finite Element Analysis

The second approach to evaluation of the ultimate strength is to use a three-dimensional finite element analysis technique in conjunction with a 3-D nonlinear constitutive model (Figure 1.1). The ultimate strength will be referred to as the failure strength whenever associated

with a 3-D finite element analysis as opposed to a fiber analysis evaluation. This report essentially comprises of evaluating the failure strength of various reinforced concrete sections using a 3-D idealization.

The first major difference between the conventional fiber analysis technique and the 3-D finite element analysis (3-D FEA) technique adopted here is the definition of the ultimate strength of the fiber analysis as compared to the failure strength of the 3-D FEA technique. Failure strength in a 3-D FEA is defined when the equivalent plastic strain in every layer of the concrete in the compression zone reaches a value of equivalent plastic strain for concrete. The equivalent plastic strain is evaluated using classical laws of plasticity. The magnitude of ultimate plastic strain is evaluated from concrete uniaxial compressive stress-strain relationships.

In a 3-D FEA, the stress and strain is usually calculated at the integration points of the 3-D finite elements as compared to the fibers in the one-dimensional fiber analysis. Thus, if the equivalent plastic strain of an integration point associated with the outermost element of concrete in compression is beyond the equivalent ultimate plastic strain, that integration point is assumed to have reached its failure strength. It can no longer resist any loads or deformations. The loads are then redistributed to the remaining elements. If the equivalent plastic strains of all integration points in the compression zone are beyond the equivalent ultimate plastic strain, then the failure strength of the section is reached.

An integration point may achieve its failure strength by three different modes. These modes are now defined:

(1) Cracking

When an integration point is in isotropic tension, and the effective stress at that point as evaluated by the 3-D constitutive material model is equal to the effective cracking stress, the cracking strength of the integration point is said to have been reached (point 1, Figure 1.1). The cracking strength of the section is reached when all the integration points in tension reach their cracking strength. This definition of cracking strength is different from the fiber analysis, meaning where once the cracking stress in the outermost fiber of concrete in tension is reached, the section cracking strength is defined.

(2) Initial Yield

Initial yield of the section in 3-D FEA is defined when the effective stress at an integration point exceeds or is equal to the equivalent stress defined by the first nonlinearity of the uniaxial compressive stress-strain relationship (point 2, Figure 1.1). Initial yield of the section may be defined where the outermost layer of concrete in compression reaches such a stress state. Note the similarity in definition of initial yield in the case of 3D FEA as compared to 1-D FA.

(3) Crushing

Crushing of an integration point in 3-D finite element analysis is defined in two ways, depending on the stress state. In a tension-compression stress state, the crushing strength is said to have been reached if the equivalent plastic strain is equal to or greater

than the equivalent plastic fracture strain, corresponding to the strain at ultimate stress of the uniaxial compressive stress-strain relationship of concrete and laws of plasticity (point 3, Figure 1.1). If on the other hand the integration point is in isotropic compression, then the crushing strength is reached when the equivalent plastic strain evaluated is greater than the equivalent ultimate plastic strain calculated using classical laws of plasticity corresponding to the ultimate strain of the uniaxial compressive stress-strain curve (point 4, Figure 1.1).

(4) Failure Strength

Section failure strength is assumed to have been reached when every integration point of all the finite elements loaded in compression crush either in compression-compression or tension-compression.

c. Comparative Summary of FA and 3-D FEA

The basic differences between the one-dimensional fiber analysis and the 3-D FEA are as follows:

1. The ultimate strength of the reinforced concrete section is assumed to have been reached in the one-dimensional analysis when the strain in the outermost fiber of concrete in compression reaches the ultimate value of strain of the uniaxial compressive stress-strain relation. In contrast, when using 3-D FEA and an associated 3-D nonlinear constitutive material model, failure strength of the section is defined when every 3-D finite element of concrete loaded in compression reaches its crushing strength.
2. While evaluating the failure strength of a section by the 3-D FEA technique, the section was subjected to a monotonically increasing deformation pattern in a fixed ratio

of displacement and rotation. Thus, the neutral axis of imposed deformations was kept fixed while these deformations were increased, until the failure strength of the section was reached. In contrast, in a fiber analysis the neutral axis of imposed deformations was kept fixed while these deformations were increased, until the failure strength of the section was reached. In contrast, in a fiber analysis the neutral axis changes position within the section as defined by the imposed strain distributions. Hence in a fiber analysis, all points in the M-θ response curve have different neutral axis positions, while in the case of 3-D FEA, with imposed deformations, the neutral axis is kept constant for all points on the M-θ and P-δ curves, for a given imposed deformation ratio.

3. No effect of confinement is considered in the 1-D analysis while the 3-D FEA with a 3-D constitutive material model, does account for the effect of confinement.
4. It is appropriate at this stage to define <u>ductility</u> of a section. The displacement or rotational ductility of the section is defined by the ratio of displacement or rotation of the section at ultimate or failure strength to displacement or rotation of the section at initial yield. The initial yield and ultimate strength for a 1-D analysis and initial yield and failure strength for a 3-D analysis have already been defined in preceding paragraphs.

A detailed description of initial yield for purposes of ductility evaluation using a 3-D analysis is now presented. As was mentioned previously, the initial discontinuous surface or initial yield is defined when the effective stress evaluated using a 3-D constitutive model is greater than the effective stress corresponding to the point where the first nonlinearity occurs on the concrete uniaxial compressive σ-ε relation. This point is arbitrary and defined by the user. To have a more consistent definition of ductility, it was assumed that for ductility calculations, initial section yield occurs when the effective stress evaluated using a 3-D material model is greater than the effective stress corresponding to 65% of ultimate uniaxial compressive σ-ε relation calculated in a similar manner.

4. SUMMARY OF REPORT CONTENT

Based on the Volume 1 literature survey of experimental results and analytical models, the constitutive relationship suggested by Chen and Chen (refs. 1 and 2) were adopted by PMB Systems Engineering for the characterization of various sections. Certain modifications were made to the proposed model, which were incorporated in a general purpose nonlinear finite element analysis program called ANSR (ref. 3). Section II describes

---

1. Chen, A.C.T., and Chen, W.F., "Constitutive Relations for Concrete," Vol. 101, No. EM4, Journal of Engineering Mechanics, August, 1975.

2. Chen, A.C.T, and Chen, W.F., "Constitutive Equations and Punch Indentation of Concrete," Vol. 101, No. EM6, Journal of Engineering Mechanics, December, 1975.

3. Mondkar, D. P., Powell, G. H., ANSR-1 General Purpose Program for Analysis of Nonlinear Structural Response, EERC Report No. 75-37, Earthquake Engineering Research Center, University of California, Berkeley, December, 1975.

these constitutive relationships and verification results. Two different geometrical sections were analyzed: a rectangular section , and a cylindrical section. Results of such analyses are presented in Section III. Applications of the proposed model are presented in Section IV. Proposed failure design curves derived from the failure envelopes of various sections are also presented in this section. An example application of the design failure envelopes for a cylindrical section is shown in Section IV. Assumptions and limitations of the proposed model are also presented in Section IV. Appendix A contains a brief description of the computer program, the user's guide, and a sample input to the program for a cylindrical section, while Appendix B shows sample calculations for the ultimate envelope using fiber analysis.

SECTION II

ANALYTICAL MODEL AND VERIFICATION RESULTS

1. GENERAL

To help understand the mechanical behavior of concrete, it is possible to study the response of concrete when subjected to uniaxial loading.

A typical stress-strain curve under uniaxial compressive loading for concrete is shown in Figure 1.2. The curve is generally nonlinear. However, the curve is linear up to stress states of 30% to 60% of ultimate stress. If unloading occurs in this range, the deformations are recoverable. If the load is increased beyond the "linear" range, permanent deformations occur, and the curve becomes nonlinear. The nonlinearity of the curve is caused by the development of internal microcracks. As the load is increased further, these cracks spread and interconnect until the ultimate stress is reached. Beyond this stress state, the curve descends with a negative modulus until the concrete is completely crushed.

The behavior of concrete when subjected to uniaxial tension is quite different from the behavior under compressive loads. The stress-strain curve in tension is linear up to the ultimate stress, when the concrete ruptures and cannot resist any further load. The tensile stress limit in one direction is affected by the introduction of compressive stresses in other directions. For a constant tensile strain in one direction, the tensile stress will decrease with the increase in compressive stresses in other directions.

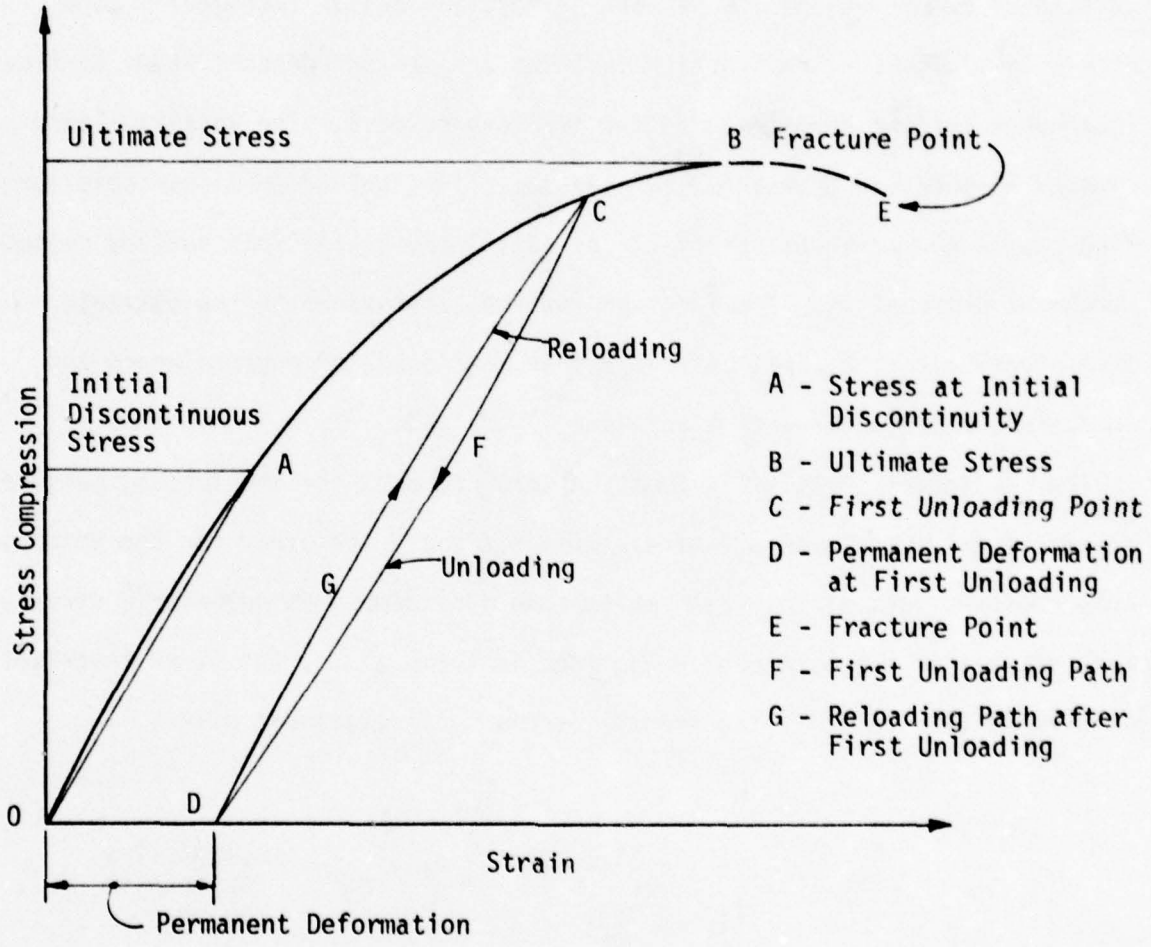

Figure 1.2 Typical Stress-Strain Curve for Concrete

2. CONSTITUTIVE RELATIONSHIPS

Chen and Chen's model (refs. 1 and 2) considers concrete as an elastic plastic strain hardening and fracture material in the isotropic compression region and in the tension-compression region. The behavior of concrete is defined by two relationships, a loading function and an incremental stress-strain law. The loading function includes the initial discontinuous surface, subsequent loading surfaces, and the fracture surface. The initial discontinuous surface can be reached by elastic action; unloading within this surface causes no permanent deformations. Straining beyond this surface causes permanent deformation. The fracture surface corresponds to the ultimate stress condition. Ultimate strain defines the state of rupture where the concrete can no longer resist any load.

Two different but similar functions are proposed for the loading surfaces, one for the isotropic compressive stress state and the other for the tension-compression stress state. Both these functions depend on deviatoric stresses and hydrostatic pressure and are defined in terms of I_1, the first invariant of stress state, and J_2, the second invariant of deviatoric stress.

$$f(\sigma_{ij}) = \frac{\left[\frac{\kappa^2}{3} J_2 - \frac{\kappa^2}{36} I_1^2 + \frac{1}{12} I_1^2 + \frac{\beta}{3} I_1\right]}{\left[1 - \frac{\alpha}{3} I_1\right]} = \tau^2 \quad \begin{matrix}(\text{compression} \\ \text{compression} \\ \text{region})\end{matrix} \qquad (1)$$

$$f(\sigma_{ij}) = \frac{\left[\frac{\kappa^2}{3} J_2 - \frac{\kappa^2}{36} I_1^2 - \frac{1}{12} I_1^2 + \frac{\beta}{3} I_1\right]}{\left[1 - \frac{\alpha}{3} I_1\right]} = \tau^2 \quad \begin{matrix}(\text{tension-} \\ \text{compression} \\ \text{region})\end{matrix} \qquad (2)$$

where $I_1 = \sigma_x + \sigma_y + \sigma_z$

$$J_2 = \frac{1}{6}\left[(\sigma_x - \sigma_y)^2 + (\sigma_y - \sigma_z)^2 + (\sigma_z - \sigma_x)^2 + 6(\tau_{xy}^2 + \tau_{yz}^2 + \tau_{zx}^2)\right]$$

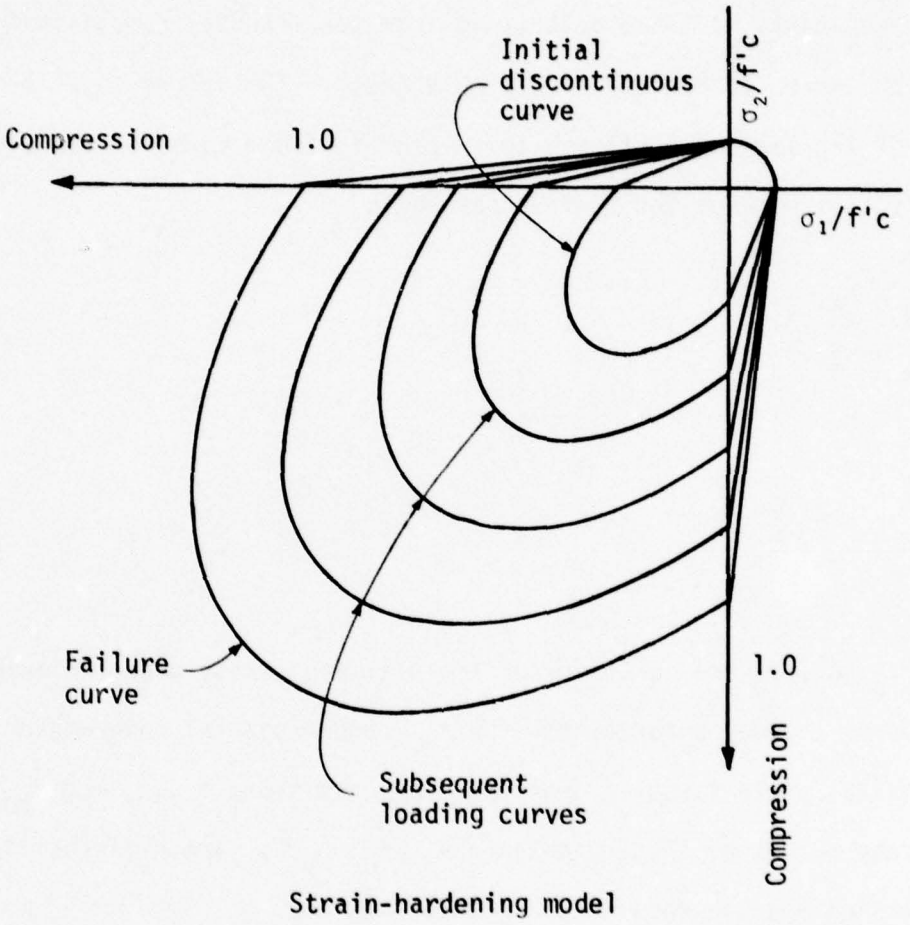

Fig. 2 Initial Discontinuous, Subsequent Loading, and Failure Curves in Biaxial Principal Stress Space

where σ_x, σ_y, σ_z are normal stresses in directions x, y, and z, respectively, and τ_{xy}, τ_{yz}, τ_{xy} are the shear stresses.

If α and β in equations (1) and (2) above are zero, the loading function reduces to a von Mises loading function.

Note that both functions are similar except for the sign of the third term. The constants α, β are determined from the material constants A_o, τ_o, A_u, τ_u which can be determined from simple tests. The values of κ^2 determine the shape of the loading surfaces; this value is found to be 3 from experimental results, which makes the surface parabolic.

$$\alpha = \frac{A_u - A_o}{\tau_u^2 - \tau_o^2} \tag{3}$$

and

$$\beta = \frac{A_o\tau_u^2 - A_u\tau_o^2}{\tau_u^2 - \tau_o^2} \tag{4}$$

where A_o, τ_o, A_u, τ_u are functions of the ultimate stress under uniaxial compression f'_c, under uniaxial tension f'_t, under biaxial compression f'_{bc}, and the initial yield stresses under similar conditions f_c, f_t and f_{bc}. Note that the values of these constants A_o, τ_o, A_u, τ_u are different in the compression and the tension-compression regions.

Thus, for the compression region

$$\frac{A_o}{f'_c} = \frac{\bar{f}_{bc}^2 - \bar{f}_c^2}{(2\bar{f}_{bc} \bar{f}_c)} \tag{5}$$

$$\frac{A_u}{f'_c} = \frac{(\bar{f}'^2_{bc} - 1)}{(2\bar{f}'_{bc} - 1)} \tag{6}$$

$$\frac{\tau_o}{f'_c}^2 = \frac{[\bar{f}_c \cdot \bar{f}_{bc} (2\bar{f}_c - \bar{f}_{bc})]}{3(2\bar{f}_{bc} - \bar{f}_c)} \tag{7}$$

$$\frac{\tau_u}{f'_c}^2 = \frac{\bar{f}'_{bc} (2 - \bar{f}_{bc})}{3(2\bar{f}'_{bc} - 1)} \tag{8}$$

and for the tension-compression region

$$\frac{A_o}{f'_c} = \frac{(\bar{f}_c - \bar{f}_t)}{2} \tag{9}$$

$$\frac{A_u}{f'_c} = \frac{1 - \bar{f}'_t}{2} \tag{10}$$

$$\frac{\tau_o}{f'_c}^2 = \frac{\bar{f}_c \cdot \bar{f}_t}{6} \tag{11}$$

$$\frac{\tau_u}{f'_c}^2 = \frac{\bar{f}'_t}{6} \tag{12}$$

where ($\bar{}$) denotes the nondimensionalized quantity of the corresponding terms to f'_c.

In the loading function (equations 1, 2), if $\tau = \tau_o$, the function reduces to the initial discontinuous surface and if $\tau = \tau_u$, the function defines the fracture surface. Between these two stress states, τ is a function of equivalent plastic strain ε^p characterized by uniaxial compressive stress-strain relationship.

Thus, $\tau = \tau(\varepsilon^p)$ where

$$\varepsilon^p = d\varepsilon^p = (d\varepsilon^p_{ij} \cdot d\varepsilon^p_{ij})^{1/2} \tag{13}$$

Beyond the ultimate stress state τ_u, unloading of concrete occurs where the loading surface decreases while the total equivalent strain increases. This state of stress continues until the equivalent plastic strain reaches the equivalent ultimate plastic strain value. At this stage the concrete is assumed to be totally crushed and cannot resist any load.

In the isotropic tension region, concrete is assumed to be a brittle, elastic-fracture material. In this region, the initial discontinuous surface is assumed to be the same as the fracture surface. If the stress state is located inside this surface, the material is assumed to behave elastically; if concrete is stressed beyond this surface, it is assumed to have cracked, and hence cannot resist any load. The loading function used is the same as the loading function of the tension-compression region.

Since the loading functions in the compression region and the tension-compression region are different, it is important to determine the correct stress-state zone, in order to calculate the correct equivalent stress. Two different criteria to check the stress state were used by researchers at Lehigh University.

a. The first one was used in the Ocean Thermal Energy Conversion Program by T. Y. Chang and W. F. Chen (Fritz Engineering Lab Report No. 414-7) (ref. 4).

---

4. Chang, T. Y., and Chen, W. F., Ocean Thermal Energy Conversion Program, Report No. 414.7, Fritz Engineering Laboratory Report, Lehigh University, August, 1976.

The compression-compresion region was established if the conditions $I_1 < 0$ and $(\sqrt{J_2} + \frac{I_1}{\sqrt{3}}) < 0$ were satisfied, and for the tension-compression region, if $I_1 < 0$ or $(\sqrt{J_2} + \frac{I_1}{\sqrt{3}}) < 0$ were satisfied. The tension-tension stress state was established if $I_1 \geq 0$ and $(\sqrt{J_2} + \frac{I_1}{\sqrt{3}}) \geq 0$.

b. The other criterion was used in program EDFFEP for OTEC structural systems by H. Suzuki and W. F. Chen (Fritz Engineering Lab Report No. 414-8)(ref. 5). Here, the compression-compression region was defined by

(1) $I_1 > f'_c$ or

(2) $-f_c > I_1 > f'_c$ and $(\sqrt{\frac{2}{3}}\ I_1 - \frac{f'_t}{100}) > J_2$

and the tension-compression region by

(1) $I_1 > f'_c$ and $I_1 > -f_c$ or

(2) $-f_c > I > -f'_c$ and $(\sqrt{\frac{2}{3}}\ I_1 - \frac{f'_t}{100}) \leq J_2$

It is believed that the stress state region is independent of the stress parameters related to any given material. Hence, the second criterion is not recommended. A discussion of the first criterion is presented later in this Section.

Once the loading function has been defined, the incremental stress-strain relationships can be derived directly from the loading surface using the normality condition. In the three-dimensional case, the incremental relationship is

5. Suzuki, H., and Chen, W. F., Ocean Thermal Energy Conversion Program, Report No. 414.8, Fritz Engineering Laboratory, Lehigh University, August, 1976.

$$\begin{Bmatrix} d\sigma_{xx} \\ d\sigma_{yy} \\ d\sigma_{zz} \\ d\sigma_{xy} \\ d\sigma_{yz} \\ d\sigma_{zx} \end{Bmatrix} = \frac{E}{(1+\nu)(1-2\nu)} \begin{bmatrix} 1-\nu-\omega\Phi_{11} & \nu-\omega\Phi_{12} & \nu-\omega\Phi_{13} & -\omega\Phi_{14} & -\omega\Phi_{15} & -\omega\Phi_{16} \\ & 1-\nu-\omega\Phi_{22} & \nu-\omega\Phi_{23} & -\omega\Phi_{24} & -\omega\Phi_{25} & -\omega\Phi_{26} \\ & & 1-\nu-\omega\Phi_{33} & -\omega\Phi_{34} & -\omega\Phi_{35} & -\omega\Phi_{36} \\ & \text{SYMMETRIC} & & \frac{1-2\nu}{2}-\omega\Phi_{44} & -\omega\Phi_{45} & -\omega\Phi_{46} \\ & & & & \frac{1-2\nu}{2}-\omega\Phi_{55} & \omega\Phi_{56} \\ & & & & & \frac{1-2\nu}{2}-\omega\Phi_{66} \end{bmatrix} \begin{Bmatrix} d\varepsilon_{xx} \\ d\varepsilon_{yy} \\ d\varepsilon_{zz} \\ d\gamma_{xy} \\ d\gamma_{yz} \\ d\gamma_{zx} \end{Bmatrix} \tag{14}$$

where

$$\frac{1}{\omega} = \{(1-2\nu)\ (2\eta^2 J_2+3\rho^2) + 9\nu\rho^2\} + \frac{mH\,(1+\nu)(1-2\nu)}{E}\sqrt{(2\eta^2 J_2 + 3\rho^2)}$$

$$\Phi_{11} = \{(1-2\nu)(\eta S_{xx} + \rho) + 3\nu\rho\}^2$$

$$\Phi_{12} = \{(1-2\nu)(\eta S_{xx} + \rho) + 3\nu\rho\}\ \{(1-2\nu)(\eta S_{yy} + \rho) + 3\nu\rho\}$$

$$\Phi_{13} = \{(1-2\nu)(\eta S_{xx} + \rho) + 3\nu\rho\}\ \{(1-2\nu)(\eta S_{zz} + \rho) + 3\nu\rho\}$$

$$\Phi_{14} = \{(1-2\nu)(\eta S_{xx} + \rho) + 3\nu\rho\}\ \{(1-2\nu)\ \eta\tau_{xy}\}$$

$$\Phi_{15} = \{(1-2\nu)(\eta S_{xx} + \rho) + 3\nu\rho\}\ \{(1-2\nu)\ \eta\tau_{yz}\} \tag{15}$$

$$\Phi_{16} = \{(1-2\nu)(\eta S_{xx} + \rho) + 3\nu\rho\}\ \{(1-2\nu)\ \eta\tau_{zx}\}$$

$$\Phi_{22} = \{(1-2\nu)(\eta S_{yy} + \rho) + 3\nu\rho\}^2$$

$$\Phi_{23} = \{(1-2\nu)(\eta S_{yy} + \rho) + 3\nu\rho\}\ \{(1-2\nu)(\eta S_{zz} + \rho) + 3\nu\rho\}$$

$$\Phi_{24} = \{(1-2\nu)(\eta S_{yy} + \rho) + 3\nu\rho\} \{(1-2\nu)\eta\tau_{xy}\}$$ (15), Cont.

$$\Phi_{25} = \{(1-2\nu)(\eta S_{yy} + \rho) + 3\nu\rho\} \{(1-2\nu)\eta\tau_{yz}\}$$

$$\Phi_{26} = \{(1-2\nu)(\eta S_{yy} + \rho) + 3\nu\rho\} \{(1-2\nu)\eta\tau_{zx}\}$$

$$\Phi_{33} = \{(1-2\nu)(\eta S_{zz} + \rho) + 3\nu\rho\}^2$$

$$\Phi_{34} = \{(1-2\nu)(\eta S_{zz} + \rho) + 3\nu\rho\} \{(1-2\nu)\eta\tau_{xy}\}$$

$$\Phi_{35} = \{(1-2\nu)(\eta S_{zz} + \rho) + 3\nu\rho\} \{(1-2\nu)\eta\tau_{yz}\}$$

$$\Phi_{36} = \{(1-2\nu)(\eta S_{zz} + \rho) + 3\nu\rho\} \{(1-2\nu)\eta\tau_{zx}\}$$

$$\Phi_{44} = \{(1-2\nu)\eta\tau_{xy}\}^2$$

$$\Phi_{45} = \{(1-2\nu)\eta\tau_{xy}\} \{(1-2\nu)\eta\tau_{yz}\}$$

$$\Phi_{46} = \{(1-2\nu)\eta\tau_{xy}\} \{(1-2\nu)\eta\tau_{zx}\}$$

$$\Phi_{55} = \{(1-2\nu)\eta\tau_{yz}\}^2$$

$$\Phi_{56} = \{(1-2\nu)\eta\tau_{yz}\} \{(1-2\nu)\eta\tau_{zx}\}$$

$$\Phi_{66} = \{(1-2\nu)\eta\tau_{zx}\}^2$$

where

$$m = 1 - \frac{\alpha}{3} I_1$$

$$\eta = \frac{\kappa^2}{3}$$

$$\rho = nI_1 + \frac{\beta + \alpha\tau^2}{3}$$

$n = \frac{3 - \kappa^2}{18}$ in the isotropic compression region

$n = \frac{-3 - \kappa^2}{18}$ in the tension-compression region

All parameters can be easily calculated, excepting the value of H. The value of H, defined as the strain hardening rate, can be written in terms of the slope of the equivalent stress-strain curve:

$$H = 2\sigma_e \cdot H' \qquad (16)$$

where

$$H' = d\sigma_e / d\varepsilon^p$$

σ_e = the equivalent stress = $\sqrt{f(\sigma_{ij})}$ defined in equations (1) and (2)

ε^p = equivalent plastic strain = $d\varepsilon^p = (d\varepsilon^p_{ij} \cdot d\varepsilon^p_{ij})^{1/2}$

The $\sigma_e \sim \varepsilon^p$ curves in the compression region and the tension-compression region are different. These nonlinear curves are assumed to be identical in form and are obtained from tests.

Since the derivation of the incremental stress-strain equation was based on the elastic-plastic model, any finite element program for elastic-plastic analysis may incorporate this material model without much difficulty.

As mentioned before, the initial discontinuous surface can be reached by elastic action only. To check if this initial discontinuous surface had been reached during loading, certain yield criteria are checked.

At each increment of strain, the elastic incremental stresses are calculated using the incremental stress-strain law. The yield criterion for the element is then checked at this stage. Thus, if $f(\sigma_{ij}) - \tau_o^2 < 0$, the element is under elastic loading, and the stress increments are calculated from the elastic incremental stress-strain law. If, however, $f(\sigma_{ij}) - \tau_o^2 > 0$, then the element is under plastic loading. In this case, then, the elastic portion of the stress increment is scaled down by a factor R which is calculated as follows:

$$f(\bar{\sigma}_{ij} + Rd\sigma_{ij}) - \tau^2 = 0 \tag{17}$$

where

$\bar{\sigma}_{ij}$ = Total stresses at previous load step

$d\sigma_{ij}$ = Stress increment at current load increment calculated from elastic stress-strain law.

This condition can be satisfied if

$$AR^2 + 2BR + C = 0 \tag{18}$$

where

$$A = \frac{\kappa^2}{3}\left(\frac{1}{2}\, d\sigma_{ij} d\sigma_{ij} - \frac{1}{6}\, d\sigma_{mm}^2\right) + n d\sigma_{mm}^2 \tag{19}$$

$$B = \frac{\kappa^2}{3}\left(\frac{1}{2}\,\bar{\sigma}_{ij}\, d\sigma_{ij} - \frac{1}{6}\,\bar{\sigma}_{mm} d\sigma_{nn}\right) + n\sigma_{mm} d\sigma_{nn} + \frac{d\sigma_{mm}}{6}(\beta + \alpha\tau^2) \tag{20}$$

$$C = \frac{\kappa^2}{3}\left(\frac{1}{2}\,\bar{\sigma}_{ij}\;\bar{\sigma}_{ij} - \frac{1}{6}\,\bar{\sigma}_{nn}^2\right) + n\bar{\sigma}_{mm}^2 + \frac{\bar{\sigma}_{mm}}{3}(\beta^2 + \alpha\tau^2) - \tau^2 \tag{21}$$

$$\text{Thus } R = \frac{-B \pm \sqrt{B^2 - AC}}{A} \tag{22}$$

Note $n = \frac{3 - \kappa^2}{18}$ in isotropic compression region

$n = \frac{-3 - \kappa^2}{18}$ in tension compression region

The minimum positive value is the required scaling factor.

The remaining portion of the incremental strain is given by

$$d\bar{\varepsilon}_{ij} = (1 - R)\, d\varepsilon_{ij}$$

Once the elastic portion of the strain and the inelastic portion of the strain increment were determined, the incremental stresses were reevaluated by forming the new constitutive matrix of equation (14). The equivalent stresses were then evaluated using appropriate loading functions after stresses and strains were updated.

During the preliminary analyses, it was found that the main difficulty of the model was the criteria used to establish the various stress states. The criteria used to check these states were the first invariant of stress state I_1, and the second invariant of the deviatoric stress J_2.

Thus, if

$$I_1 < 0 \quad \underline{\text{and}} \quad \sqrt{J_2} + \frac{I_1}{\sqrt{3}} < 0$$

then the stress state that existed was in the isotropic compressive zone. These criteria were found to be inconsistent with the loading function. This can also be shown as follows:

$$f(\sigma_{ij}) = \frac{\frac{\kappa^2}{3} J_2 - \frac{\kappa^2}{36} I_1^2 \pm \frac{1}{12} I_1^2 + \frac{\beta}{3} I_1}{1 - \alpha/3 I_1} = \tau^2 \tag{23}$$

The equivalent stress is then defined as

$$\sigma_e = \sqrt{f(\sigma_{ij})} \tag{24}$$

For σ_e to be a real value, the function $f(\sigma_{ij})$ must be positive. However, in certain cases it was found that $f(\sigma_{ij})$ was negative. This negative value could be possible if either $(1 - \frac{\alpha}{3} I_1)$ was negative while the numerator of the expression for $f(\sigma_{ij})$ was positive or vice versa. In most cases the value of this numerator is positive. Hence, $f(\sigma_{ij})$ is usually positive if $1 - \frac{\alpha}{3} I_1$ is positive, and $f(\sigma_{ij})$ is usually negative if the value of $(1 - \frac{\alpha}{3} I_1)$ is negative. Let us now examine the condition under which this would be a negative value.

In the tension zone:

$$\alpha = \frac{A_u - A_o}{\tau_u^2 - \tau_o^2} \tag{25}$$

where

$$\frac{A_u}{f'_c} = \frac{\bar{f}'_c - \bar{f}'_t}{2} \tag{26}$$

$$\frac{A_o}{f'_c} = \frac{\bar{f}_c - \bar{f}_t}{2} \tag{27}$$

$$\left(\frac{\tau_u}{\bar{f}'_c}\right)^2 = \frac{\bar{f}'_c \, \bar{f}'_t}{6} \tag{28}$$

$$\left(\frac{\tau_o}{\bar{f}'_c}\right)^2 = \frac{\bar{f}_c \, \bar{f}_t}{6} \tag{29}$$

Substituting the values of A_u, A_o, τ_u, τ_o in the expression for α in equation 25, we get α as a function of f_b, f'_c, f_t, f'_t.

Thus

$$\alpha = \frac{3}{\bar{f}'_c} \frac{(\bar{f}'_c - \bar{f}'_t) - (\bar{f}_c - \bar{f}_t)}{(\bar{f}'_c \, \bar{f}'_t - \bar{f}_c \, \bar{f}_t)}$$

Thus, for $1 - \frac{\alpha}{3} I_1$ to be greater than zero, we must have $1 > \frac{\alpha}{3} I_1$, or

$$\frac{\alpha}{3} I_1 = \frac{I_1}{\bar{f}'_c} \frac{(f'_c - f'_t) - (f'_c - f_t)}{(\bar{f}'_c \, \bar{f}'_t - \bar{f}_c \bar{f}_t)} < 1$$

If we now have a stress state where

$$\sigma_{11} = f'_t, \; \sigma_{22} = \sigma_{33} = \tau_{12} = \tau_{23} = \tau_{31} = 0$$

then

$$I_1 = f'_t$$

or

$$\frac{f'_t}{\bar{f}'_c} \frac{(\bar{f}'_c - \bar{f}_t) - (\bar{f}_c - \bar{f}_t)}{(\bar{f}'_c \, \bar{f}'_t - \bar{f}_c \bar{f}_t)} < 1$$

This condition can be achieved since in most cases f'_t is about 10 percent of f'_c so that the value of the expression in the brackets can be guessed to be approximately 10. Now, if we somehow have a stress state where I_1/f'_c is greater than f'_t/f'_c, it may result in a negative value of $f(\sigma_{ij})$ so that the effective stress is a complex number. Such a value of effective stress has no physical meaning. However, it has been found that if the effective stress (assuming a tension-compression region) is evaluated as a negative quantity, and we use the material constants of α and β of the compression region and then reevaluate the effective stress, this value turns out to be a positive value, hence the effective stress is real. This could imply that the criteria used to check the various stress states may not be sufficient and may be inconsistent with the loading function.

Hence, a new modification was introduced in the program: if the stress state was established by the condition of I_1, and (I_1 and J_2) was satisfied or otherwise, and the effective stress so calculated was found to be a complex number, then the stress state was switched to the opposite one. This was done for the compression region and the compression-tension region only. Thus, if the stress state established by the criteria proposed by Chen and Chen indicated the stress to be in the compression-tension region and the effective stress calculated using the loading function of that region was found to be negative, then it was assumed that the stress state was actually in the compression region. Thus, the material constants for this region were reevaluated and the effective stress calculated using the appropriate loading function. A similar course of logic would be applied to the compression region, and it can be shown that the loading function is negative for certain stress states which could be avoided if the stress states were switched as mentioned above.

To summarize, there are three different stress states possible:

a. Compression-compression stress state is established if $I_1 < 0$ and $\sqrt{J_2} + \frac{I_1}{\sqrt{3}} < 0$. Once this state has been established, the program sets the parameter identified as IDTC as 1. The yield code printed with the results of the element is the product of IDTC and the parameter defined KODY. The parameter KODY defines the nonlinear behavior of concrete in this region as shown in Figure 3, a plot of equivalent stress and strain. Thus, if the equivalent stress $\sigma_e < \tau_o$, where τ_o is defined in equation 7, KODY = 0, thereby establishing that the stress state is elastic. If $\varepsilon < \varepsilon_f$, and the equivalent stress σ_e is less than τ_u (as defined in equation 8), then the behavior is plastic and KODY is then set to 1. If the equivalent stress is greater than τ_u and the equivalent plastic strain is greater than or equal to equivalent plastic fracture strain, then the fracture state is assumed to have been reached. KODY is now set to a value of 2. If the equivalent plastic strain is greater than equivalent plastic ultimate strain, the concrete is assumed to have crushed and KODY is set to 3.

b. Tension-compression region is established if $I_1 \geq 0$ or $\sqrt{J_2} + \frac{I_1}{\sqrt{3}} \geq 0$. Once this state is established, the program sets the parameter IDTC to -1. The nonlinear behavior of concrete in this region is shown in Figure 4. Note that for this region, the descending portion of the stress-strain curve is absent. The values of KODY = 0 and 1 have the same significance as for the isotropic compression region. For this region, however, KODY = 2 represents the crushing of concrete.

c. Tension-tension region is established if $I_1 \geq 0$ and $\sqrt{J} + \frac{I}{\sqrt{3}} \geq 0$. In this case, the parameter IDTC is set to -6. The stress-strain

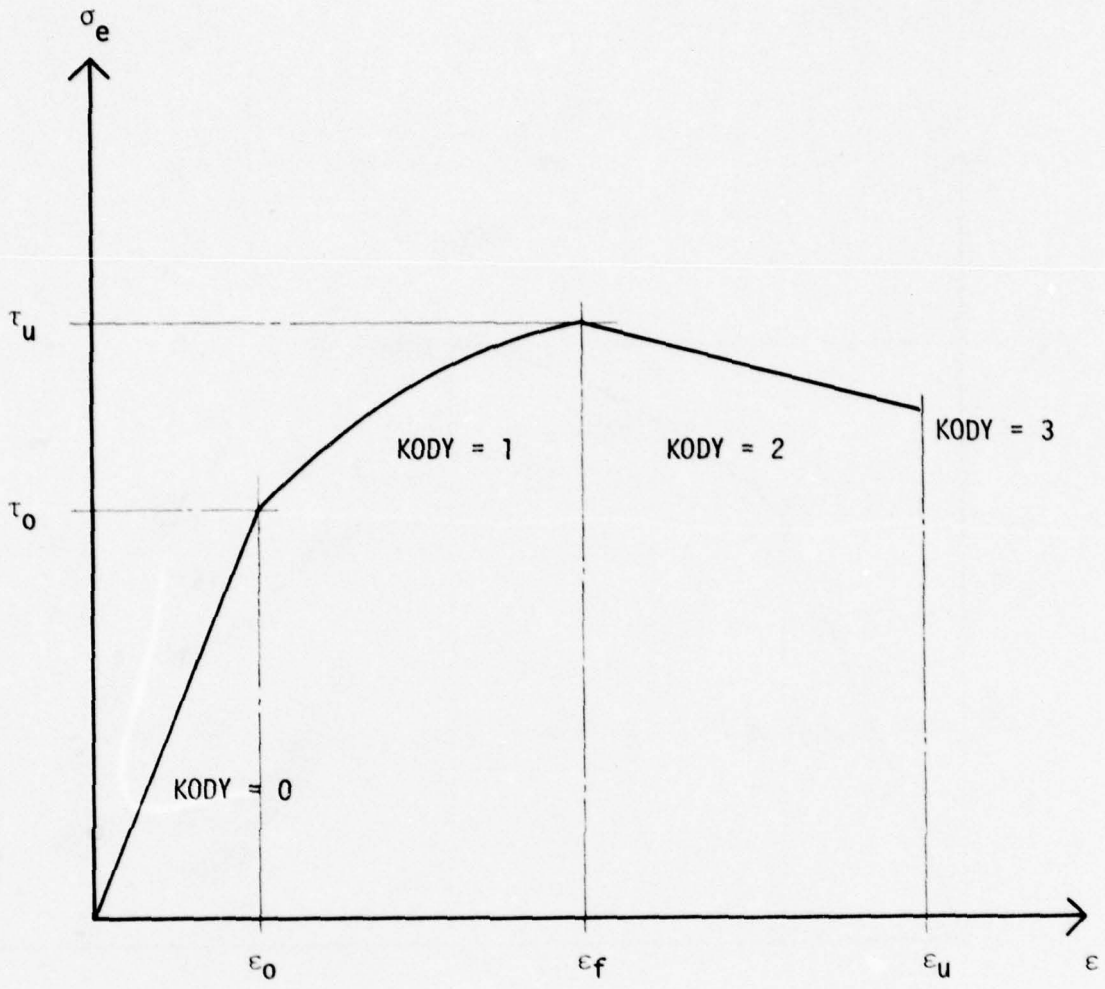

If $\sigma_e < \tau_o$ - elastic state KODY = 0

($\varepsilon < \varepsilon_f$): $\tau_u > \sigma_e \geq \tau_o$ - elastic plastic state KODY = 1

$\sigma_e > \tau_u$ - fracture state KODY = 2
$\varepsilon \geq \varepsilon_u$ - crushing state KODY = 3

Note: τ_o and τ_u values evaluated from equations 7 and 8 for the compression-compression region.

$$d\varepsilon = (d\varepsilon_{ij} \cdot d\varepsilon_{ij})^{1/2}$$

Fig. 3 Criterion for Different Stress States in Isotropic Compression Region

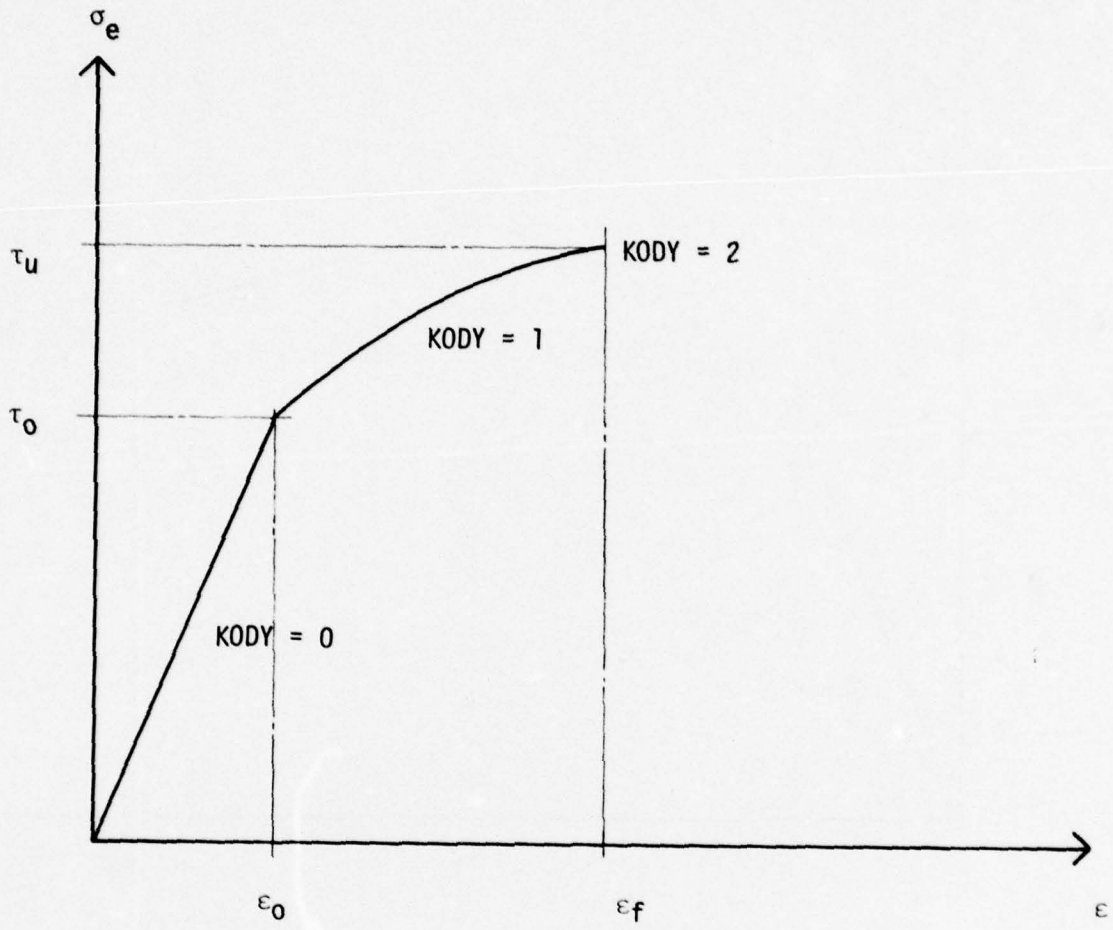

If $\sigma_e < \tau_o$ - elastic state KODY = 0

$\varepsilon < \varepsilon_f$: $\tau_u > \sigma_e \geq \tau_o$ - elastic state KODY = 1
$\sigma_e \geq \tau_u$ or $\varepsilon \geq \varepsilon_f$ - crushing state KODY = 2

Note: τ_o and τ_u are evaluated from equations 11 and 12 for tension-compression region.

Fig. 4 Criterion for Different Stress States in Tension-Compression Region

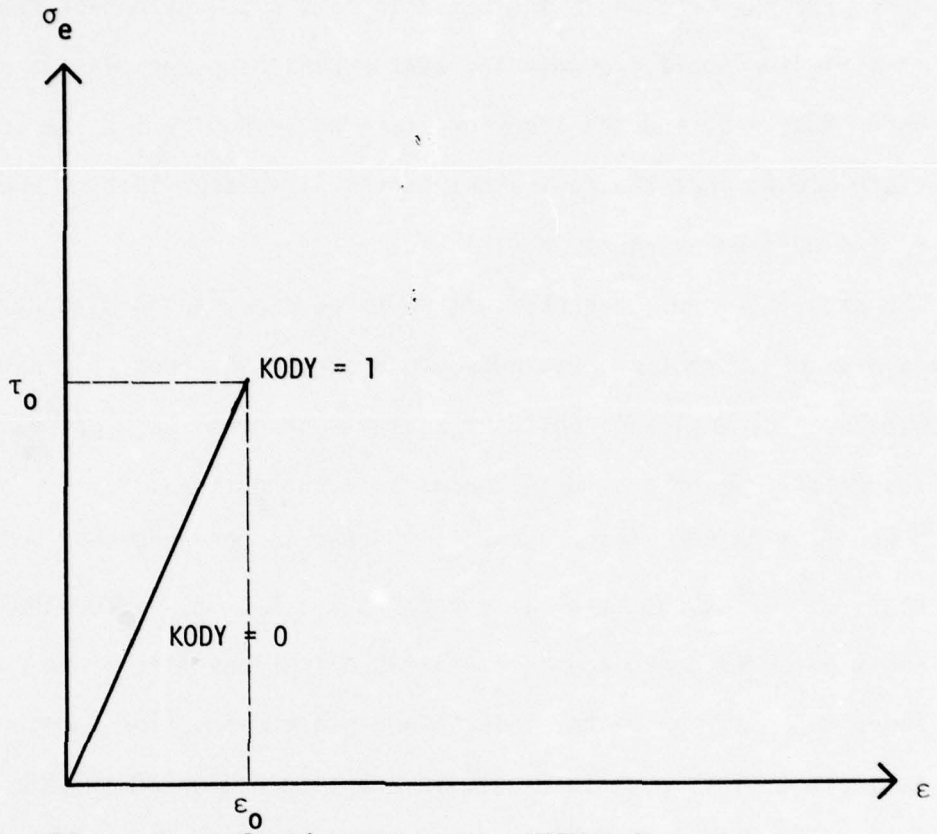

If $\sigma_e < \tau_o$ elastic state KODY = 0
$\sigma_e \geq \tau_o$ cracking state KODY = 1

Note: τ_o used is the same as for tension-compression region

Fig. 5 Criterion for Different Stress States in Tension-Tension Region

curve for this region is indicated in Figure 5. As can be seen from this figure, there are only two states possible; the elastic state where KODY = 0, and the cracking state where KODY = 1. The cracking state occurs once the equivalent stress is greater than or equal to τ_o [as defined by equation (11)].

The material model, together with a three-dimensional 8 to 20 node finite element subroutine, was added to program ANSR (ref. 3), a general purpose three-dimensional nonlinear analysis program. The material model was essentially incorporated in three basic subroutines:

a. SUBROUTINE MATP45, which essentially read in the necessary material data, evaluated the material constants A_o, A_u, τ_o, τ_u for the compression and tension regions, and also evaluated the constants α and β using the above material constants. Equivalent plastic fraction strain and equivalent plastic ultimate strain are also evaluated in this subroutine.
b. SUBROUTINE CMAT45, which evaluated the elasticity matrix defining the incremental stress-strain relationship.
c. SUBROUTINE MRES45, which evaluated the response.

These three basic subroutines in conjunction with a few other minor routines were used to define the material behavior of concrete using the constitutive relationships mentioned above. The main program ANSR was also modified to impose displacements and rotation on a section instead of imposing forces. The imposed displacements could be applied in either of the directions of the coordinate axes x, y, and z or in all three directions, or any combination thereof.

3. NUMERICAL STABILITY OF SOLUTION PROCESS

The program ANSR to which the elastic-plastic failure strain hardening material model for concrete was incorporated, has various options of numerical solution schemes. The two basic schemes available are the Newton-Raphson scheme and the constant stiffness iteration scheme. The solution scheme utilized was a mix of the two techniques. Within each load step, iteration cycles were prescribed to allow for stiffness reformation, and constant stiffness iterations were employed within in each cycle to ensure convergence of the solution.

Concrete is modeled as a mesh of discrete three-dimensional 8-to-20 node finite elements. To ensure the stability of the solution scheme, several steps had to be taken. Suppose a reinforced concrete section is modeled as shown in Figure 6.1 using concrete solid elements and three-dimensional truss elements for reinforcing steel. If this section is subjected to an imposed deformation pattern of extension and rotation in a certain ratio, and this constant deformation ratio of δ/θ is increased in a number of load steps, a stress state will be created such that the bottom four gauss points of the bottom element in the tensile zone crack. Once this stress state occurs, the stiffness contribution of these four gauss points is reduced to a percentage of the original stiffness (say 10%) for the next stiffness reformation. If in the next load step the top four gauss points of this same element also crack, then the stiffness of this element is set to zero. At selected degrees of freedom the steel truss bar elements do not contribute any stiffness, so that the resulting stiffness would be zero. The system of equations $\underline{K}\,\underline{r} = \underline{R}^{(a)}$ is solved using Gaussian elimination. However, during the factorization of $\underline{K}$ into $\underline{L}\,\underline{D}\,\underline{L}^T$, the elements of the D diagonal are checked for small numbers resulting from the zero stiffness of cracked elements. Such a

(a) Bar below letters indicates matrices.

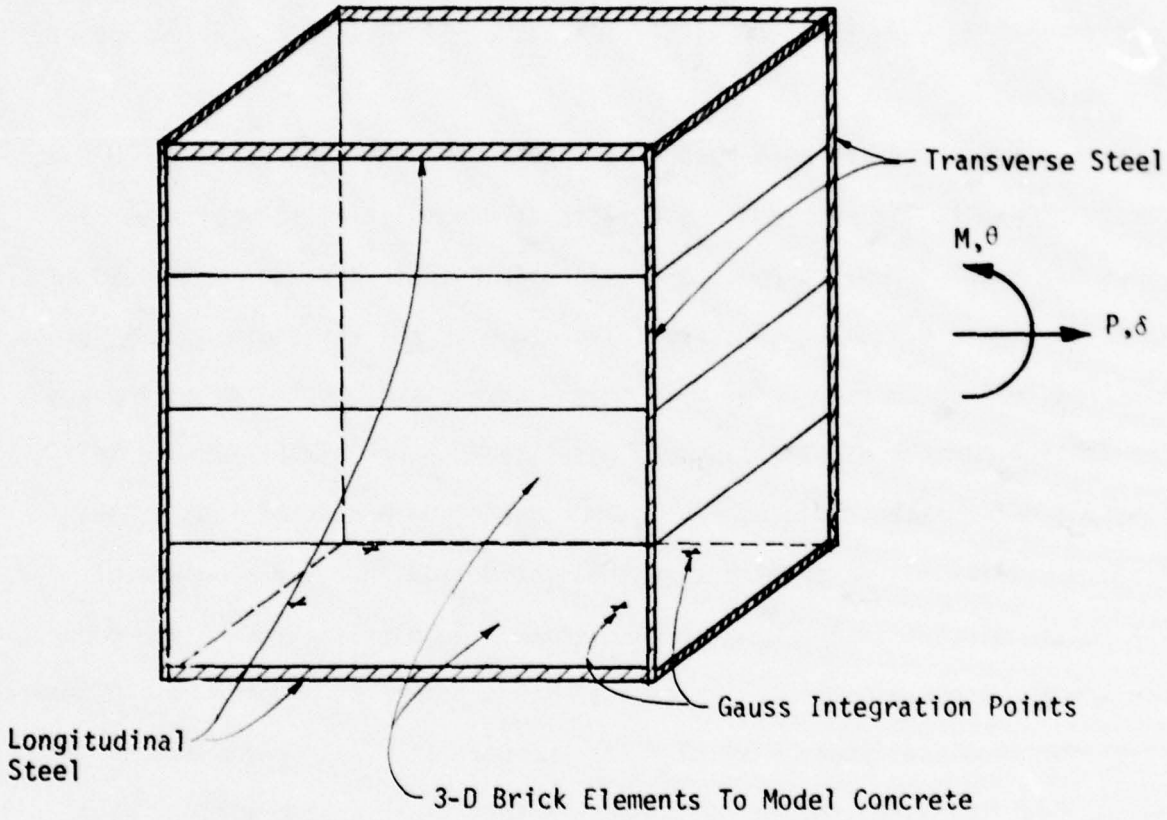

Note: Concrete Cover Was Not Considered

Figure 6.1 Reinforced Concrete Section. Finite Element Model.

condition could cause large nodal displacements resulting in large displacements and imminent numerical instability. Thus, if during the factorization of K the element of the D matrix produces numbers smaller than 10^{-5}, the diagonal element was replaced with a very large number of the order of 10^{14} to stabilize the solution. Note that both 10^{-5} and 10^{14} are arbitrary numbers. Thus, to summarize, the following steps ensure numerical stability:

a. If a gauss point in an element cracked or crushed, then the stiffness contribution of this gauss point to the element stiffness is reduced to a certain percentage of its original stiffness. This number is specified by the user as an input to the program. A value of 10 percent is recommended.

b. After the element stiffnesses are assembled into the structure stiffness matrix, the diagonals produced during the factorization are checked for small numbers. If any element in the diagonal is found to be less than 10^{-5}, this element is replaced by a large number of the order 10^{14}.

4. VERIFICATION RESULTS

The material model incorporated into program ANSR was checked by comparing the analytical results against experimental results. Since Chen and Chen (refs. 1 and 2) had already checked their constitutive relationships and presented their results compared to the experimental results of Kupfer, et al., (ref. 6) it was decided to check the model against the results of Chen and Chen and Kupfer, et al.

Hence, a series of runs was carried out using a single brick element of concrete 7.9 ins. by 7.9 ins. by 2 ins. (20 cm by 20 cm by 5 cm). The

---

6. Kupfer, H., Hilsdorf, H. K., and Rush, H., "Behavior of Concrete under Biaxial Stresses," Vol. 66, No. 8, pp. 656-666, Proceedings, Journal of American Concrete Institute, August, 1969.

uniaxial compressive stress-strain curve used is shown in Figure 6.2. This brick was subjected to biaxial forces in a ratio of σ_1/σ_2, the principal stresses in two directions. This ratio was varied for biaxial compressive forces, i.e., ratios of σ_1/σ_2 of -1/-1, -1/0, -1/-0.522, -1/-0.0001, and for tension compression forces of -1/0.103, -1/0.204, and -1/0.052. The results obtained from these analyses were plotted against the experimental results of Kupfer, et al and the analytical results of Chen and Chen. The results are presented in Figures 7 through 14.

Figure 7, which plots σ_1 versus ε_1 for σ_1/σ_2 of -1/-1, shows that the present model has more stiffness than the Chen and Chen or Kupfer, et al. results. In this analysis the uniaxial stress-strain curve input to the program was assumed to be linear up to a stress of 30 percent of the ultimate stress f'_c. Chen and Chen (ref. 2) have indicated in their report that the normality condition was best satisfied using a linear uniaxial stress-strain relationship up to a stress euqal to 60 percent of the ultimate stress. Thus this relevant parameter was changed and the results of the new analysis are indicated in Figure 8. It can still be observed that the present model response has more stiffness associated with it than the results of Kupfer, et al. and Chen and Chen.

Figure 9 indicates the results of the applied forces σ_1/σ_2 in the ratio of -1/-0.522. The correlation in this case is much better than for equal biaxial imposed forces. The correlation in this case is much better than for equal biaxial imposed forces. Figures 10 and 11 indicate results for σ_1/σ_2 of -1/-0.0001 where the change in the modeling between the two analyses is the value of initial yield point of uniaxial stress-strain relationships of concrete.

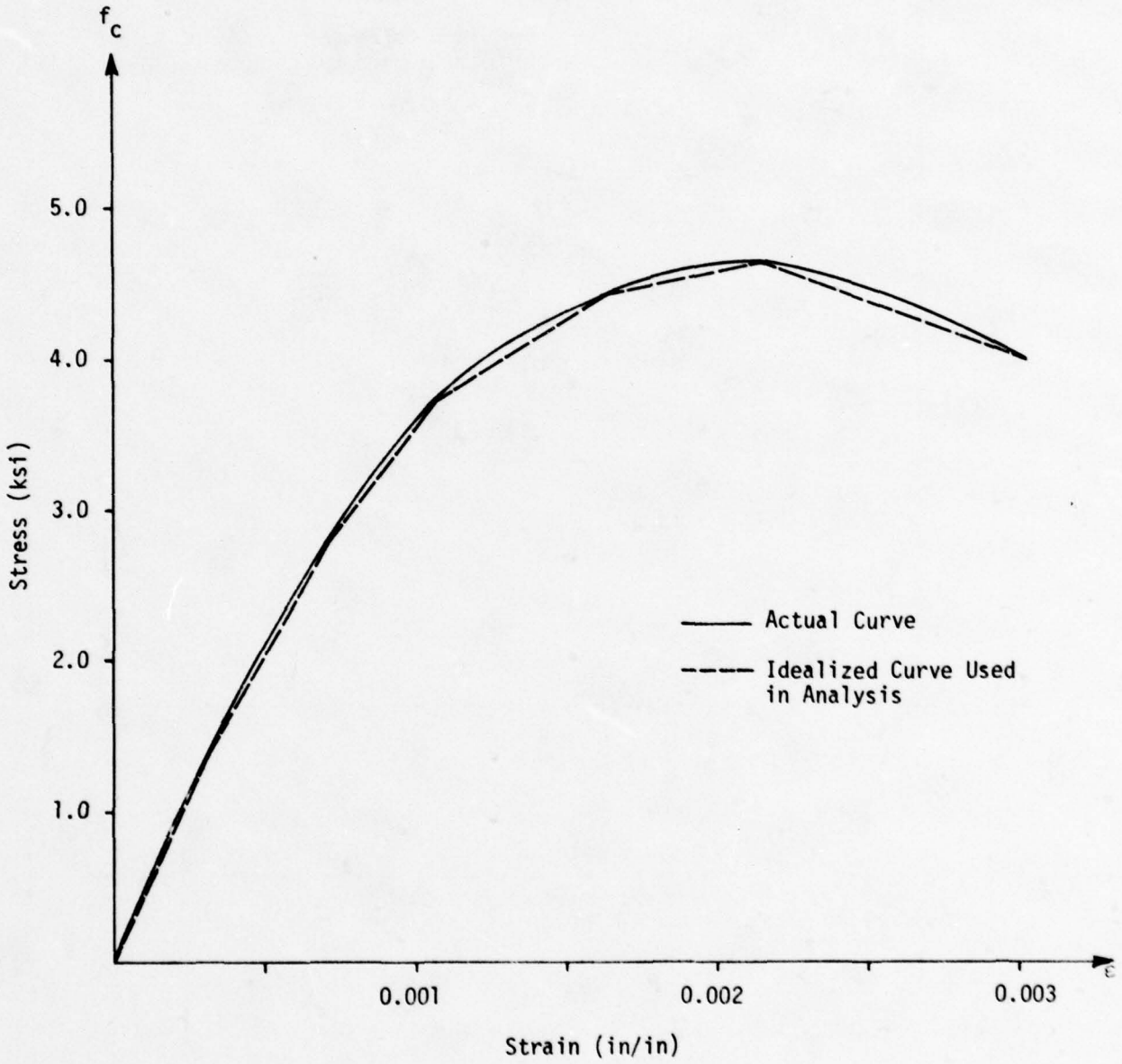

Figure 6.2 Stress-Strain Curve for Concrete

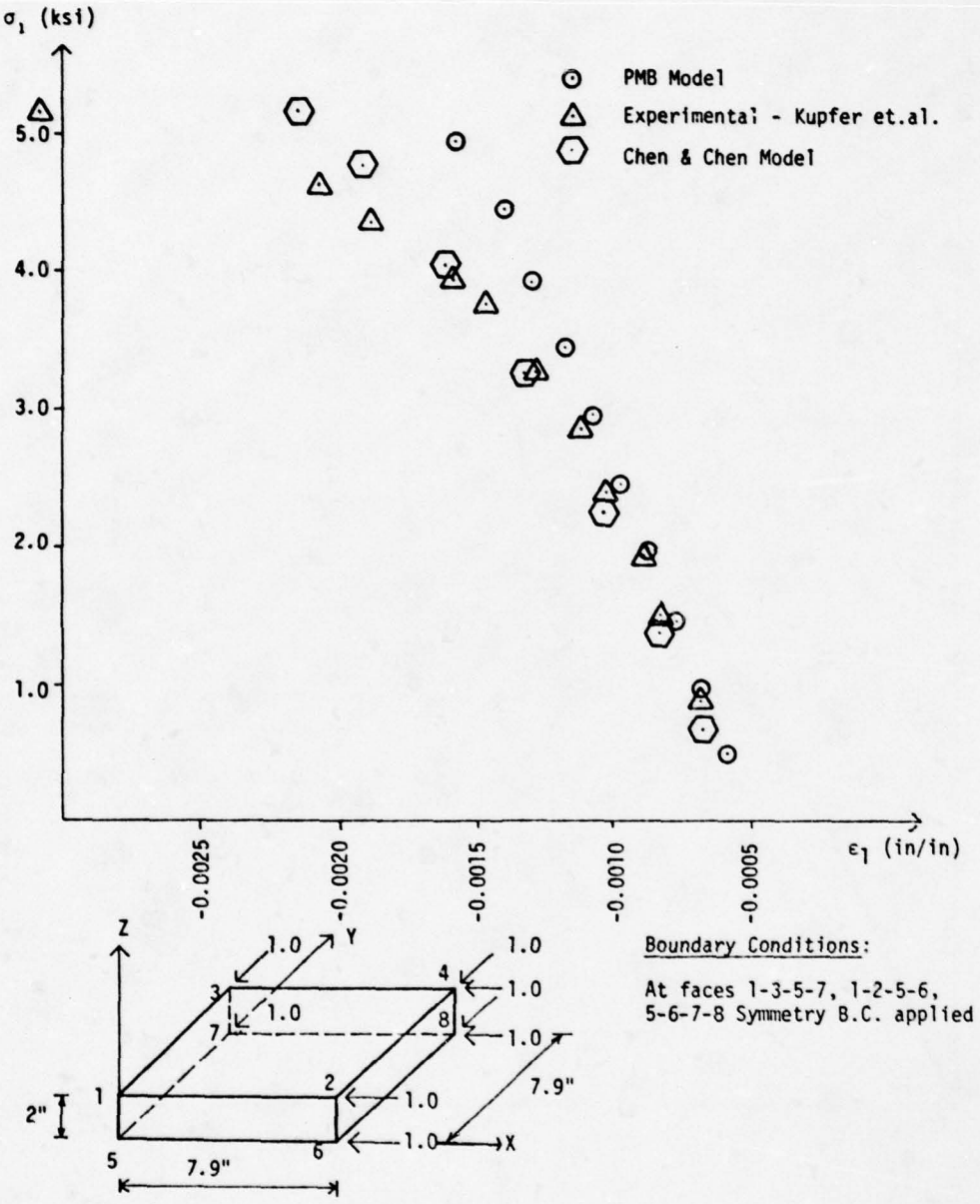

Fig. 7 Analytical Results. Biaxial Compressive Forces Imposed.

$\sigma_1/\sigma_2 = -1/-1$. $f_c/f'_c = 0.30$

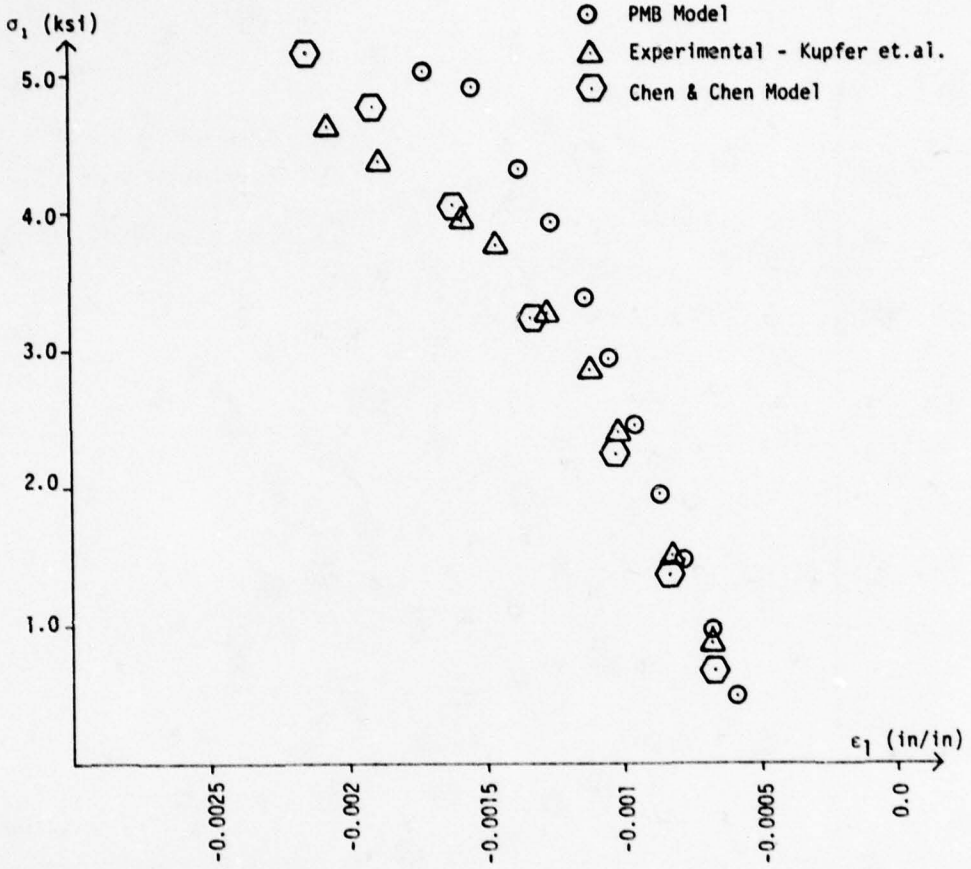

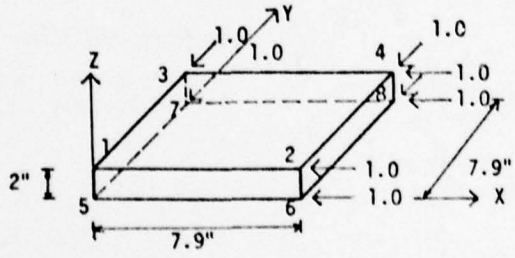

Boundary Conditions:

At faces 1-3-5-7, 1-2-5-6, and 5-6-7-8, Symmetry B.C. applied.

Fig. 8 Analytical Results. Biaxial Compressive Forces Imposed.
$\sigma_1/\sigma_2 = -1/-1.$ $f_c/f'_c = 0.60$

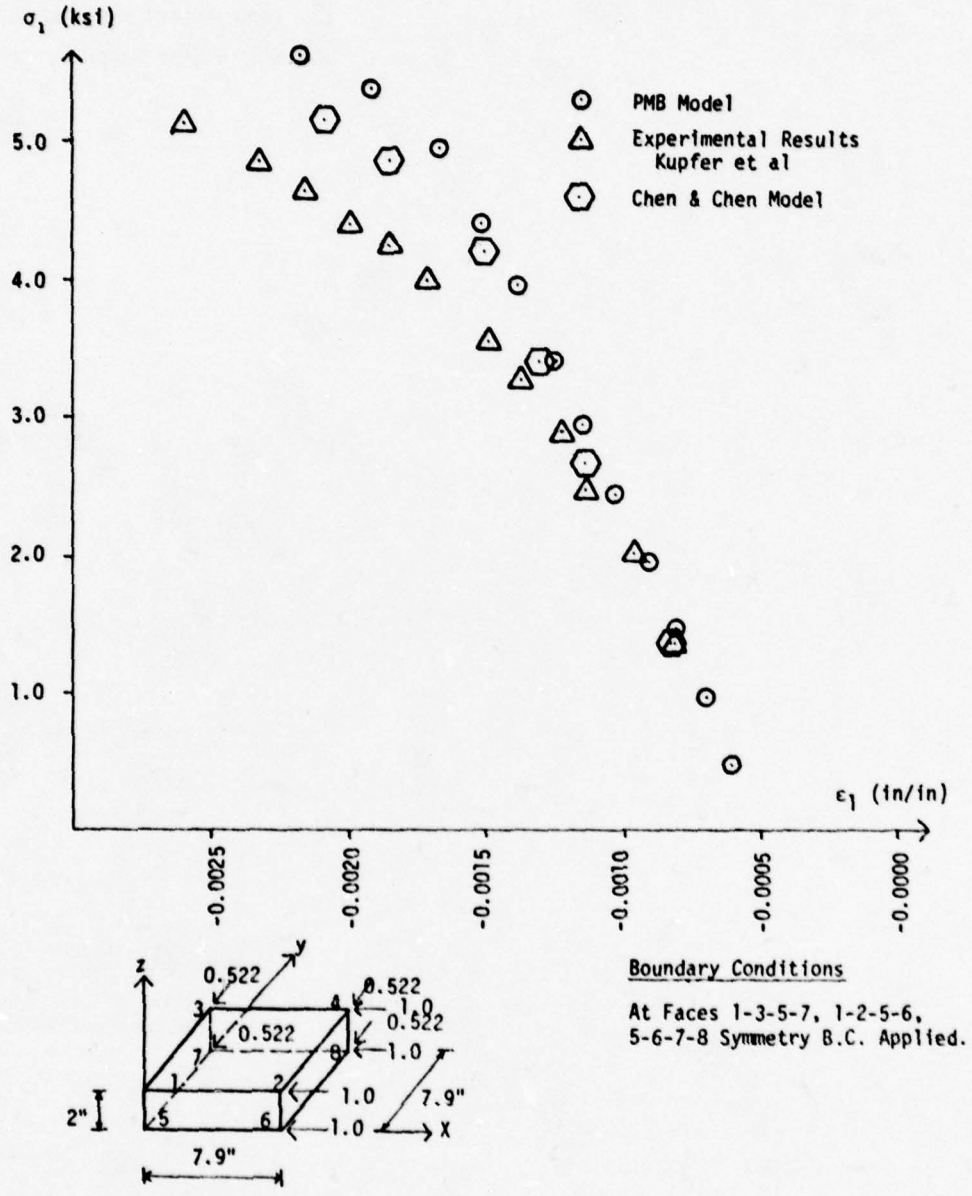

Fig. 9 Analytical Results. Biaxial Compressive Forces Imposed.
σ_1/σ_2 = -1/-0.522 f_c/f'_c = 0.30

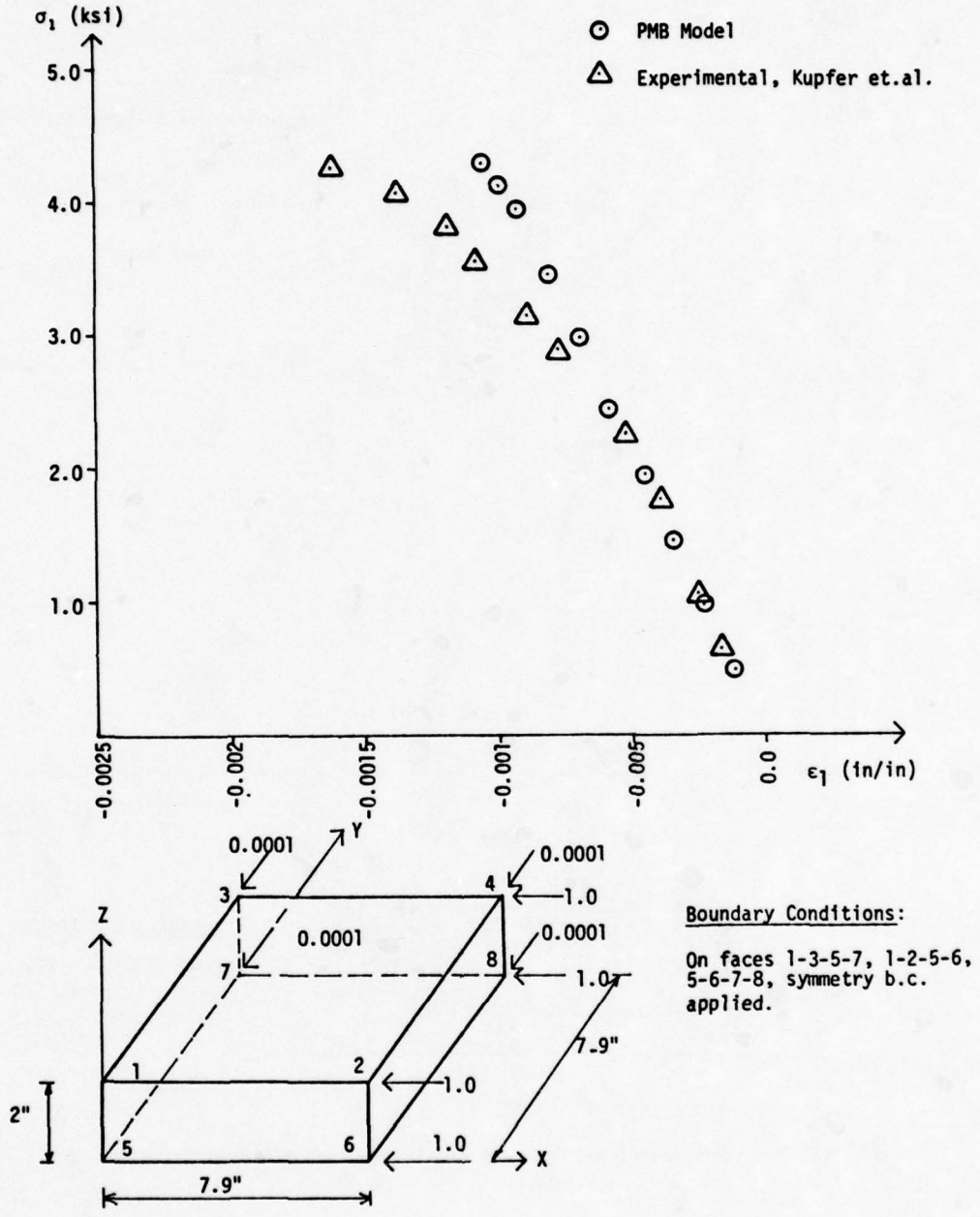

Boundary Conditions:

On faces 1-3-5-7, 1-2-5-6, 5-6-7-8, symmetry b.c. applied.

Fig. 10 Analytical Results. Biaxial Compressive Forces Imposed. $\sigma_1/\sigma_2 = -1/-0.0001$. $f_c/f'_c = 0.60$

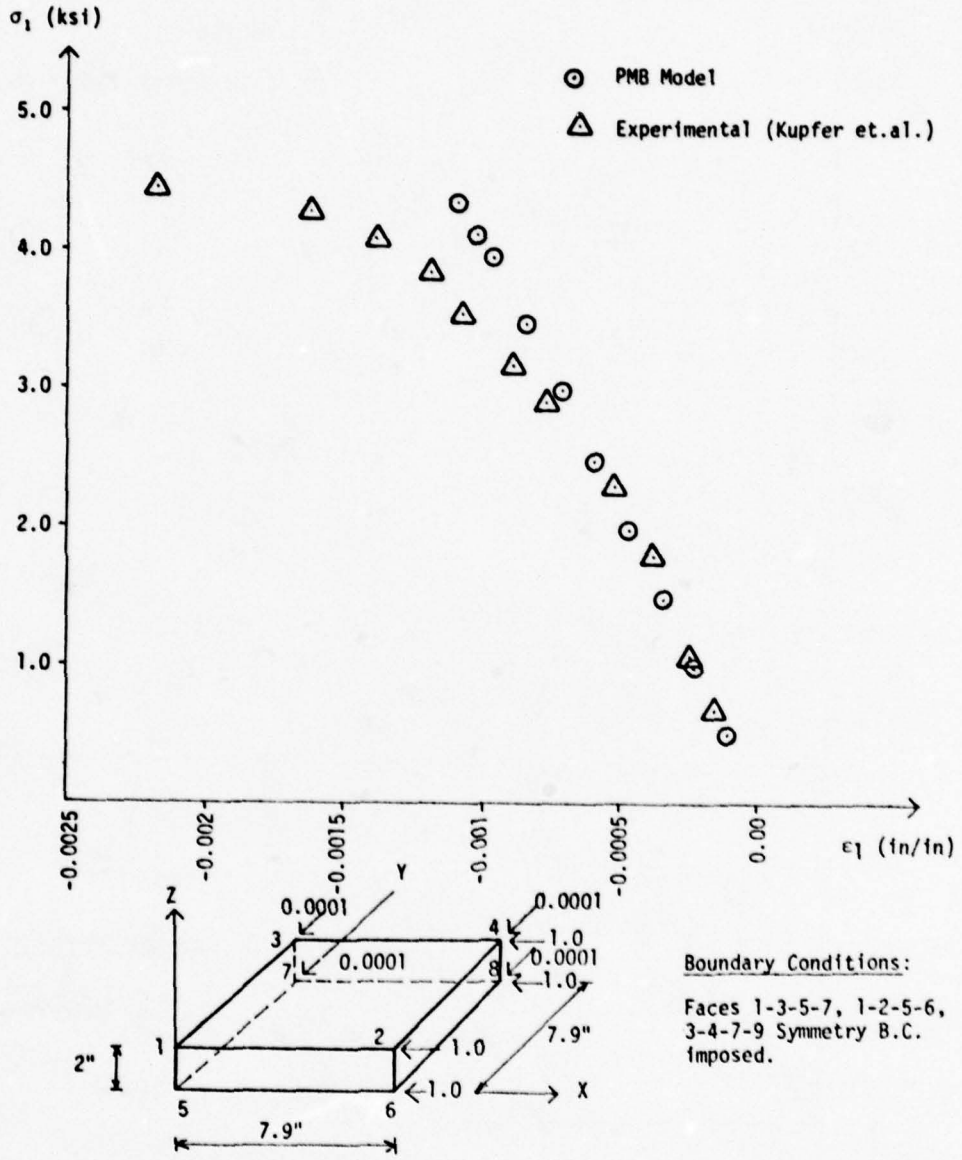

Fig. 11 Analytical Results. Biaxial Compressive Forces Imposed. $\sigma_1/\sigma_2 = -1/-0.0001$. $f_c/f'_c = 0.30$

The correlation in the case of tension-compression applied forces seems to be better than in the biaxial compressive applied forces. Figures 12 through 14 indicate the results of the analysis for various ratios of loading.

The general conclusion that can be drawn from the above analysis is that the present model has more stiffness associated with it. This stiffness is sensitive to the type of uniaxial stress-strain relationship input to the model. The exact parameters for the uniaxial σ-ε curve used by Chen and Chen in their analysis were not known. In this case, the curve assumed may be different, which can account for the difference in stiffness.

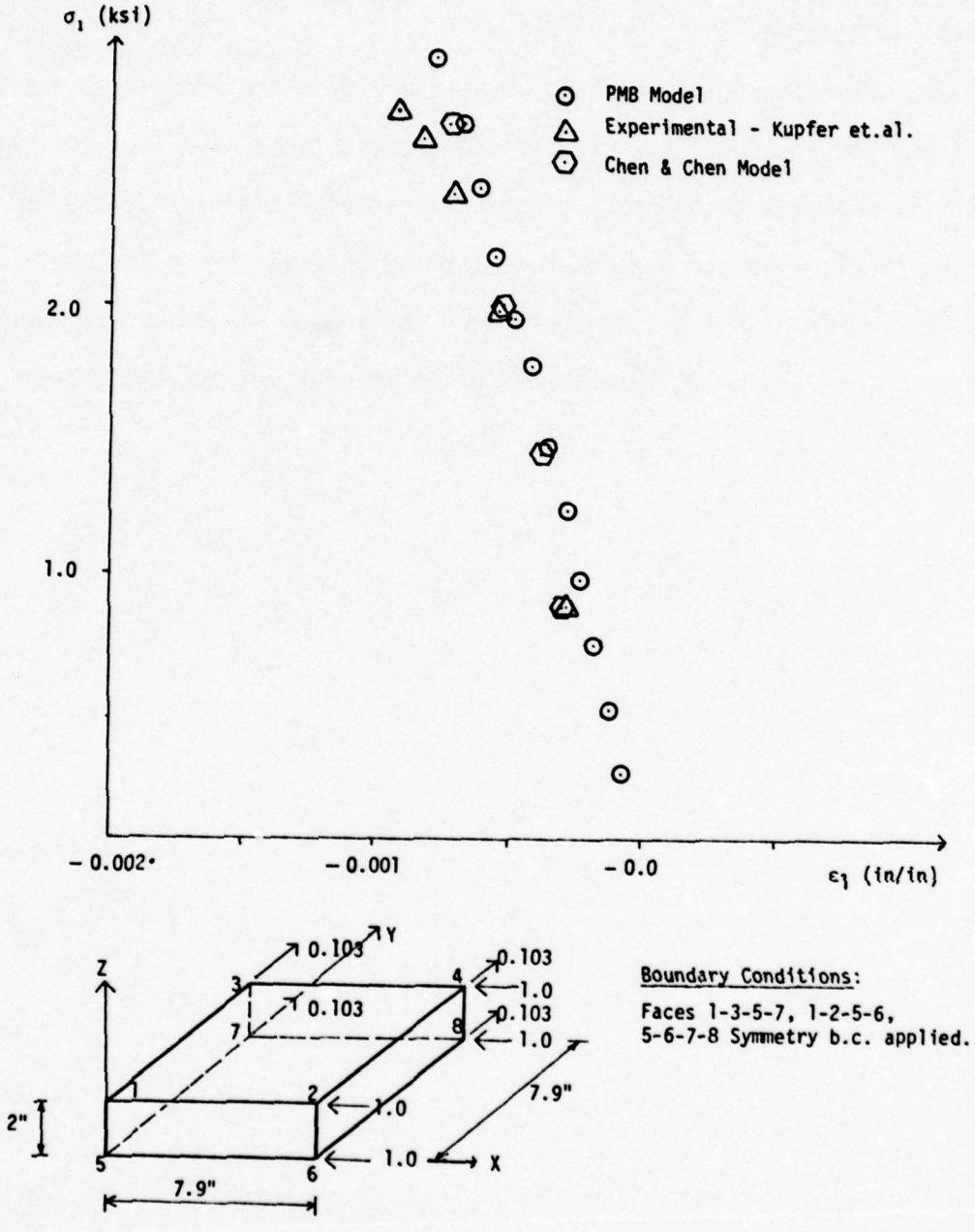

Boundary Conditions:

Faces 1-3-5-7, 1-2-5-6, 5-6-7-8 Symmetry b.c. applied.

Fig. 12 Analytical Results. σ_1/σ_2 = -1/+0.103. f_c/f'_c = 0.30

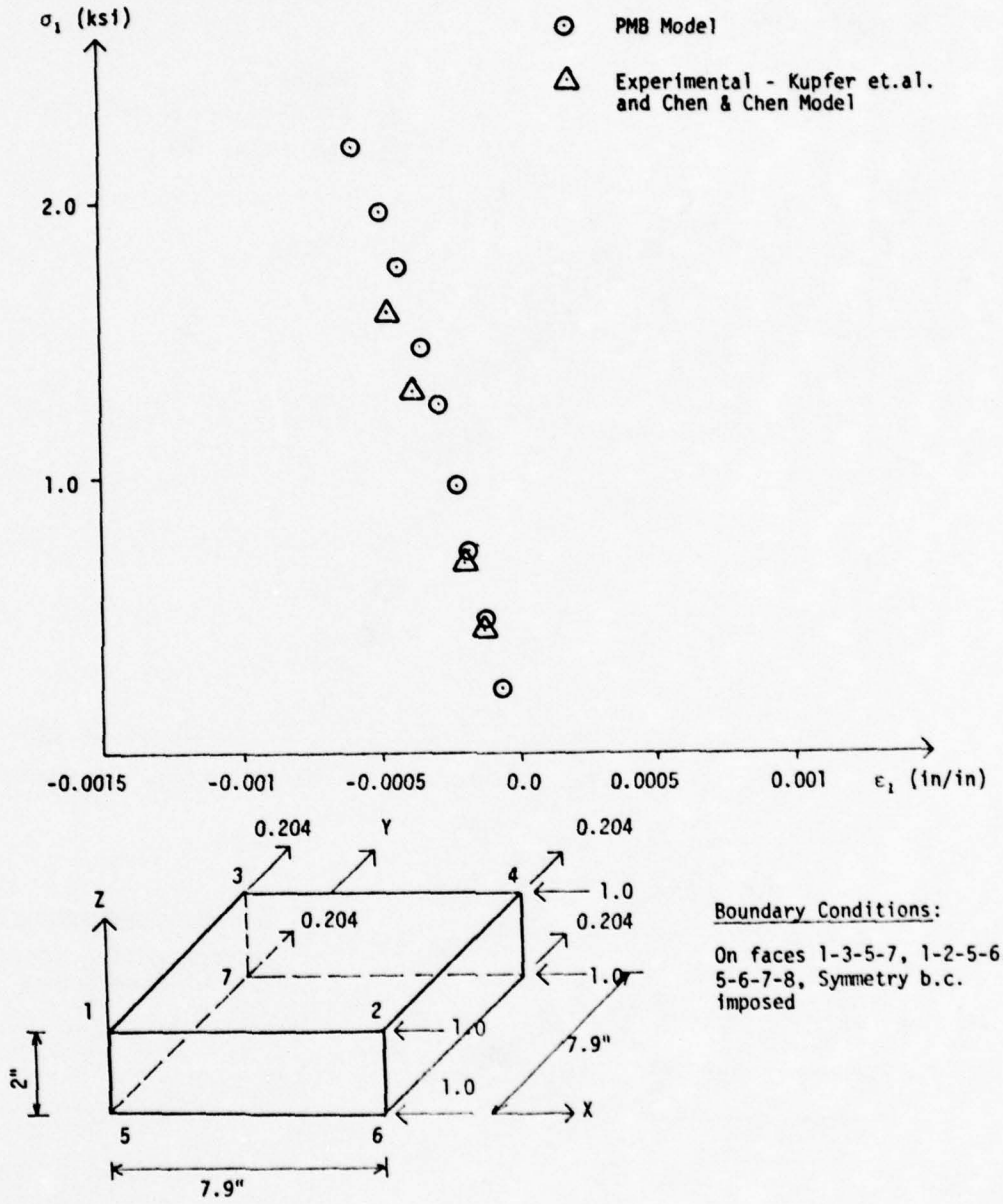

Fig. 13 Analytical Results. σ_1/σ_2 = -1/0.204 f_c/f'_c = 0.60

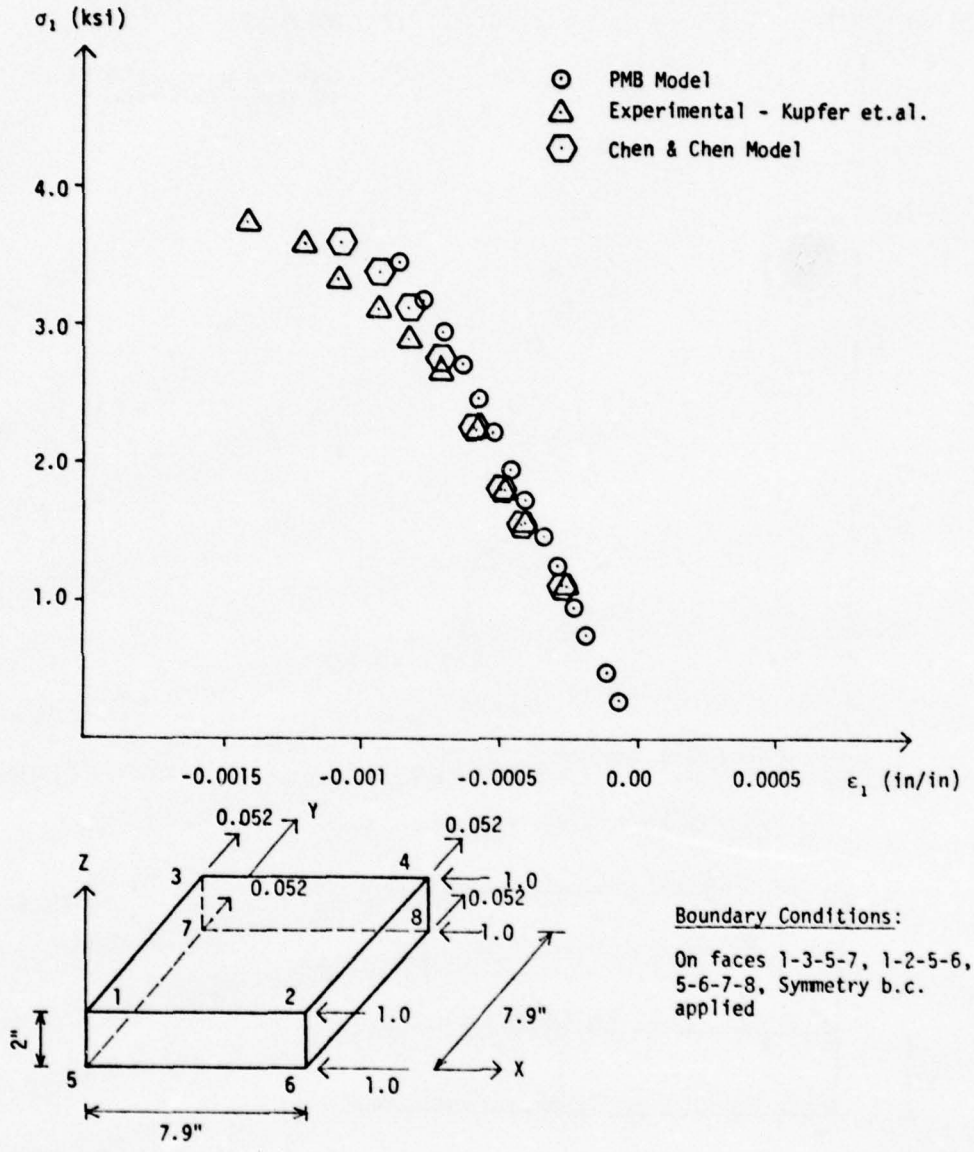

Fig. 14 Analytical Results. $\sigma_1 / \sigma_2 = -1/0.052$ $f_c/f'_c = 0.60$

SECTION III

PARAMETRIC DATA

1. GENERAL

Once the model was tested and the results indicated in the preliminary analysis found to be adequate, the analysis of two types of sections was considered: the rectangular section and the cylindrical section. The analysis consisted of imposing monotonically increasing values of a specific ratio of axial to rotational deformation to a given section. After such an increment of deformation, total stresses in the concrete and steel were computed to determine if the concrete had cracked, yielded, crushed or failed, or the steel had yielded.

Stresses for the concrete were calculated at the integration points of the three-dimensional finite elements. These stresses were integrated over the volume of the section to give equivalent loads at the nodes of the element. The generalized axial force and bending moment on the section were also calculated using these nodal loads and the loads in the steel.

For concrete, yield of an integration point was defined when the effective stress at that point (equation 1 and 2) exceeded the effective yield stress. The effective yield stress τ_o was calculated using equation 7 for an isotropic compression state of stress and by equation 11 for a tension-compression state of stress.

For an isotropic compression state of stress at an integration point, crushing was defined when the effective stress (equation 1) exceeded the effective ultimate stress τ_u (equation 8) and the equivalent plastic strain

at that point exceeded the equivalent ultimate plastic strain. The equivalent plastic strain is defined by equation 13 while the equivalent ultimate plastic strain is calculated using laws of plasticity corresponding to the ultimate strain of the uniaxial compressive stress-strain curve.

For the tension-compression state of stress, crushing of the integration point occurs when the effective stress of that point (equation 2) exceeds the effective ultimate stress (equation 12) and the equivalent plastic strain (equation 13) exceeds the equivalent fracture plastic strain. The equivalent fracture plastic strain is calculated using laws of plasticity corresponding to the strain at ultimate stress of the uniaxial compression stress-strain relation.

Cracking of an integration point in isotropic tension is defined when the effective stress of that point (equation 2) exceeds the effective cracking stress (equation 11).

Once an integration point of the three-dimensional finite element cracked in isotropic tension state of stress, or crushed in isotropic compression or tension-compression state of stress, the stiffness contribution of that integration point to the element stiffness was considered as zero. If all the integration points of all the elements loaded in compression were crushed in isotropic compression or in tension-compression, the failure strength of the section was reached. Thus, depending on the loading on the section, as a consequence, the depth of the concrete section loaded in compression, the failure strength of the section would vary. Thus, a series of values of failure strengths for the section could be obtained as a function of the loading on the section, resulting in an envelope, now defined as the failure strength envelope or simply the failure envelope.

The main purpose of the analysis then was to obtain a failure envelope for each type of section analyzed. In order to achieve this, the section was imposed with monotonically increasing deformations in a fixed ratio of axial to rotational, until the failure strength of the section was attained.

Since the ratio of imposed deformations, axial to rotational was fixed while monotonically increasing the value of these deformations, the neutral axis of imposed deformations was fixed. Each section was subjected to seven deformation ratios or patterns: pure compression, pure extension, pure rotation, extension/rotation of 5.0, extension/rotation of 15.0, compression/rotation of 5.0 and compression/rotation of 15.0. For each section, seven failure strengths were obtained corresponding to the seven deformation ratios or patterns. These failure strengths were plotted to give the failure envelope for the section. The failure envelope was plotted in terms of deformations which were reduced to dimensionless quantities of strains and curvatures. Note that the section was imposed with deformations rather than forces. This approach was adopted since the final aim was to obtain the failure envelope in terms of deformations rather than forces. A typical failure envelope is indicated in Figure 15. As the deformations on the section were monotonically increased, at each load step increment, the axial force and bending moment on the section were also calculated. These response quantities were plotted as moment-rotation ($M-\theta$) and axial force deformation ($P-\delta$) curves for each section. Note that the $M-\theta$ and $P-\delta$ curves were referenced to the geometric centroid of the section. The failure envelopes also indicated strains and curvatures at failure at the centroid of the section. Note also that only confined sections were studied.

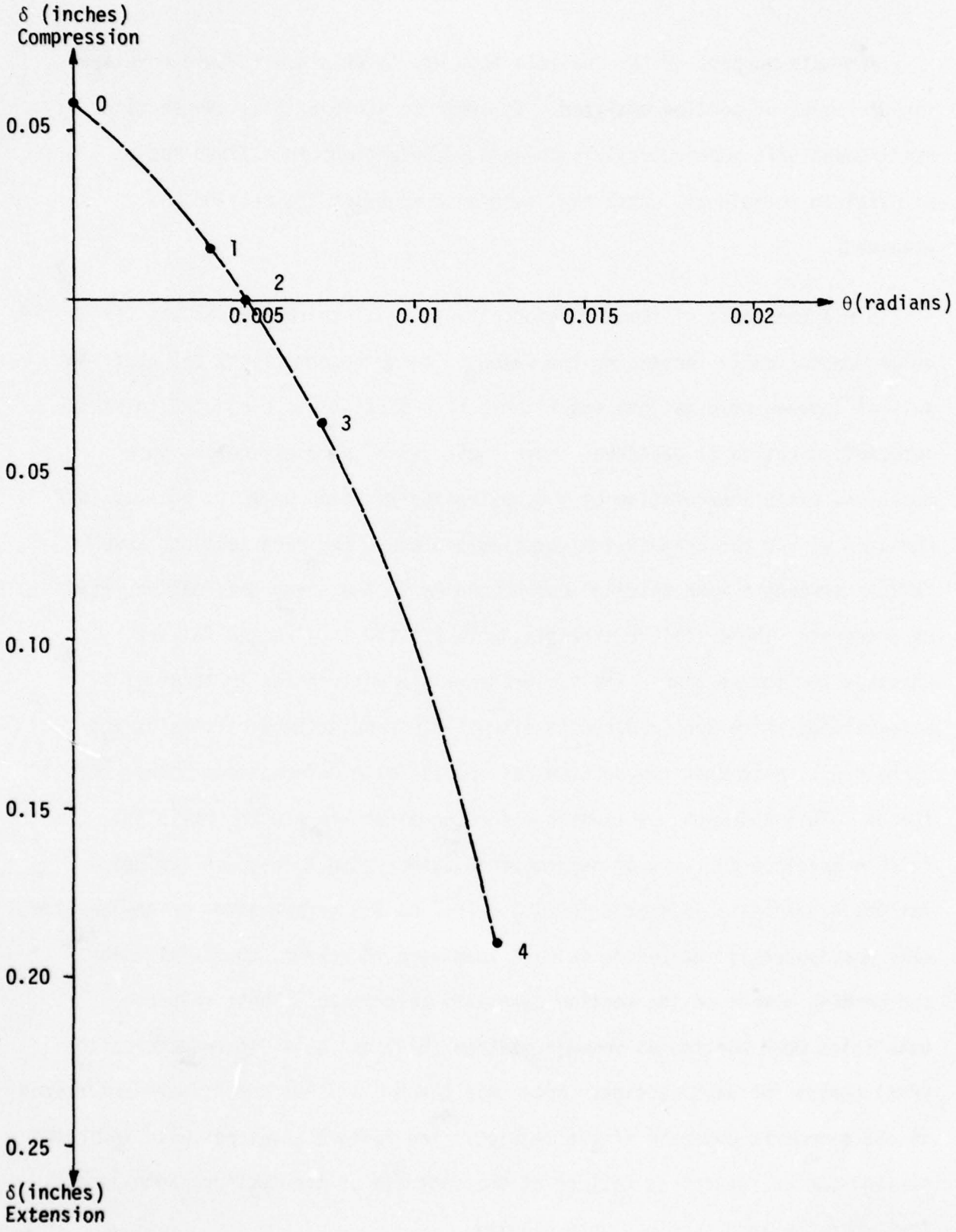

Figure 15. Typical Failure Envelope in Terms of Deformations

2. RECTANGULAR SECTION RESULTS

The total number of cases analyzed for the confined rectangular section (CRS) is indicated in Table 1. The strength of concrete, the percentage of longitudinal reinforcement, and the area of confining steel were selected as the parameters that would be varied. The first two sections analyzed were CRS #3 and CRS #7 (Table 1). Each of the above two sections contained 2 percent longitudinal reinforcement both in tension and compression zones ($p = p' = 2\%$). The area of transverse steel per leg was 3.50 in^2 over a length of 19.685 inches, calculated on the basis of ACI 1971 code requirements for seismic resistant design. The only difference between the two was the strength of concrete; the ultimate uniaxial compressive stress of concrete for CRS #3 was 5 ksi, while that of CRS #7 was 6 ksi. CRS #4 and #8 were sections with $p = p' = 1/4\%$, while the ultimate uniaxial compressive stresses for concrete were 5 ksi and 6 ksi, respectively. CRS #11 had $p = p' = 2\%$ and an ultimate uniaxial compressive stress of concrete of 9.0 ksi. CRS #11.1 was similar to CRS #11 with the exception of the uniaxial compression stress-strain relationship for the concrete, which was different. Section CRS #6 was analyzed with 1 percent longitudinal reinforcement at each face and an ultimate uniaxial concrete compressive stress of 5.0 ksi. While keeping the section size, the percentage of longitudinal reinforcement and the properties of concrete constant and equal to that of CRS #4, the transverse reinforcement was varied to study the effect of confinement on the failure envelope (CRS #4.2). The effect of refinement of mesh in the response characteristics and the failure envelope was studied in the analysis of Section CRS #4.1.

TABLE 1 CONFINED RECTANGULAR SECTION (CRS)
PARAMETRIC STUDY LAYOUT

DEFORMATION RATIOS:[a] $\delta/\theta = \pm\infty, 0, \pm 5, \pm 15$														
Identification No.	Ult. Compressive Stress f'c (ksi)				Reinforcement %[b]				Confining Transverse Reinforcement Area $A_{sh}(in^2)$ [c]				Mesh Type	
	5	6	7	9	¼	½	1	2	3.50	2.713	1.36	0.60	4-Layer Mesh	8-Layer Mesh
CRS3	X								X				X	
CRS4	X				X							X	X	
CRS4.1	X				X							X		X
CRS4.2	X				X				X				X	
CRS6	X						X			X			X	
CRS7		X						X	X				X	
CRS8		X			X							X	X	
CRS11				X				X	X				X	
CRS11.1				X				X	X					X

[a] Positive value of δ/θ ratio indicates extension combined with rotation.
[b] Reinforcement ratios expressed as a percentage at each face of the section,
[c] Minimum area required as per ACI 1971 Code for seismic requirements.

a. Analytical Modeling For Concrete And Steel

The dimensions of the section were kept constant throughout the analysis. No cover was considered in the analysis, since the cover would spall at a very early stage of loading, thereby not contributing significantly to the ultimate capacity of the section. Inclusion of the cover would also cause numerical stability problems. Concrete was modeled using three-dimensional node finite elements. Most of the sections were analyzed using a four layer system. Some sections were analyzed using eight layers of brick elements.

Steel was modeled as three-dimensional truss elements. These elements were connected at the nodes of the concrete brick elements. The confined section under consideration is shown in Figure 16.1 while an analytical model is shown in Figure 16.2.

Boundary conditions imposed on the section were as follows: symmetry boundary conditions were imposed on the face 1-11-15-5 (Figure 16.2) in the X-direction while nodes 10 and 20 were restrained in the Y-direction. To prevent rigid body modes of deformation in the Z-direction, face 1-5-10-6 was fixed in this direction. Nodes 3-8-18-13 defined the horizontal plane passing through the centroidal axis of the section (Figure 16.2). Displacements (extension or compression) were imposed on the plane defined by nodes 6, 10, 16, 20, while this same plane (nodes 6-10-16-20) was subjected to rotations about the horizontal plane through the centroidal axis of the section (nodes 3-8-18-13).

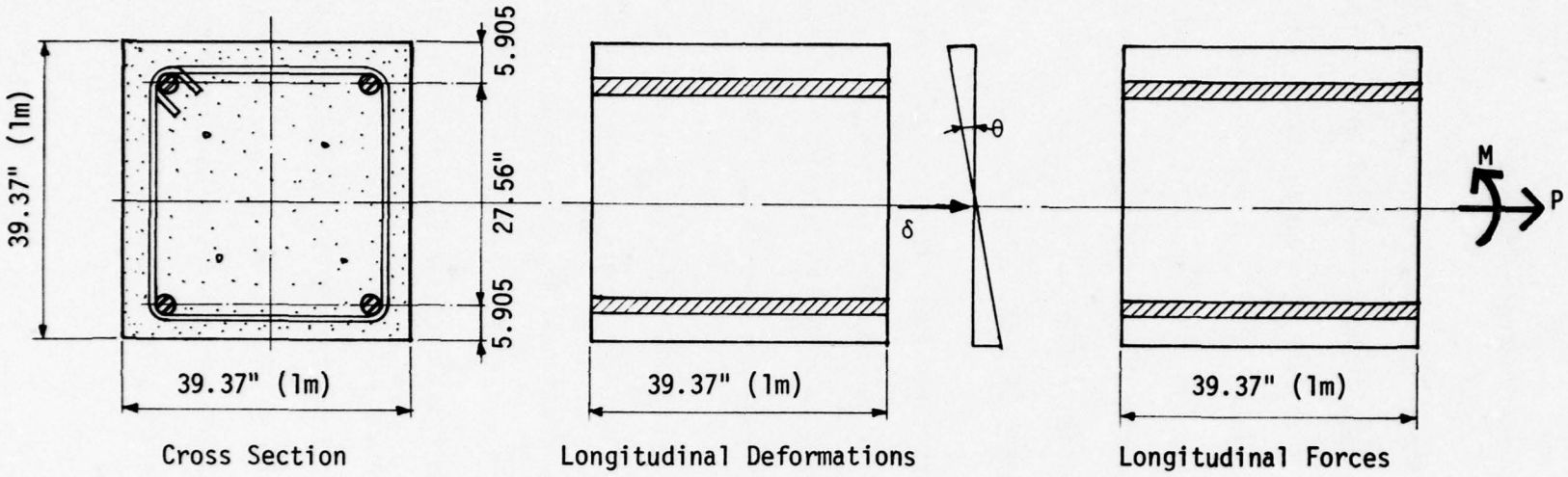

Figure 16.1 Rectangular Section. Dimensions, Reinforcement Layout, and Definition of Longitudinal Deformations and Forces

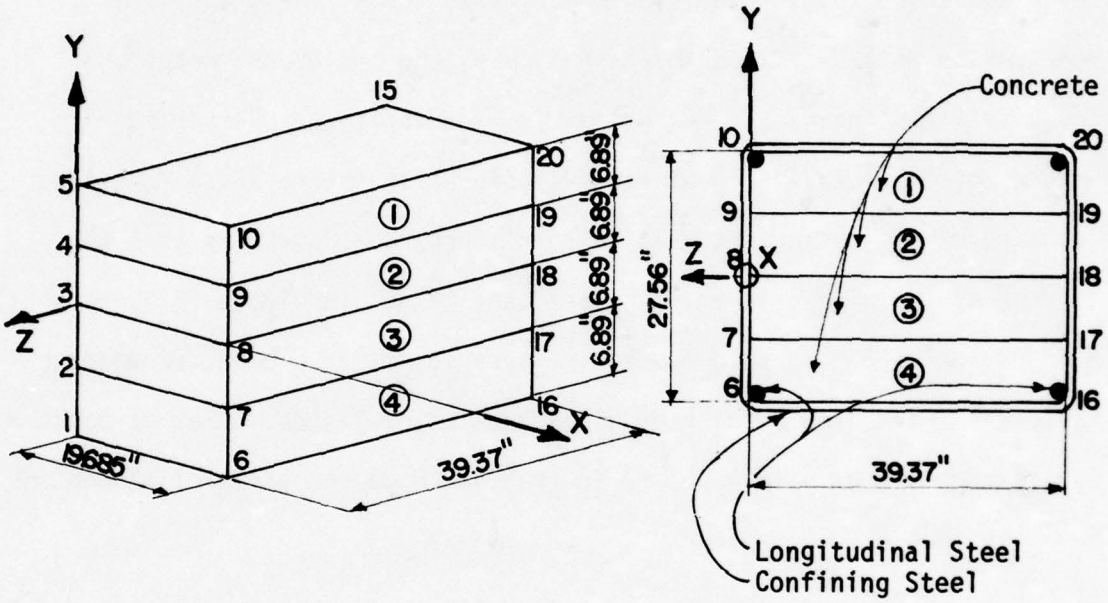

Figure 16.2 Finite Element Model for Rectangular Section

The moment and axial force measured as response quantities were measured at the geometric centroidal axis. Thus, the M-θ curves and the P-δ curves were plotted at the centroidal axis of that section.

The history of nonlinearities that occur throughout the loading history are presented as events in tabular form on the plots of M-θ and P-δ curves. Each event is identified by a number (for example, refer to Figure 26.3). The events are described at the gaussian integration points defined in these figures and tables as "nodes". Thus, if a nonlinear event occurs during loading (e.g., "cracking of 3 nodes of element #4", identified as point 1 in Figure 26.3) in effect cracking of 3 gaussian integration points occurs. Note also that the current status of each element is defined. Thus, in Figure 26.3, at point 5 identified in this figure, 7 gauss points of element #2 undergo yield while at point 8 the remaining gauss point yields. Thus at point 8, the current status of element #2 is that all 8 gauss points of element #2 have yielded.

(1) Response Of CRS #3

Confined rectangular section CRS #3 had concrete with an ultimate uniaxial compressive stress of 5.0 ksi. The uniaxial stress strain curve used for concrete in the analysis is indicated in Figure 17. The idealized curve is shown by the dashed line. Note that concrete behavior is assumed elastic and linear up to the point where the stress is 0.48 times the ultimate compressive stress. After this point the nonlinear behavior is idealized by three linear portions of nonelastic behavior as shown in Figure 17. Ultimate strain was assumed to be 0.003 in/in. The

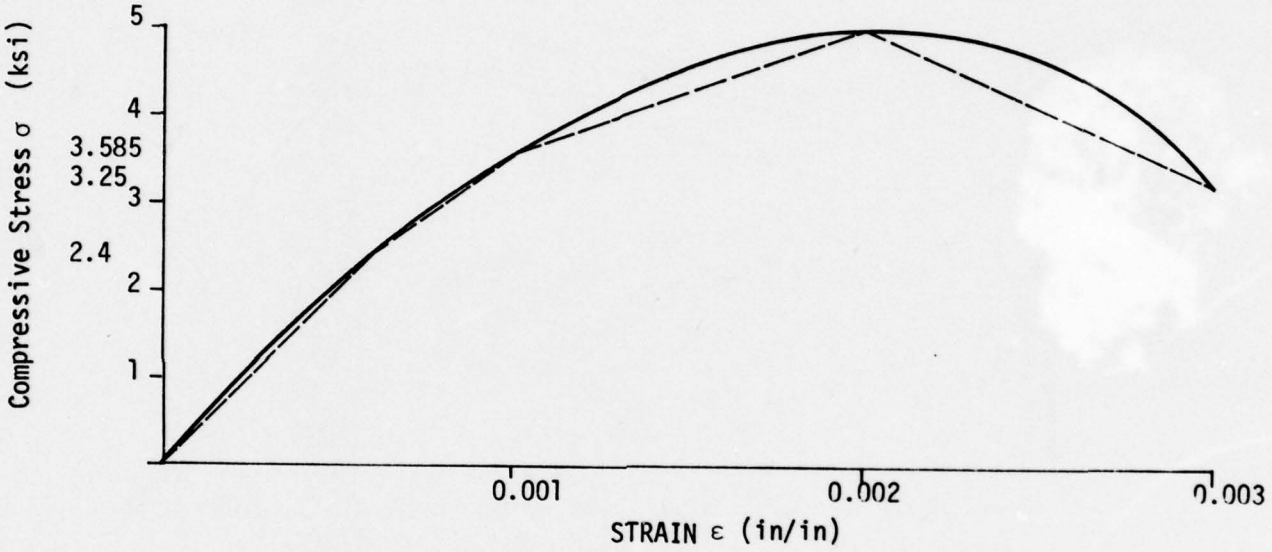

a. Obtained from Ref. 8, pp. 12. Ultimate strain was assumed to be 0.003 in/in.

Note: This stress-strain relation used for all cases except CRS #7, CRS #8, CRS #11, CRS #11-1

Figure 17. Stress-Strain Curve for Concrete

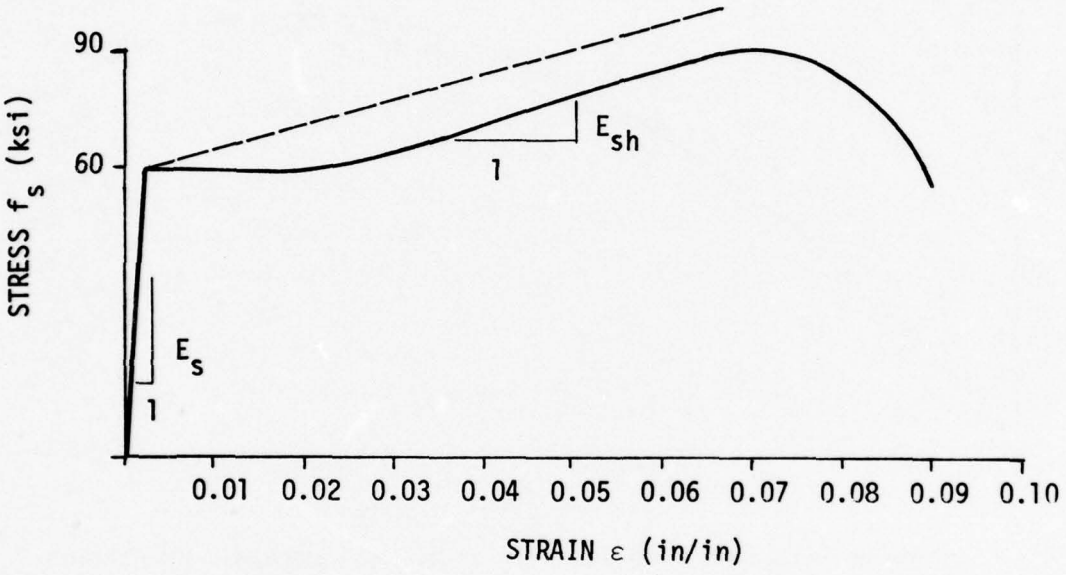

——— Idealized model used in analytical response prediction.

——— Typical stress-strain curve.

Note: E_{sh}/E_s = 0.02 where

E_s = Initial modulus of elasticity

E_{sh} = Slope of strain hardening portion of the curve.

Figure 18 Stress-Strain Curve for Steel. Grade 60 ASTM

stress-strain curve used for steel is shown in Figure 18. It was idealized as a bilinear curve with a strain hardening ratio of 0.02; i.e., $E_{sh}/E_s = 0.02$ where E_{sh} is the slope of the strain hardening curve and E_s is the initial modulus of elasticity of steel. The failure envelope for this section using the above material properties is shown in Figure 23, while the response of this section to various deformation ratios is indicated in Figures 24.1 through 24.7 in terms of M-θ and P-δ curves. Interpretation of each of these response curves is discussed for this section in detail. For concrete sections presented later in this section of the report only the main differences are discussed.

Figure 24.1 shows the plot of P vs. δ for a pure extension case. The response is linear up to the point prior to 1 indicated in Figure 24.1. At point 1 cracking of the whole section occurs and the total resistance is then due to the longitudinal steel. At point 2 in Figure 24.1, the yield of longitudinal steel occurs. Failure of this section under pure extension is then controlled by serviceability rather than strength. A ductility ratio, defined as a ratio of maximum strain in longitudinal steel to the initial yield strain of longitudinal steel, of 10 to 15 would be an appropriate value where failure would be defined. However, on the plot of failure envelope for this section (Figure 23), this point is not plotted.

In Figure 24.2, the response P versus the deformation δ for a case of imposed pure compressive deformation is indicated. Here the response is linear up to the point 1 where the yield of concrete

section occurs in compression. Yield of the section is defined when the effective stress σ_e (equation 1) is greater than τ_o, the initial effective yield stress (equation 7). At point 2 in Figure 24.2, the deformations have been increased to a point where the yield of longitudinal bars occurs in compression. In the next load step, after the yield of re-bars has occurred, crushing of concrete occurs in compression. Failure of the section was defined at this point, which is indicated on the failure envelope (Figure 23).

The response of the section to pure rotation imposed deformations is shown in Figure 24.3. The section remains elastic up to point 1. In the load step defined by point 2, cracking of the bottom element occurs. As deformations are increased further, the bottom half of the section cracks completely in tension [element nos. 3, and 4, (Figure 16.2)]. Note that the cracking of elements is followed by a loss of stiffness as indicated by the M-θ curve. As deformations are increased further, certain integration points of the top element #1 crush in tension-compression. Following the yield of re-bars in tension and compression (point 8 in Figure 24.3), successive crushing of gauss points of elements 1 and 2 occurs in isotropic compression and in tension-compression until at point 13, all the elements, loaded in compression, crush completely. After this point the only resisting force is due to the strain hardening effect of steel. Failure of the section for this imposed deformation is thus defined when all the elements of concrete loaded in compression crush completely in an isotropic compression or a tension-compression state of stress. The deformation (curvature) associated

with the section at this point is shown on the failure envelope in Figure 23.

For the imposed deformation ratio of extension/rotation of 5.0, the deformations imposed were such that the neutral axis lies between the element boundaries of element #2 (Figure 19). Thus, element #1 and top portion of element #2 are in the compression zone while the bottom portion of element #2, as well as all of elements #3 and #4 are in tensile zone. The position of this neutral axis is now fixed while the deformations are monotonically increased. It can be seen from Figure 24.4 that the axial force on the element is initially tensile in nature. Increase of the imposed deformations results in the cracking of elements #3 and #4 and the bottom four integration points of element #2 (point 3 in Figure 24.4). However, in the next load step, the top four integration points yield in tension-compression, an event which causes an out-of-balance force in the solution process. The process of iterating the solution to convergence causes the stress state to change to a pure tension state, resulting in the cracking of the top four nodes of the element #2. Once the cracking of the tensile zone has occurred, most of the forces resulting from the imposed deformations are resisted by the longitudinal tensile steel, which is still elastic, while a small portion is resisted by compressive steel and the concrete in the compressive zone. Hence, the axial force in the section is still tensile and increases with the increase in deformation. As soon as the tensile steel yields in tension, the forces resulting from a further increase in deformation are resisted mainly by the steel in compression and the concrete compressive block. The increase in

force in the tensile steel is very small. Such a force distribution causes a drop in the axial force which is tensile and eventually leads to a compressive axial force P on the section. At point 10 in Figure 24.4, the re-bars in compression yield. Further increases in deformation cause crushing of the integration points of the concrete in the compressive zone until at point 13, crushing of the whole concrete compressive block occurs. At this stage any increase in deformation is resisted by the steel in tension and compression, both of which have already undergone yield. Failure of the section for this deformation ratio is defined by point 13, where all the concrete loaded in compression has crushed, which is shown on the plot of the failure envelope in terms of strains and curvatures in Figure 23.

Response of the section when subjected to a monotonically increasing deformation ratio of extension/rotation of 15 is indicated in Figure 24.5. In this case, the neutral axis of deformations lies outside the section, thereby forcing the whole section to be in tension (Figure 20). Thus, the case is a trivial case where the increase in deformation eventually cracks the whole section in isotropic tension (point 3 in Figure 24.5). After the section has cracked, any additional deformation is resisted by the longitudinal steel which is elastic up to point 4, where the bottom re-bars yield in tension. Hence, the response is controlled by steel rather than concrete, and failure in this case is defined similar to failure in the pure extension case. The failure point has not been plotted for the deformation ratio on the failure envelope in Figure 23.

Deformation ratio of compression/rotation of 5.0 is opposite to extension rotation of 5.0 as far as the location of the neutral axis of deformation is concerned. Element #4 and the bottom portion of element #3 are in tension, while elements #1, #2 and the top portion of element #3 are in compression (Figure 21).

The response of the section to this deformation pattern is indicated in Figure 24.6. As a contrast to the response of the section to a deformation pattern of extension/rotation of 5, it can be observed that the axial force on the member is always compressive in nature. This behavior is expected as the compressive zone is the main contributor to the resisting mechanism. Once the bottom element has cracked in tension, causing some loss of initial stiffness, future behavior to increase in deformation is controlled by the steel and the concrete in the compressive zone. With successive increase in deformation the concrete in the compressive zone crushes. Failure of the section to this deformation pattern is defined when the concrete section in the compressive zone is completely crushed. Such a deformation condition is plotted on the failure envelope of Figure 23.

The last deformation pattern imposed on the section was a combination of compressive displacement to rotation of 15. This deformation pattern was such that the neutral axis of imposed deformations was outside the section, thereby imposing compressive deformations on the section (Figure 22). The response of the section is indicated in Figure 24.7. As can be seen from this figure, as the deformations are monotonically increased, certain elements

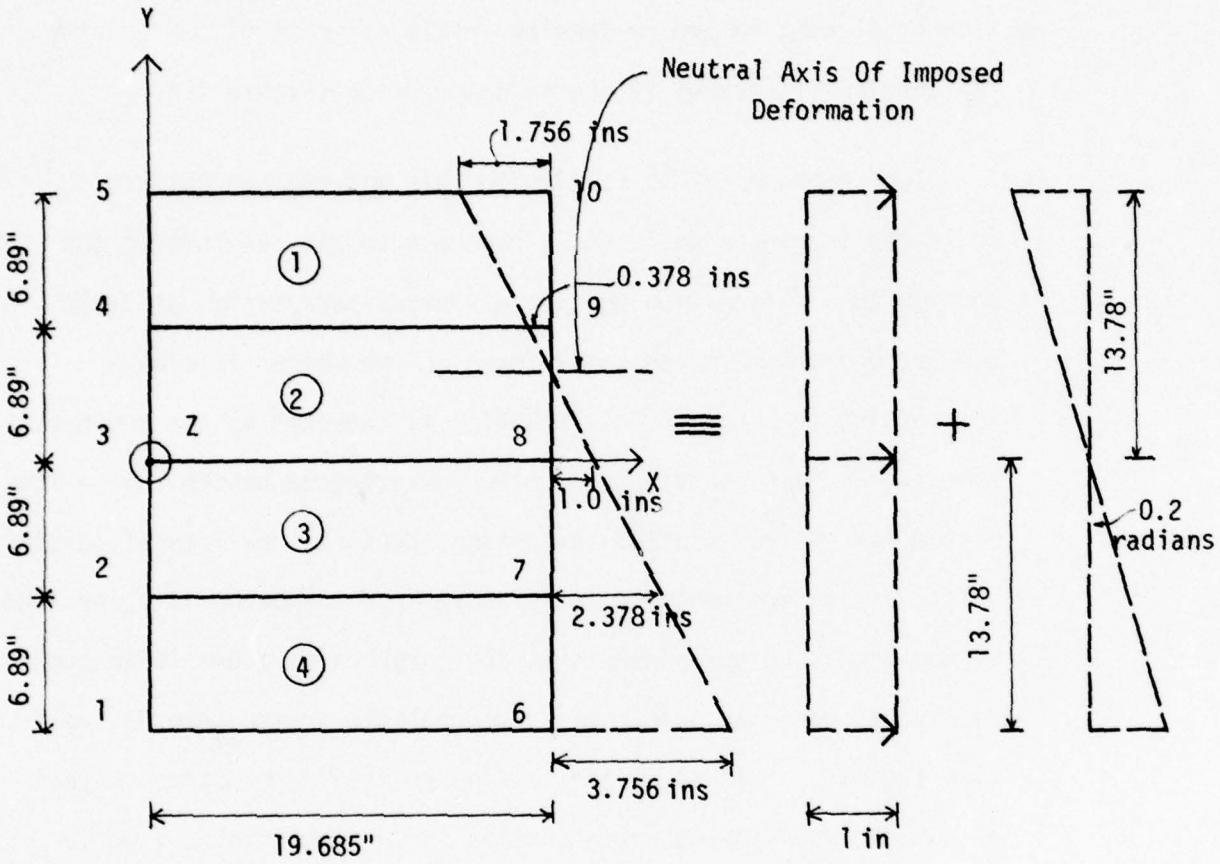

Fig. 19 Deformation Pattern. Extension/Rotation = δ/θ = 5.0

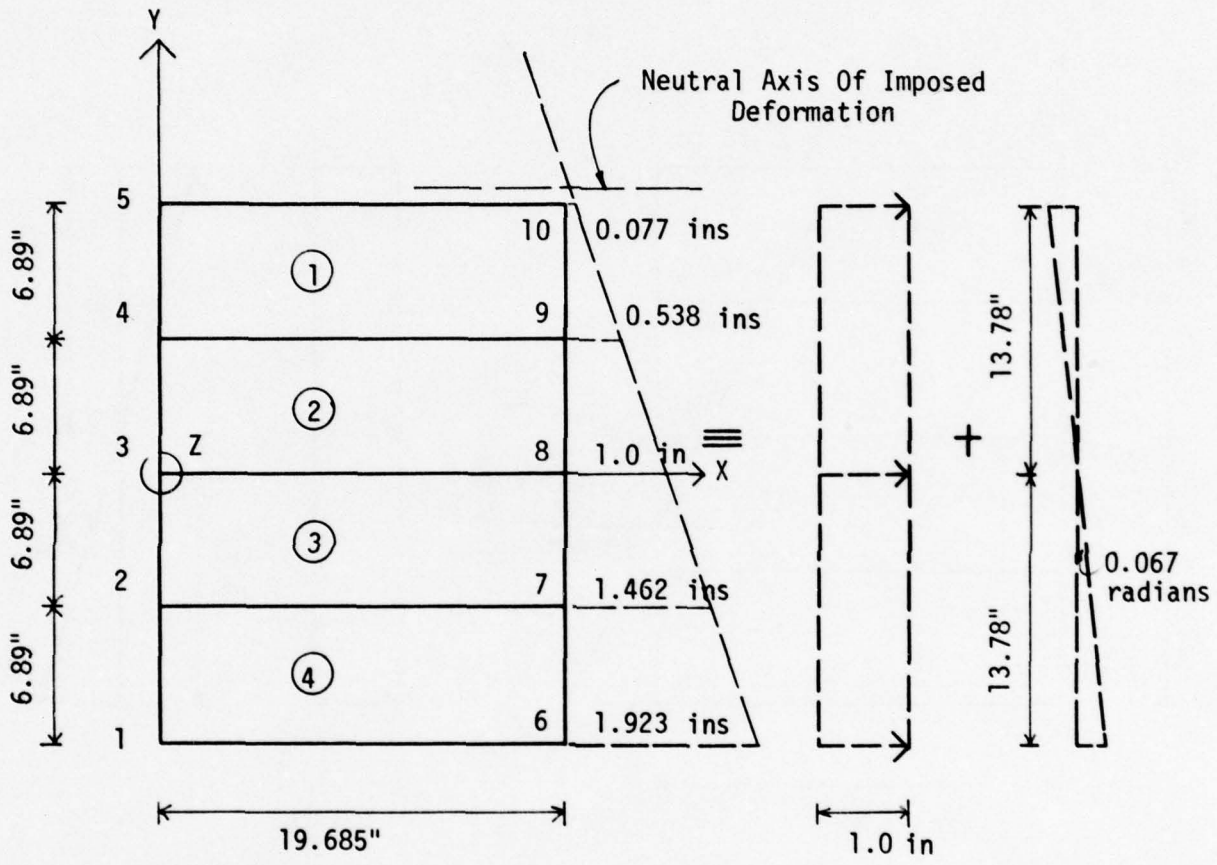

Fig. 20 Deformation Pattern. Extension/Rotation = 15.0

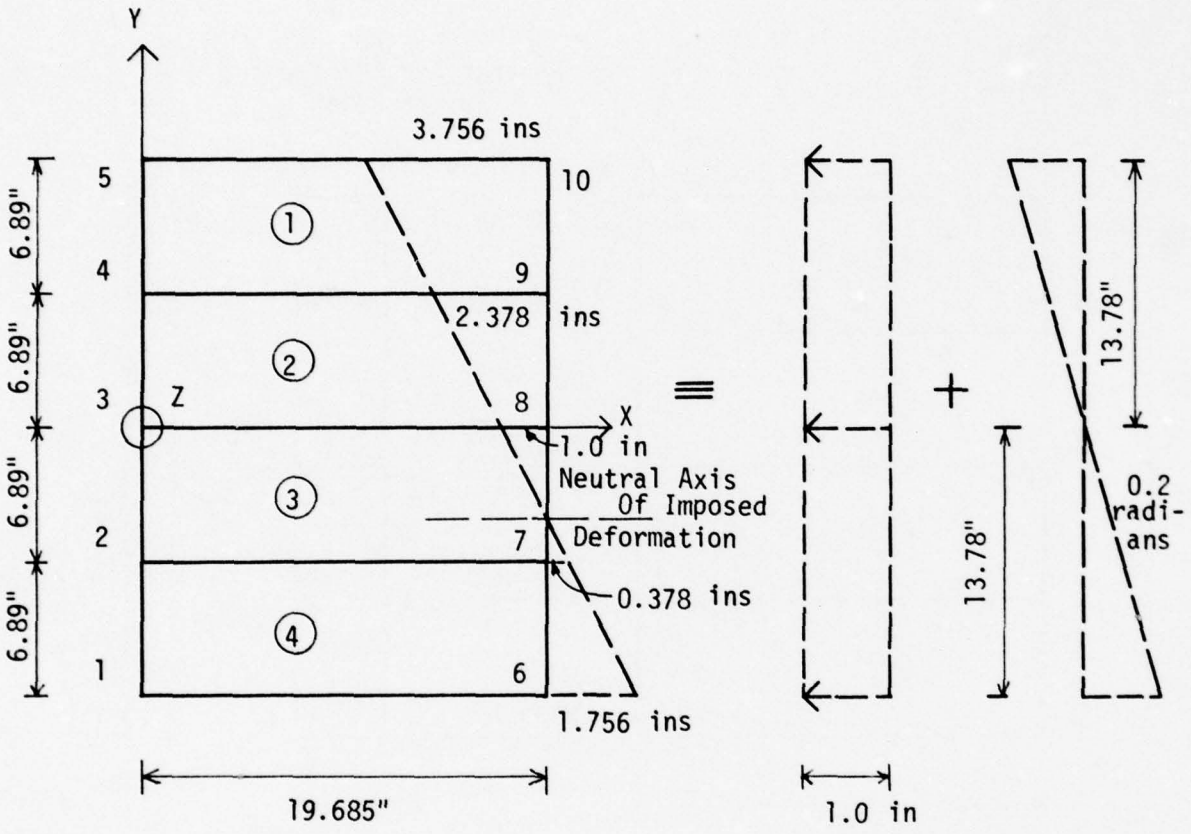

Fig. 21 Deformation Pattern. Compression/Rotation = 5.0

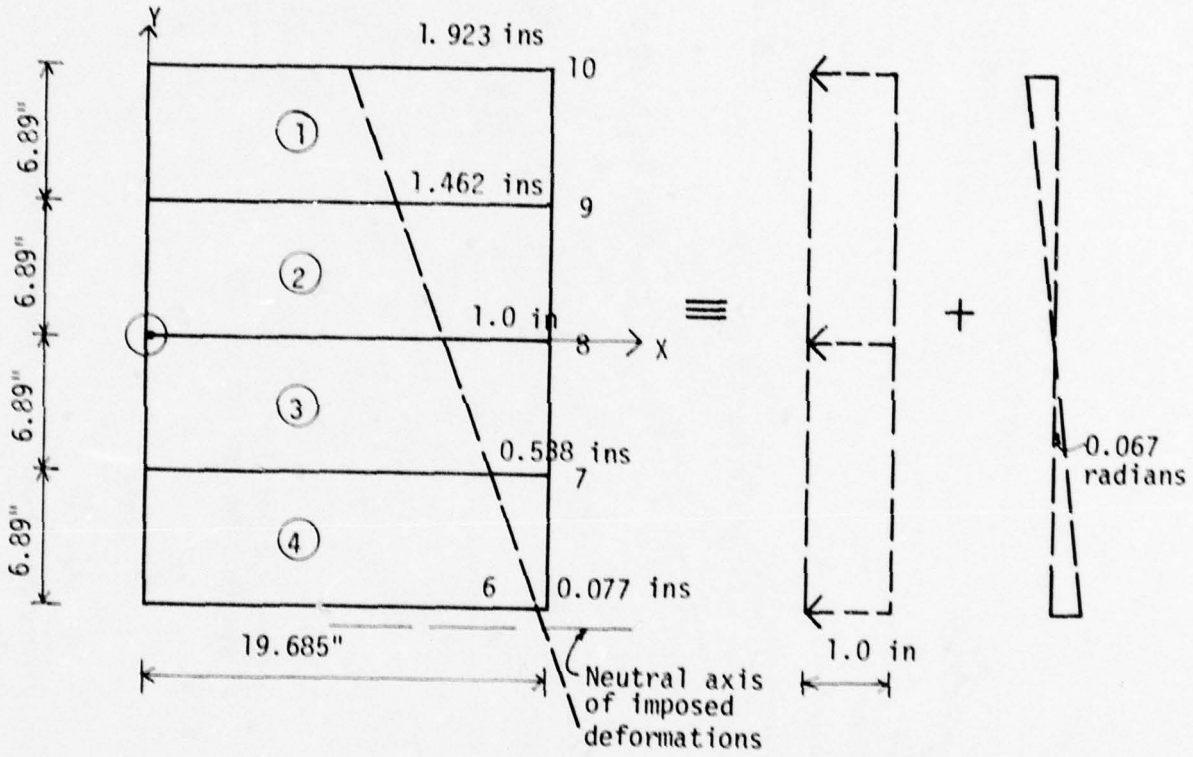

Fig. 22 Deformation Pattern. Compression/Rotation = 15.0.

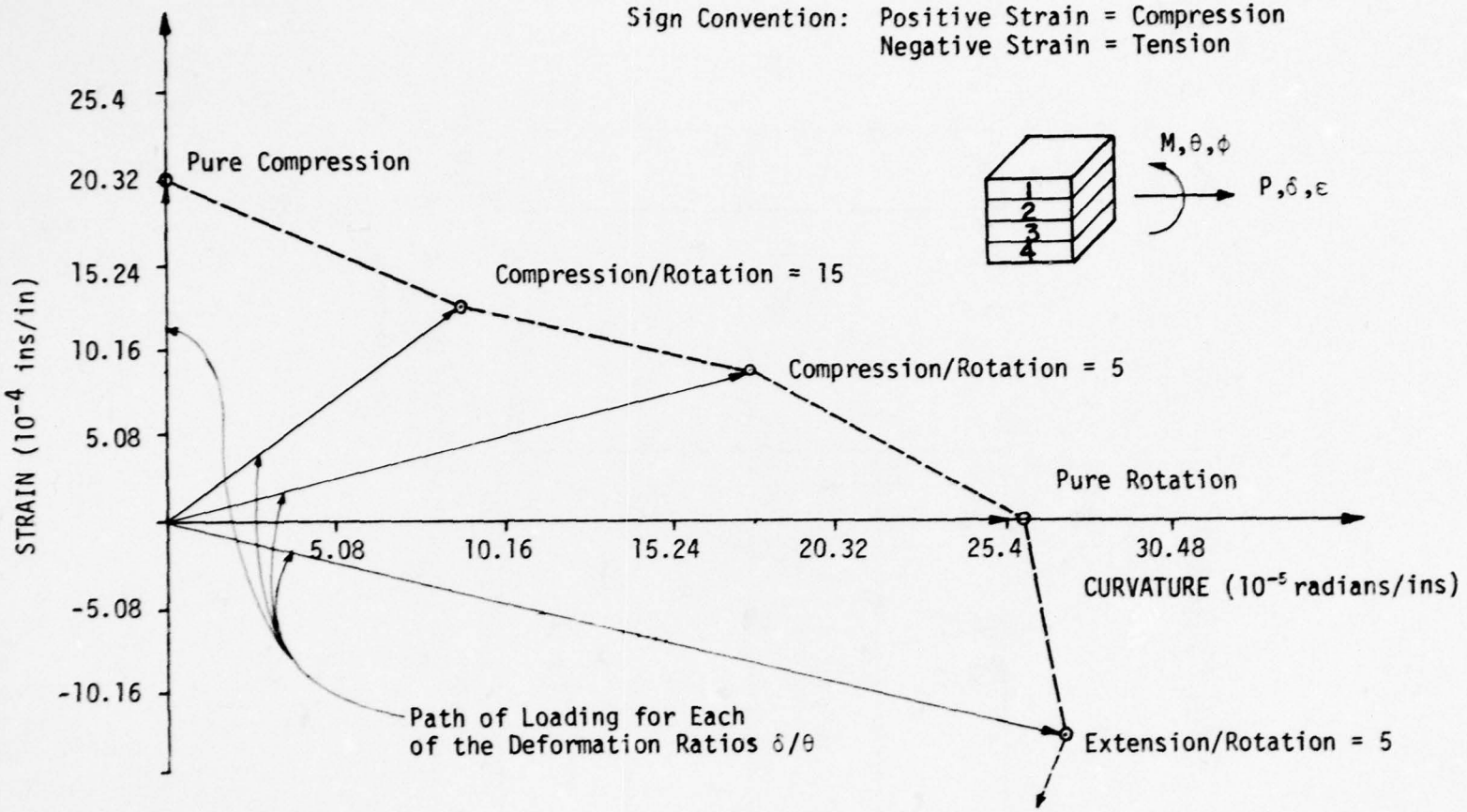

Figure 23 CRS #3 Failure Envelope

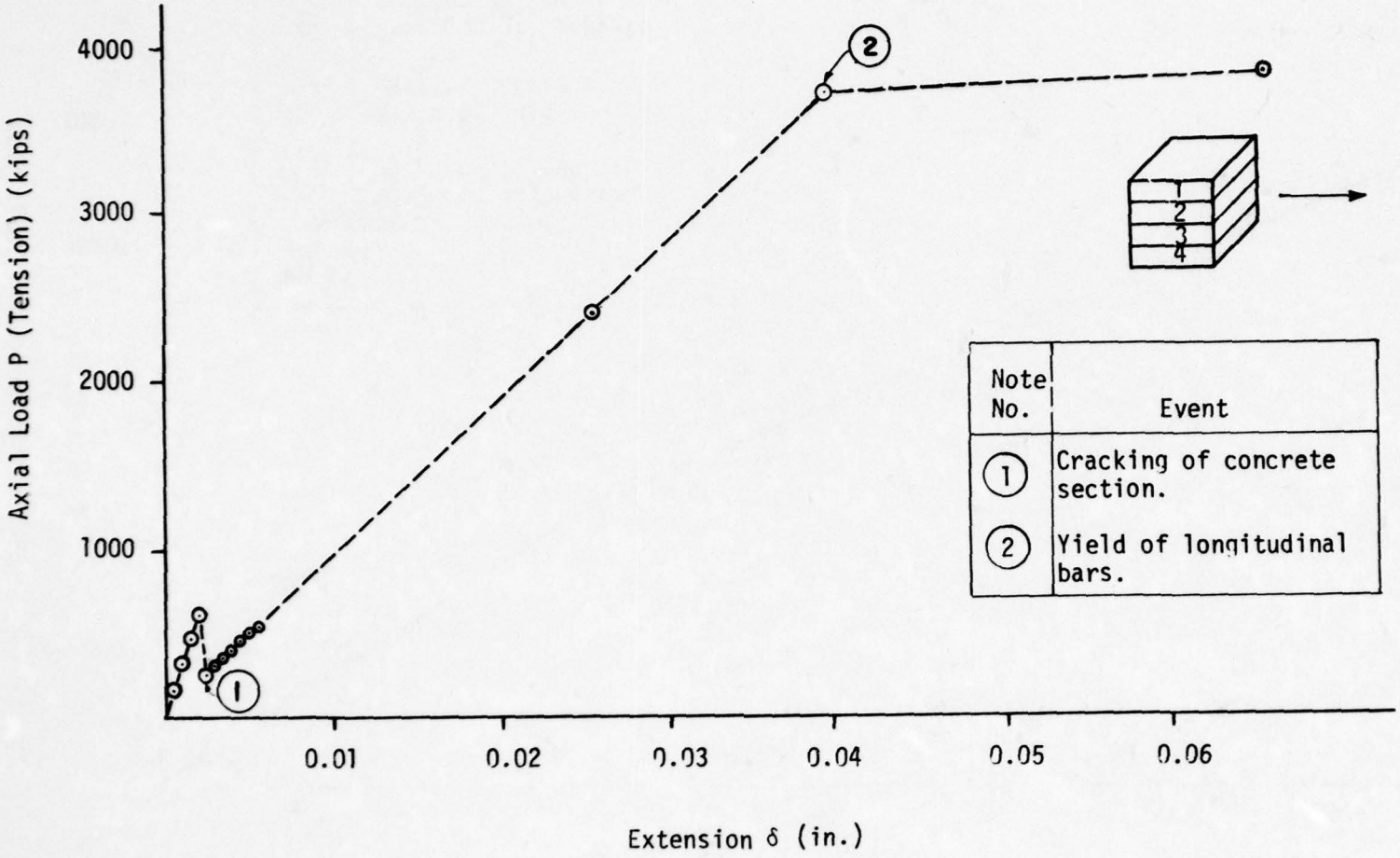

Fig. 24.1 CRS #3 - Pure Extension

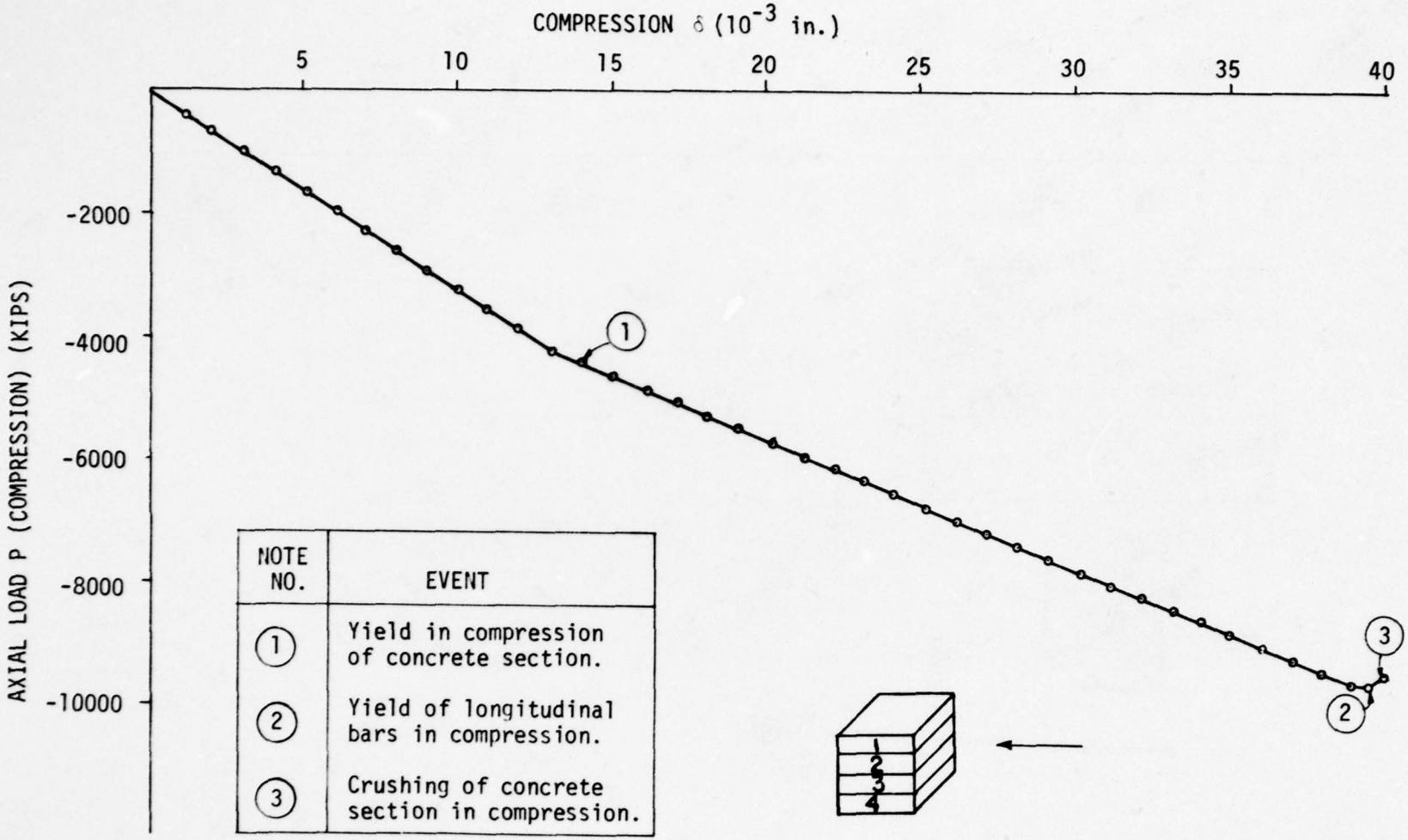

Figure 24.2 CRS #3 Pure Compression

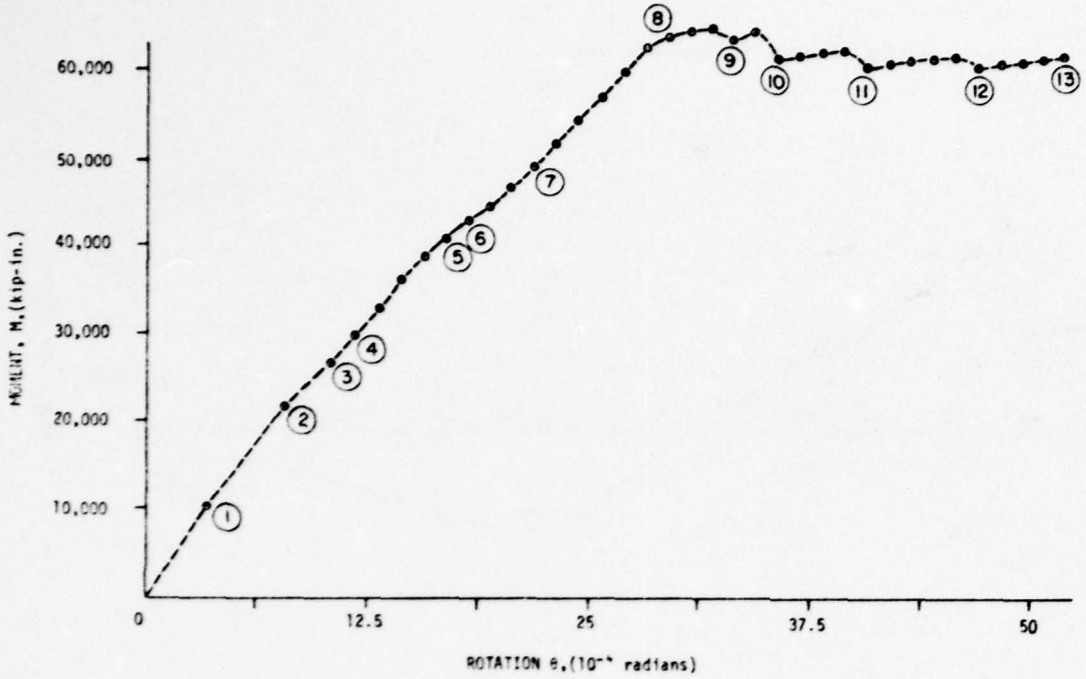

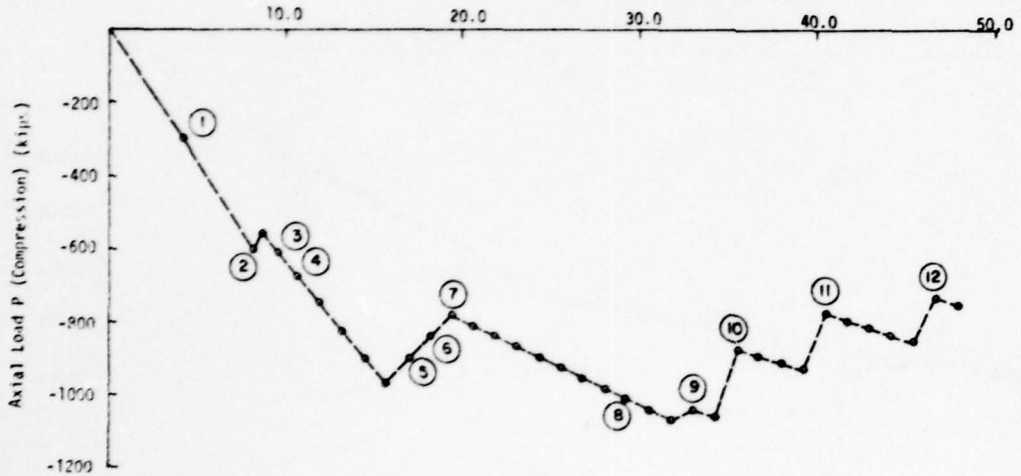

NOTE NO.	EVENT
(1)	Cracking of Elem. #4.
(2)	Cracking of Elem. #3.
(3)	Compressive yield of Elem. #1 (partial). Cracking (4 nodes) and crushing of Elem #2 (2 nodes).
(4)	Compressive yield of remaining nodes of Elem #2
(5)	Crushing of 3 nodes of Elem #2 and 1 node of Elem #1.
(6)	Crushing of 2 nodes of Elem #1.
(7)	Crushing of 3 nodes of Elem #1.
(8)	Compressive and tensile yield of re-bars.
(9)	Crushing of 4 nodes of Elem #1.
(10)	Crushing of 5 nodes of Elem #1.
(11)	Crushing of 6 nodes of Elem #1.
(12)	Crushing of 4 nodes of Elem #2.
(13)	Crushing of total section occurs.

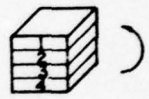

Figure 24.3 CRS #3 - Pure Rotation

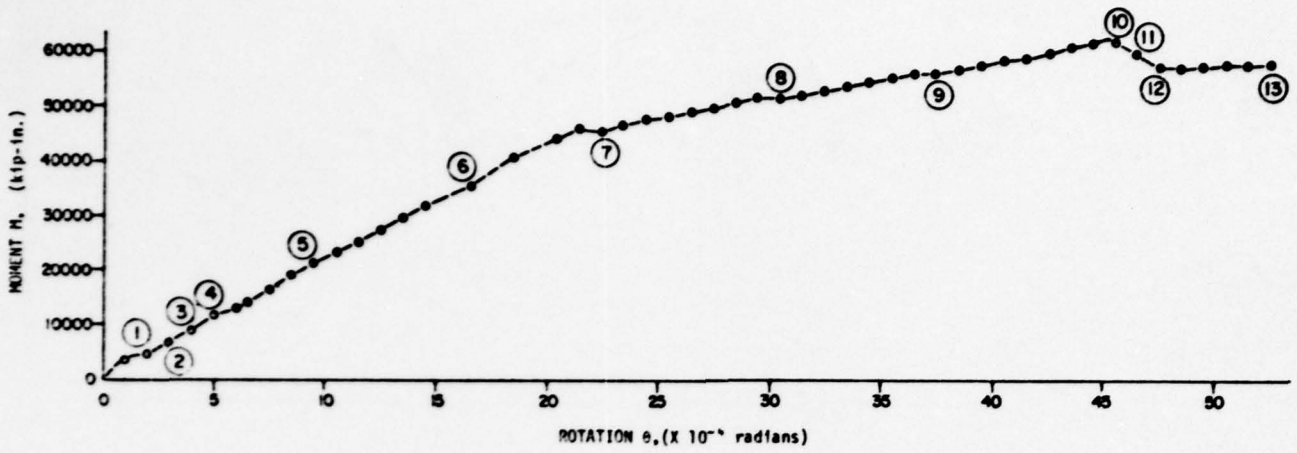

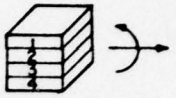

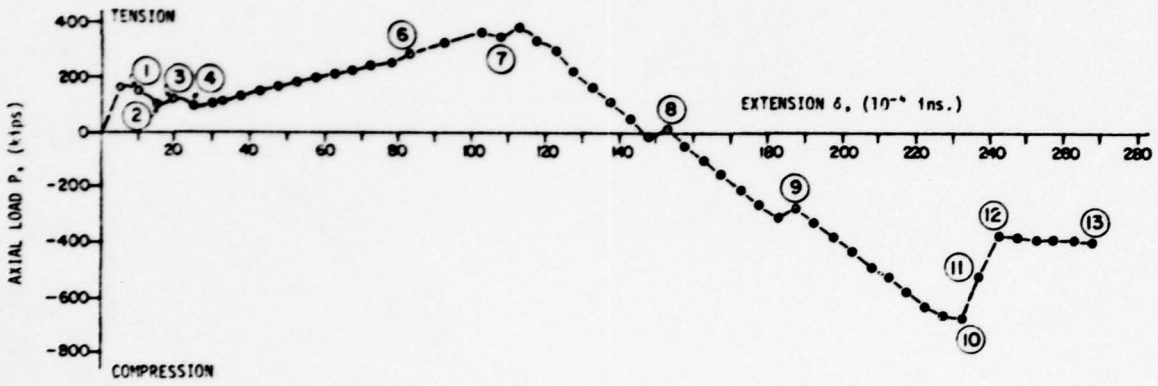

NOTE NO.	EVENT
(1)	Cracking of Elem #4.
(2)	Partial cracking of Elem #3.
(3)	Complete cracking of Elem #3 and partial cracking of Elem #2.
(4)	Complete cracking of Elem #2.
(5)	Partial compressive yield of Elem #1 (4 nodes).
(6)	Complete compressive yield of Elem #1.
(7)	Crushing of 2 nodes of Elem #1 and tensile yield of re-bars.
(8)	Crushing of 3 nodes of Elem #1.
(9)	Crushing of 4 nodes of Elem #1.
(10)	Compressive yield of re-bars.
(11)	Crushing of 5 nodes of Elem #1.
(12)	Crushing of 6 nodes of Elem #1.
(13)	Failure of complete section.

Figure 24.4 CRS #3 - Extension/Rotation = 5.0

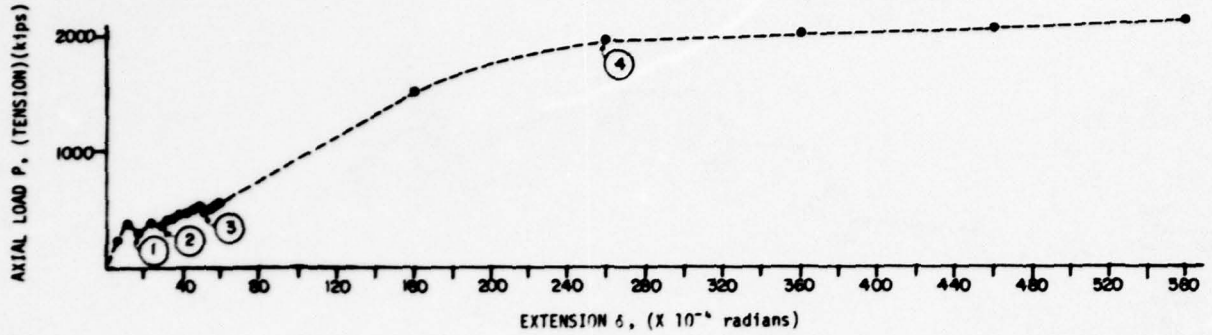

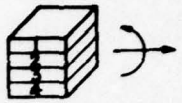

NOTE NO.	EVENT
1	Cracking of Elem. #4 and partial cracking of Elem. #3 (6 nodes)
2	Cracking of Elem. #3 complete and Elem. #2 partial (6 nodes)
3	Cracking of Elem. #1 and #2
4	Yield of tensile re-bars

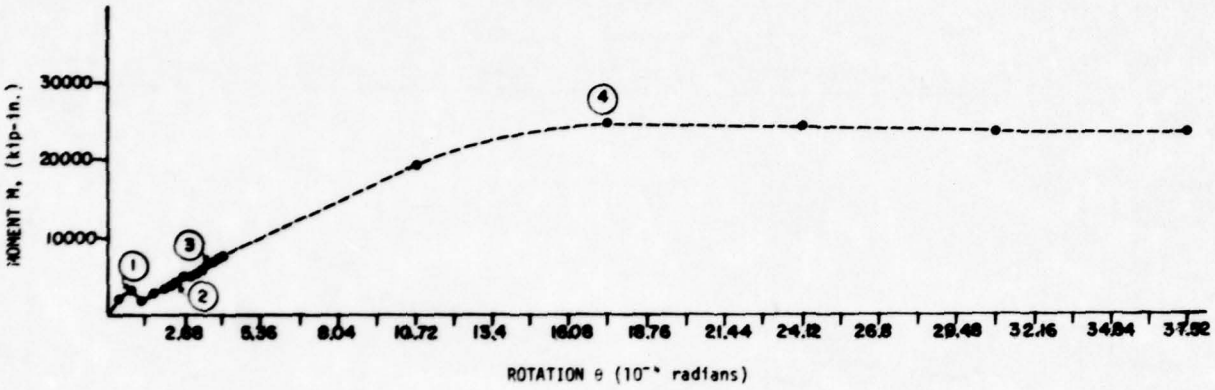

Figure 24.5 CRS #3 - Extension/Rotation = 15.0

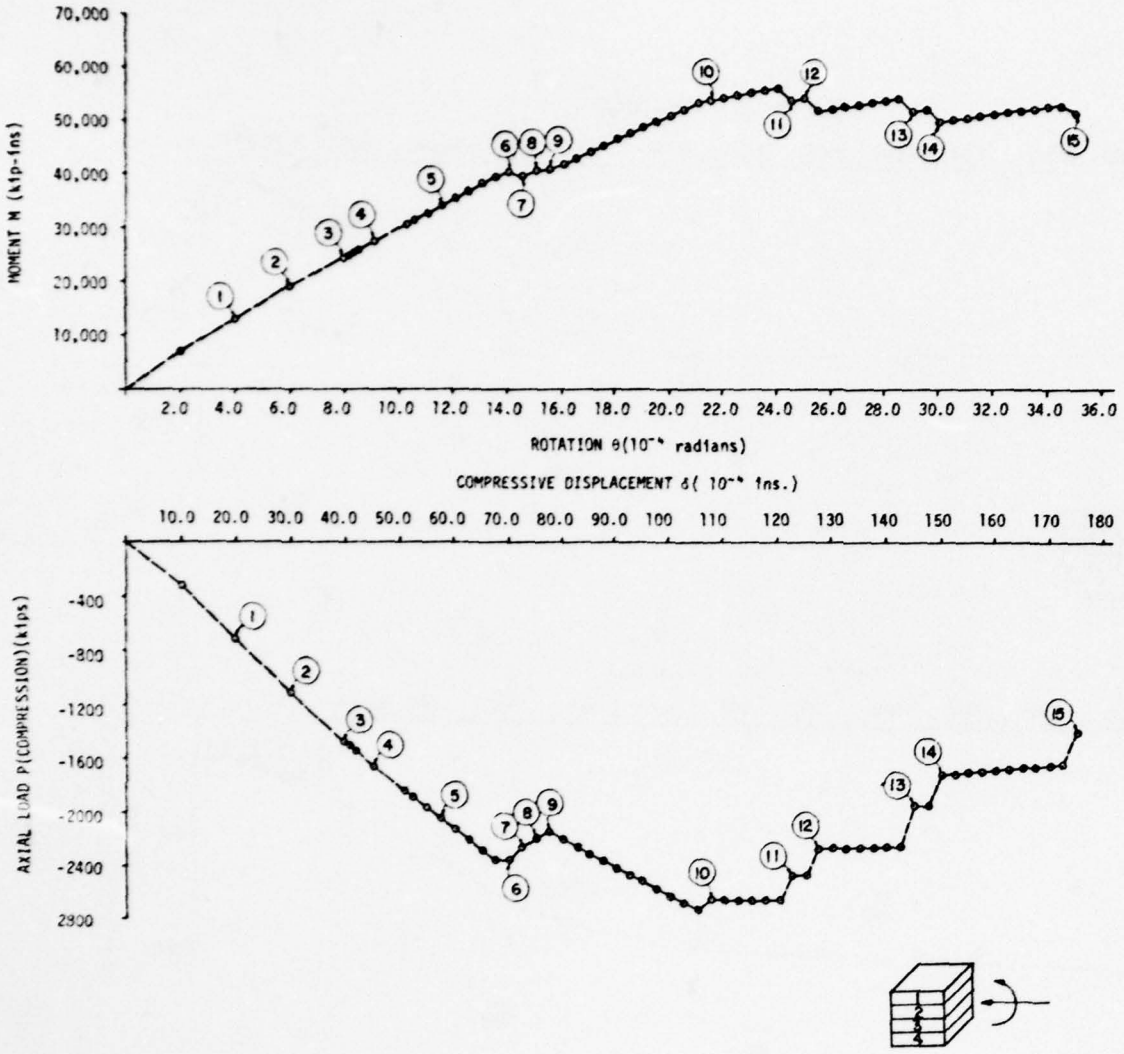

NOTE NO.	EVENT
(1)	Cracking of Element #4 (4 nodes.
(2)	Cracking of Element #4 (8 nodes)
(3)	Cracking of Element #3 (5 nodes). Crushing of 1 node of Element #3 in t-c.
(4)	Yield of Element #1 (8 nodes in compression.)
(5)	Yield of Element #2 (6 nodes in t-c, 2 nodes in compression).
(6)	Crushing of Element #1 (1 node in t-c).
(7)	Crushing of Element #1 (2 nodes in t-c).
(8)	Crushing of Element #2 (2 nodes in t-c).
(9)	Crushing of Element #2 (3 nodes in t-c).
(10)	Crushing of Element #2 (4 nodes in t-c). Yield of re-bars in compression.
(11)	Crushing of Element #1 (1 node in compression, 2 nodes in t-c).
(12)	Crushing of Element #1 (2 nodes in t-c).
(13)	Crushing of Element #1 (3 nodes in compression, 2 nodes in t-c).

NOTE NO.	EVENT
(14)	Crushing of Element #1 (4 nodes in compression, 2 nodes in t-c).
(15)	Crushing of Element #1 (5 nodes in compression, 2 nodes in t-c), failure of section assumed.

Figure 24.6 CRS #3 - Compression/Rotation = 5.0

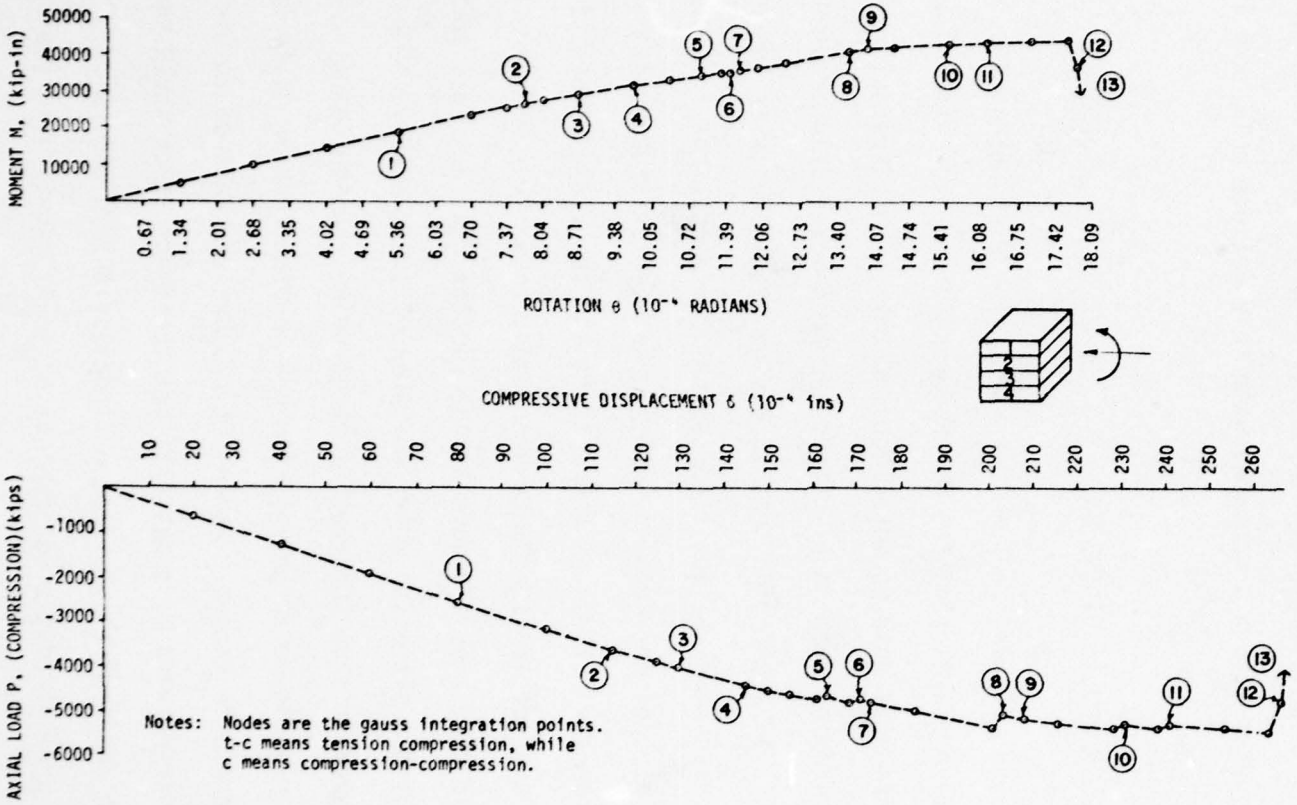

NOTE NO.	EVENT
(1)	Yield of Element #1 (total in compression.)
(2)	Yield of Element #2 (4 nodes in compression, 4 nodes in t-c).
(3)	Yield of Element #3 (2 nodes in t-c, 6 nodes in compression).
(4)	Yield of Element #4 (8 nodes in t-c).
(5)	Crushing of Element #2 (1 node in t-c).
(6)	Crushing of Element #2 (2 nodes in t-c).
(7)	Yield of Element #4 (8 nodes in t-c).
(8)	Crushing of Element #3 (3 nodes in t-c).
(9)	Yield of re-bars in compression.
(10)	Crushing of Element #3 (4 nodes in t-c).
(11)	Crushing of Element #3 (5 nodes in t-c).
(12)	Crushing of Element #4 (1 node in t-c).
(13)	Failure of concrete section.

Figure 24.7 CRS #3 - Compression/Rotation = 15.0

yield in isotropic compression, while some yield in tension-compression. Further successive increases in deformation cause the top re-bars to yield in compression and then the bottom re-bars to yield in compression. Failure for this section is defined when the concrete section, loaded in compression, totally crushes either in isotropic compression or tension-compression state of stress. The deformations associated with this failure point are indicated in Figure 23.

(2) Response Of CRS #4

CRS #4 has the same stress-strain relationship for concrete and steel properties as CRS #3 (Figures 17 and 18). Four layers of bricks were used to model the concrete. Longitudinal reinforcement was 1/4% at each face. Since the transverse reinforcement required by ACI 1971 code for seismic design requirements is independent of the percentage of longitudinal reinforcement, but is dependent on the size of the section, spacing between stirrups, ultimate uniaxial compressive stress of concrete f'_c and the yield stress of steel f_y, the area of transverse reinforcement to be provided for this section would have been the same as for section CRS #3. This would have created a situation where the area of transverse reinforcement would be greater than the area of longitudinal reinforcement. Such a situation would be an unrealistic one and the problem would be only academic in nature. Hence, it was decided instead to use an arbitrary area of transverse reinforcement which would seem reasonable compared to the area of longitudinal reinforcement. Since the area of confining steel is so small, as is also the area of

longitudinal steel, this section is similar to an unconfined section. The response of the section to imposed deformations would be controlled by the behavior of concrete, with little effect of the behavior of longitudinal steel. In effect, it is very close to a plain concrete model. Since the confining effect of transverse reinforcement is almost negligible, the value of Poisson's ratio was set to 10^{-7}. This also stabilized the numerical solution process. The failure envelope for this section is indicated in Figure 25, while the response of the section to various deformation ratios is presented in Figures 26.1 through 26.7.

In Figure 26.1, the pure extension imposed displacements case, it can be seen that the initial stiffness and load carrying capacity is mainly due to the concrete section. Once the section completely cracks, the resistance to imposed deformation is due to steel. Comparing the CRS #4 response to that of Figure 24.1 of section CRS #3, Figure 24.1 reveals that in the response of CRS #3, longitudinal steel was the main source of strength, and the resisting force was mainly due to the forces in steel.

In Figure 26.2, where the imposed deformations are pure compressive displacements, it can be observed that the crushing of concrete in isotropic compression occurs before the yield of longitudinal bars, unlike the failure of CRS #3 when subjected to a similar deformation pattern. Failure of the section in this case was also defined by point 2 (Figure 26.2) where the concrete section totally crushes in compression-compression.

Figure 26.3, the pure rotation imposed deformations case, indicates all the events that occur throughout the deformation history. Failure of the section was defined when all the concrete loaded in compression crushed in isotropic compression or tension-compression stress states. Note that the longitudinal steel yields before crushing of the concrete section occurs.

Failure of the section when subjected to an imposed deformation pattern of extension/rotation = 5.0 occurs before the longitudinal steel yields. Failure is defined by the deformation at which the concrete loaded in the compression zone totally crushes (Figure 26.4).

In Figure 26.7, which shows the response of the section to an imposed deformation pattern of compression/rotation of 15, failure of the concrete section occurs after the yield of top re-bars in compression. Note that, unlike the response of CRS #3 to a similar deformation ratio (Figure 24.7), the bottom re-bars of Section CRS #4 do not yield.

The failure envelope of Section CRS #4 shown in Figure 25 is quite different from the one indicated in Figure 19 for Section CRS #3. Section CRS #4 behaves essentially like an unconfined plain concrete section. Since behavior is mainly controlled by the behavior of concrete, the response is very sensitive to the mesh size. A four-layer mesh may be a coarse mesh which does not accurately account for the nonlinear behavior through the depth of the section. This could be the cause of the difference in shape of the failure envelopes of Sections CRS #3 and CRS #4. Hence, section CRS #4 was reanalyzed, refining the mesh, using an eight layer mesh

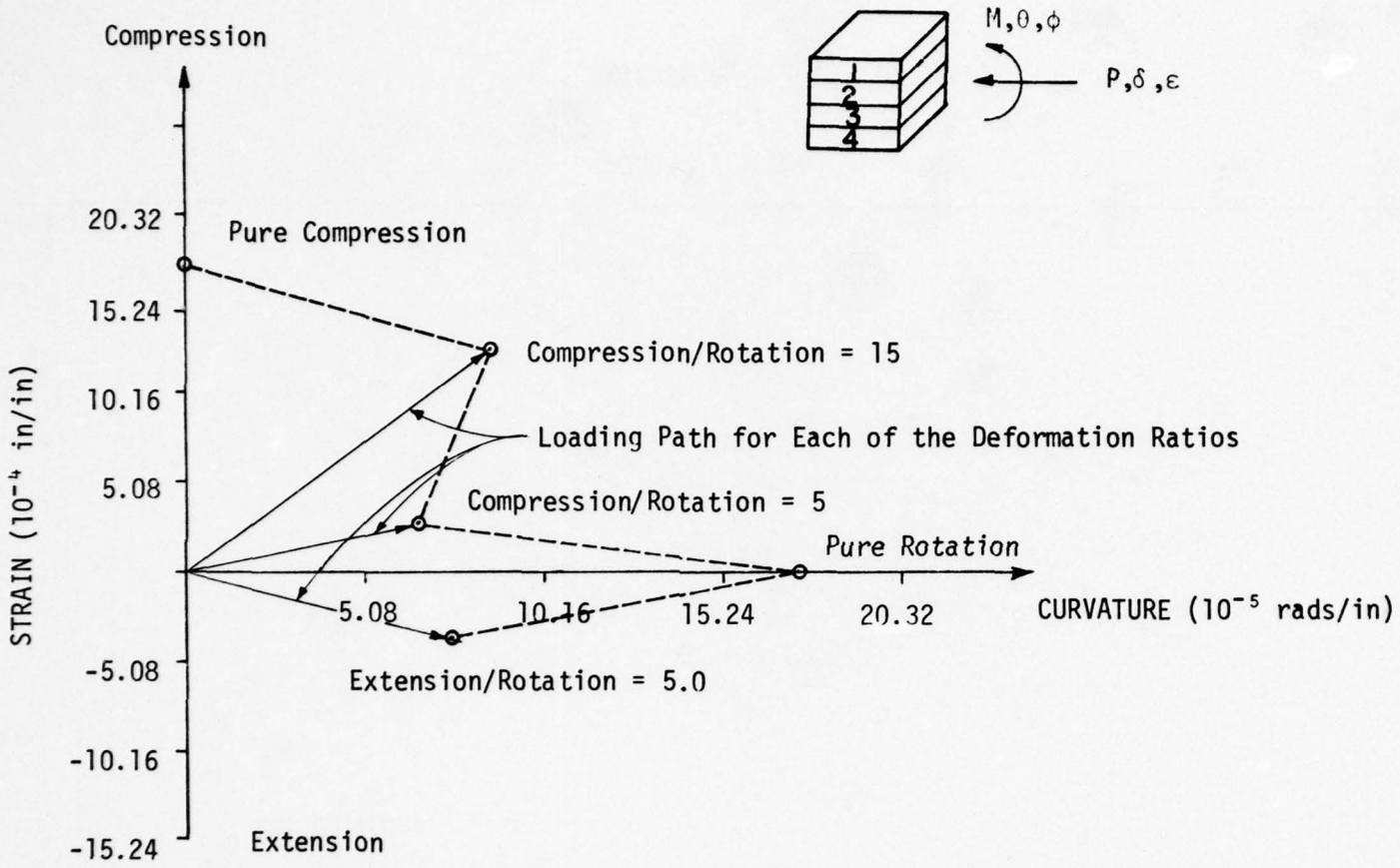

Figure 25 CRS #4 - Failure Envelope

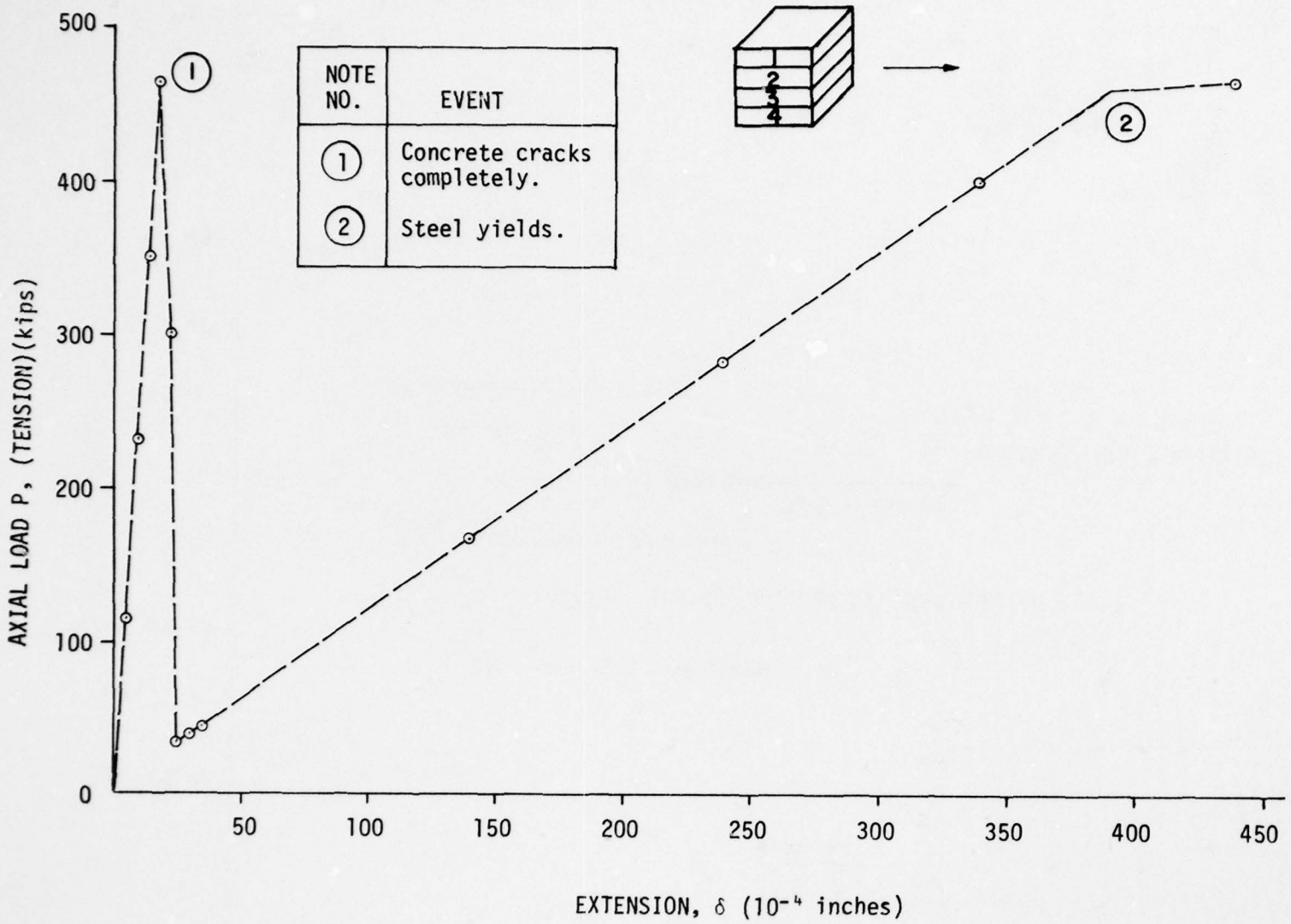

Figure 26.1 CRS #4 - Pure Extension

AD-A070 644 PMB SYSTEMS ENGINEERING INC SAN FRANCISCO CA F/G 11/2
FAILURE CRITERIA FOR REINFORCED CONCRETE STRUCTURES. VOLUME II.--ETC(U)
MAY 79 R W LITTON, J M GIDWANI F29601-76-C-0135
UNCLASSIFIED AFWL-TR-77-239-VOL-2 NL

2 OF 3
AD A070644

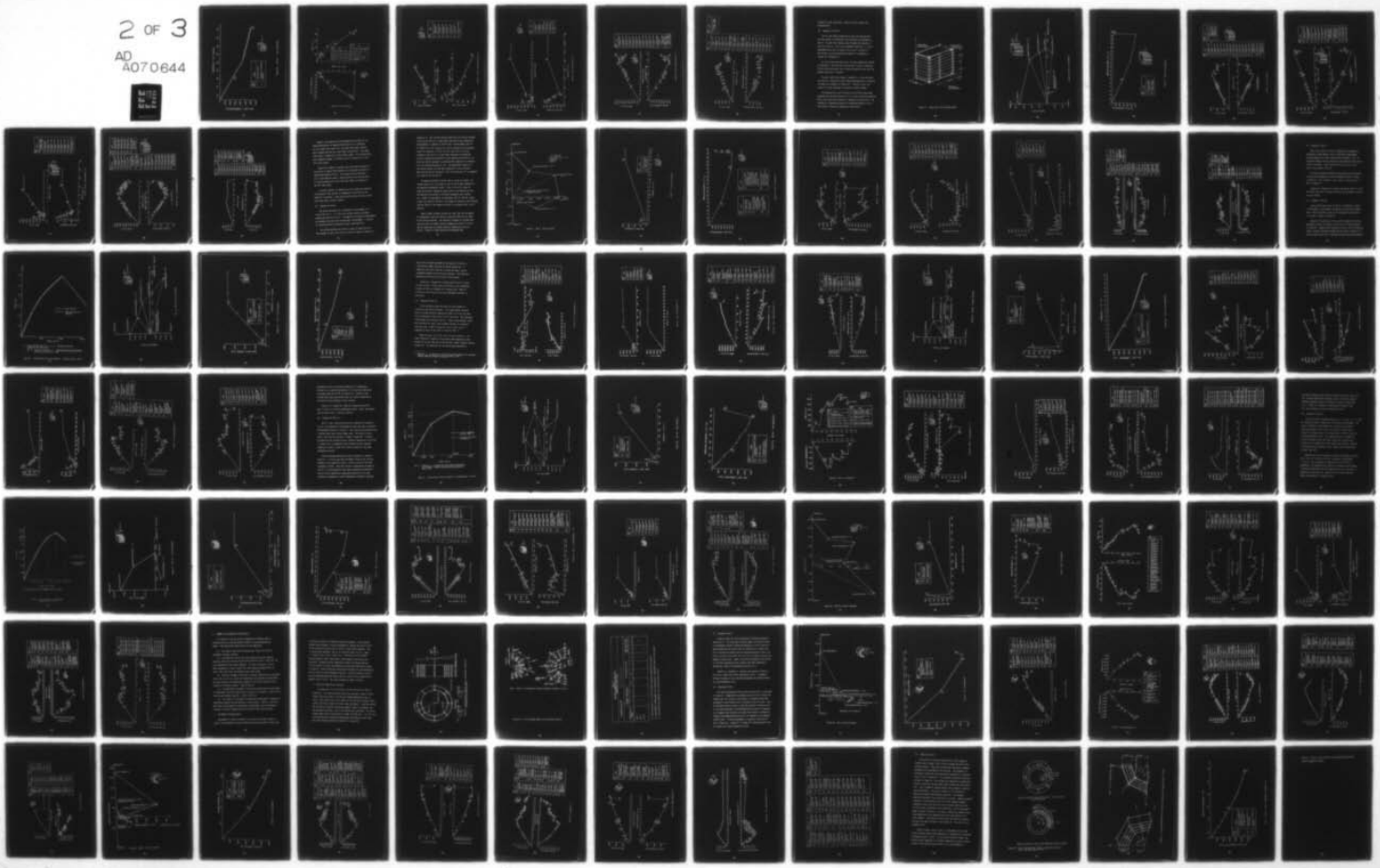

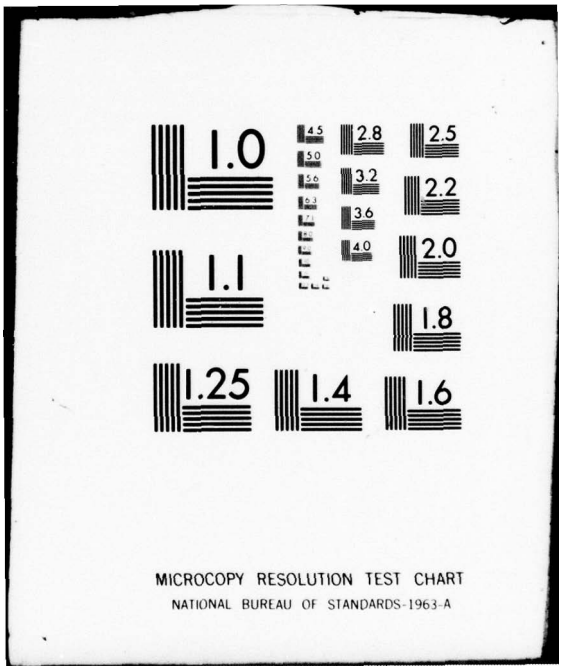
1.0
1.1
1.25
4.5
5.0
5.6
6.3
7.1
2.8
3.2
3.6
4.0
2.5
2.2
2.0
1.8
1.4
1.6
MICROCOPY RESOLUTION TEST CHART
NATIONAL BUREAU OF STANDARDS-1963-A

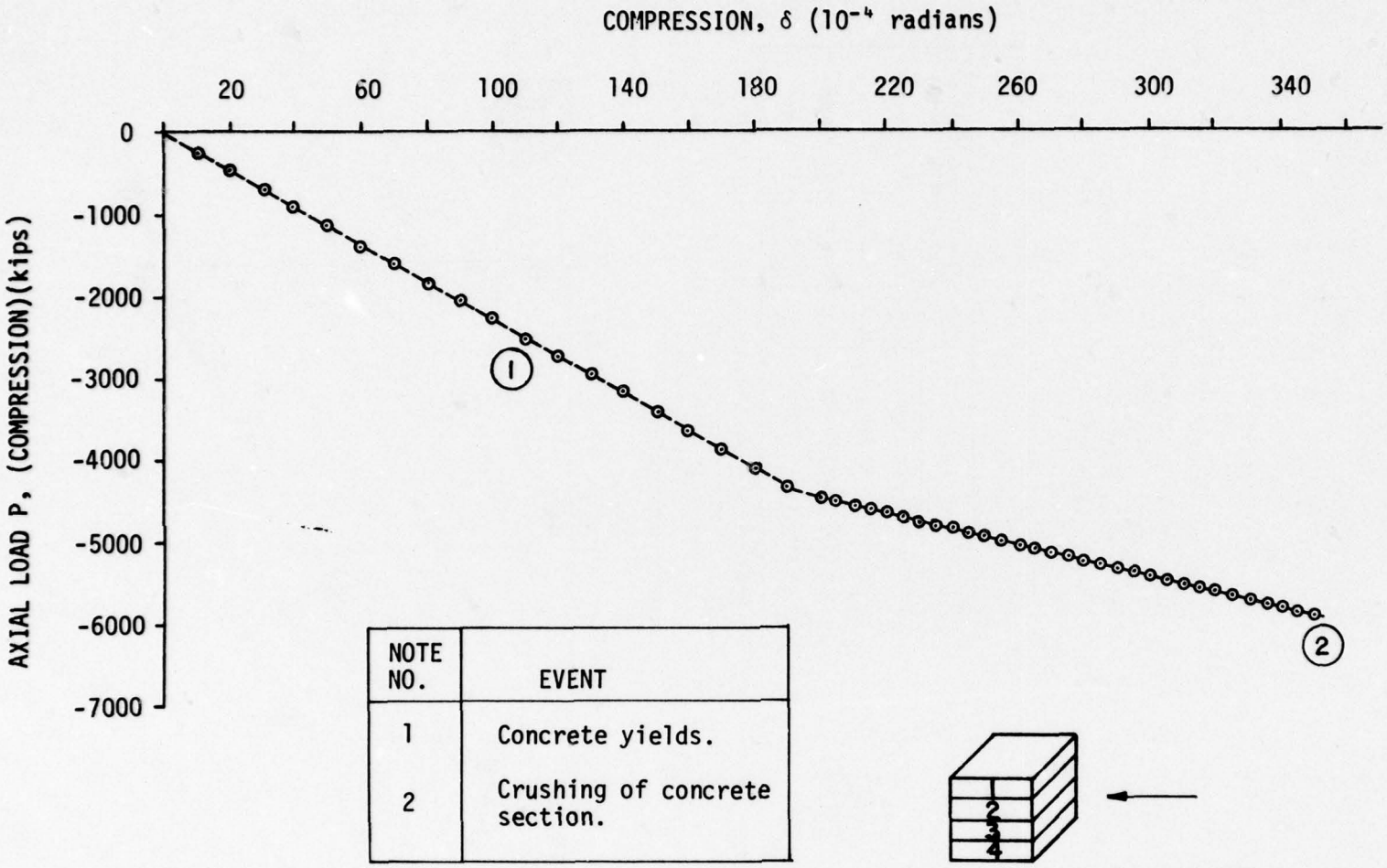

Figure 26.2 CRS #4 - Pure Compression

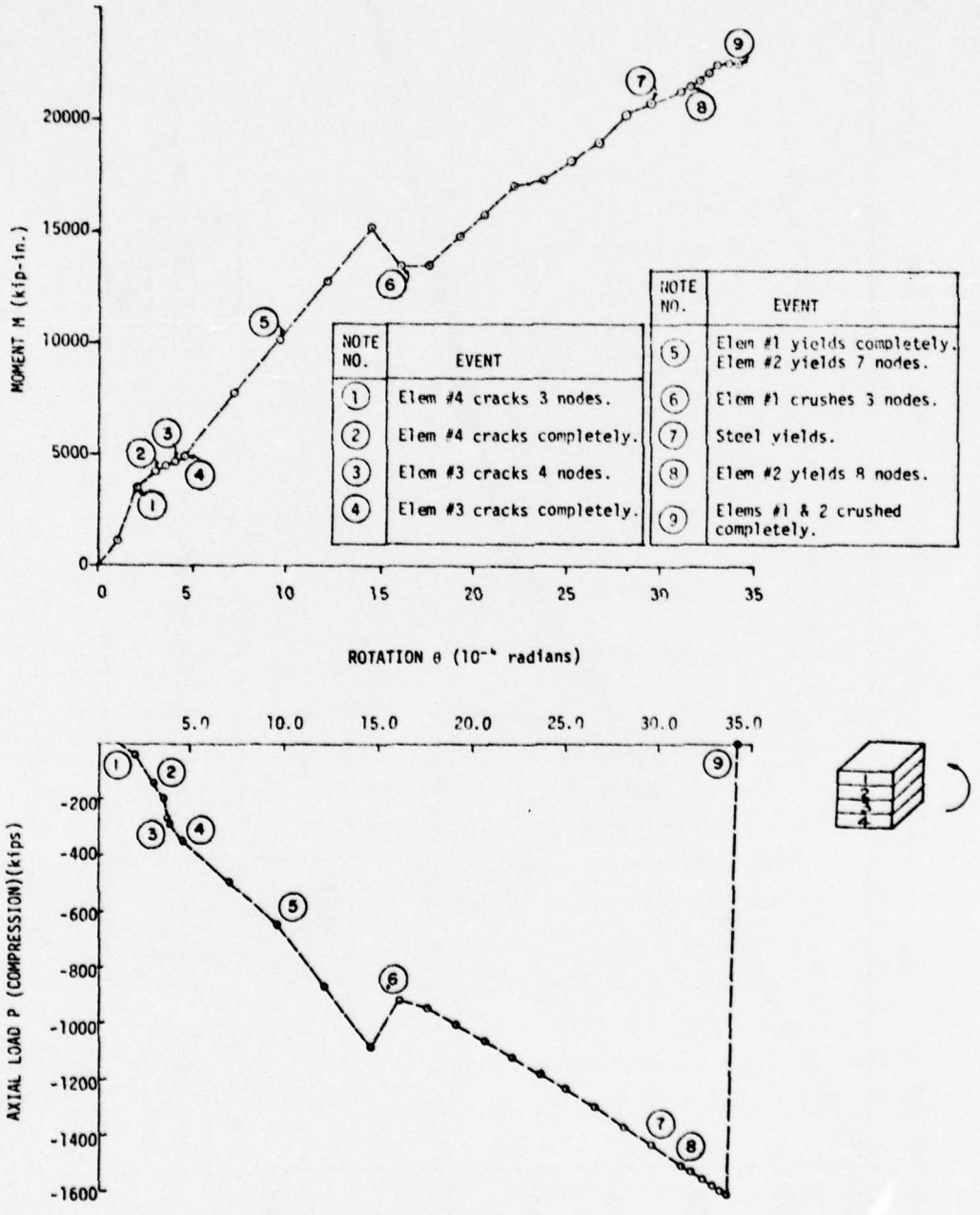

Figure 26.3 CRS #4 - Pure Rotation

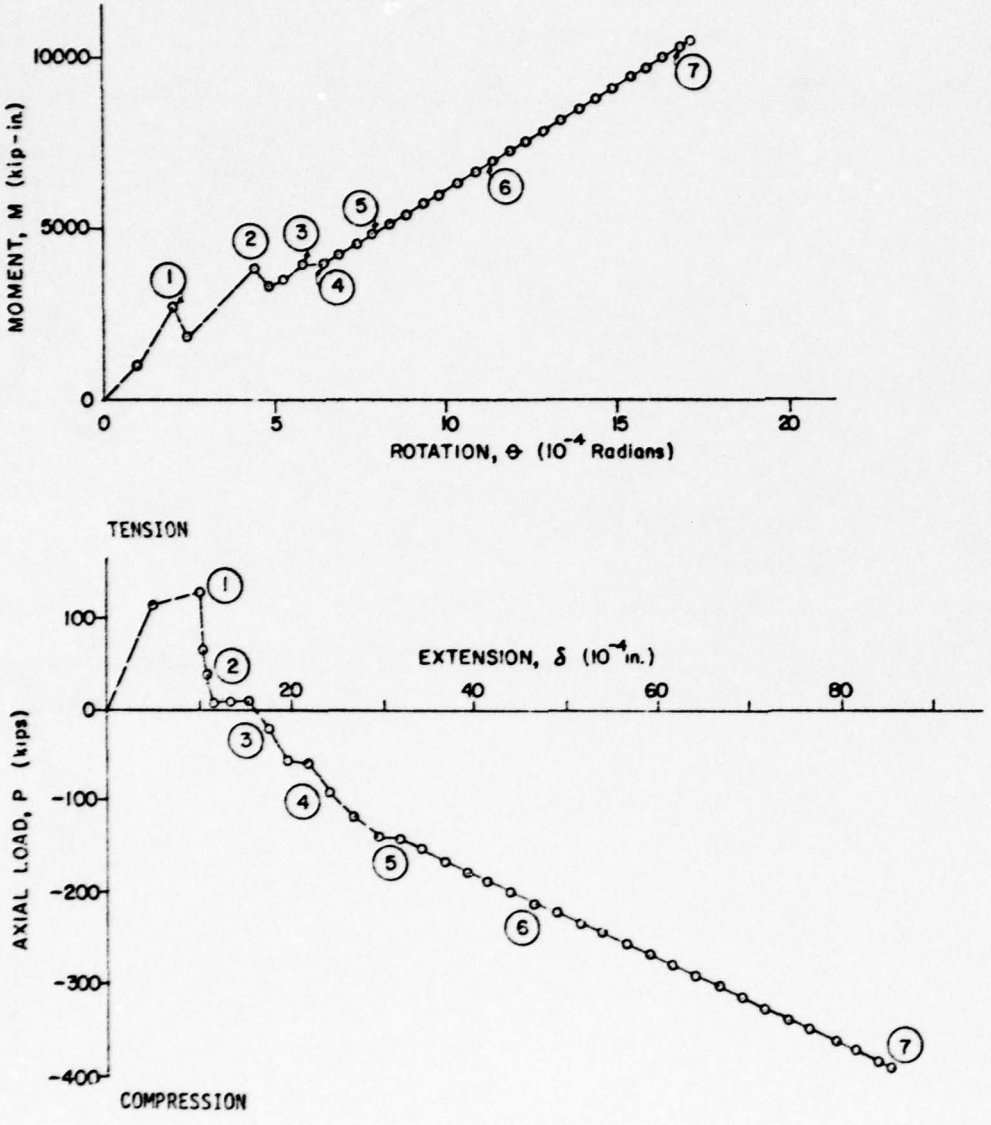

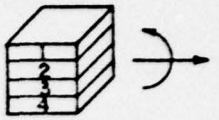

NOTE NO.	EVENT
1	Elem #4 cracks completely.
2	Elem #3 cracks (4 nodes).
3	Elem #3 cracks completely.
4	Elem #2 cracks (4 nodes).
5	Elem #2 cracks completely.
6	Elem #1 begins to yield.
7	Elem #1 completely crushed.

Figure 26.4 CRS #4 - Extension/Rotation = 5.0

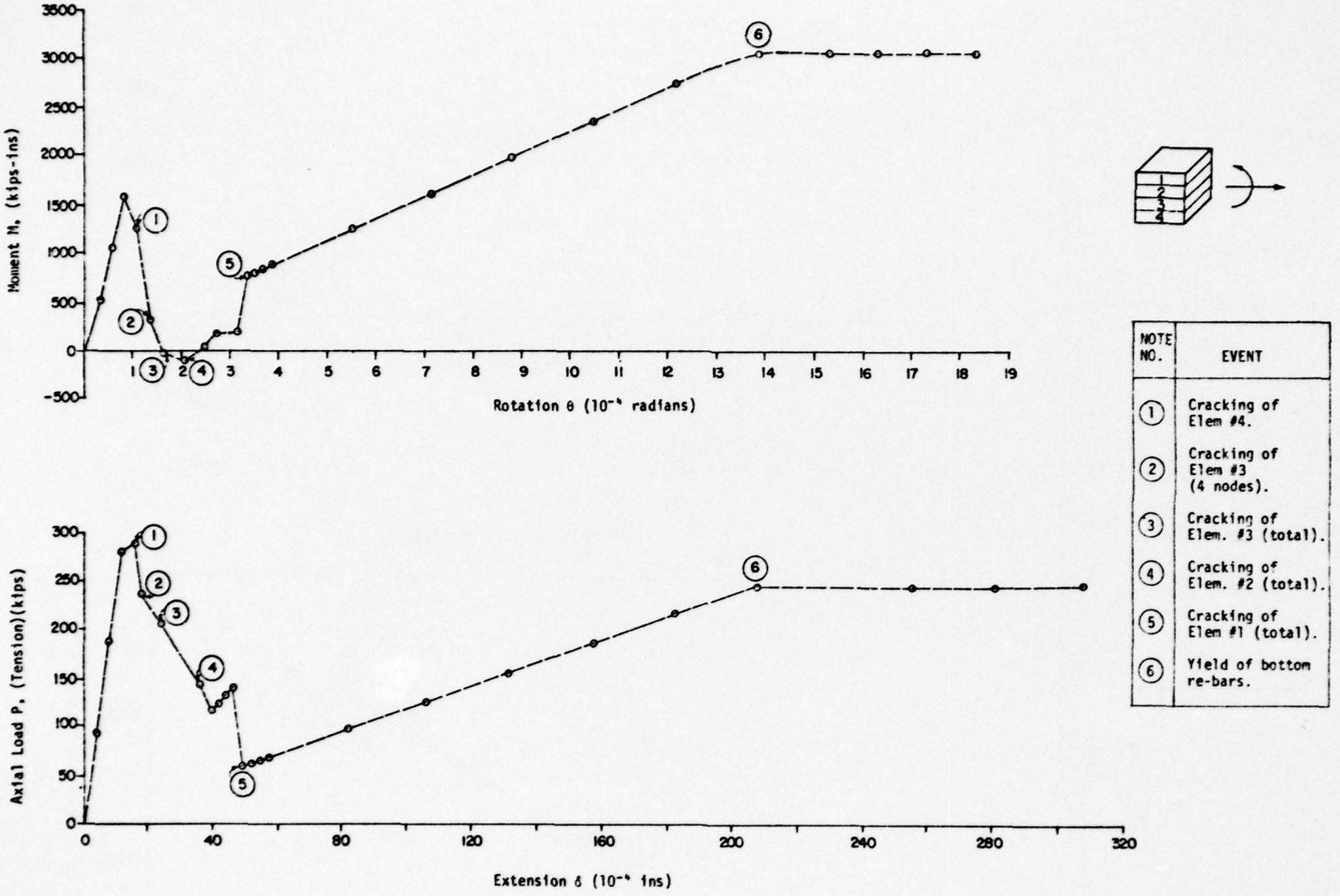

Figure 26.5 CRS #4 - Extension/Rotation = 15.0

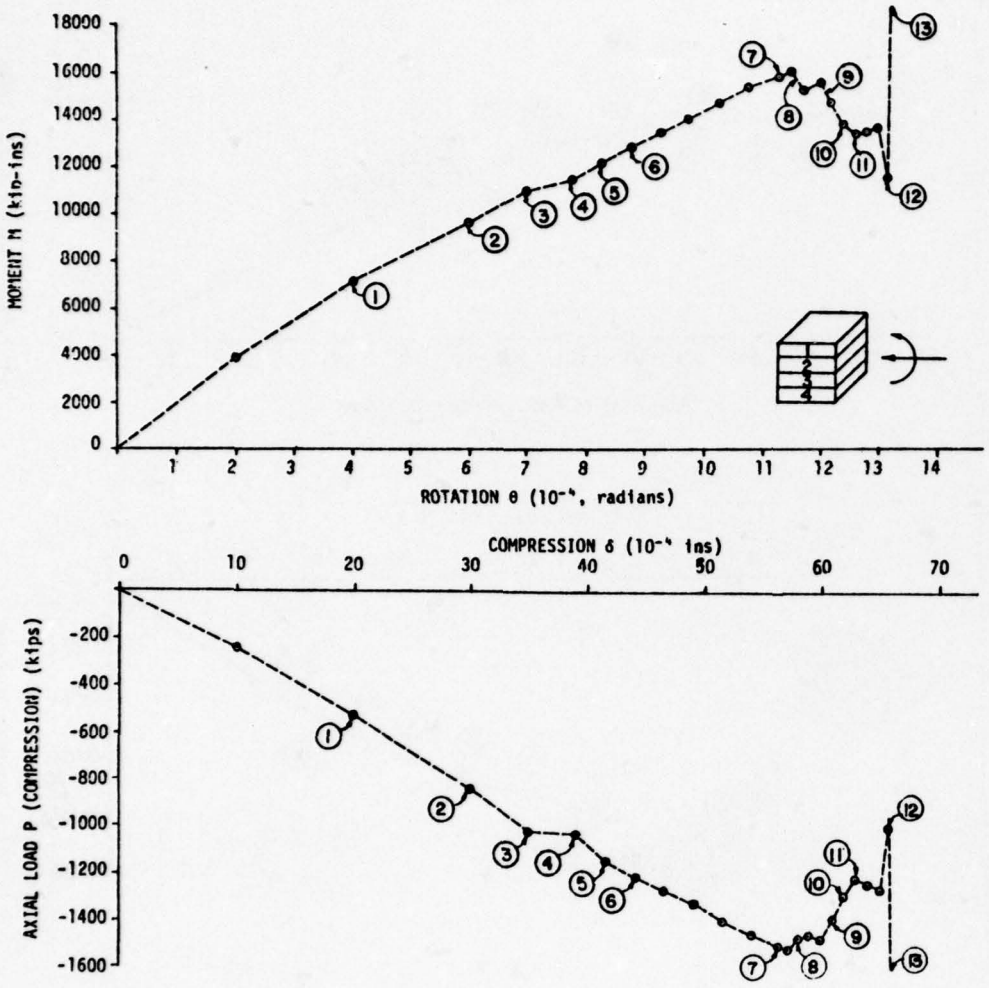

NODE NO.	EVENT
①	Elem #4 cracks 4 nodes.
②	Elem #4 cracks 8 nodes.
③	Elem #1 yields 8 nodes.
④	Elem #3 cracks 7 nodes.
⑤	Elem #2 yields 4 nodes.
⑥	Elem #2 yields 7 nodes.
⑦	Elem #2 yields 8 nodes.
⑧	Elem #1 crushes 1 node.
⑨	Elem #1 crushes 2 nodes
⑩	Elem #1 crushes 3 nodes.
⑪	Elem #2 crushes 1 node.
⑫	Elem #1 crushes 4 nodes. Elem #2 crushes 3 nodes.
⑬	Elem #1 crushes 7 nodes. Elem #2 crushes 4 nodes. Elem #2 cracks 4 nodes. Elem #3 crushes 1 node. Solution does not converge.

Figure 26.6 CRS #4 - Compression/Rotation = 5.0

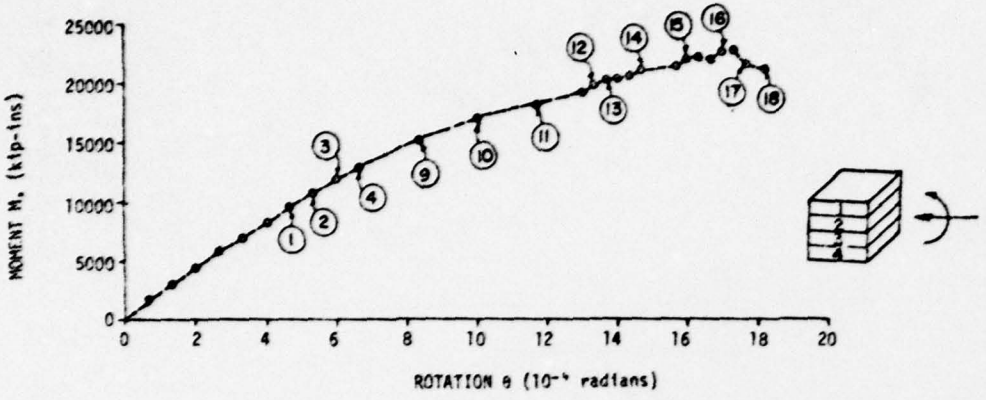

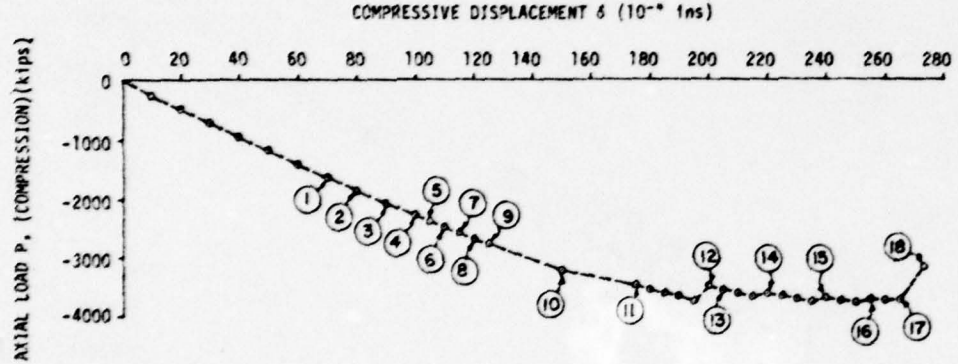

NOTE NO.	EVENT
1	Element #1 yields 4 nodes.
2	Element #1 yields completely.
3	Element #2 yields 2 nodes.
4	Element #2 yields 6 nodes.
5	Element #2 yields 7 nodes.
6	Element #2 yields completely. Element #3 yields 1 node.
7	Element #3 yields 2 nodes. Element #4 yields 3 nodes.
8	Element #3 yields 3 nodes.
9	Element #3 yields 6 nodes. Element #4 yields 4 nodes.
10	Elements #3, 4 yield completely.
11	Element #2 crushes 1 node.
12	Element #3 crushes 3 nodes.
13	Top re-bars yield in compression.
14	Element #3 crushes 4 nodes.
15	Element #3 crushes 5 nodes.
16	Element #4 crushes 1 node.
17	Element #1 crushes 1 node.
18	Element #1 crushes 4 nodes. Element #4 crushes 2 nodes.

Figure 26.7 CRS #4 - Compression/Rotation = 15.0

instead of a four layer mesh. Results of this analysis are presented next.

(3) Response of CRS #4.1

CRS 4.1 had similar properties of steel and concrete and the same amount of longitudinal and transverse reinforcement as CRS #4. An eight layer mesh was used to model the concrete as shown in Figure 27. The failure envelope (Figure 28) is a great improvement over that of Figure 25 for CRS #4. Response of the section to various deformation patterns is indicated in Figures 29.1 through 29.6.

As can be seen from Figure 29.1, for pure compression imposed displacements, a more distinct and refined P-δ curve is obtained with an eight layer mesh, with a distinct negative slope after the maximum load point is reached.

The most significant change in response is in the case where the section is imposed with pure rotation deformations as indicated in Figure 29.2 compared to Figure 26.3. Failure in this case occurs at a lower magnitude of rotation of 0.0017 radians.

The deformation at which failure of the section occurs when subjected to extension/rotation of 5.0 is close to the one predicted with a four layer mesh (Figure 29.3 compared to Figure 26.4). The response to a deformation pattern of extension/rotation of 15 is also similar (Figure 29.4 compared to Figure 26.5).

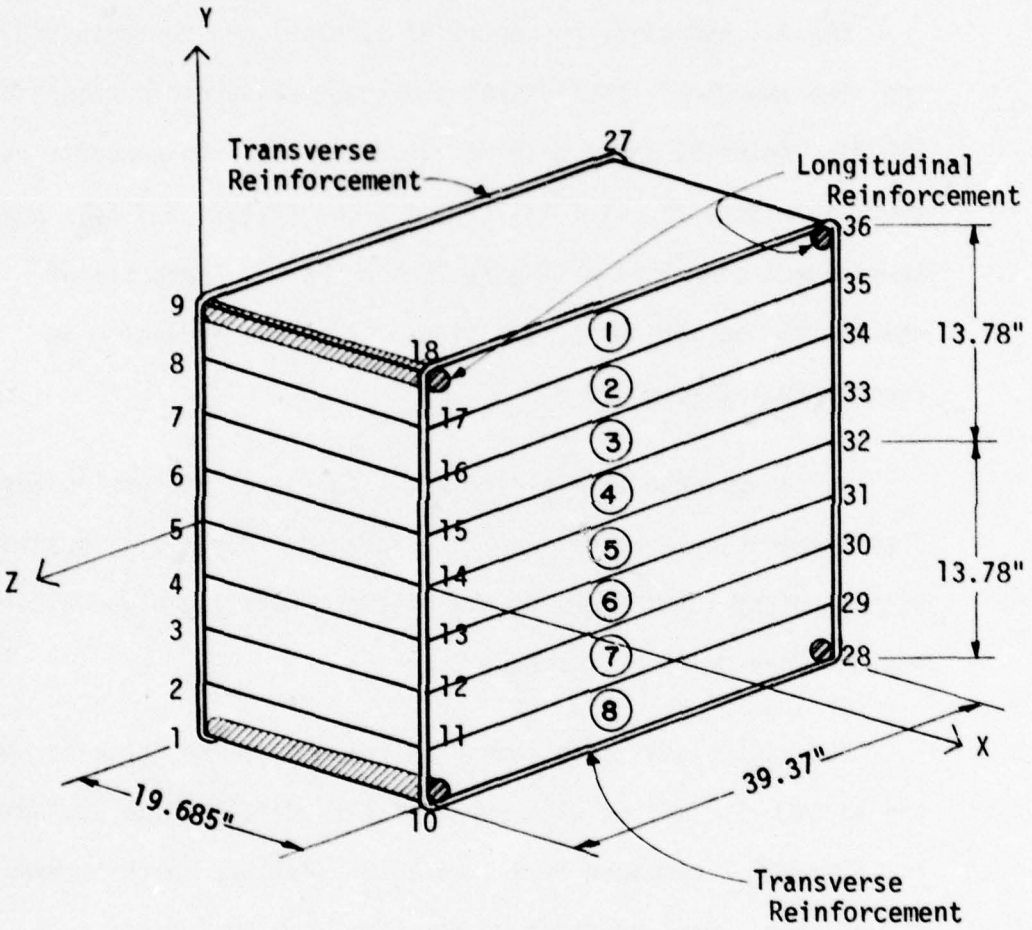

Figure 27 Eight Layer Finite Element Model

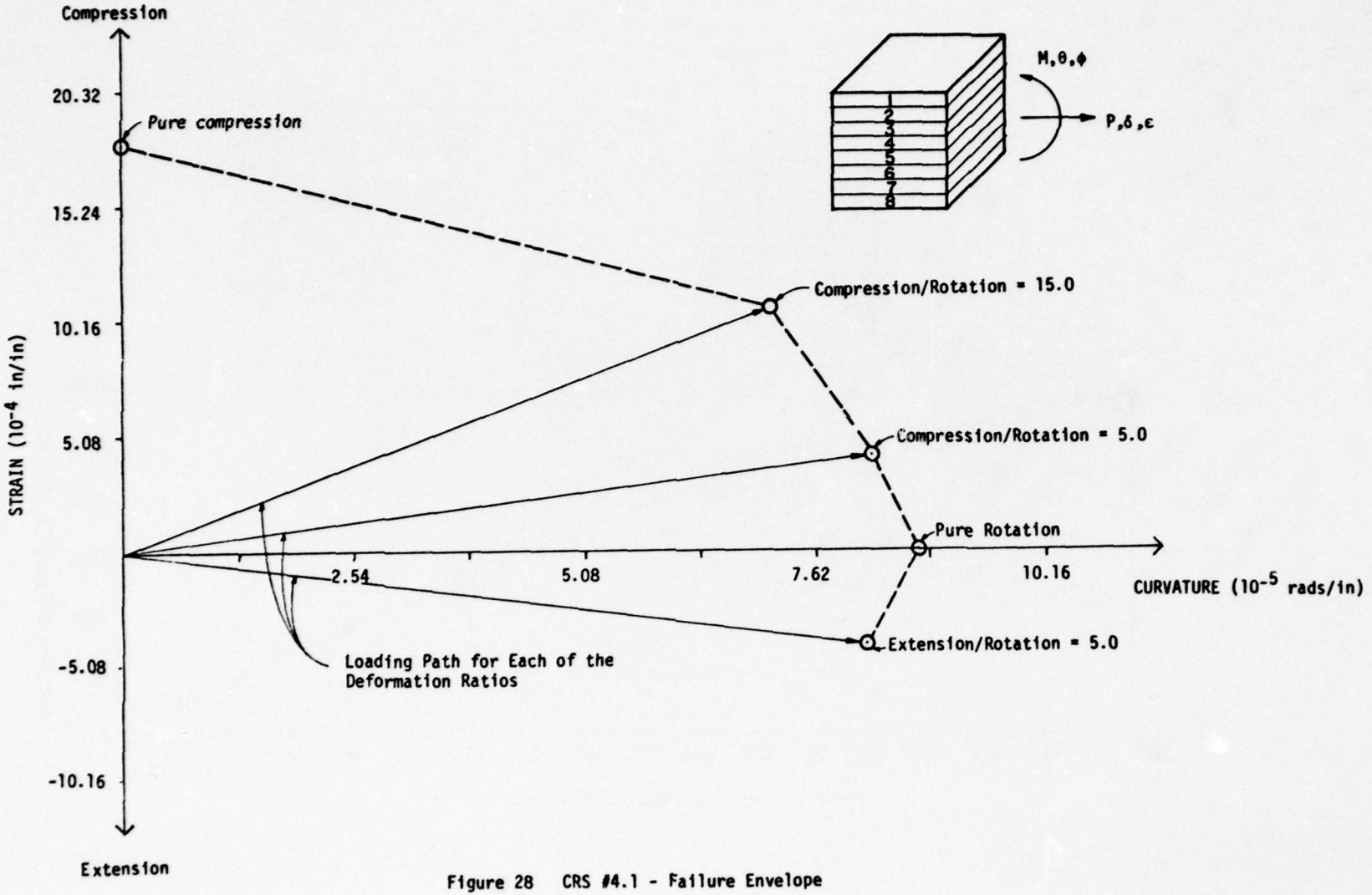

Figure 28 CRS #4.1 - Failure Envelope

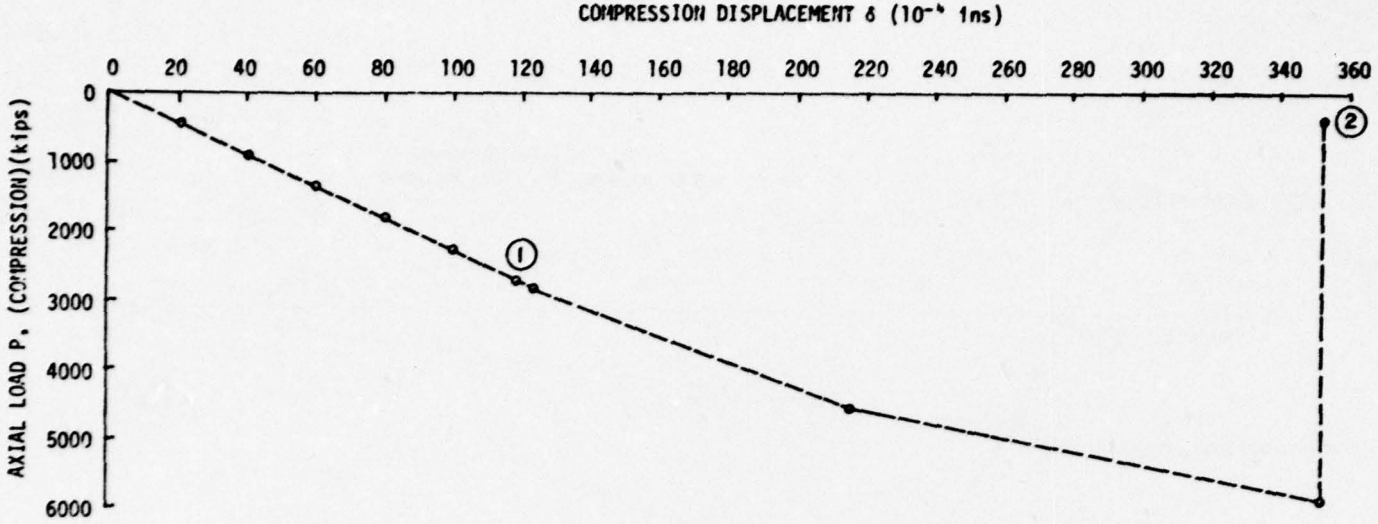

NOTE NO.	EVENT
1	Entire concrete section yields.
2	Entire concrete section crushes.

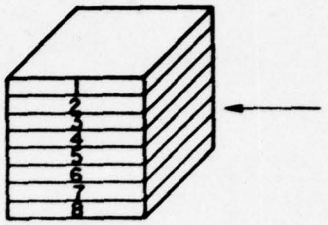

Figure 29.1 CRS #4.1 - Pure Compression

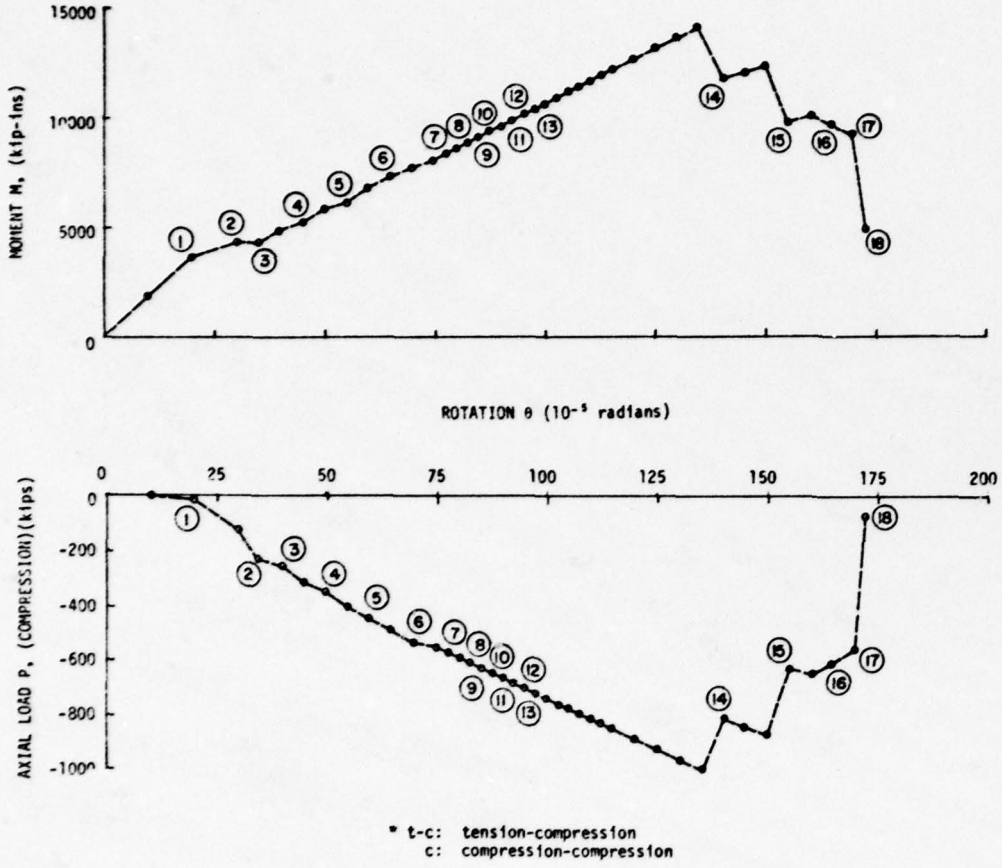

* t-c: tension-compression
c: compression-compression

NOTE NO.	EVENT
1	Element #8 cracks 4 nodes.
2	Elements #7, 8 crack 8 nodes.
3	Element #6 cracks 4 nodes.
4	Element #6 cracks 8 nodes.
5	Element #5 cracks 4 nodes.
6	Element #5 cracks 8 nodes.
7	Element #1 yields 4 nodes (t-c).
8	Element #1 yields 8 nodes (t-c).
9	Element #4 yields 4 nodes (t-c).
10	Element #2 yields 4 nodes (t-c).
11	Element #2 yields 8 nodes (t-c).
12	Element #4 yields 8 nodes (t-c).
13	Element #3 yields 8 nodes (t-c).
14	Element #1 crushes 4 nodes (t-c).
15	Element #1 crushes 6 nodes (t-c). Element #2 crushes 3 nodes (t-c).
16	Element #2 crushes 4 nodes (t-c).
17	Element #2 crushes 5 nodes (t-c). Element #3 crushes 1 node (t-c).

NOTE NO.	EVENT
18	Element #1 crushes 7 nodes (t-c). Element #2 crushes 8 nodes (t-c). Element #3 crushes 8 nodes (t-c). Element #4 crushes 8 nodes (t-c).

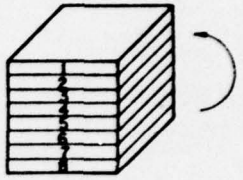

Figure 29.2 CRS #4.1 - Pure Rotation

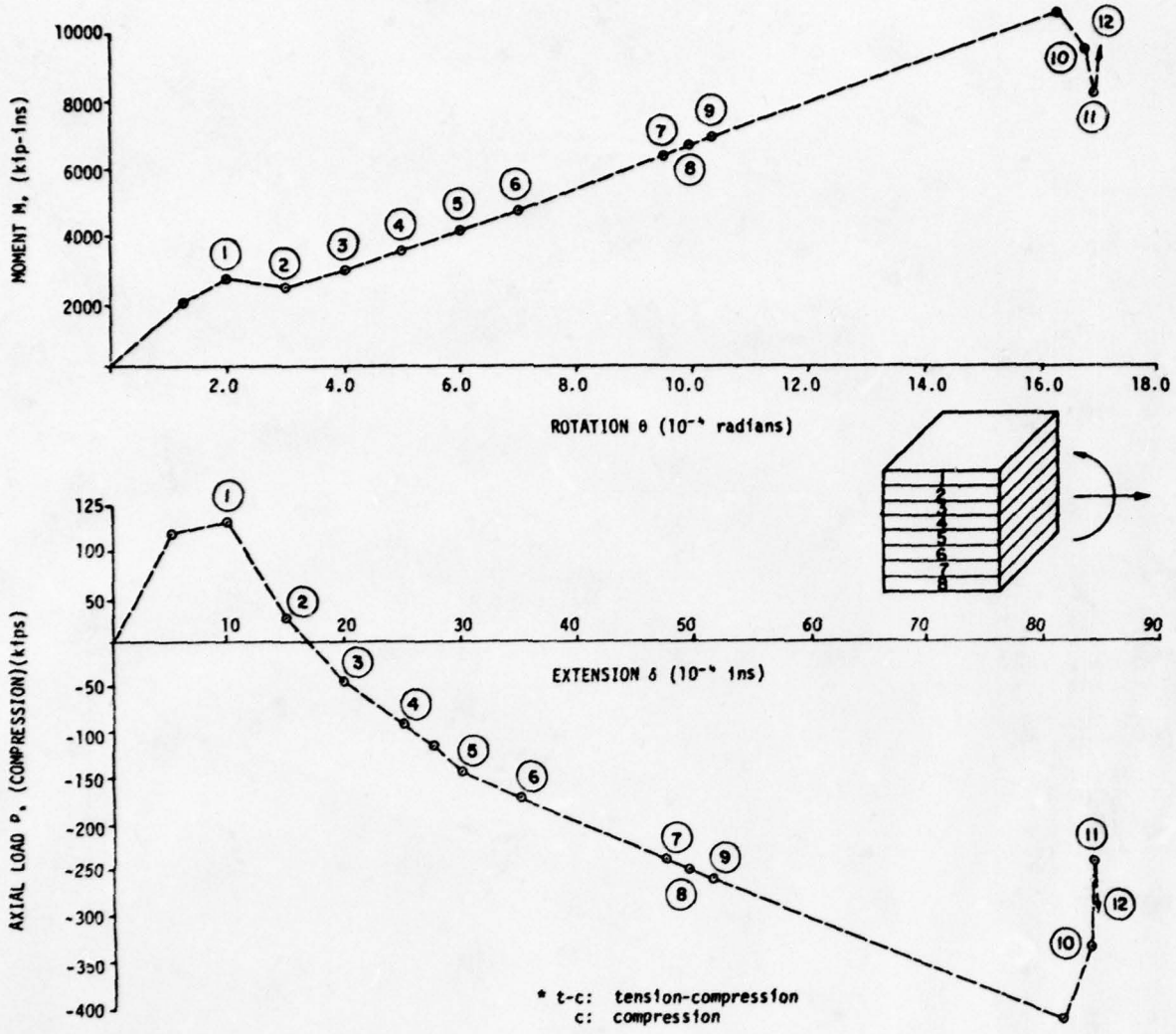

NOTE NO.	EVENT
(1)	Cracking of elements #7, 8 total.
(2)	Cracking of element #6 (total) element #5 (4 nodes).
(3)	Cracking of element #5 (total).
(4)	Cracking of element #4 (4 nodes).
(5)	Cracking of element #4 (total).
(6)	Cracking of element #3 (4 nodes).
(7)	Yield of element #4 (4 nodes in t-c).
(8)*	Complete yield of element #1 in t-c. Yield of element #2 (4 nodes in t-c).
(9)	Complete yield of element #2 in (t-c). Yield of element #3 (4 nodes in t-c).
(10)	Crushing of element #1 (2 nodes in t-c).
(11)	Crushing of element #1 (4 nodes in t-c).
(12)	Failure of section.

Figure 29.3 CRS #4.1 - Extension/Rotation = 5.0

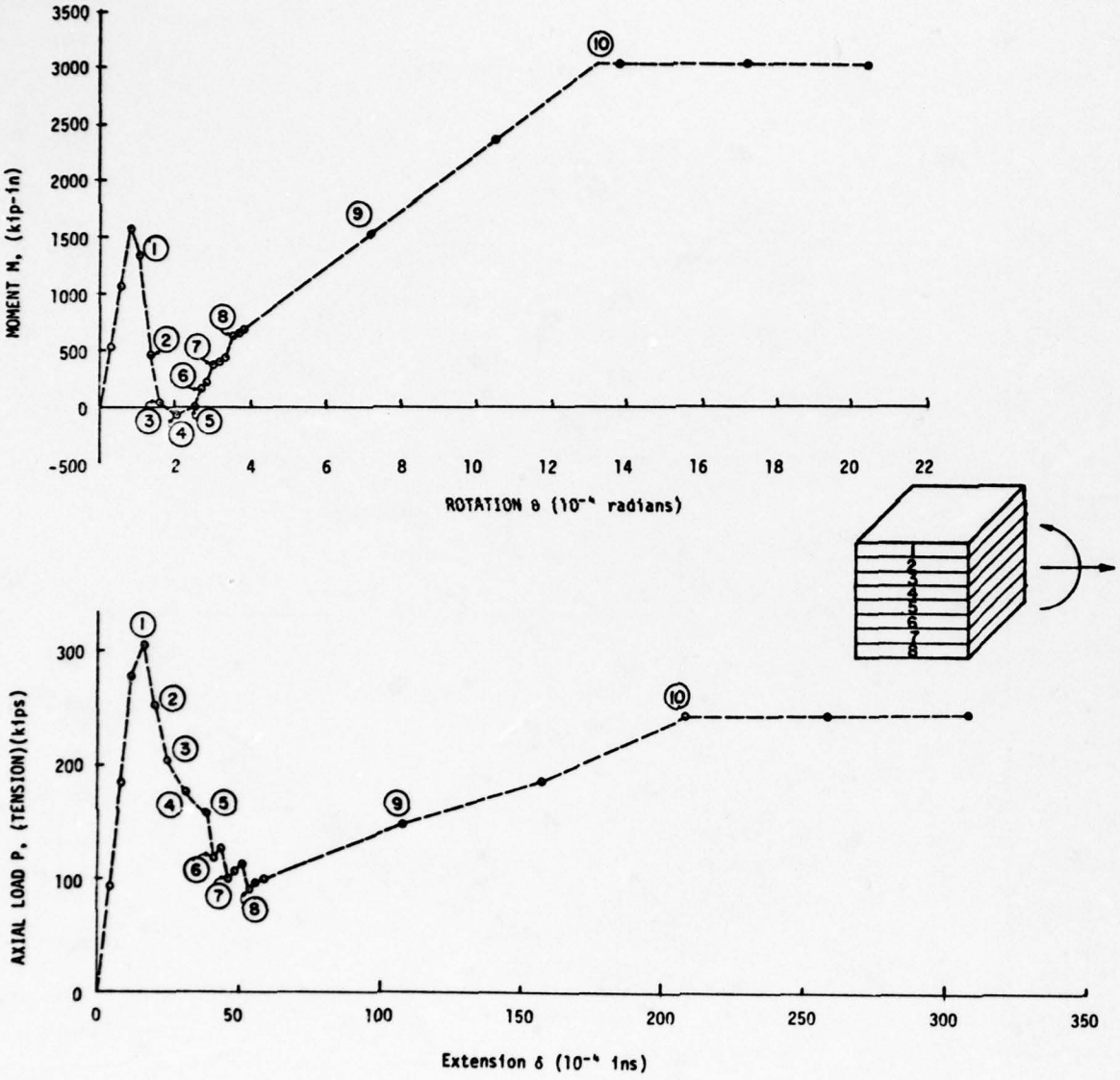

NOTE NO.	EVENT
(1)	Element #8 cracks 8 nodes. Element #7 cracks 4 nodes.
(2)	Elements #7, 6 crack 8 nodes.
(3)	Element #5 cracks 8 nodes.
(4)	Element #4 cracks 8 nodes.
(5)	Element #3 cracks 4 nodes.
(6)	Element #3 cracks 8 nodes.
(7)	Element #2 cracks 4 nodes.
(8)	Element #2 cracks 8 nodes.
(9)	Element #1 cracks 8 nodes.
(10)	Bottom longitudinal steel yields.

Figure 29.4 CRS #4.1 - Extension/Rotation = 15.0

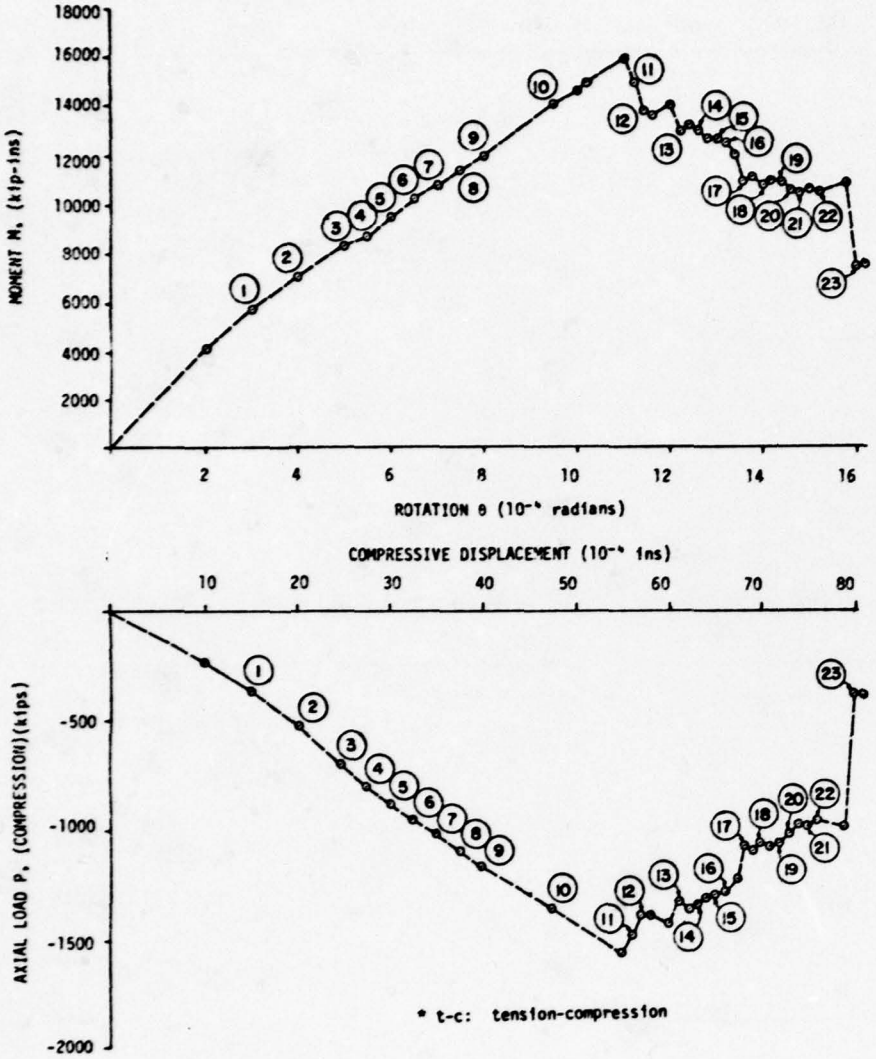

* t-c: tension-compression

Figure 29.5 CRS #4.1 - Compression/Rotation = 5.0

NOTE NO.	EVENT
(1)	Cracking of element #8 (4 nodes).
(2)	Cracking of element #8 complete.
(3)	Cracking of element #7 (4 nodes).
(4)	Cracking of element #7 complete.
(5)*	Yield of element #1 in (t-c).
(6)	Yield of element #2 (4 nodes in t-c). Cracking of element #6 (4 nodes).
(7)	Cracking of element #6 (7 nodes). Yield of element #2 complete in (t-c).
(8)	Yield of element #3 (5 nodes in t-c).
(9)	Complete yield of element #3 in t-c.
(10)	Complete yield of element #4 in (t-c).
(11)	Crushing of element #1 (3 nodes in t-c).
(12)	Crushing of element #1 (4 nodes in t-c).
(13)	Crushing of element #2 (2 nodes in t-c).
(14)	Crushing of element #2 (3 nodes in t-c).
(15)	Crushing of element #2 (4 nodes in t-c).
(16)	Crushing of element #2 (5 nodes in t-c).
(17)	Crushing of element #2 (6 nodes in t-c). Crushing of element #3 (3 nodes in t-c).

NOTE NO.	EVENT
(18)	Crushing of element #3 (4 nodes in t-c).
(19)	Crushing of element #3 (5 nodes in t-c).
(20)	Crushing of element #3 (6 nodes in t-c).
(21)	Crushing of element #4 (1 node in t-c).
(22)	Crushing of element #4 (2 nodes in t-c).
(23)	Failure of elements 3, 4, 5, 6. Yield of transverse rebars. Failure of section assumed.

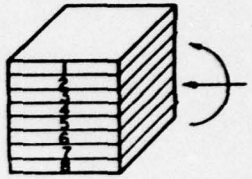

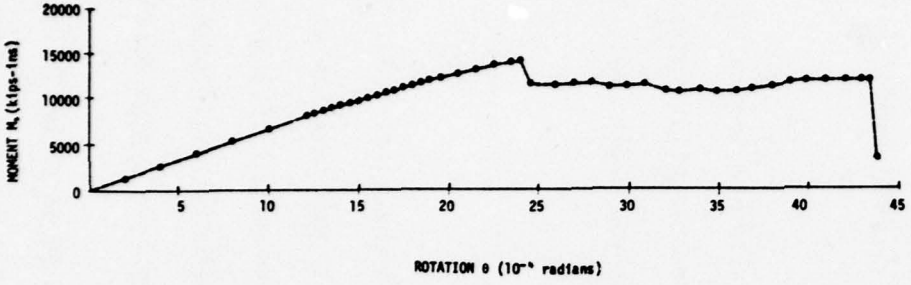

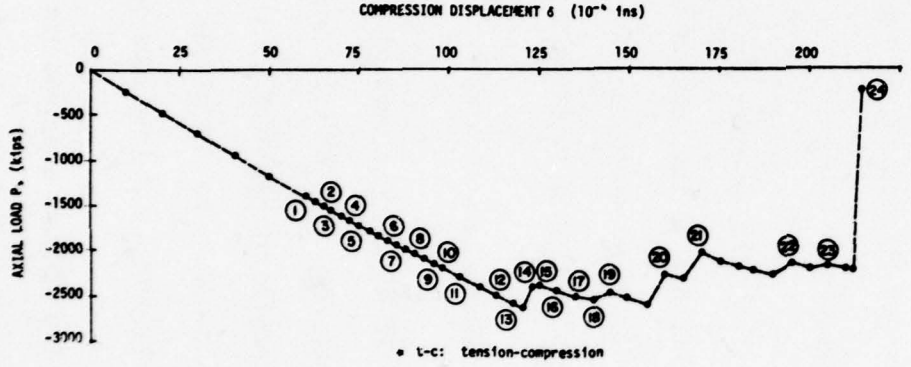

* t-c: tension-compression

NOTE NO.	EVENT
①	Element #1 yields 4 nodes (t-c).
②	Element #1 yields 8 nodes (4t-c, 4c).
③	Element #2 yields 4 nodes (t-c).
④	Element #2 yields 8 nodes (t-c).
⑤	Element #3 yields 4 nodes (t-c).
⑥	Element #3 yields 8 nodes (t-c).
⑦	Element #4 yields 4 nodes (t-c).
⑧	Element #4 yields 8 nodes (t-c).
⑨	Element #5 yields 1 node (t-c).
⑩	Element #5 yields 4 nodes (t-c).
⑪	Element #5 yields 8 nodes (t-c).
⑫	Element #6 yields 4 nodes (t-c).
⑬	Element #13 yields 8 nodes (t-c).
⑭	Element #2 crushes 5 nodes (t-c).
⑮	Element #2 crushes 6 nodes (t-c). Element #7 yields 4 nodes (t-c).
⑯	Element #7 yields 8 nodes (t-c). Element #8 yields 4 nodes (t-c).
⑰	Element #8 yields 8 nodes (t-c).

NOTE NO.	EVENT
⑱	Element #3 crushes 1 node (t-c).
⑲	Element #3 crushes 3 nodes (t-c).
⑳	Element #3 crushes 4 nodes (t-c). Element #4 crushes 6 nodes (t-c).
㉑	Element #4 crushes 7 nodes (t-c). Element #5 crushes 5 nodes (t-c). Solution does not converge.
㉒	Element #6 crushes 2 nodes (t-c).
㉓	Element #5 crushes 6 nodes (t-c). Top re-bar yields in compression. Solution does not converge.
㉔	Failure of section.

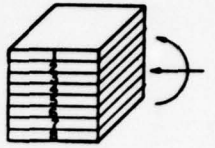

Figure 29.6 CRS #4.1 - Compression/Rotation = 15.0

However, the response and the deformation at failure for an imposed deformation of compression/rotation of 5 is different. As can be seen from Figure 29.5, the eight layer model predicts more strength than the four layer model (Figure 26.6). The eight layer model is numerically a more stable system. The nonlinearities and consequent changes in stiffness are not as drastic as in the four layer system.

Figure 29.6, however, indicates that the failure strength of the section is smaller when subjected to a deformation pattern of compression/rotation of 15.0. This could be due to the multi-axial stress behavior where a larger portion of the section fails in tension-compression in the eight layer model as compared to the four layer model.

It should, however, be emphasized at this stage that whenever the response of the section is predominantly controlled by the behavior of concrete, a finer mesh would give more accurate results and a more stable solution process.

(4) Response Of CRS #6

CRS #6 was analyzed with a longitudinal reinforcement of 1% on each face ($p = p' = 1\%$) and with concrete having an ultimate compressive stress of 5.0 ksi. The amount of transverse reinforcement was assumed to be 40% of the longitudinal reinforcement. A section so reinforced would be expected to have a high ductility.

The failure envelope for CRS #6 is shown in Figure 30 while the response in terms of M-θ and P-δ curves is shown in Figures 31.1

through 31.6. This failure envelope shows that the failure strength of the section CRS #6 is higher when subjected to pure compressive displacements as compared to CRS #3 with a reinforcement ratio of 2% (Figure 23), when subjected to similar compressive displacements. Figure 30 (compared to Figure 23) also shows that the failure strength of the section is higher when subjected to deformation ratios of compression/rotation of 5 and compression/rotation of 15, while the failure strength is decreased when subjected to a deforma- ratio of extension/rotation of 5.0. The deformation capacity of the section remains the same when subjected to a pure rotation. Note that the value of Poisson's ratio for CRS #6 was 10^{-6} as compared to a value of 0.2 for CRS #3.

The general pattern of the M-θ and P-δ curves in Figures 31.1 through Figure 31.6 is the same as that of CRS #3 when subjected to corresponding deformation ratios. Thus, in the first stage of study the uniaxial compressive stress-strain relationship was kept the same while the effect of different parameters were studied; e.g., change in longitudinal reinforcement (CRS #4, CRS #6), change in mesh size (CRS #4, CRS #4.1), and change in transverse reinforcement (CRS #4, CRS #4.2, the response of which is discussed later in this section).

Hence, higher strength concrete was used, and only the amount of longitudinal steel was varied to study the effect on the shape of the failure envelope. Two different strengths of concrete were used; one with an ultimate uniaxial compressive stress of 6.0 ksi and the other with an ultimate uniaxial compressive stress of 9.0 ksi. Results of these analyses are presented next.

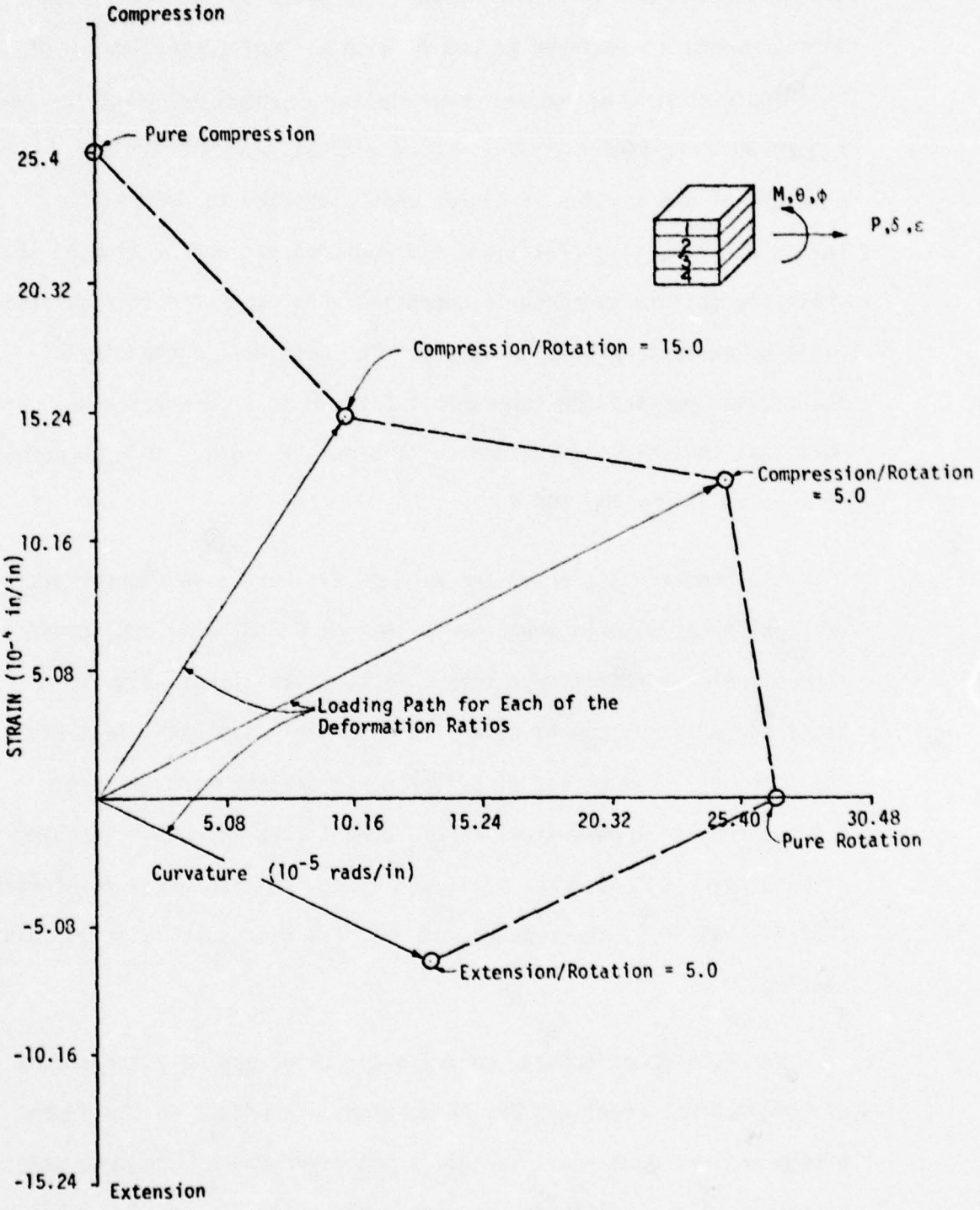

Figure 30 CRS #6 Failure Envelope

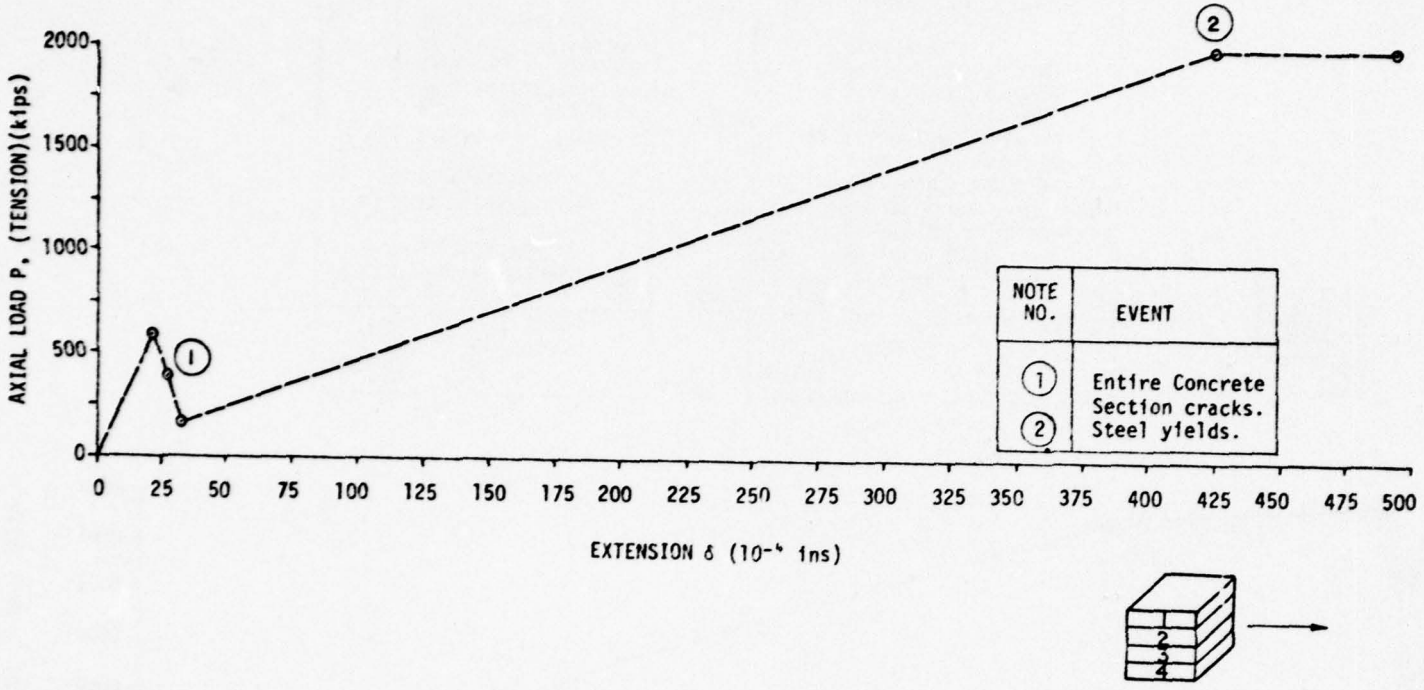

Figure 31.1 CRS #6 - Pure Extension

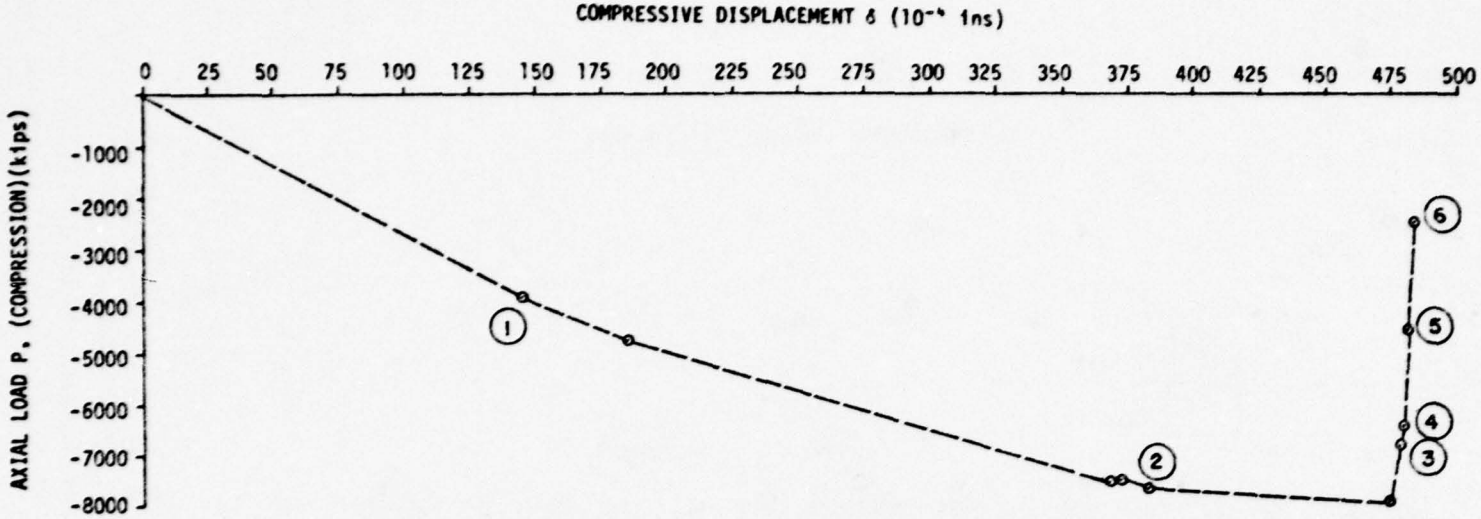

NOTE NO.	EVENT
1	Entire Concrete Section yields.
2	Steel yields in compression.
3	Crushing of Element #2, 3 (2 nodes each in compression). Crushing of Element #1, 4 (1 node each in compression).
4	Crushing of Element #4 (2 nodes each in compression).

NOTE NO.	EVENT
5	Crushing of Element #1 (4 nodes in compression). Crushing of Element #2 (5 nodes in compression). Crushing of Element #3 (4 nodes in compression). Crushing of Element #4 (5 nodes in compression).
6	Crushing of Elements #2, 3, 4 in compression (total). Yield of transverse rebars. Failure of section assumed.

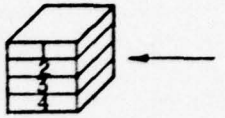

Figure 31.2 CRS #6 - Pure Compression

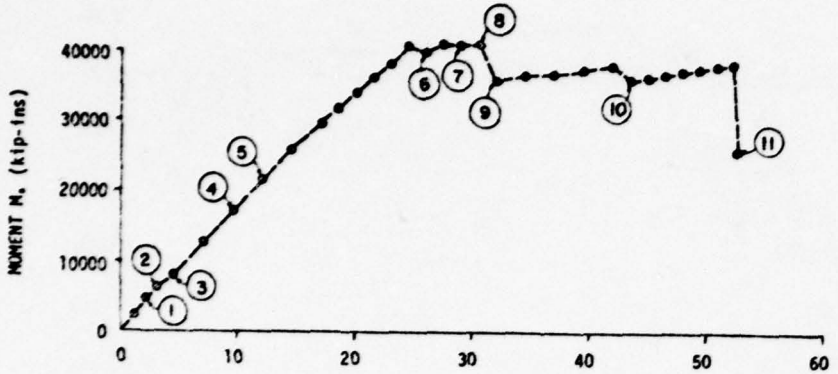

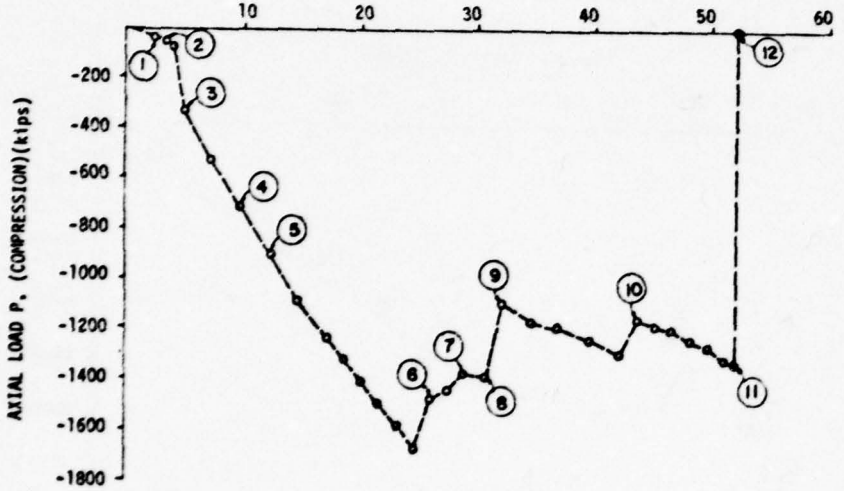

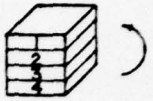

NOTE NO.	EVENT
1	Element #4 cracks 4 nodes.
2	Element #4 cracks completely.
3	Element #3 cracks completely.
4	Element #1 yields 8 nodes. Element #2 yields 4 nodes.
5	Element #2 yields 8 nodes.
6	Element #1 crushes 2 nodes.
7	Element #2 crushes 4 nodes and steel yields.
8	Element #1 crushes 3 nodes.
9	Element #1 crushes 4 nodes.
10	Element #1 crushes 5 nodes.
11	Elements #1, 2 crush completely.

Figure 31.3 CRS #6 - Pure Rotation

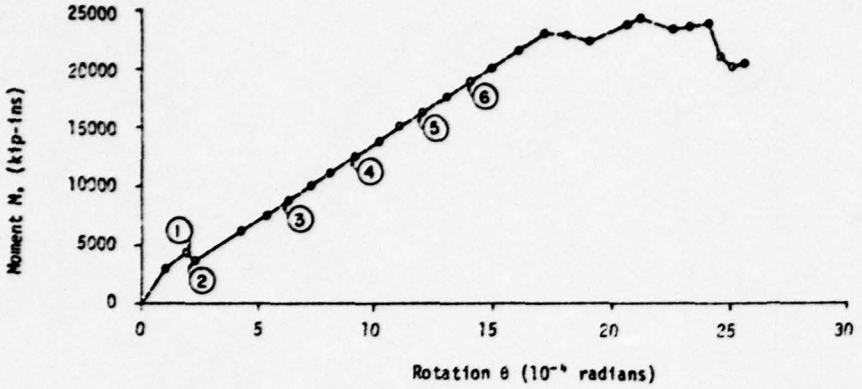

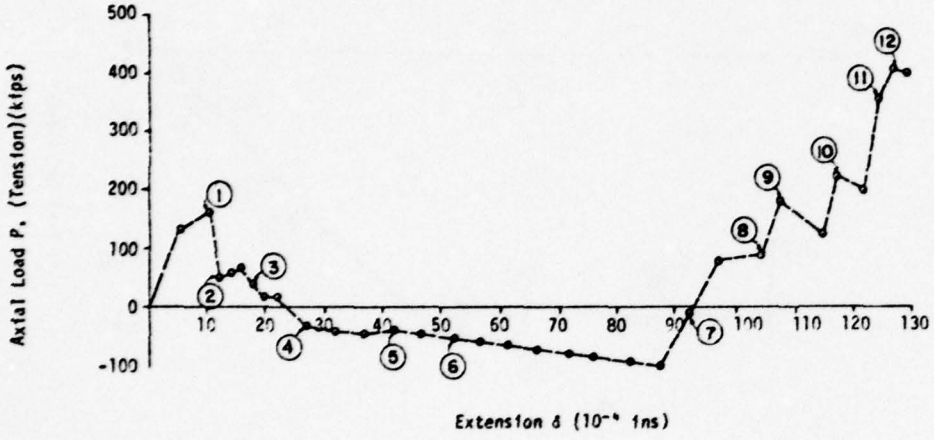

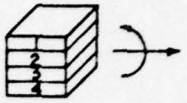

NOTE NO.	EVENT
①	Element #4 cracks completely.
②	Element #3 cracks 4 nodes.
③	Element #3 cracks 8 nodes.
④	Element #2 cracks 4 nodes.
⑤	Element #2 cracks completely.
⑥	Element #1 yields 8 nodes.
⑦	Element #1 crushes 1 node.
⑧	Element #1 crushes 2 nodes.
⑨	Element #1 crushes 3 nodes. Steel yields.
⑩	Element #1 crushes 4 nodes.
⑪	Element #1 crushes 7 nodes. Solution does not converge.
⑫	Element #1 crushes completely.

Figure 31.4 CRS #6 - Extension/Rotation = 5.0

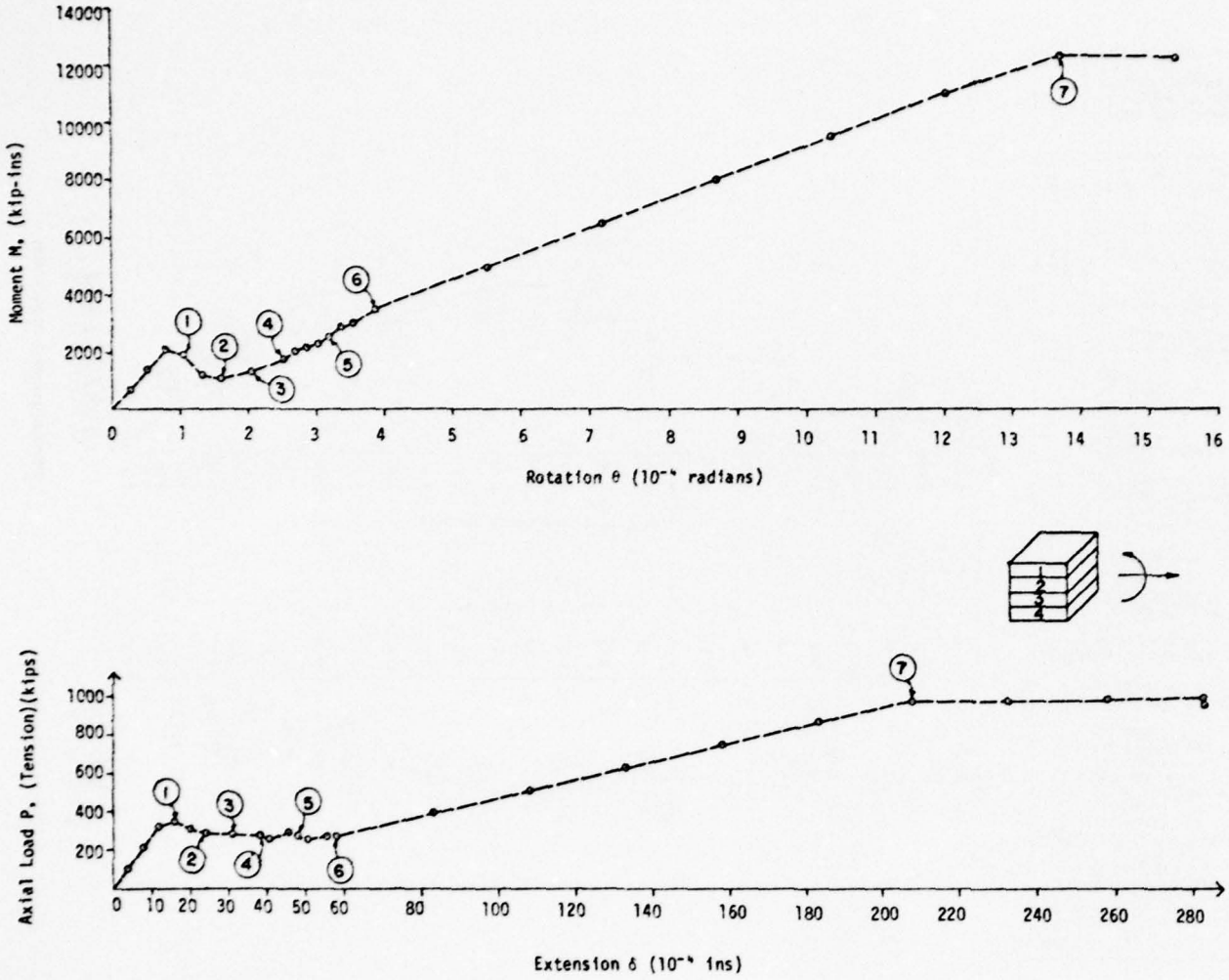

NOTE NO.	EVENT
1	Element #4 Cracks Completely.
2	Element #3 cracks completely.
3	Element #2 cracks 4 nodes.
4	Element #2 cracks completely.
5	Element #1 cracks 4 nodes.
6	Element #1 cracks completely.
7	Steel yields.

Figure 31.5 CRS #6 - Extension/Rotation = 15.0

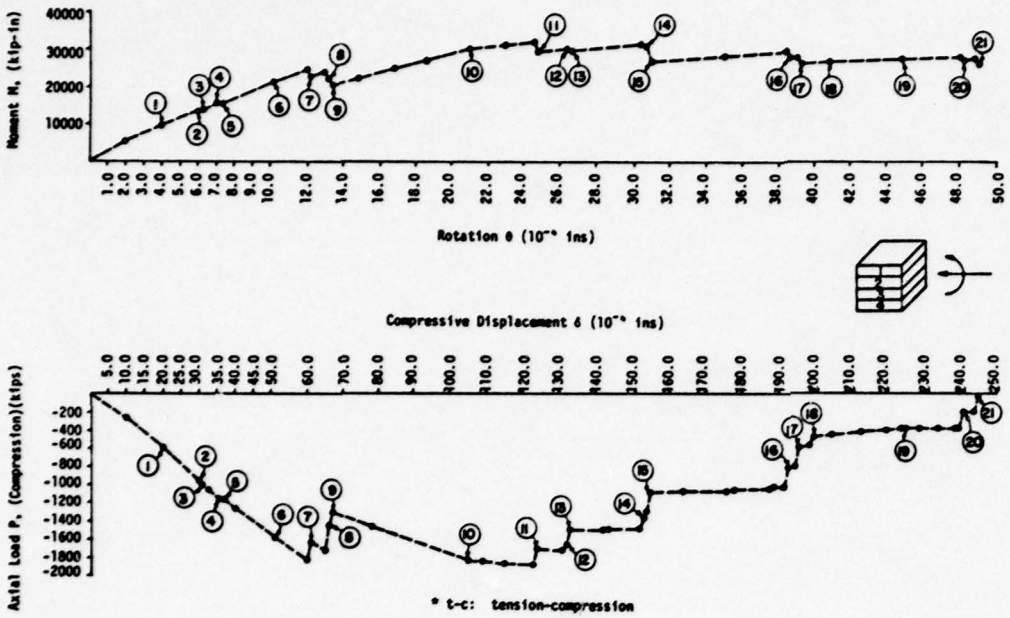

* t-c: tension-compression

NOTE NO.	EVENT
①	Cracking of Element #4 (4 nodes).
②	Cracking of Element #4 (total).
③*	Yield of Element #1 (4 nodes in t-c).
④	Yield of Element #1 (8 nodes in t-c).
⑤	Cracking of Element #3 (6 nodes).
⑥	Yield of Element #2 (8 nodes in t-c).
⑦	Crushing of Element #1 (2 nodes in t-c).
⑧	Crushing of Element #2 (4 nodes in t-c).
⑨	Crushing of Element #1 (3 nodes in t-c). Crushing of Element #3 (1 node in t-c).
⑩	Yield of re-bars in compression.
⑪	Crushing of Element #1 (1 node in compression.)
⑫	Crushing of Element #2 (5 nodes in t-c).
⑬	Crushing of Element #2 (6 nodes in t-c).
⑭	Crushing of Element #1 (2 nodes in compression, 3 nodes in t-c).
⑮	Crushing of Element #1 (3 nodes in compression, 3 nodes in t-c).
⑯	Crushing of Element #1 (4 nodes in compression, 3 nodes in t-c).

NOTE NO.	EVENT
⑰	Failure of Element #1.
⑱	Failure of Element #3.
⑲	Yield of re-bars in tension.
⑳	Crushing of Element #2 (1 node in compression, 6 nodes in t-c).
㉑	Failure of concrete section.

Figure 31.6 CRS #6 - Compression/Rotation = 5.0

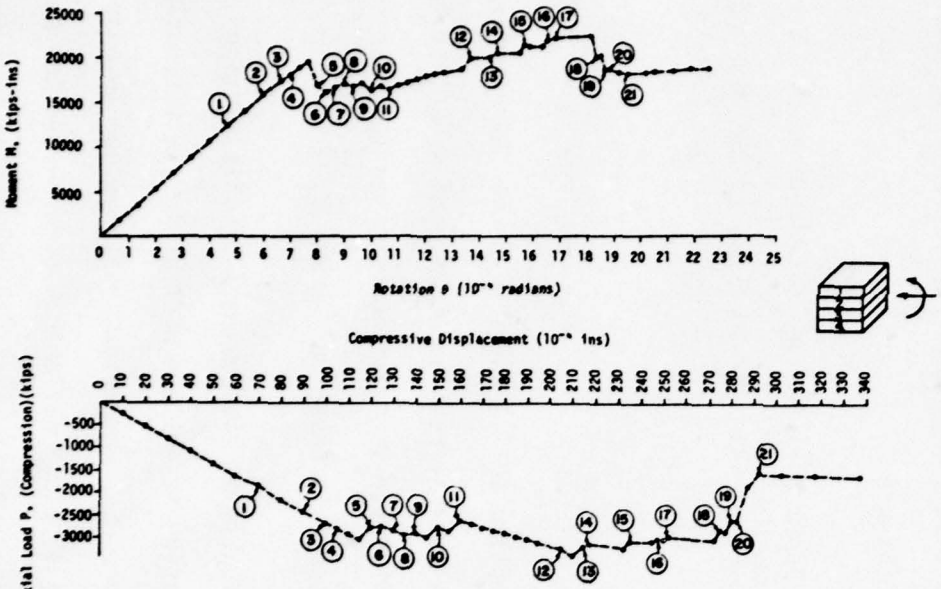

NOTE NO.	EVENT
①	Element #1 yields 4 nodes.
②	Element #1 yields 7 nodes.
③	Element #1 yields completely. Element #2 yields 2 nodes. Element #3 yields 4 nodes.
④	Element #2 yields 4 nodes.
⑤	Element #1 crushes 3 nodes.
⑥	Element #1 crushes 4 nodes. Element #2 yields 6 nodes.
⑦	Element #2 yields completely. Element #3 yields completely. Element #4 yields 4 nodes.
⑧	Element #4 yields 8 nodes.
⑨	Element #2 crushes 1 node.
⑩	Element #2 crushes 3 nodes.
⑪	Element #2 crushes 6 nodes.
⑫	Top re-bars yield in compression.
⑬	Element #3 crushes 1 node.
⑭	Element #3 crushes 2 nodes.
⑮	Element #3 crushes 4 nodes.
⑯	Element #4 crushes 1 node.
⑰	Element #4 crushes 2 nodes.

NOTE NO.	EVENT
⑱	Element #4 crushes 3 nodes.
⑲	Element #4 crushes 4 nodes. Element #1 crushes 6 nodes Solution does not converge.
⑳	Element #4 crushed completely.
㉑	Element #2 crushes 7 nodes. Element #1 crushes 7 nodes. Element #3 crushed completely. Failure of section assumed.

Figure 31.7 CRS #6 - Compression/Rotation = 15.0

(5) Response Of CRS #7

CRS #7 was similar to CRS #3 in dimensions, percentage of longitudinal reinforcement, area of transverse reinforcement, and the properties of steel (stress-strain relation). The only difference between the two sections was the uniaxial stress-strain curve for concrete. Figure 32 shows the stress-strain curve used in the analysis of CRS #7.

The failure envelope plotted from the results of the analyses of the section subjected to various deformation ratios is shown in Figure 33. This envelope is very similar in shape to that of CRS #3 (Figure 23).

Figures 34.1 through 34.6 indicate that the M-θ and P-δ curves for CRS #7 are similar to those of CRS #3, and the modes of failure are also similar.

(6) Response of CRS #8

Section CRS #8 was similar to CRS #4, in dimensions, amount of longitudinal reinforcement, and amount of transverse reinforcement. The stress-strain curve used to represent the properties of concrete is shown in Figure 32.

Results of the analyses of this section subjected to various deformation ratios are plotted in the form of a failure envelope in Figure 35. Comparing this envelope to that of CRS #4 (Figure 25) shows a distinct difference between the two curves, especially for the case when the section is subjected to pure rotation deformation.

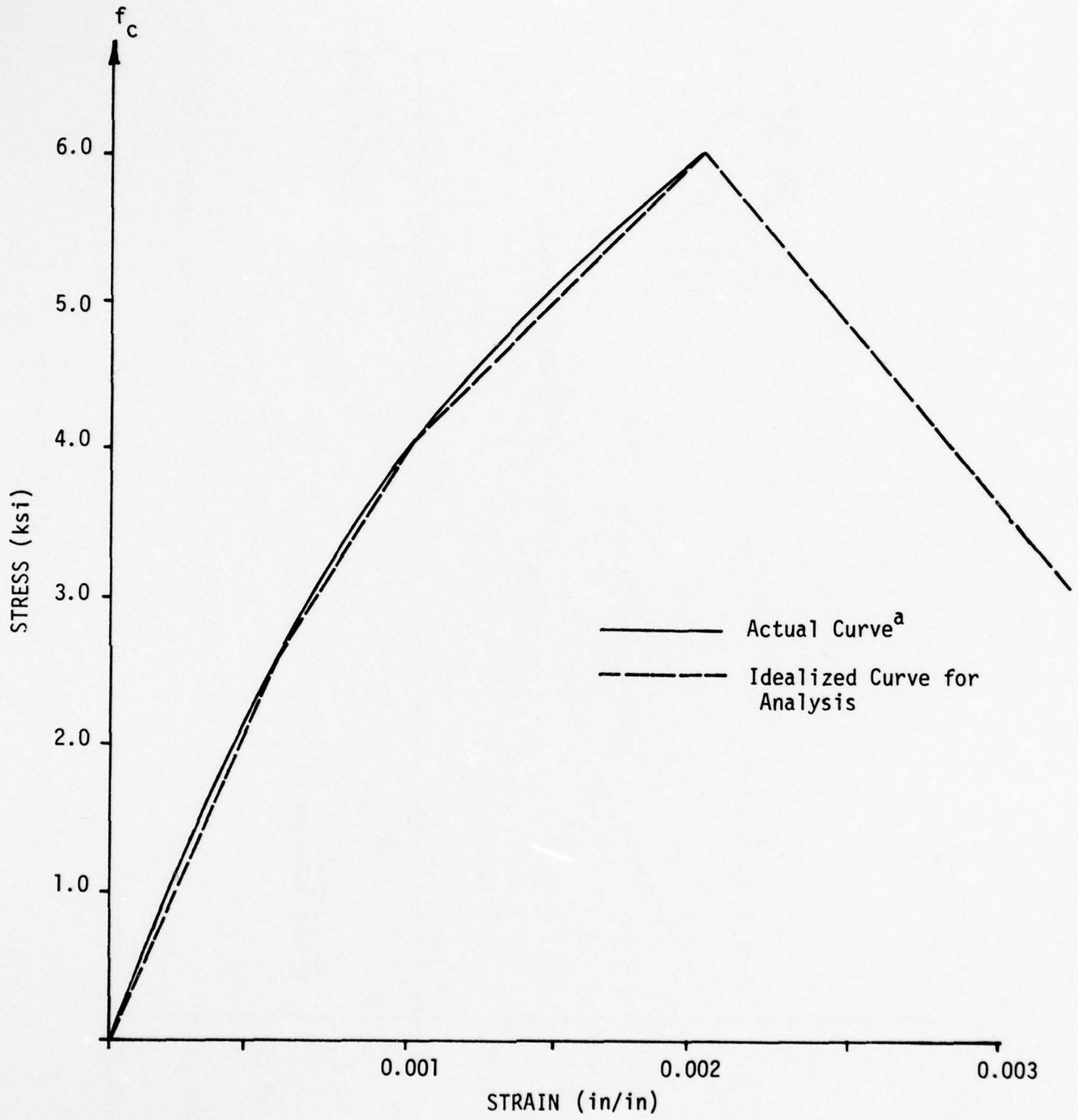

a) Curve obtained from ref. 8, p. 12. Ultimate strain was assumed to be 0.003 in/in.

Ref. 8: Park, R., and Paulay, T., Reinforced Concrete Structures, John Wiley & Sons, Inc., 1975

Figure 32 Stress-Strain Curve for Concrete. Ultimate Stress = 60 ksi

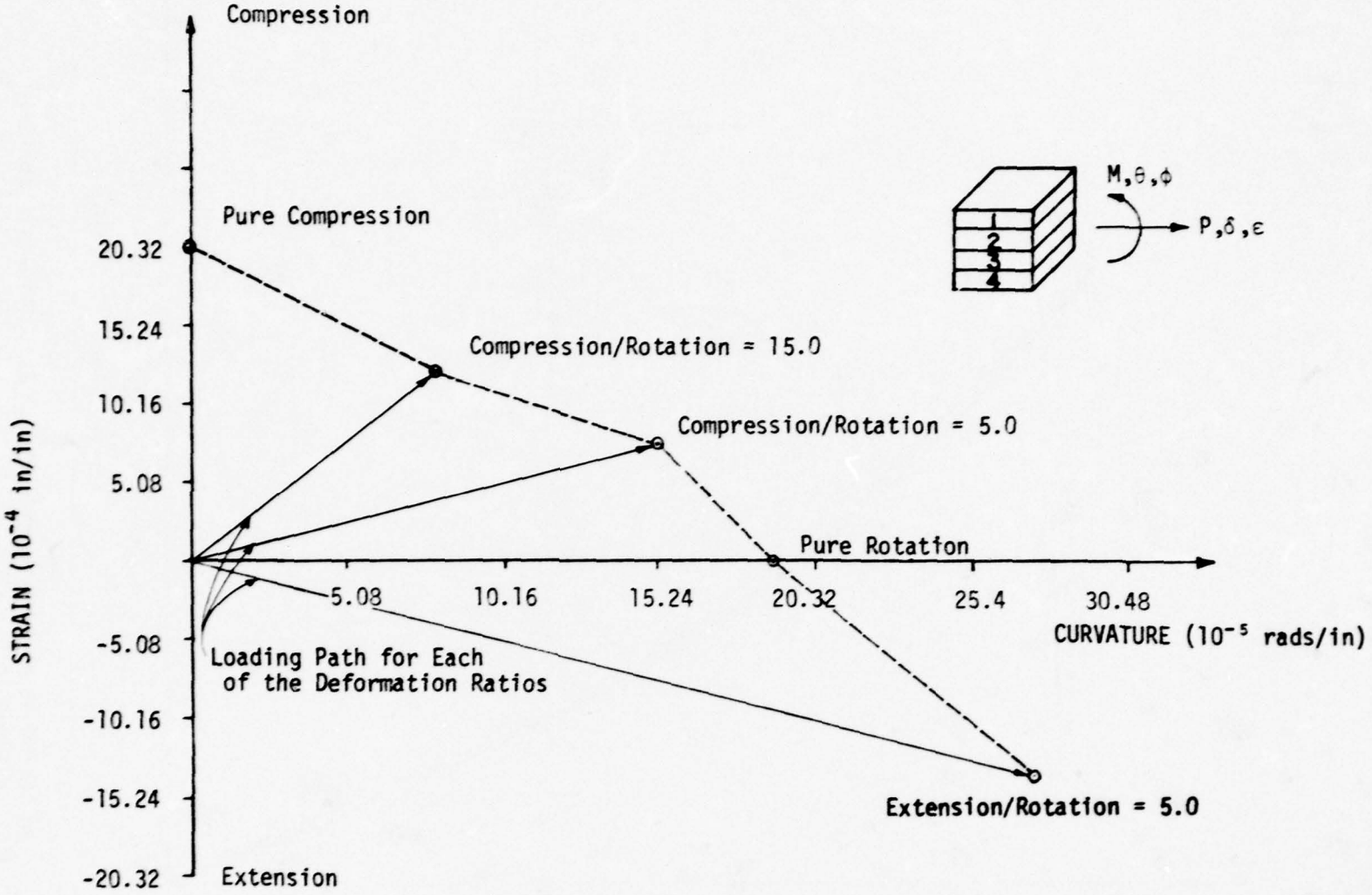

Fig. 33 CRS #7 Failure Envelope

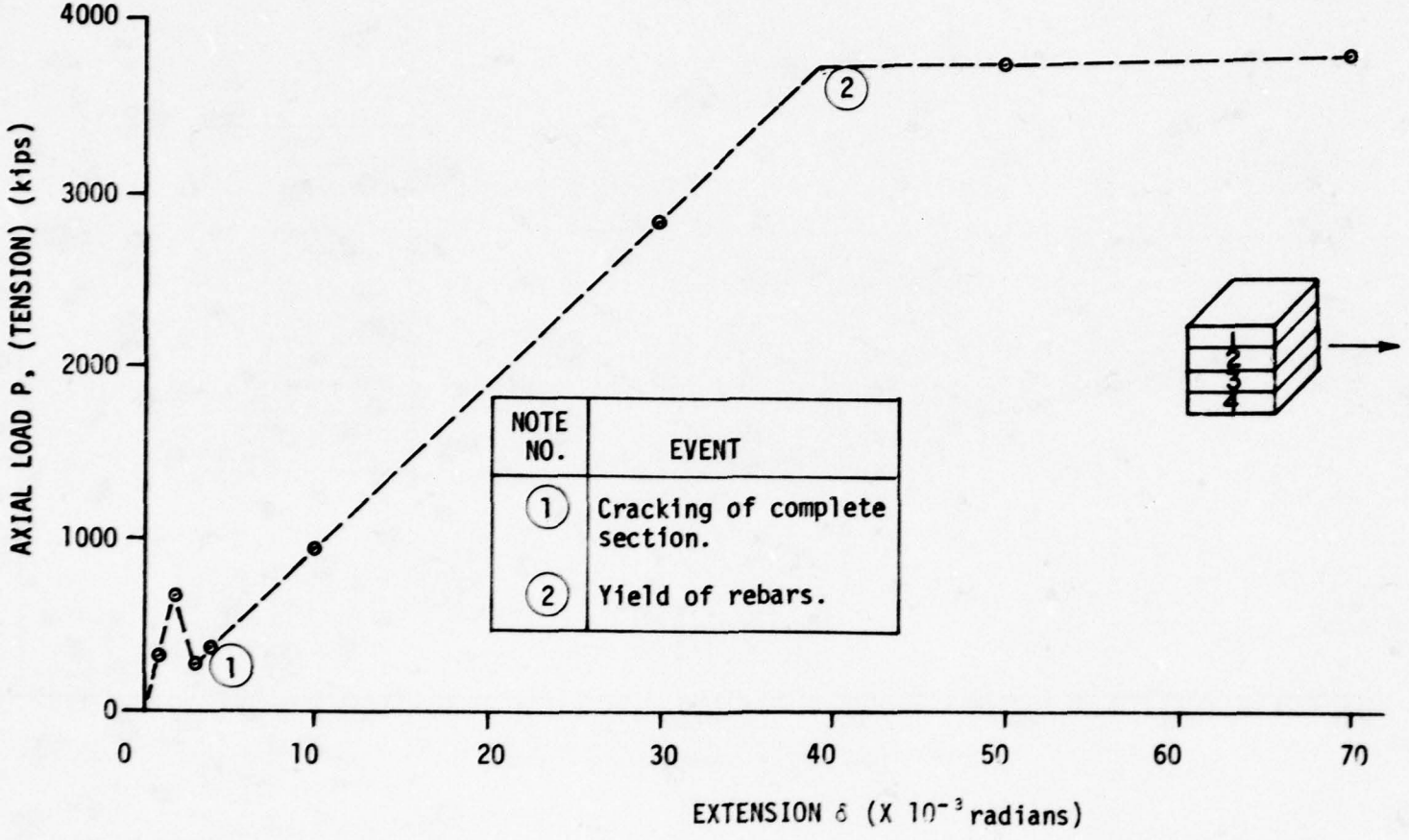

Figure 34.1 CRS #7 Pure Extension

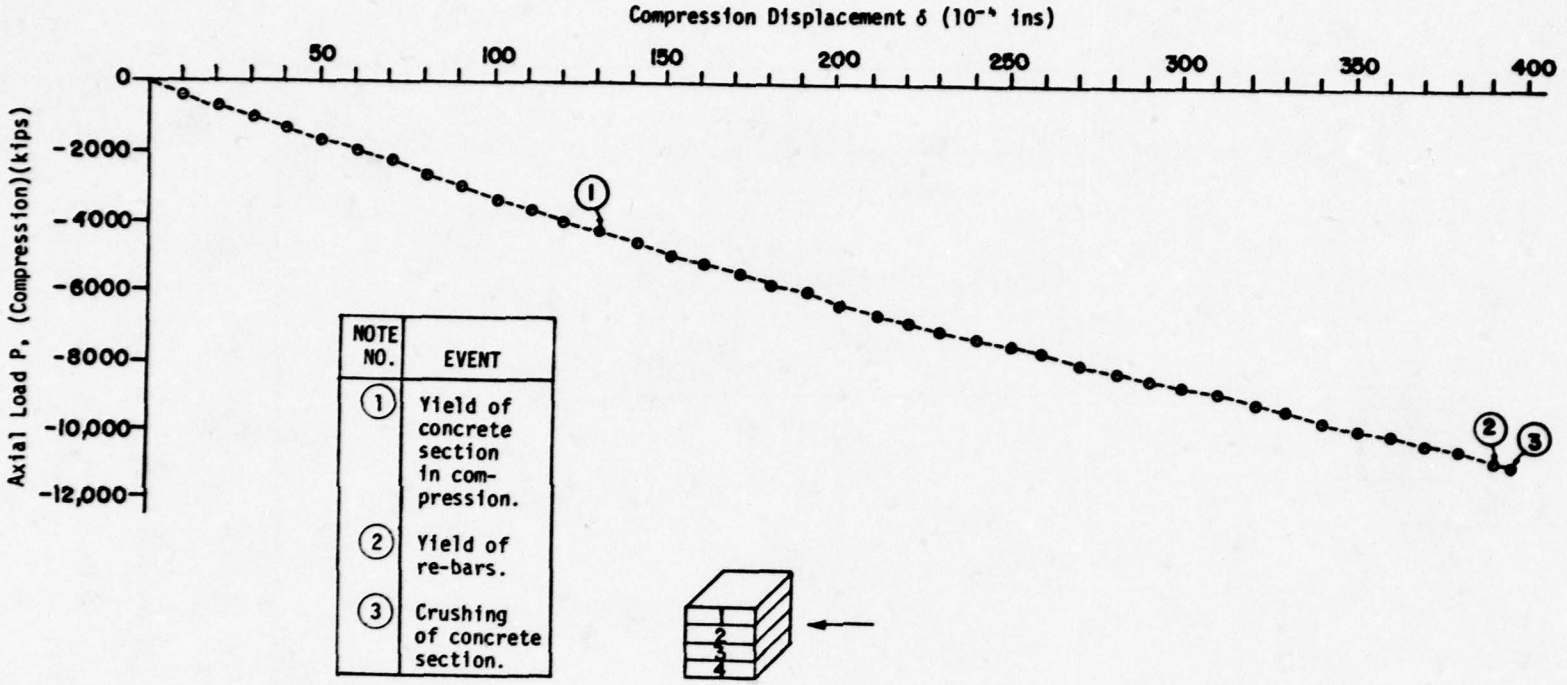

Figure 34.2 CRS #7 - Pure compression

The failure strength estimated by the analysis of CRS #4 is significantly higher than that of CRS #8 (Figure 35). A comparison with that of CRS #4.1 (Figure 38) shows a better resemblance between the two failure envelopes. The shape and magnitude of the two curves follow a close pattern.

Figures 36.1 through 36.7 indicate the M-θ and P-δ curves for this section. These curves also follow a close resemblance to those of CRS #4.1 (Figures 29.1 through 29.6). Modes of failure are also similar for various deformation patterns in both cases.

(7) Response Of CRS #11

It was decided to study the effect of the strength of concrete on the failure envelope. As an upper bound, concrete with an ultimate uniaxial compressive stress of 9.0 ksi was used with a longitudinal steel ratio of 2% at each face. The transverse reinforcement area used was 3.50 in^2. Since no experimental curves were available for such a high strength concrete, an analytical curve was used. Figure 37 shows the stress-strain curve as suggested by Saenz in the paper by Popovics (Ref. 7).

Figure 38 shows the failure curve of such an analysis. The figure indicates a capacity of the section when subjected to pure rotation to be less than that of CRS #3 with a lower strength concrete (Figure 23). The capacities of the section when subjected to

---

7. Popovics, S., "A Review of Stress-Strain Relationships for Concrete", Journal, American Concrete Institute, March, 1970.

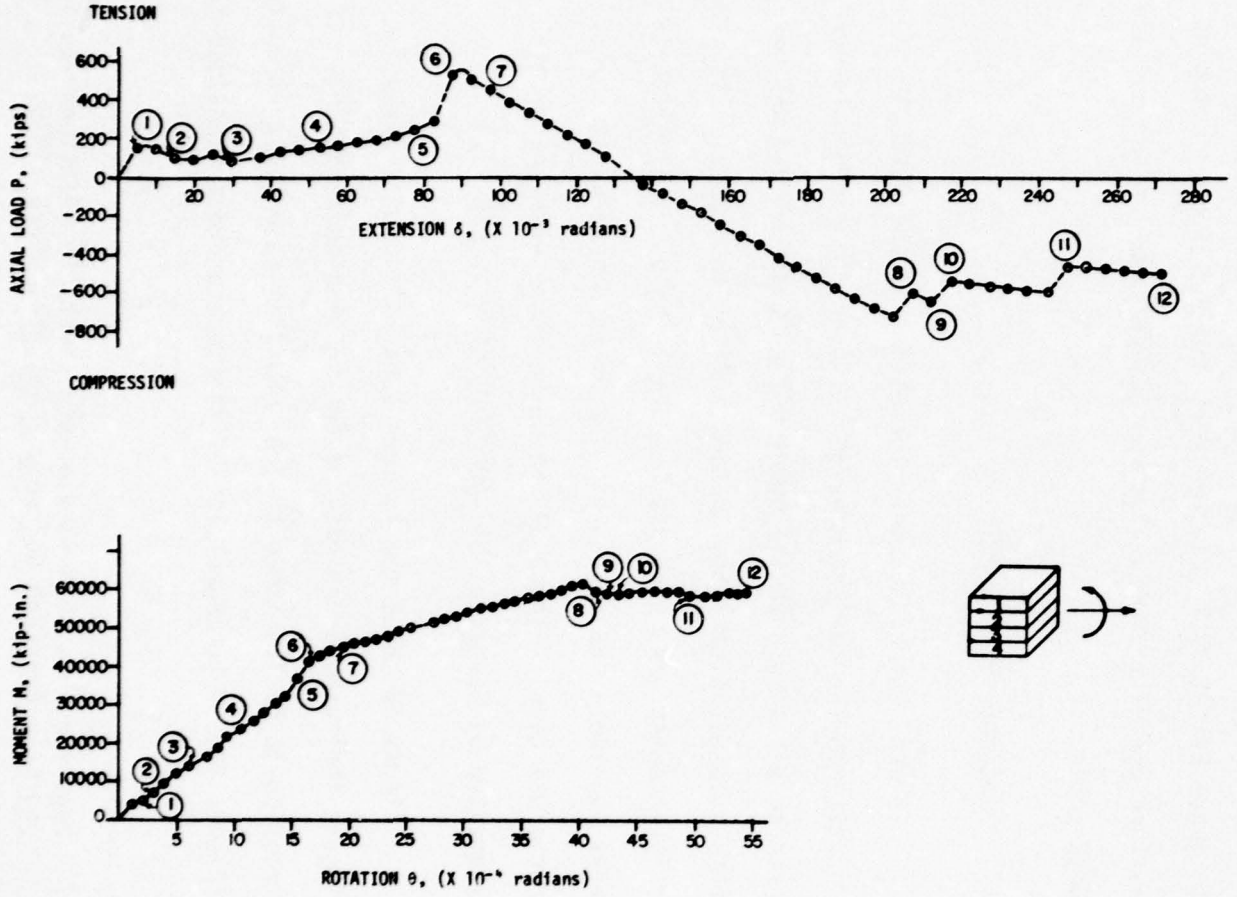

NOTE NO.	EVENT
(1)	Cracking of Elem #4.
(2)	Cracking of Elem #3.
(3)	Cracking of Elem #2.
(4)	Compressive yield of Elem #1 (4 nodes).
(5)	Complete yield of Elem #1 in compression.
(6)	Crushing of 3 nodes of Elem #1.
(7)	Yield of tensile reinforcement.
(8)	Crushing of 4 nodes of Elem #1.
(9)	Yield of longitudinal steel.
(10)	Crushing of 5 nodes of Elem #1.
(11)	Crushing of 6 nodes of Elem #1.
(12)	Failure of total section.

Figure 34.3 CRS #7 - Extension/Rotation = 5.0

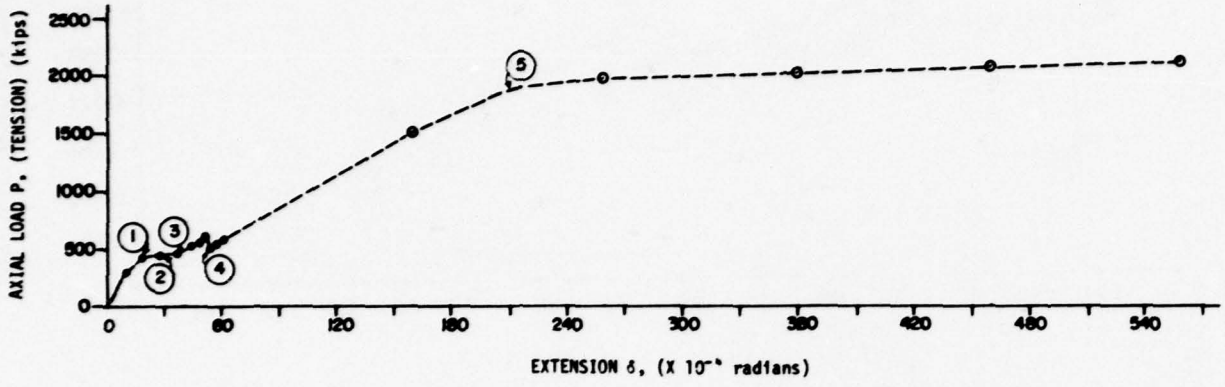

NOTE NO.	EVENT
1	Cracking of Elem #4.
2	Cracking of Elem #3.
3	Cracking of Elem #2 partial.
4	Cracking of total section.
5	First yield of bottom re-bars.

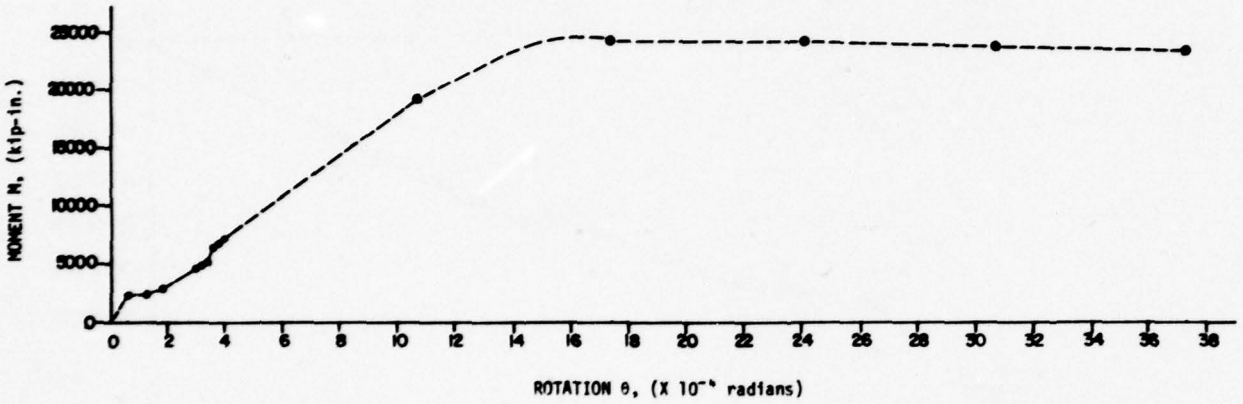

Figure 34.4 CRS #7 - Extension/Rotation = 15.0

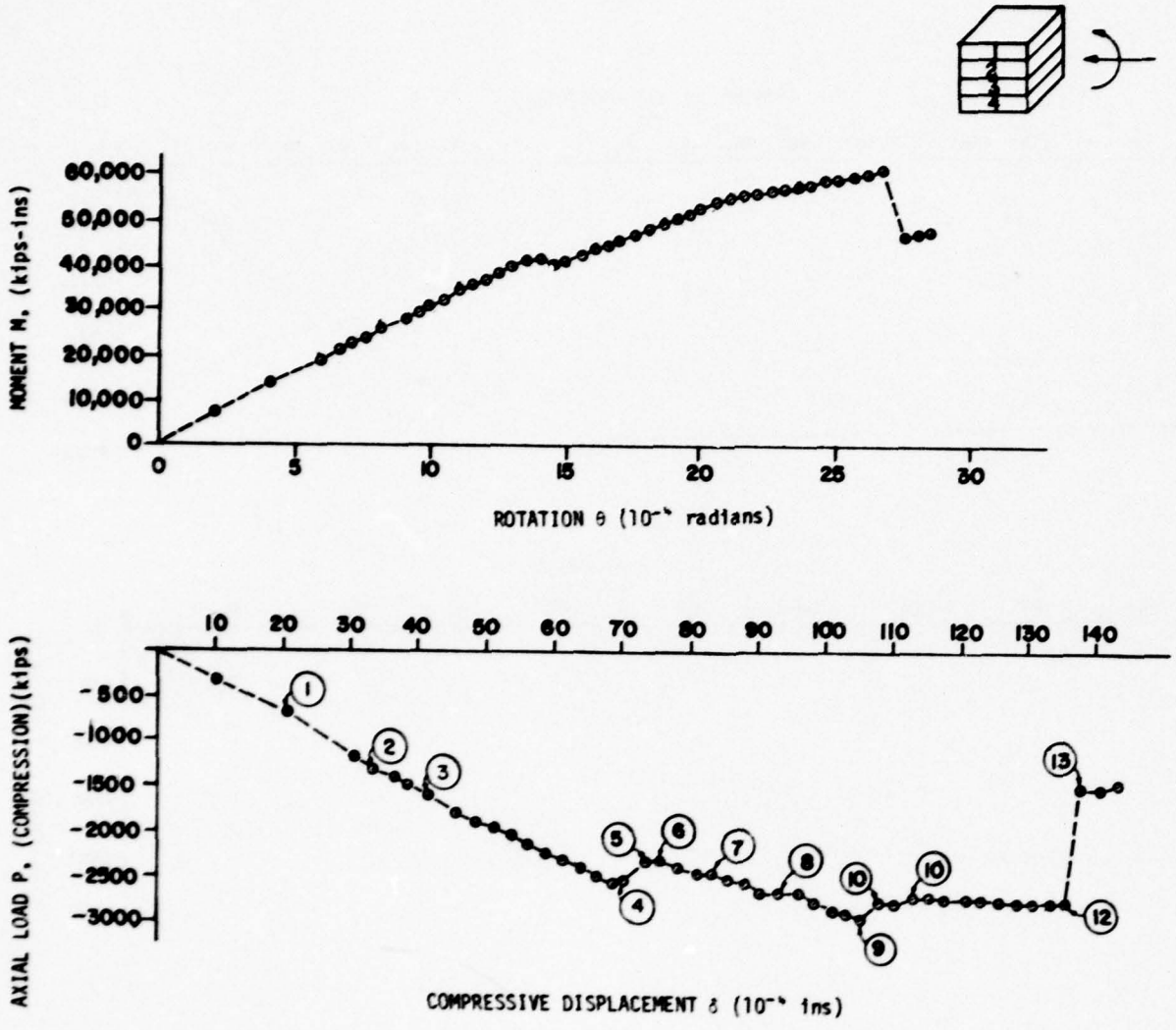

NOTE NO.	EVENT
1	Cracking of Elem #4.
2	Cracking of Elem #3 (2 nodes).
3	Yield of Elem #1 (total). Elem #2 (2 nodes). Elem #3 cracks 4 nodes. Elem #3 crushes 1 node.
4	Elem #1 crushes 2 nodes.
5	Elem #1 crushes 3 nodes.
6	Elem #2 crushes 1 node.
7	Elem #2 crushes 2 nodes.
8	Elem #3 crushes 2 nodes.
9	Top re-bars yield in compression.
10	Elem #2 crushes 4 nodes.
11	Elem #3 crushes 3 nodes.
12	Elem #3 crushes 4 nodes.
13	Failure of concrete section.

Figure 34.5 CRS #7 - Compression/Rotation = 5.0

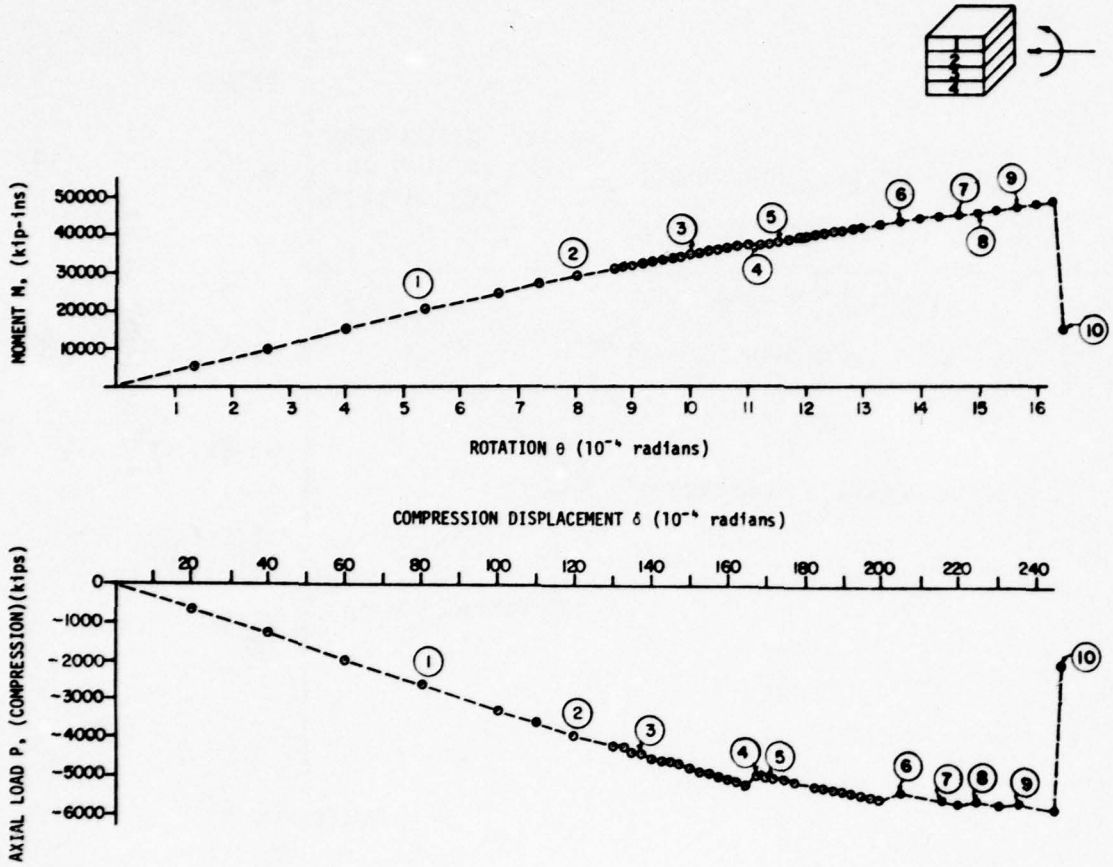

NOTE NO.	EVENT
1	Yield in compression of Elem #1 (total) and Elem #2 (6 nodes)
2	Yield in compression of Elems #3 and #4 (2 nodes each).
3	Complete yield in compression of concrete section.
4	Crushing of 2 nodes of Elem #2.
5	Crushing of 1 node of Elem #2.
6	Yield of top re-bars.
7	Crushing of Elem #3.
8	Crushing of Elem #3 (4 nodes).
9	Crushing of Elem #3 (5 nodes)
10	Yield of transverse steel occurs, the concrete section is crushed, failure of section assumed.

Figure 34.6 CRS #7 - Compression/Rotation = 15.0

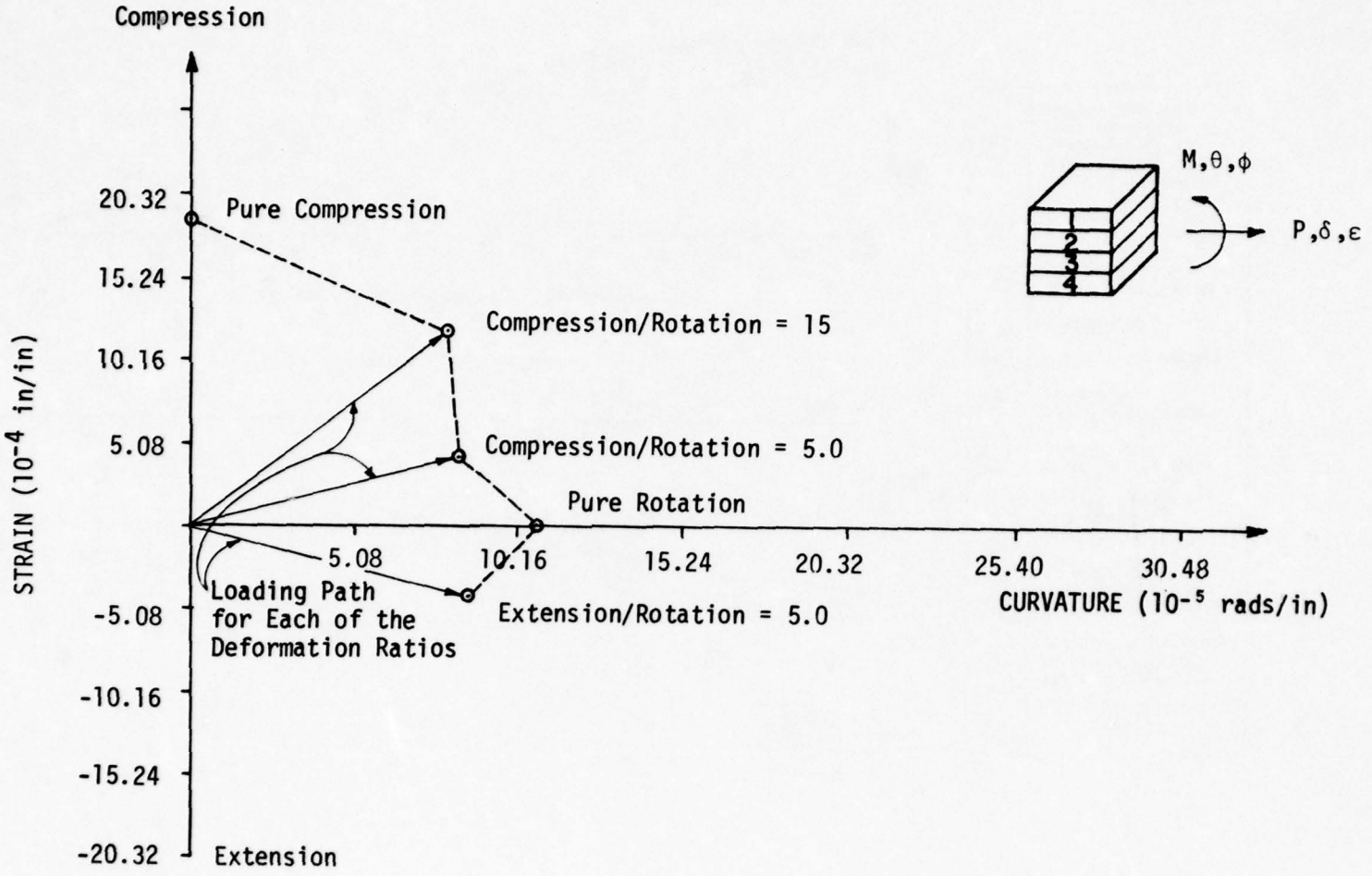

Figure 35 CRS #8 - Failure Envelope

NOTE NO.	EVENT
(1)	Concrete cracks completely.
(2)	Steel yields.

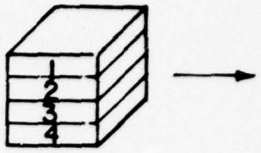

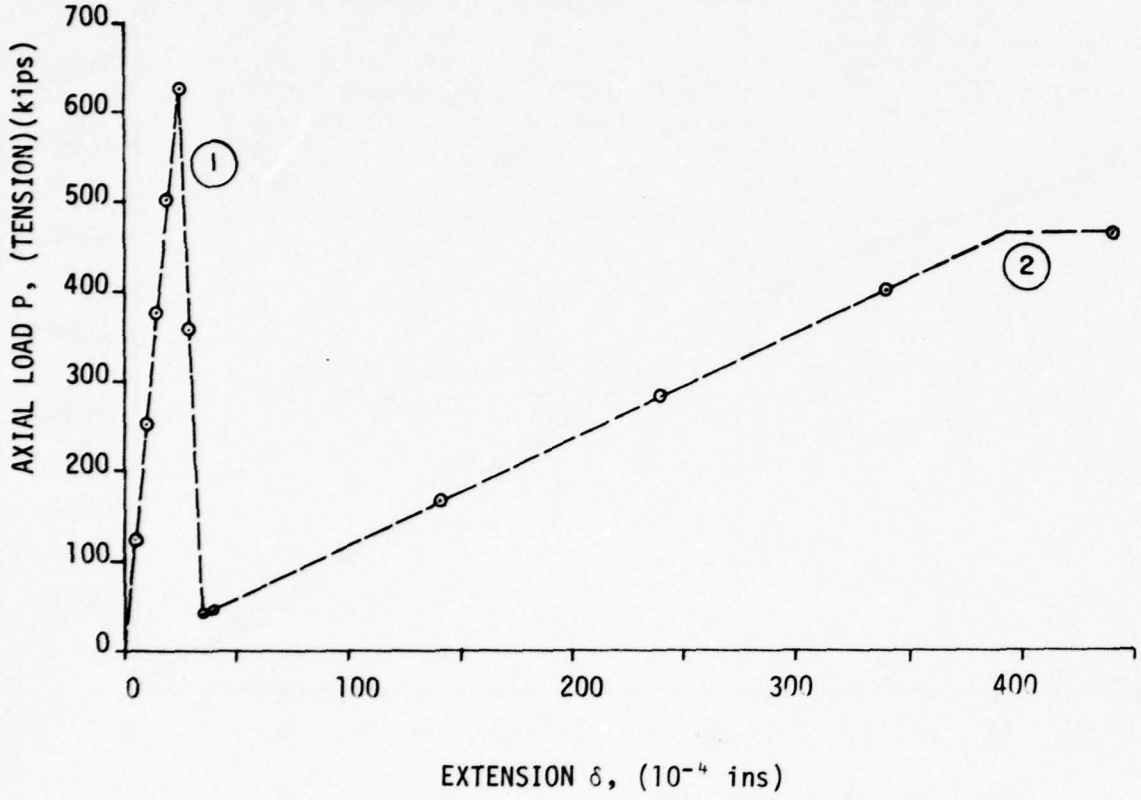

Figure 36.1 CRS #8 - Pure Extension

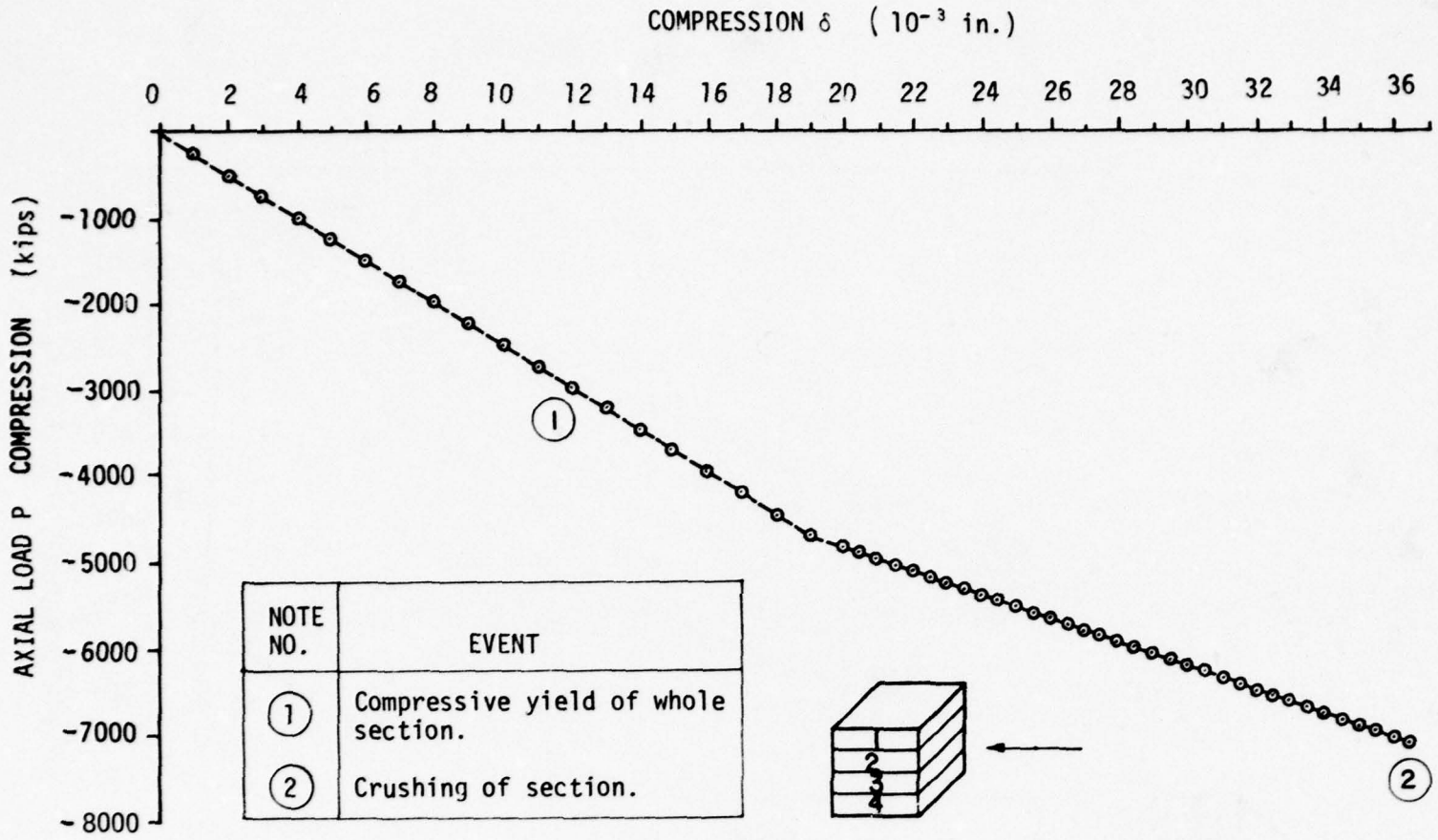

Figure 36.2 CRS #8 - Pure Compression

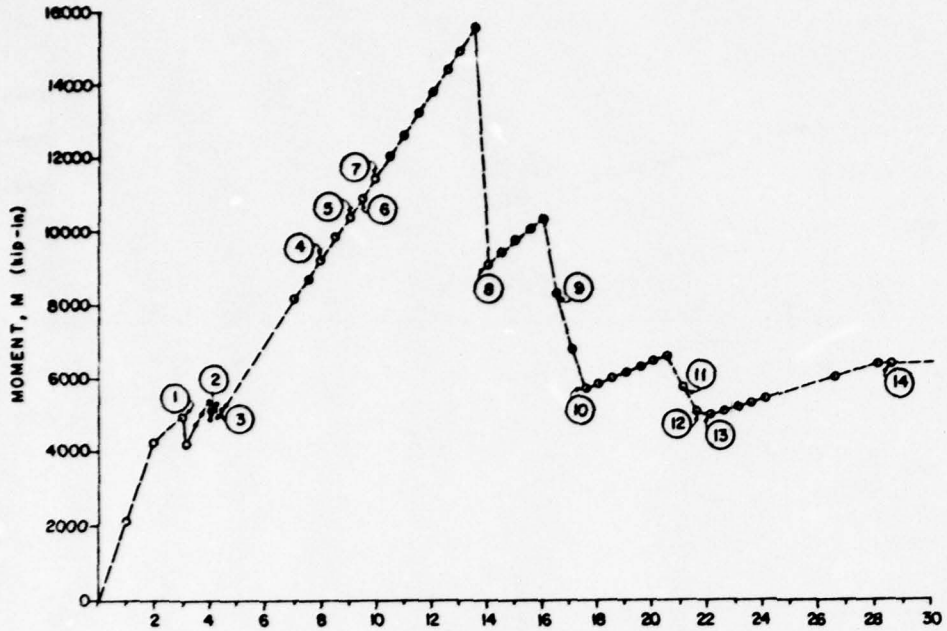

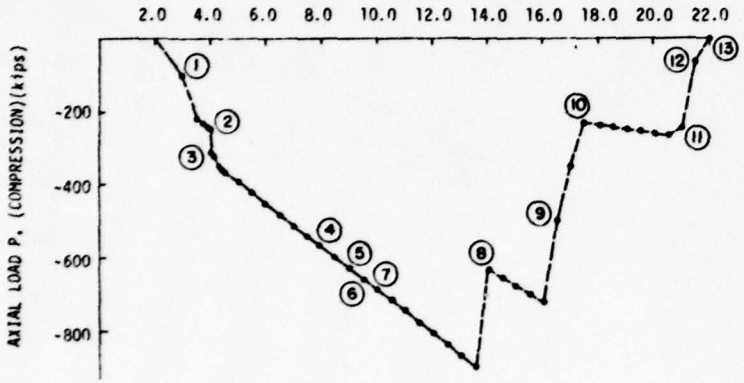

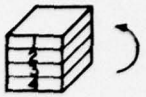

NOTE NO.	EVENT
(1)	Cracking of Elem #4.
(2)	Cracking of Elem #3 (4 nodes)
(3)	Cracking of Elem #3 (total).
(4)	Yield of Elem #1 (4 nodes).
(5)	Yield of Elem #1 (total).
(6)	Yield of Elem #2 (4 nodes).
(7)	Yield of Elem #2 (total).
(8)	Crushing of 4 nodes of Elem #1.
(9)	Crushing of Elem #1 (total).
(10)	Crushing of Elem #2 (2 nodes).
(11)	Crushing of Elem #2 (4 nodes).
(12)	Crushing of Elem #2 (5 nodes).
(13)	Crushing of Elem #2 (total).
(14)	Yield of re-bars.

Figure 36.3 CRS #8 - Pure Rotation

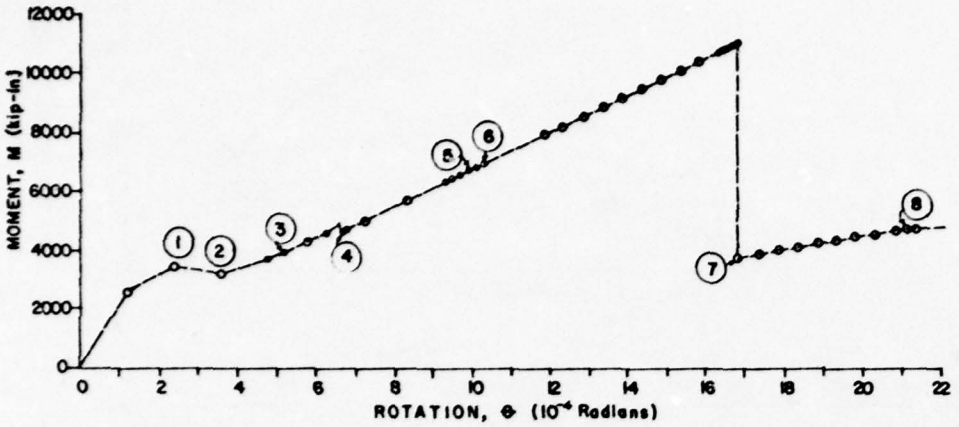

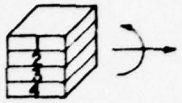

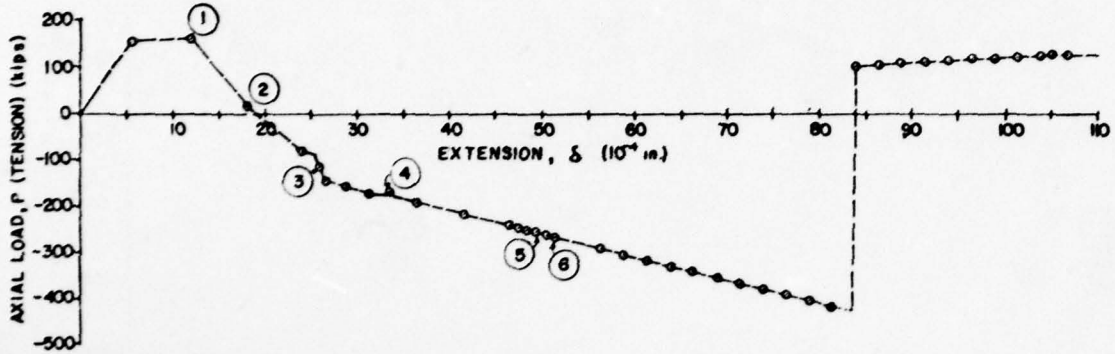

NOTE NO.	EVENT
1	Cracking of Elem #4.
2	Cracking of Elem #3.
3	Cracking of 4 nodes of Elem #2.
4	Complete cracking of Elem #2.
5	Compressive yield of 4 nodes of Elem #1.
6	Complete yield of Elem #1.
7	Crushing of Elem #1 in tension-compression.
8	Yield of bottom re-bars.

Figure 36.4 CRS #8 - Extension/Rotation = 5.0

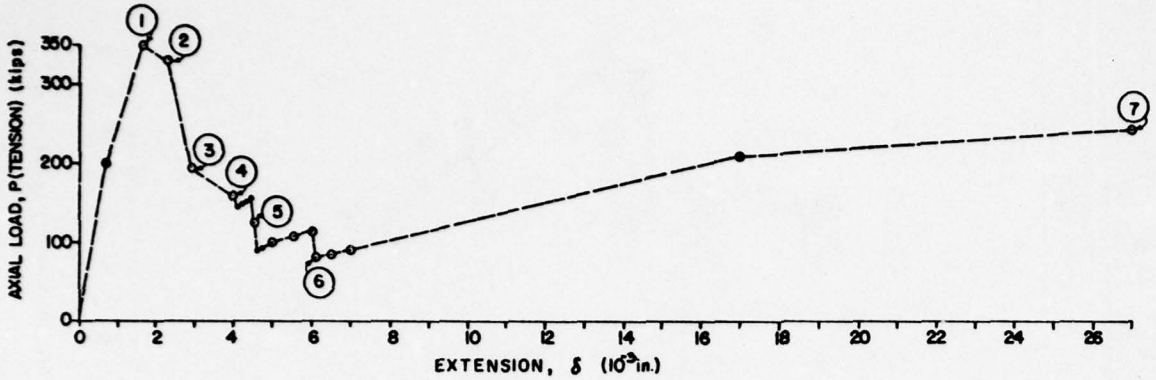

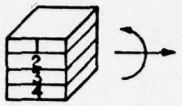

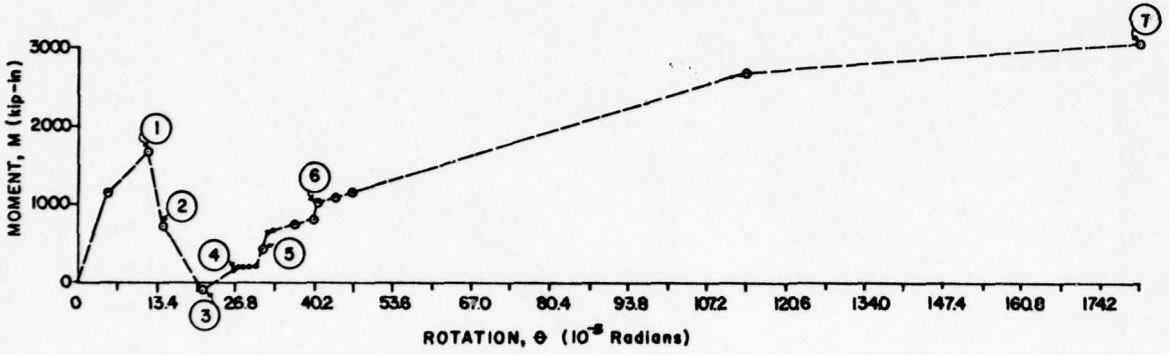

NOTE NO.	EVENT
1	Cracking of 4 nodes of Elem #4.
2	Complete cracking of Elem #4 and cracking of 4 nodes of Elem #3.
3	Complete cracking of Elem #3 and 4 nodes of Elem #2.
4	Complete cracking of Elem #2.
5	Cracking of 4 nodes of Elem #1.
6	Complete cracking of Elem. #1
7	Yield of bottom re-bars.

Figure 36.5 CRS #8 - Extension/Rotation = 15.0

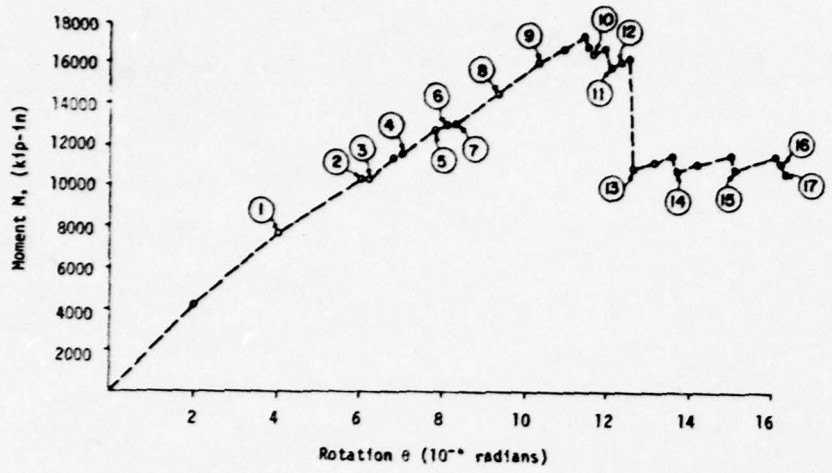

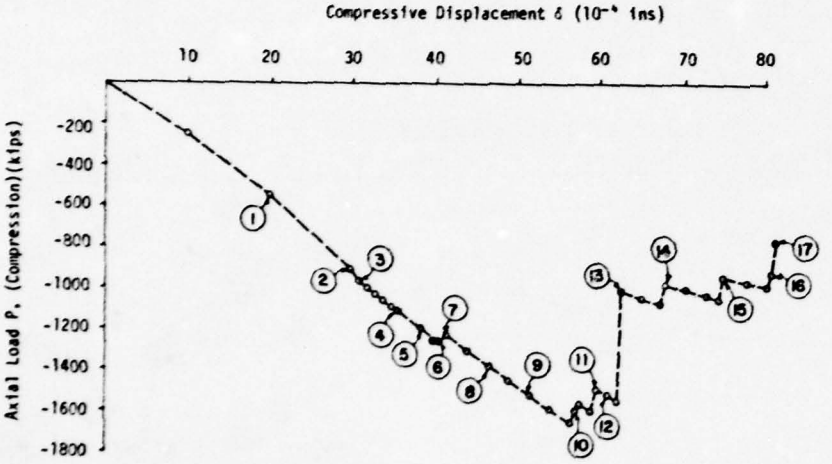

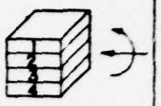

NOTE NO.	EVENT
(1)	Cracking of Element #4 (4 nodes).
(2)	Cracking of Element #4 complete.
(3)	Yield of Element #1 in tension-compression (4 nodes).
(4)	Complete yield of Element #1.
(5)	Cracking of Element #3 (4 nodes).
(6)	Yield of Element #2 (3 nodes). Element #3 (1 node). Cracking of Element #3 (5 nodes).
(7)	Cracking of Element #3 (7 nodes).
(8)	Yield of Element #2 (4 nodes).
(9)	Complete yield of Element #2.
(10)	Crushing of Element #1 in tension-compression (1 node).
(11)	Crushing of Element #1 in tension-compression (2 nodes).
(12)	Yield of Element #3 in tension-compression (2 nodes).
(13)	Crushing of Element #1 in tension-compression (5 nodes). Crushing of Element #2 in tension-compression (2 nodes).

NOTE NO.	EVENT
(14)	Crushing of Element #2 in tension-compression (3 nodes).
(15)	Crushing of Element #2 in tension-compression (4 nodes).
(16)	Crushing of Element #2 in tension-compression (5 nodes).
(17)	Failure of Element #2. Yield of transverse reinforcement.

Figure 36.6 CRS #8 - Compression/Rotation = 5.0

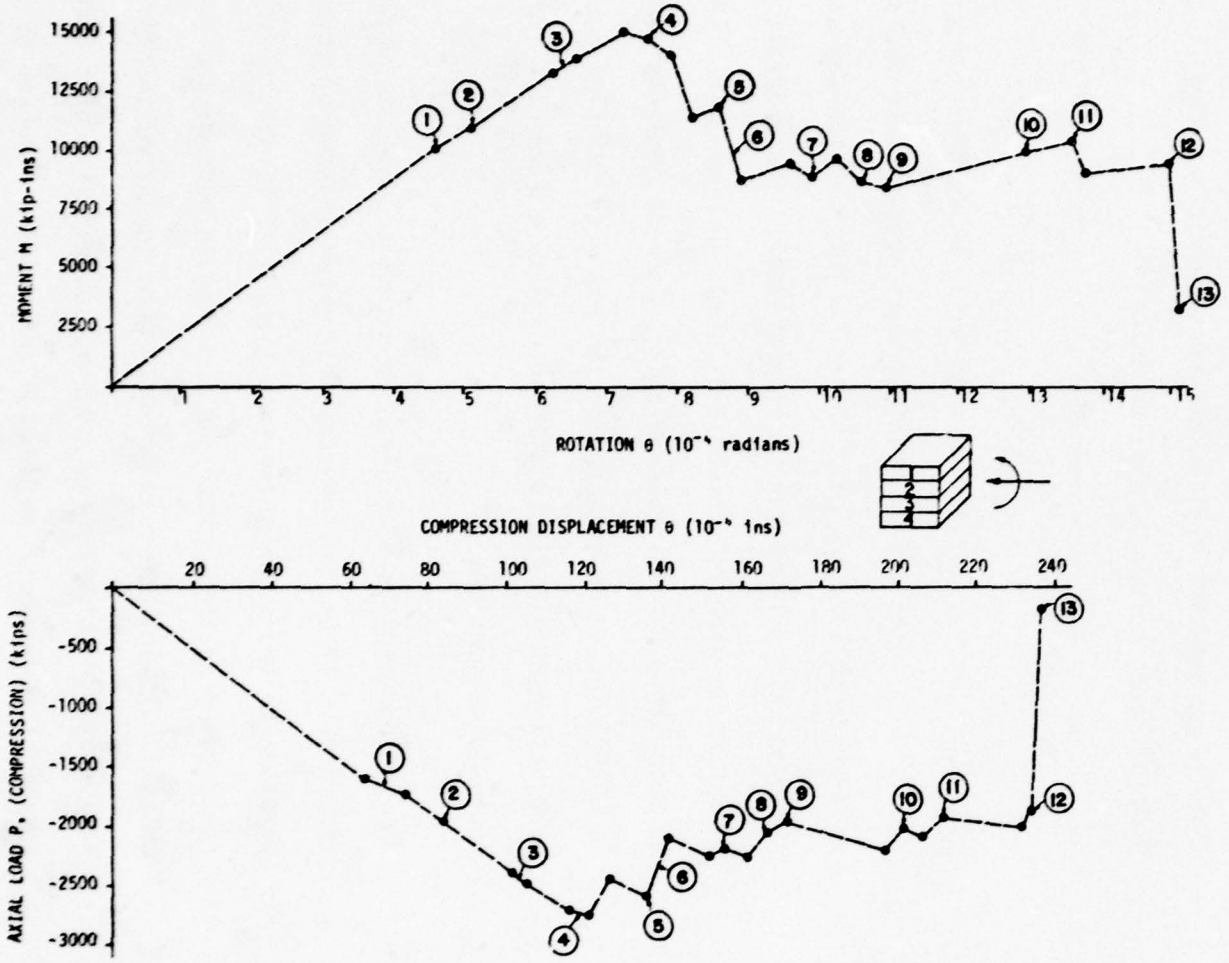

NOTE NO.	EVENT
(1)	Yielding of Elem #1.
(2)	Yielding of Elem #2.
(3)	Yielding of Elem #3.
(4)	Crushing of Elem #1 (4 nodes).
(5)	Yielding of Elem #4.
(6)	Crushing of Elem #2 (4 nodes).
(7)	Crushing of Elem #2 (5 nodes).
(8)	Crushing of Elem #2 (7 nodes).
(9)	Crushing of Elem #2 (total).
(10)	Crushing of Elem #3 (2 nodes).
(11)	Crushing of Elem #3 (3 nodes). Yield of top re-bars in compression.
(12)	Crushing of Elem #3 (5 nodes).
(13)	Failure of section.

Figure 36.7 CRS #8 - Compression/Rotation = 15.0

deformation ratios of extension/rotation of 5, compression/rotation of 5, compression/rotation of 15, and pure compression are higher than that of CRS #3 (Figure 19). Possibly a more refined eight layer mesh would result in a better estimation of the capacity when subjected to pure rotation.

Figures 39.1 through 39.7 shows the response curves ($M-\theta$ and $P-\delta$ curves) for various deformation ratios. Again, the general form of these curves is similar to CRS #3.

(8) Response Of CRS #11.1

CRS #11.1 was a section with uniaxial compressive strength of 9.3 ksi, 2% longitudinal reinforcement at each face and a transverse reinforcement area A_{sh} of 3.50 ins^2. This section was analyzed using a refined eight layer finite element mesh. The uniaxial stress-strain curve used for concrete is shown in Figure 40. It should be noted that the ultimate uniaxial concrete compressive strain used is 0.0045 in/in, as compared to the ultimate uniaxial concrete compressive strain of 0.003 in/in used to analyze all the other rectangular sections.

Failure envelope obtained from such an analysis is shown in Figure 41. It can be seen that the general shape of this failure envelope in the compression zone is similar to that of the other rectangular section. Note the increase in deformation strength of CRS #11.1 in the compression zone (when subjected to deformation ratios of pure compression, compression/rotation of 5.0, pure rotation) as compared to similar deformation strength of sections

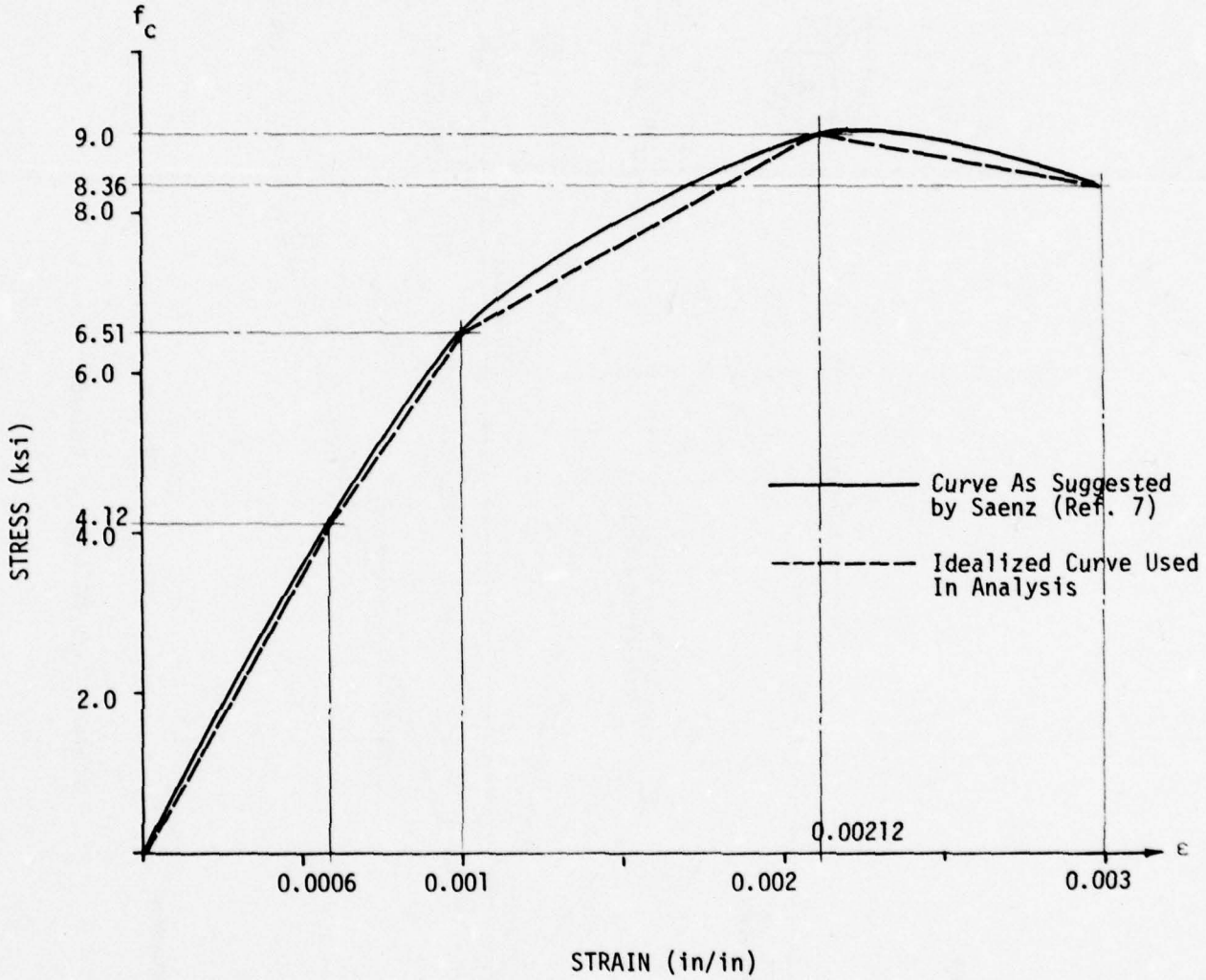

Ref. 7: Popovics, S., "A Review of Stress-Strain Relationships for Concrete," Journal, American Concrete Institute, March, 1970.

Figure 37 Stress-Strain Curve for Concrete. Ultimate Stress = 9.0 ksi

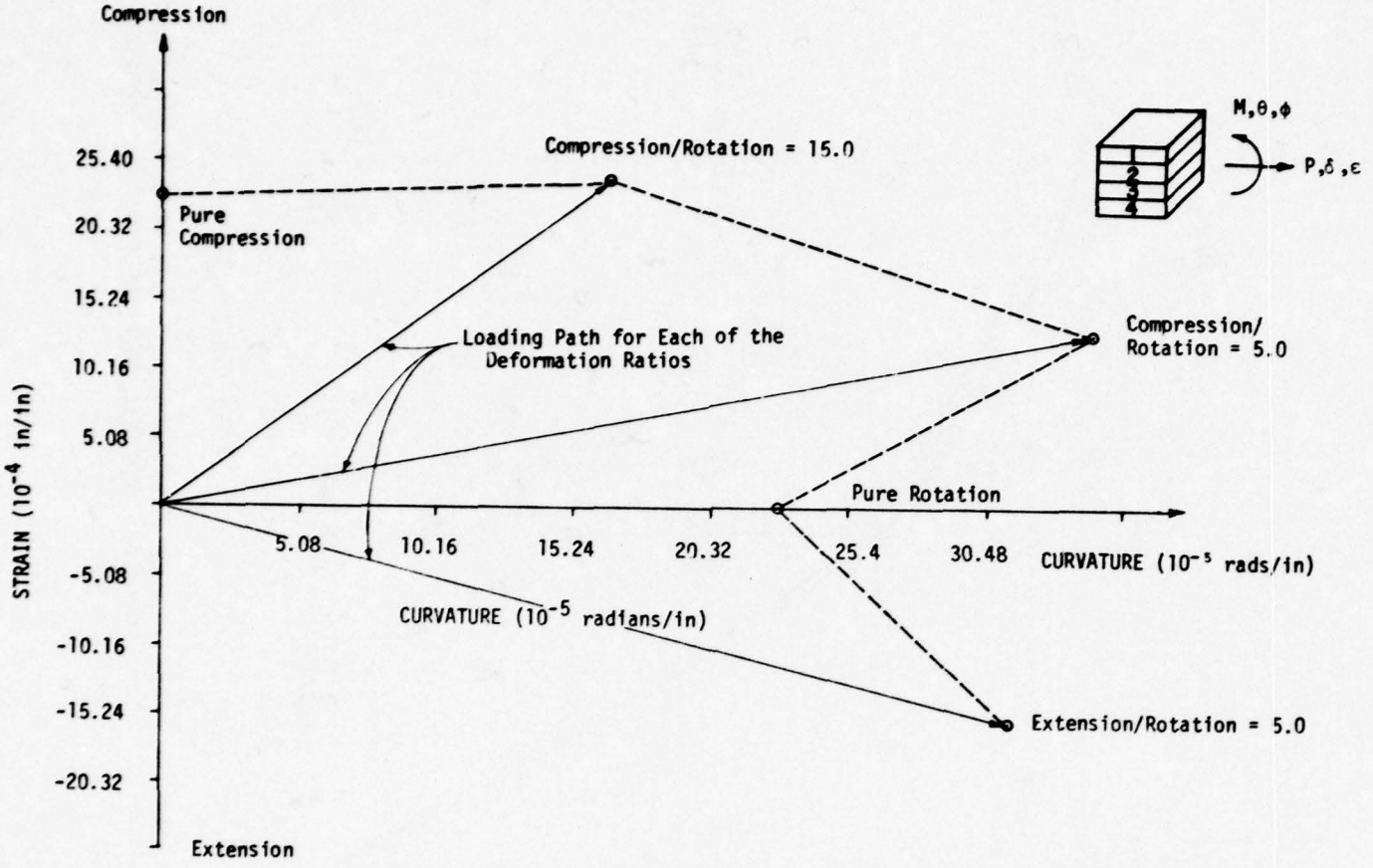

Figure 38 CRS #11 - Failure Envelope

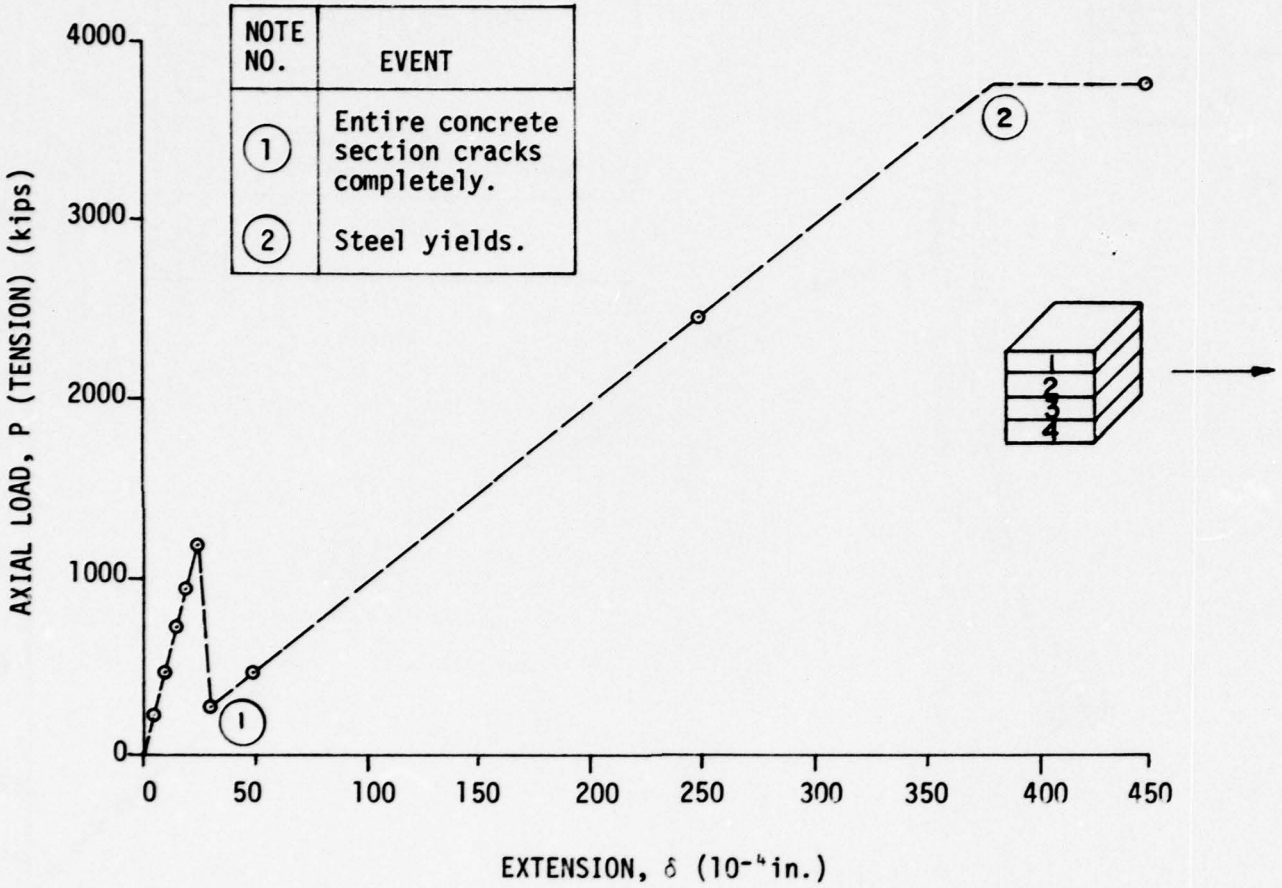

Figure 39.1 CRS #11 - Pure Extension

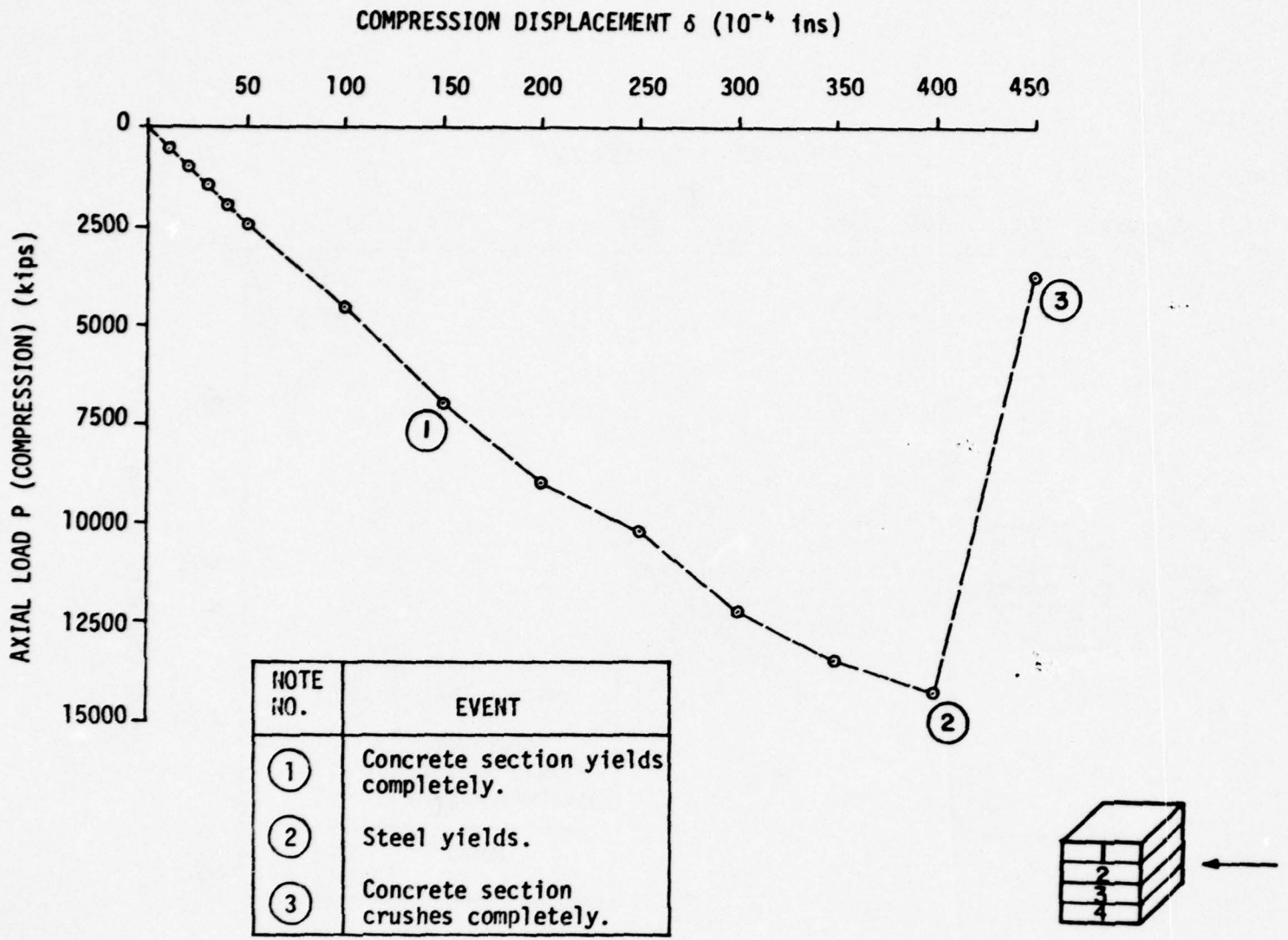

Figure 39.2 CRS #11 - Pure Compression

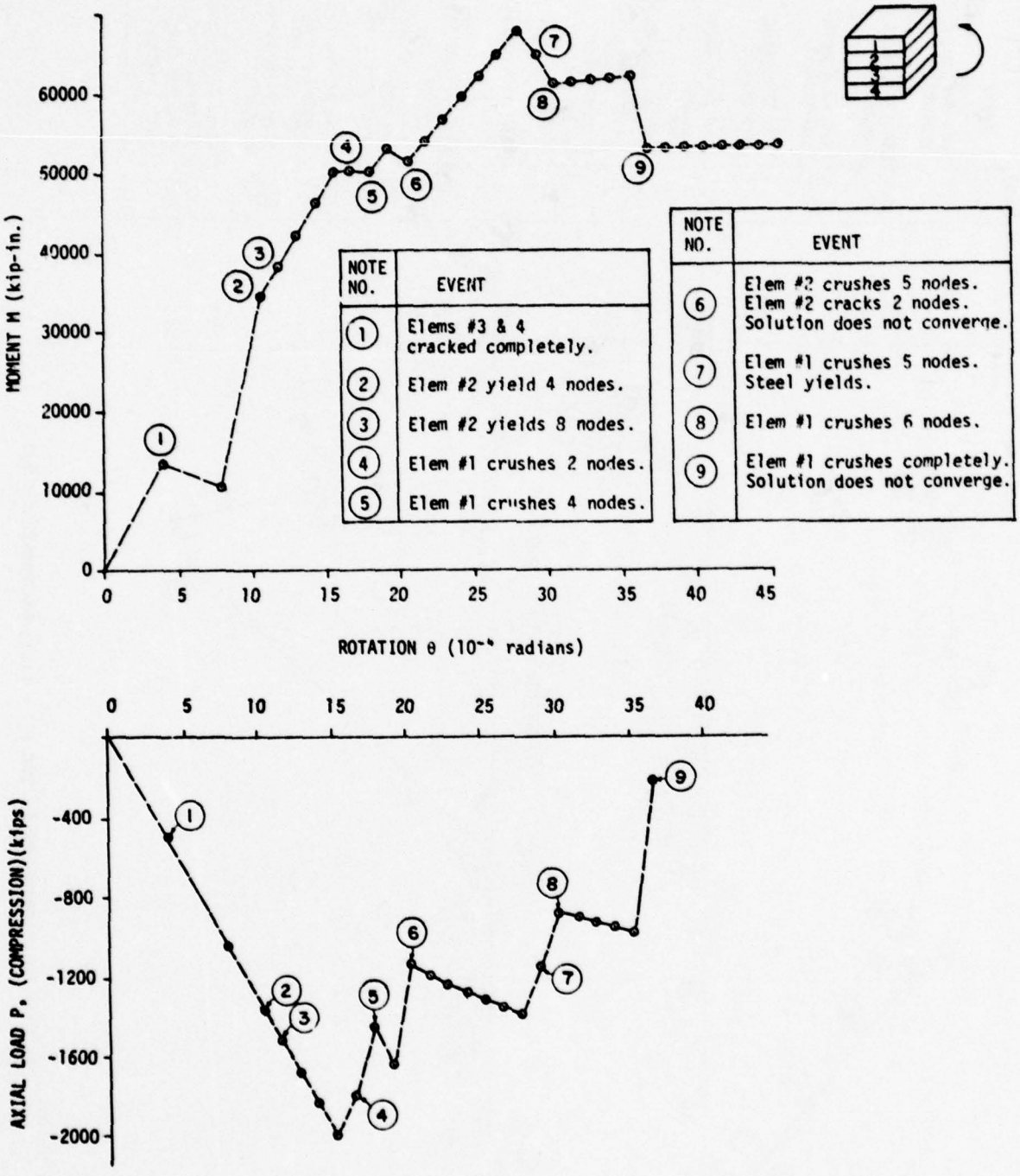

Figure 39.3 CRS #11 - Pure Rotation

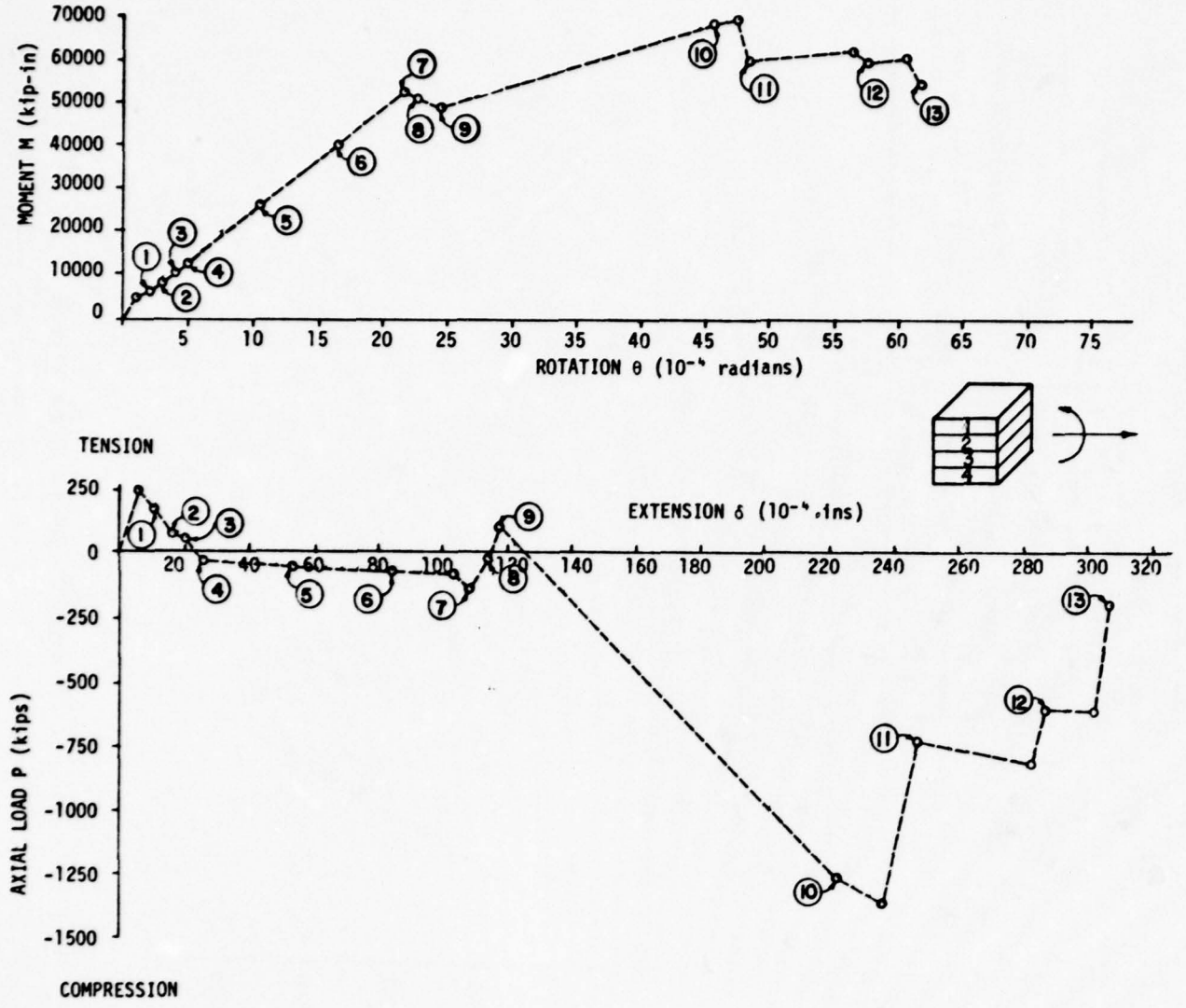

NOTE NO.	EVENT
1	Elem #4 cracks completely.
2	Elem #3 cracks 6 nodes.
3	Elem #3 cracks completely.
4	Elem #2 cracks completely.
5	Elem #1 yields 4 nodes.
6	Elem #1 yields 8 nodes.
7	Bottom rebar yields in tension.
8	Elem #1 crushes 1 node.
9	Elem #1 crushes 2 nodes.
10	Top rebar yields in compression.
11	Elem #1 crushes 5 nodes.
12	Elem #1 crushes 6 nodes.
13	Elem #1 crushes 7 nodes. Solution does not converge.

Figure 39.4 CRS #11 - Extension/Rotation = 5.0

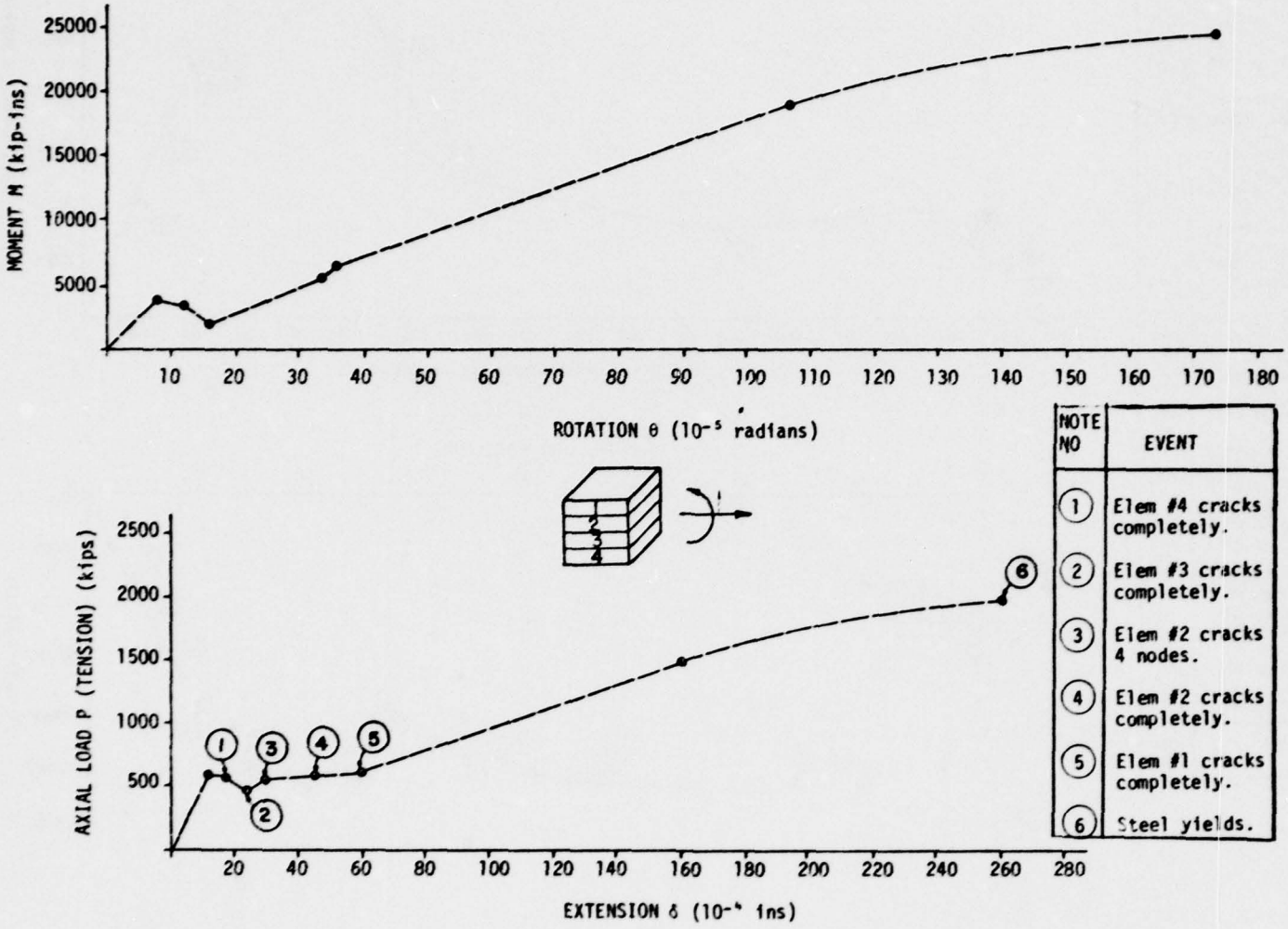

Figure 39.5 CRS #11 - Extension/Rotation = 15.0

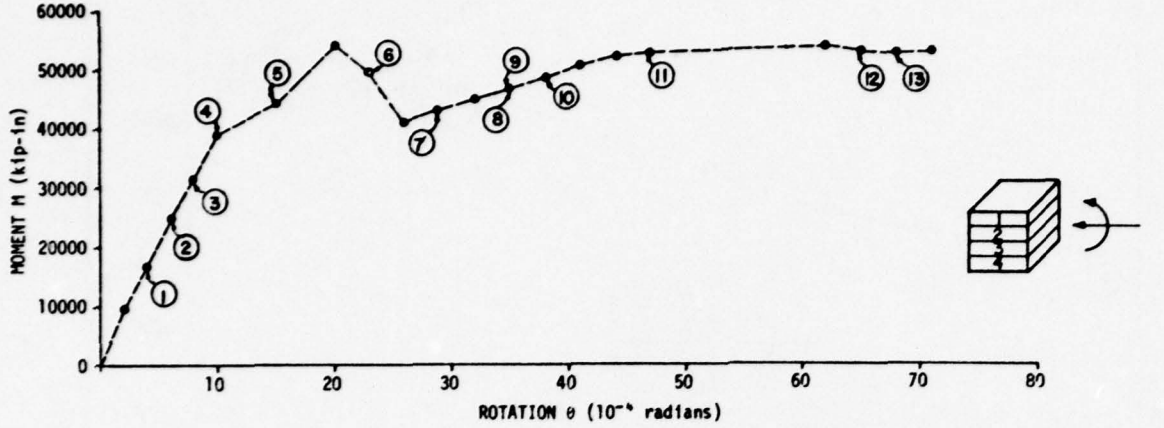

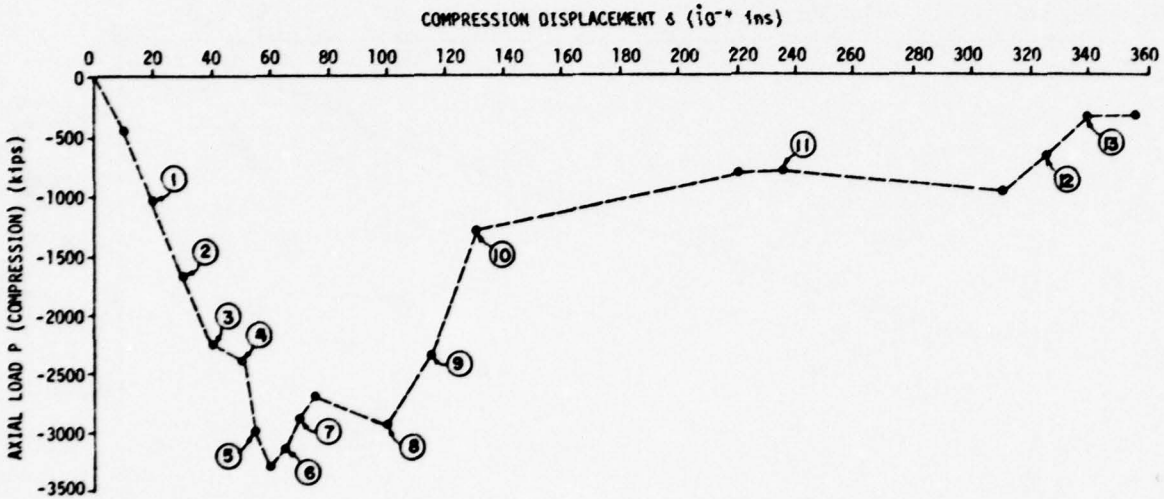

NOTE NO.	EVENT
(1)	Elem #4 cracks 4 nodes.
(2)	Elem #4 cracks completely.
(3)	Elem #1 yields 4 nodes. Elem #3 cracks 5 nodes. Elem #3 crushes 1 node. Solution does not converge.
(4)	Elem #1 yields 4 nodes. Elem #2 yields 1 node.
(5)	Elem #1 yields 6 nodes. Elem #2 yields 2 nodes. Elem #3 yields 1 node.
(6)	Elem #1 crushes 2 nodes.
(7)	Elem #1 crushes 4 nodes.
(8)	Elem #2 crushes 4 nodes. Elem #1 yields 2 nodes.
(9)	Top rebar yields in compression. Elem #1 crushes 6 nodes. Solution does not converge.
(10)	Elem #1 crushes completely. Elem #2 crushes 6 nodes. Elem #3 crushes 2 nodes.
(11)	Bottom rebar yields in tension.
(12)	Elem #1 crushes 7 nodes.
(13)	Elem #1 crushes completely.

Figure 39.6 CRS #11 - Compression/Rotation = 5.0

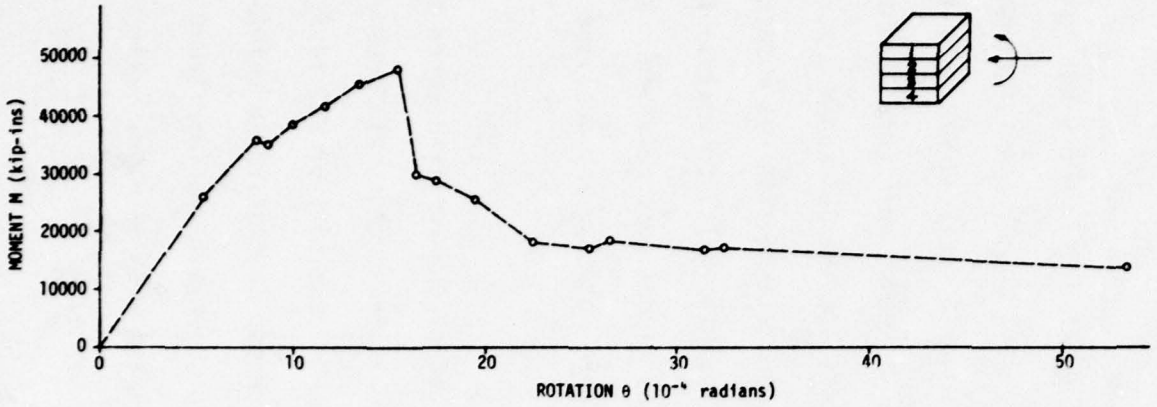

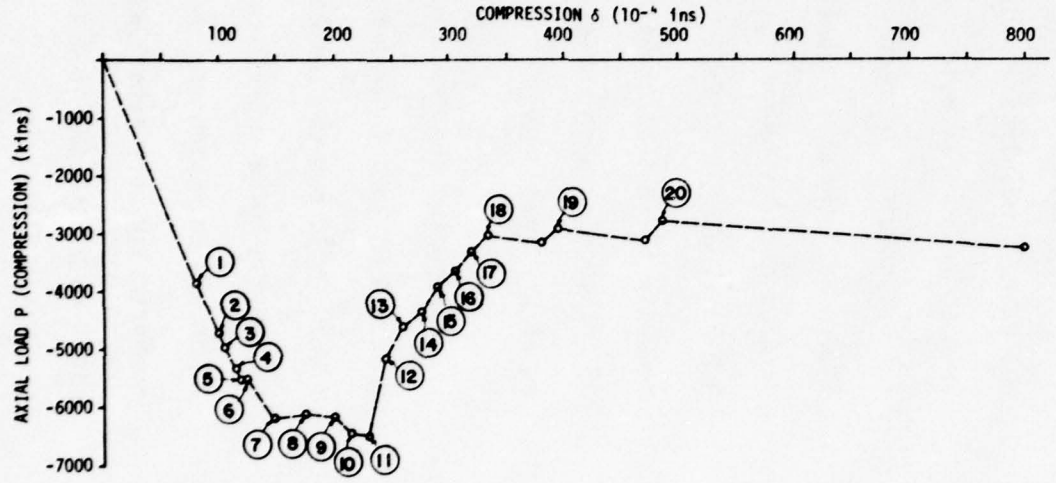

NOTE NO.	EVENT
1	Elem #1 yields 8 nodes.
2	Elem #2 yields 4 nodes.
3	Elem #2 yields 8 nodes.
4	Elem #3 yields 3 nodes.
5	Elem #3 yields 6 nodes. Elem #4 yields 1 node.
6	Elem #1 crushes 1 node.
7	Elem #1 crushes 2 nodes.
8	Elem #2 crushes 4 nodes. Elem #4 yields 4 nodes.
9	Elem #3 crushes 3 nodes.
10	Elem #4 yields 8 nodes. Top rebar yields in compression.
11	Elem #3 crushes 4 nodes.
12	Elem #1 crushes 7 nodes. Elem #3 crushes 5 nodes. Solution does not converge.
13	Elem #3 crushes 6 nodes. Elem #4 crushes 1 node. Solution does not converge.
14	Solution does not converge. Elem #1 crushes completely.
15	Elem #2 crushes 5 nodes. Elem #3 crushes 7 nodes.
16	Elem #2 crushes 6 nodes.
17	Elem #2 crushes 7 nodes. Elem #4 crushes 2 nodes. Solution does not converge.
18	Elem #2 crushes completely.
19	Elem #4 crushes 4 nodes.
20	Elem #3 crushes completely.

Figure 39.7 CRS #11 - Compression/Rotation = 15.0

with lower strength concrete (CRS #3, Figure 23; CRS #7, Figure 33). This increased deformation strength is due to the higher uniaxial ultimate compressive strain of 0.0045 in/in used to analyze CRS #11.1. Figure 42.1 through 42.6 indicate the response of CRS #11.1 when subjected to various deformation ratios.

(9) Response Of CRS #4.2

CRS #4 (confined rectangular section, f'_c = 5.0 ksi, p = p' = 1/4%) was reanalyzed using a higher area of transverse reinforcement. The area of transverse reinforcement used in analysis was 3.50 in^2. Failure envelope of such a section is shown in Figure 43 while Figure 44.1 through Figure 44.7 indicate the P-δ and M-θ curves for various deformation ratios. The concrete section was modeled as 3-D brick elements (four layer mesh, Figure 16) to analyze the response for all deformation ratios except pure rotation. Response of the section when subjected to pure rotation was analyzed using an eight layer mesh.

Comparing the failure envelopes of CRS #4 (transverse reinforcement = 0.60 in^2) to that of CRS #4.2 (transverse reinforcement = 3.50 in^2), one can observe a higher ductility of CRS #4.2, a phenomenon to be expected with increase in transverse reinforcement. It should be mentioned, that the problem using a four layer mesh is numberically very sensitive. Analysis with an eight layer mesh might have resulted in a smoother curve.

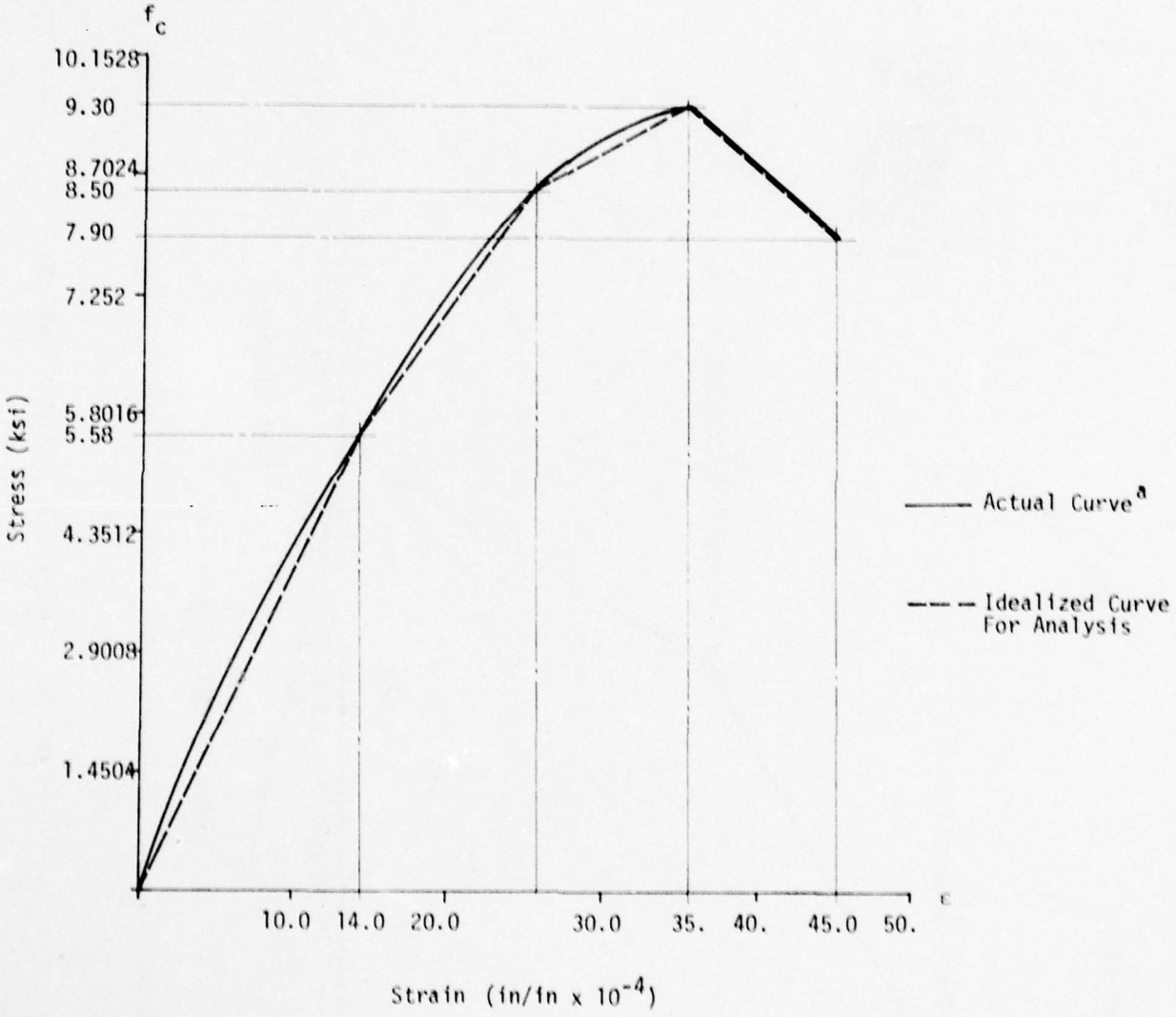

[a] Curve given by Air Force Weapons Laboratory (AFWL)

Figure 40 Stress Strain Curve for Concrete
Ultimate Stress = 9.3 ksi

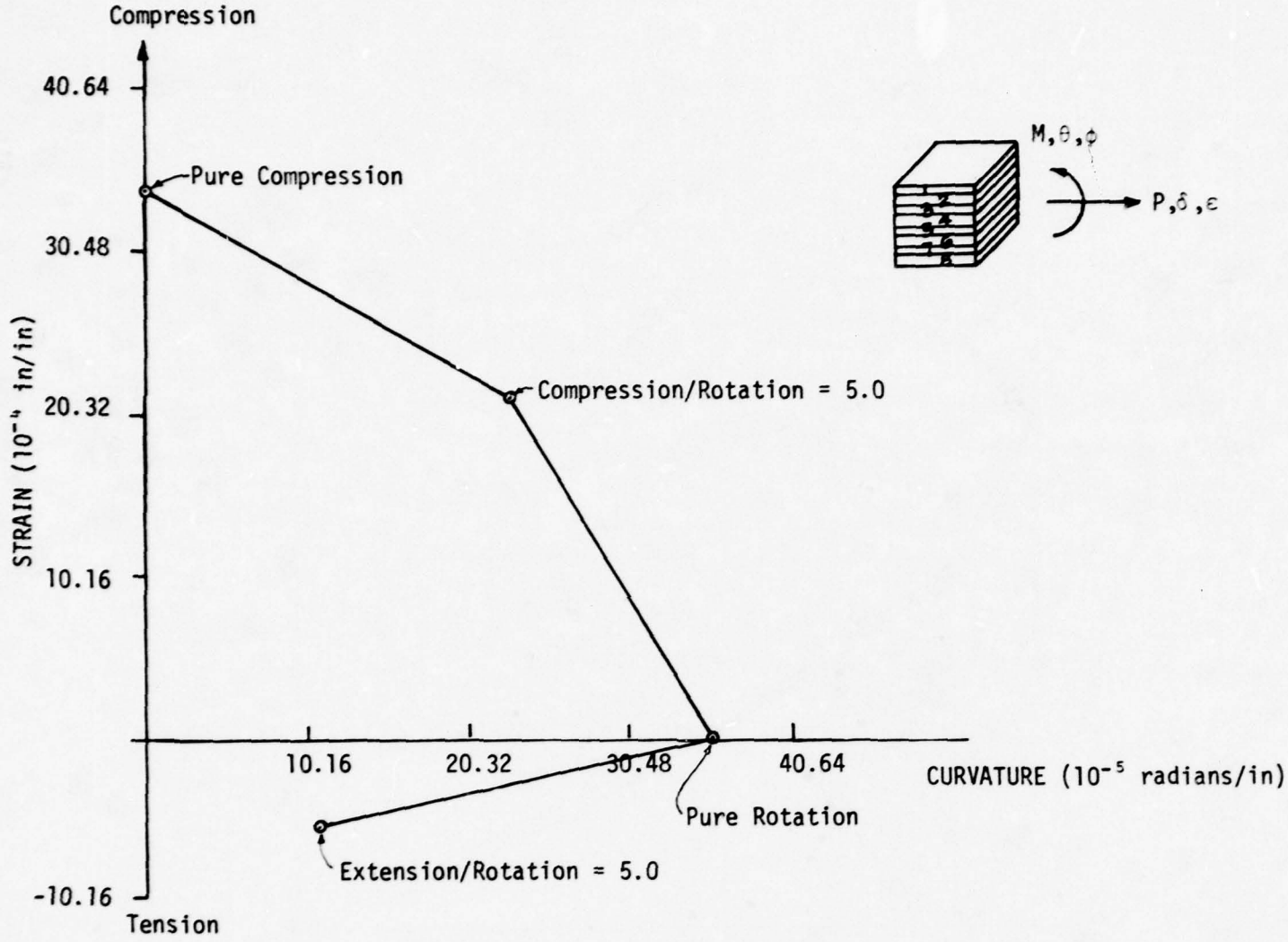

Figure 41 CRS #11.1 Failure Envelope

NOTE NO.	EVENT
(1)	Cracking of complete section.
(2)	Yield of re-bars.

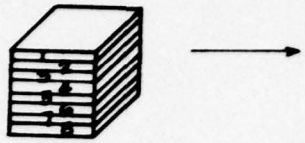

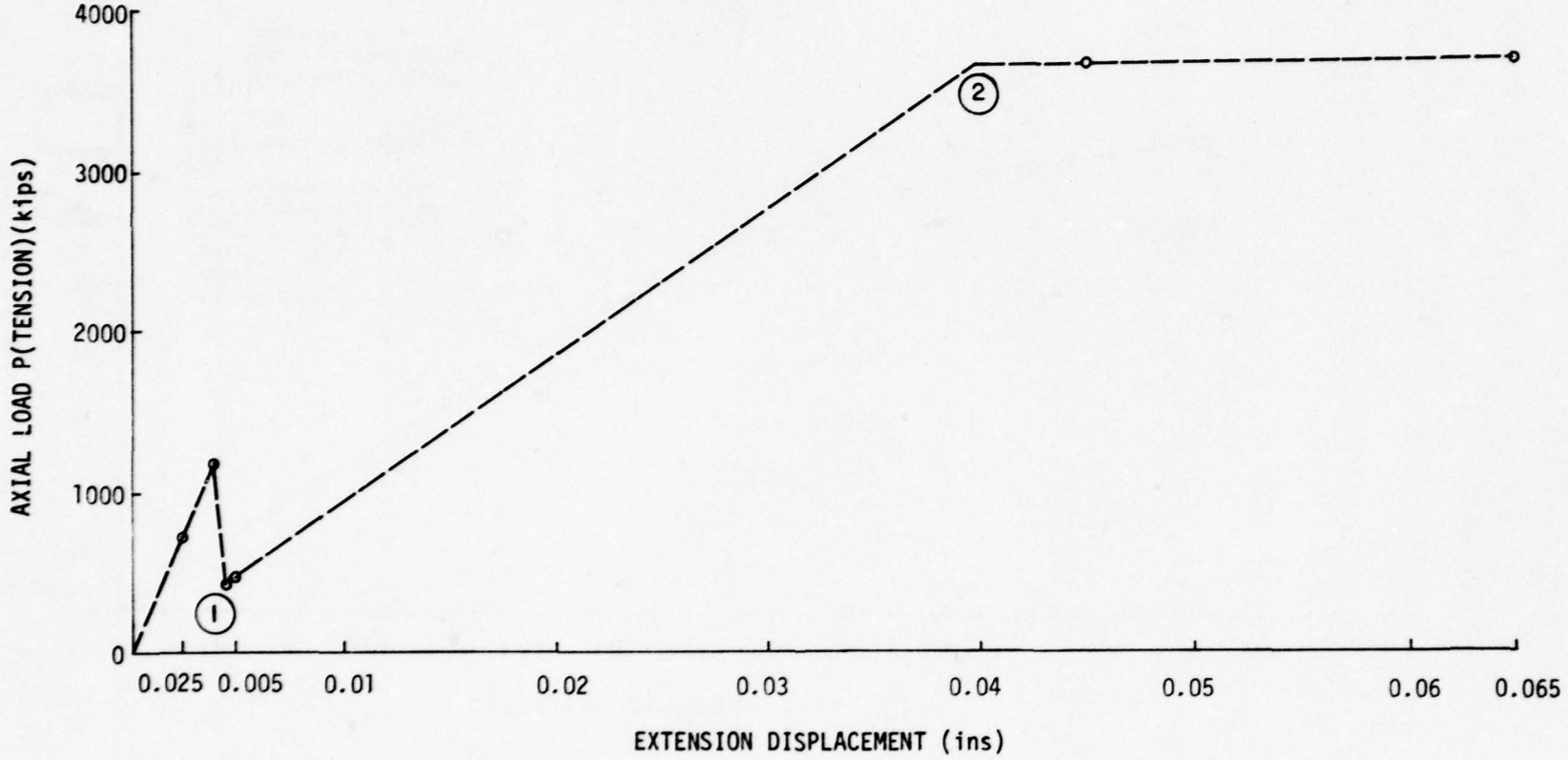

Figure 42.1 CRS #11.1 Pure Extension

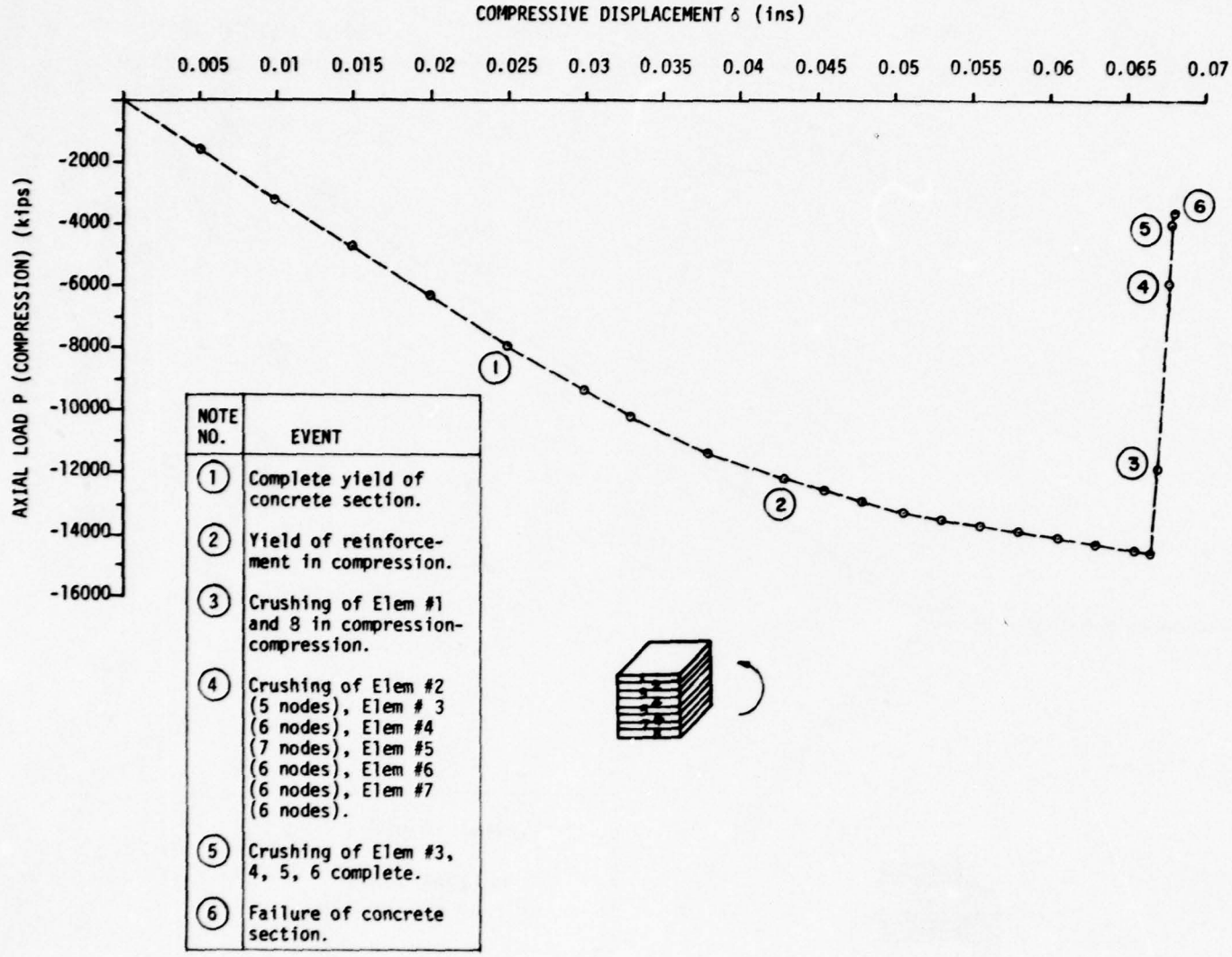

Figure 42.2 CRS#11.1 Pure Compression

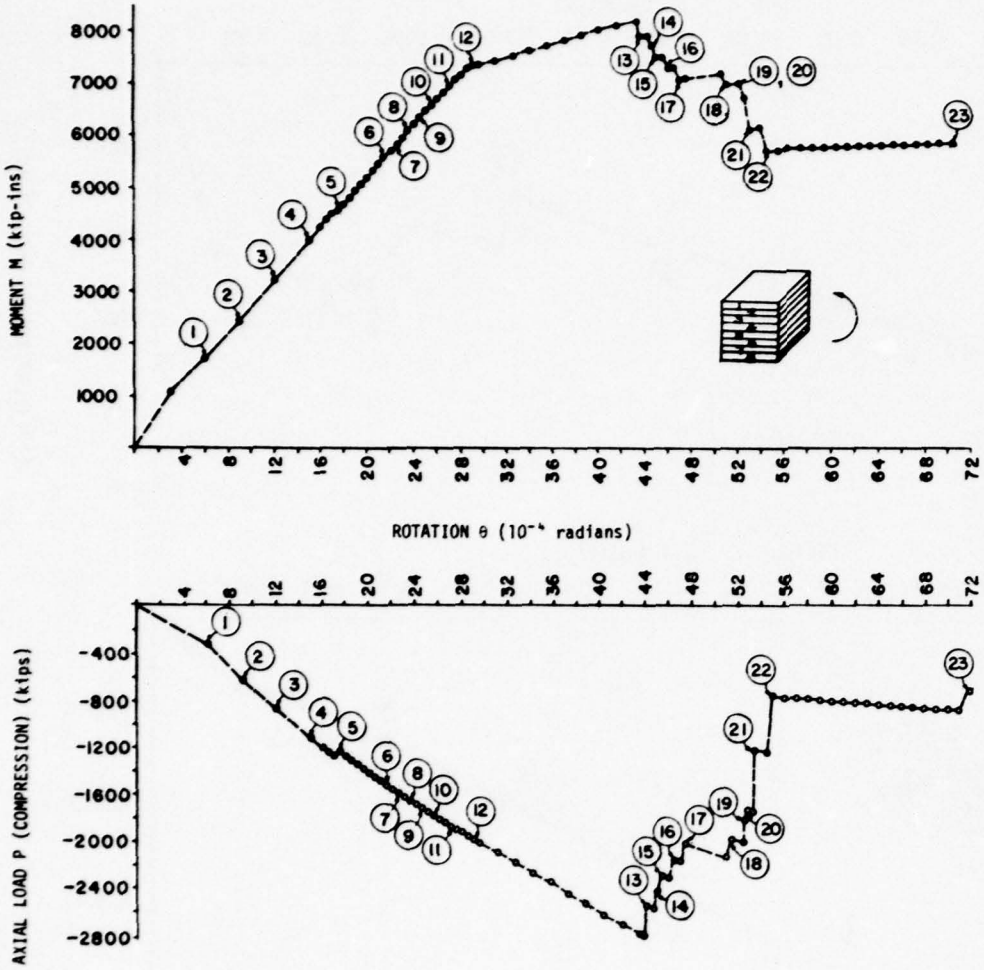

Figure 42.3 CRS #11.1 Pure Rotation

NOTE NO.	EVENT
(1)	Cracking of Element #7, 8 (total).
(2)	Cracking of Element #6 (total).
(3)	Cracking of Element #5 (4 nodes).
(4)	Cracking of Element #5 (total).
(5)	Cracking of Element #4 (5 nodes); Crushing of Element #4 (3 nodes in t-c).
(6)	Yield of Element #1, (4 nodes in compression).
(7)	Yield of Element #3 (4 nodes in t-c).
(8)	Yield of Element #1 (4 nodes in compression, 4 nodes in t-c).
(9)	Yield of Element #2 (4 nodes in t-c).
(10)	Yield of Element #3 (8 nodes in t-c).
(11)	Yield of Element #2 (8 nodes in t-c).
(12)	Yield of re-bars in tension and compression.
(13)	Crushing of Element #1 (2 nodes in t-c).
(14)	Crushing of Element #1 (2 nodes in t-c, 1 node in compression).

NOTE NO.	EVENT
(15)	Crushing of Element #1 (2 nodes in t-c, 2 nodes in compression).
(16)	Crushing of Element #1 (2 nodes in t-c, 3 nodes in compression).
(17)	Crushing of Element #1 (2 nodes in t-c, 4 nodes in compression).
(18)	Crushing of Element #1 (2 nodes in t-c, 5 nodes in compression).
(19)	Failure of Element #1.
(20)	Crushing of Element #3 (1 node in t-c).
(21)	Crushing of Element #2 (1 node in t-c, 1 node in compression). Crushing of Element #3 (4 nodes in t-c).
(22)	Crushing of Element #2 (1 node in t-c, 4 nodes in compression). Crushing of Element #3 (5 nodes in t-c).
(23)	Failure of Section Assumed

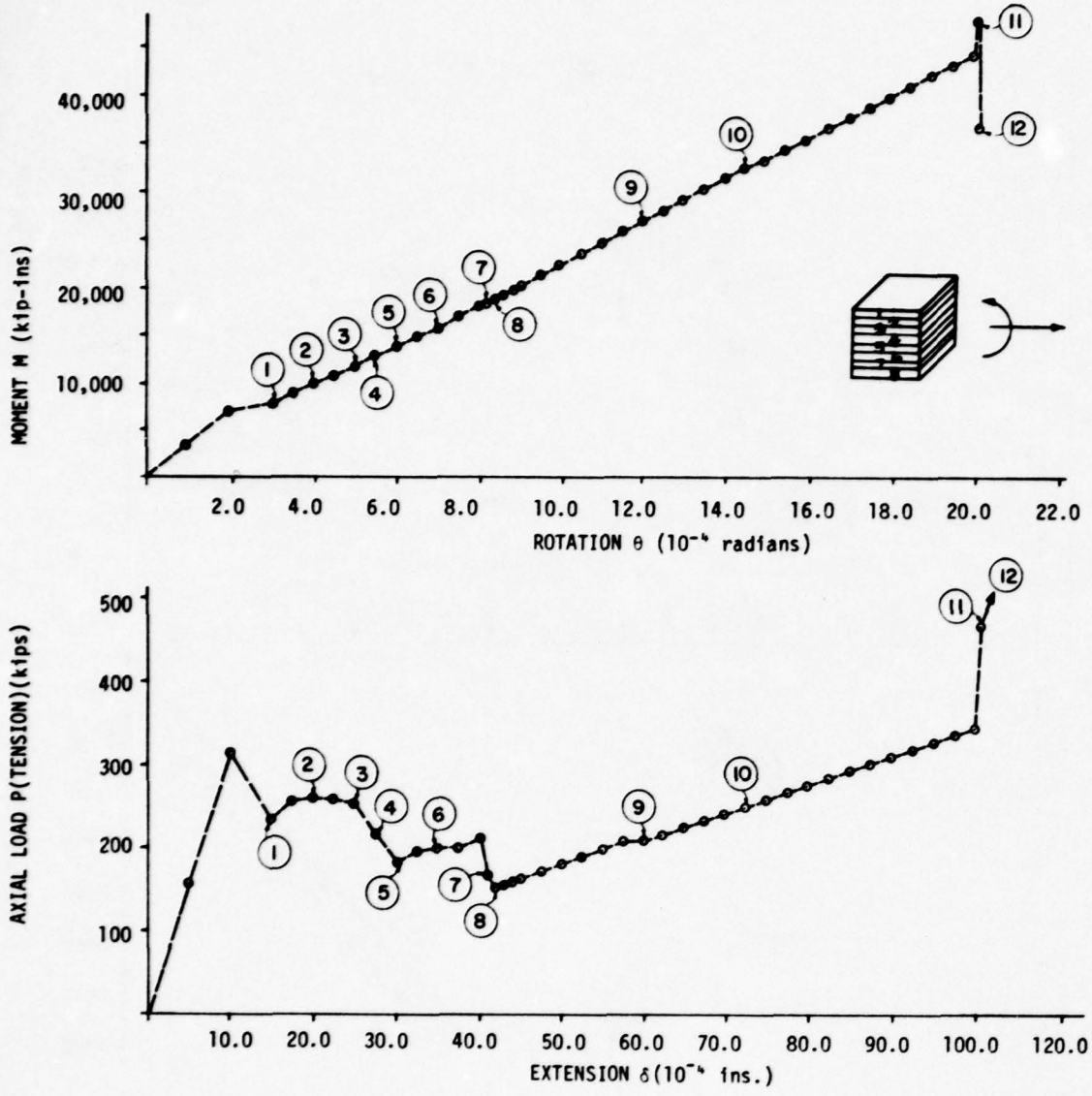

NOTE NO.	EVENT
(1)	Cracking of Element #7, #8.
(2)	Cracking of Element #6 (4 nodes).
(3)	Cracking of Element #6 (8 nodes).
(4)	Cracking of Element #5 (4 nodes).
(5)	Cracking of Element #5 (6 nodes).
(6)	Cracking of Element #5 (8 nodes).
(7)	Cracking of Element #4 (4 nodes).
(8)	Cracking of Element #4 (7 nodes).
(9)	Cracking of Element #4 (8 nodes).
(10)	Cracking of Element #3 (5 nodes). Crushing of Element #3 (2 nodes in t-c).
(11)	Cracking of Element #2 (5 nodes). Crushing of Element #2 (2 nodes in t-c). Yield of Element #2 (1 node in t-c.
(12)	Failure of concrete section.

Figure 42.4 CRS #11.1 - Extension/Rotation = 5.0

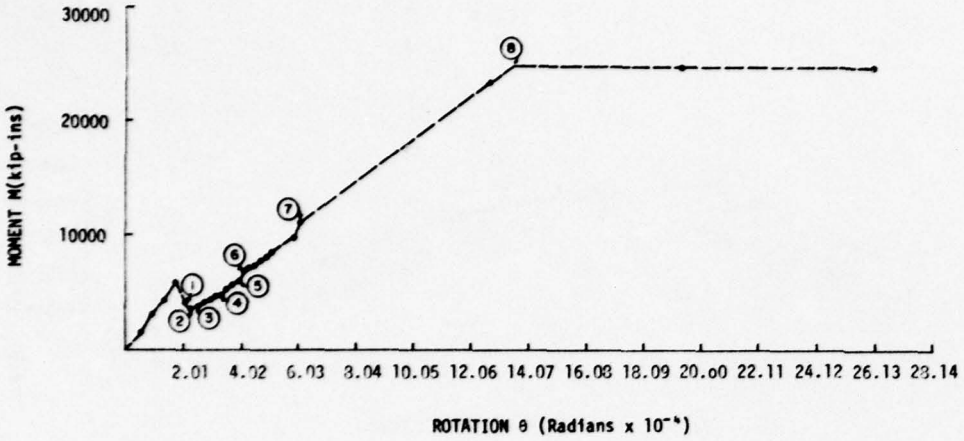

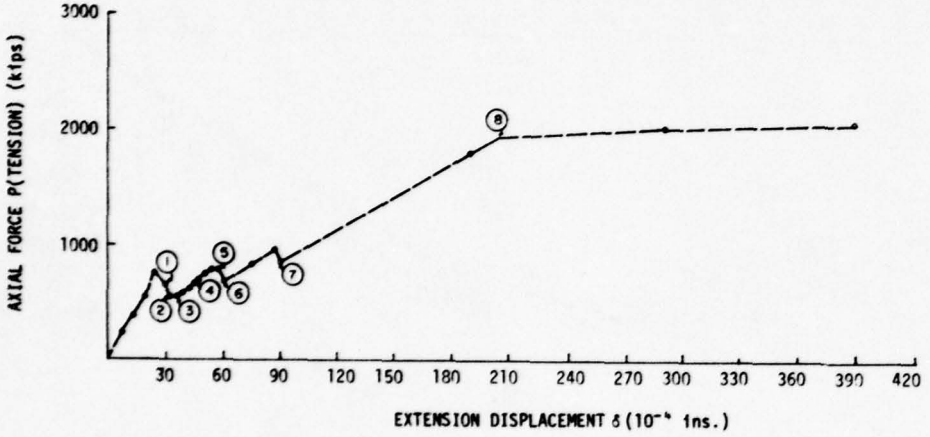

NOTE NO.	EVENT
1	Cracking of element #4.
2	Cracking of element #3 (6 nodes).
3	Cracking of element #3 (7 nodes).
4	Cracking of element #3 (complete).
5	Cracking of element #2 (2 nodes).
6	Cracking of element #2 (complete).
7	Cracking of element #1 (complete).
8	Yield of re-bars in tension.

Figure 42.5 CRS #11.1 Extension/Rotation = 15.0.

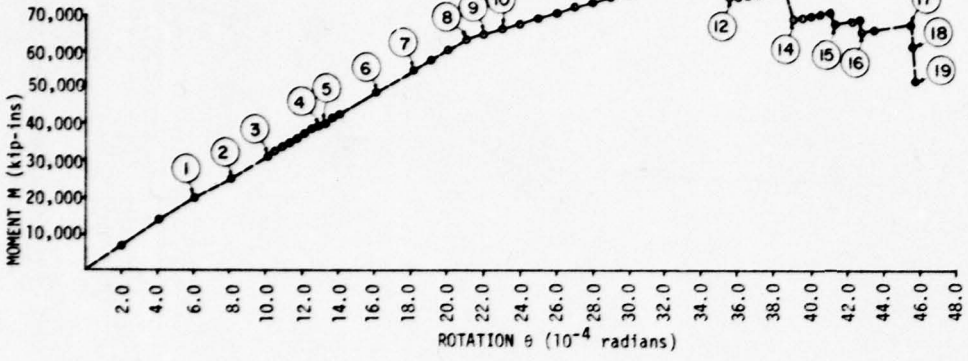

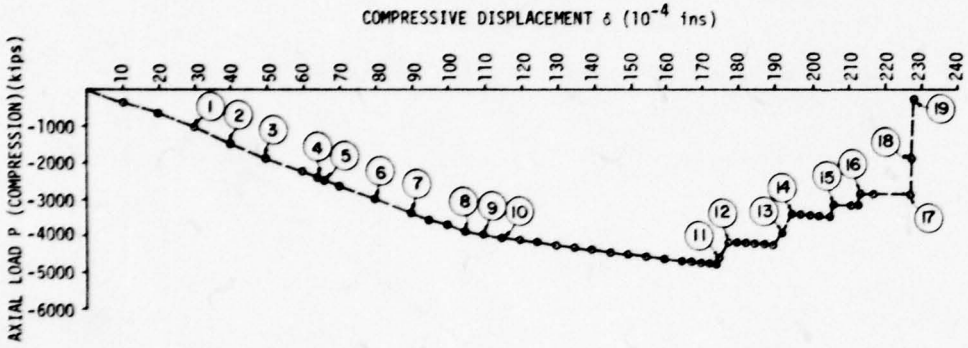

NOTE NO.	EVENT
1	Cracking of Element #8 (8 nodes).
2	Cracking of Element #7 (6 nodes).
3	Cracking of Element #7 (8 nodes).
4	Cracking of Element #6 (6 nodes).
5	Cracking of Element #6 (8 nodes).
6	Yield of Element #1 (4 nodes in compression).
7	Yield of Element #1 (8 nodes in compression).
8	Yield of Element #2 (4 nodes in compression, 4 nodes in t-c).
9	Yield of Element #3, #4 (4 nodes each in t-c). Yield of Element #5 (8 nodes in t-c). Yield of re-bars in compression.
10	Yield of Element #3, #4 (8 nodes in t-c).
11	Crushing of Element #1 (1 node in compression).
12	Crushing of Element #1 (4 nodes in compression).
13	Crushing of Element #1 (6 nodes in compression).

NOTE NO.	EVENT
14	Failure of Element #1 in compression. Crushing of Element #2 (1 node in t-c).
15	Crushing of Element #2 (2 nodes in compression, 1 node in t-c).
16	Crushing of Element #2 (4 nodes in compression).
17	Yield of re-bars in tension.
18	Crushing of Element #2 (5 nodes in compression, 1 node in t-c). Crushing of Element #3 (1 node in compression, 2 nodes in t-c). Crushing of element #5 (5 nodes in t-c).
19	Failure of concrete section.

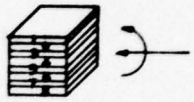

Figure 42.6 CRS #11.1 - Compression/Rotation = 5.0

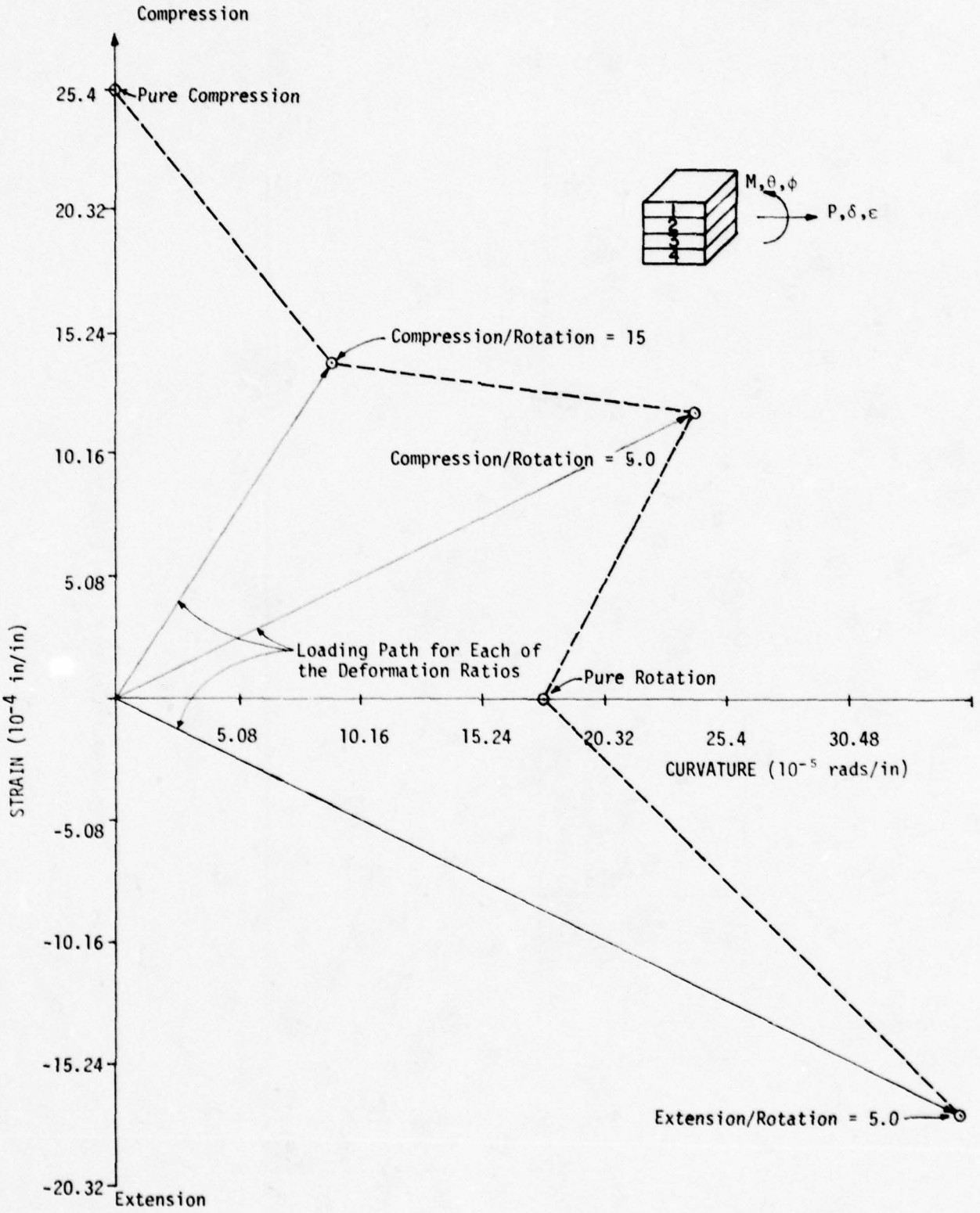

Figure 43. CRS #4.2 Failure Envelope

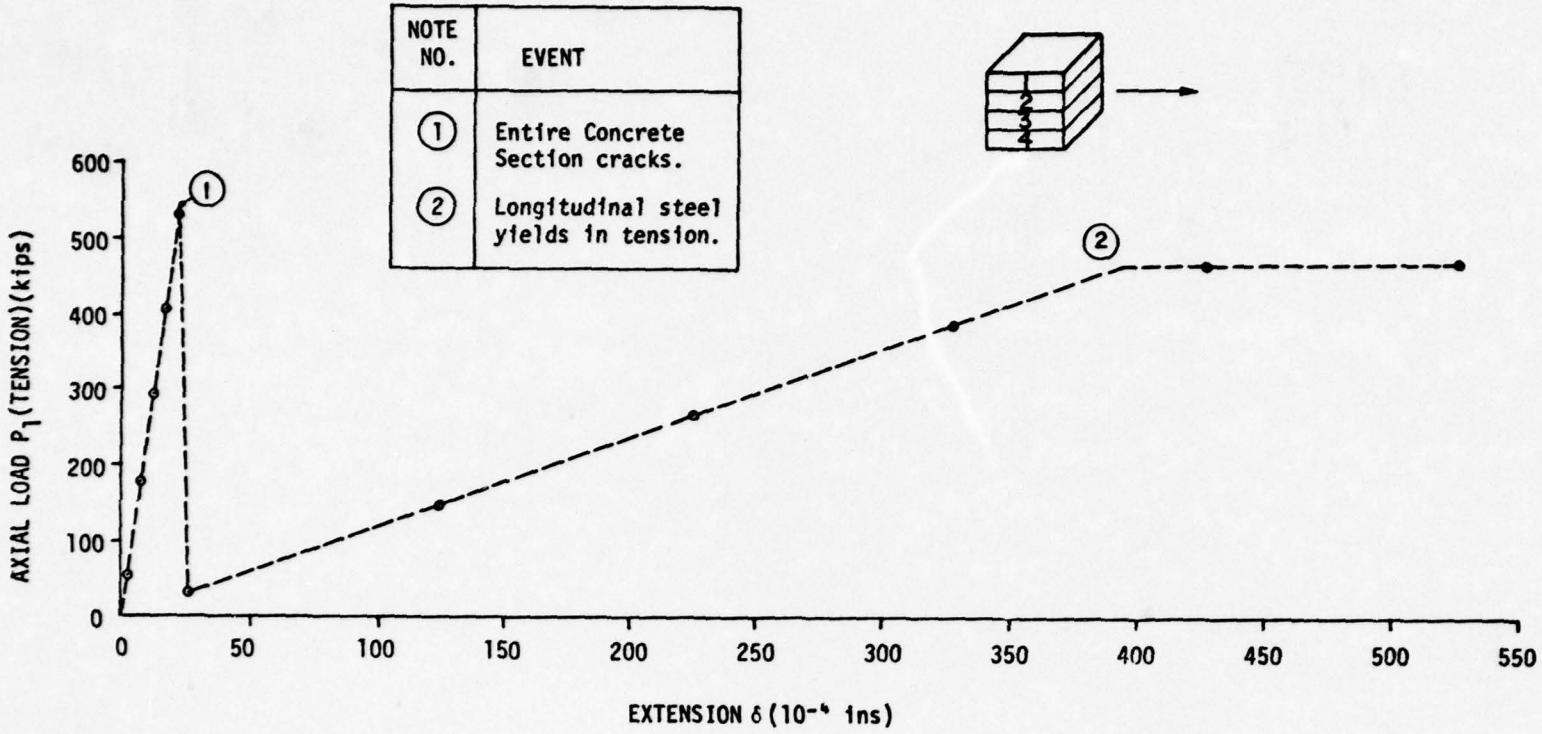

Figure 44.1 CRS #4.2 Pure Extension

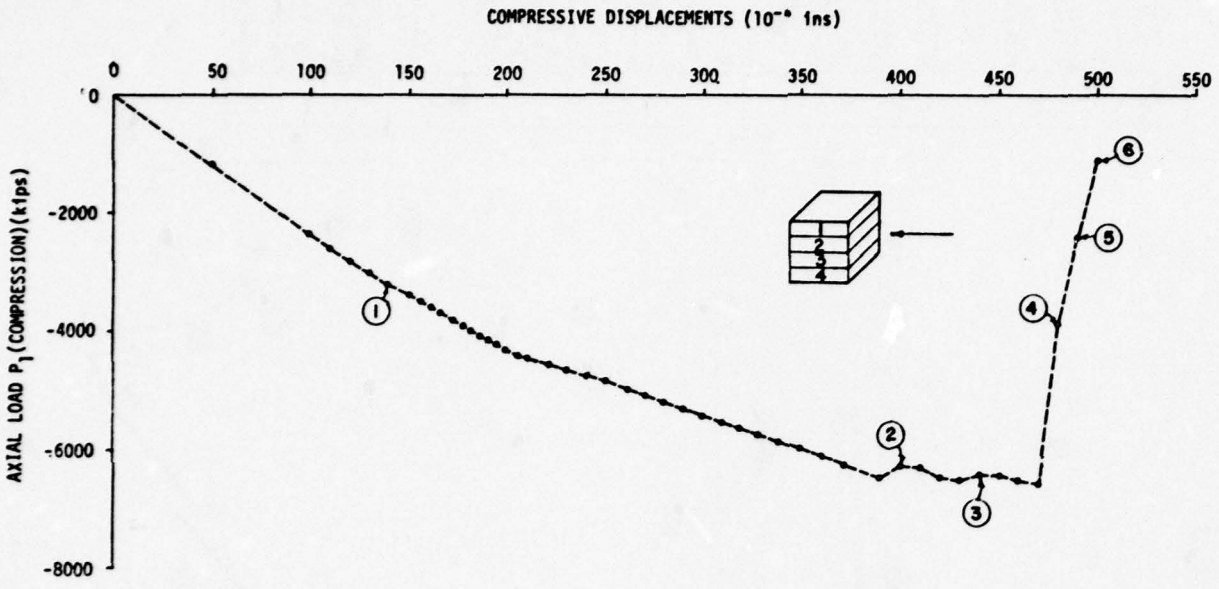

NOTE NO.	EVENT
(1)	Entire concrete section yields.
(2)	Steel yields in compression.
(3)	Element #1 crushes 1 node.
(4)	Element #1 crushes 5 nodes. Element #2 crushes 3 nodes. Element #3 crushes 5 nodes. Element #4 crushes 5 nodes. Solution does not converge.
(5)	Elements #3, 4 crush completely. Elements #1, 2 crush 6 nodes. Solution does not converge.
(6)	Element #2 crushes completely. Element #1 crushes 7 nodes. Solution does not converge.

Figure 44.2 CRS #4.2 - Pure Compression

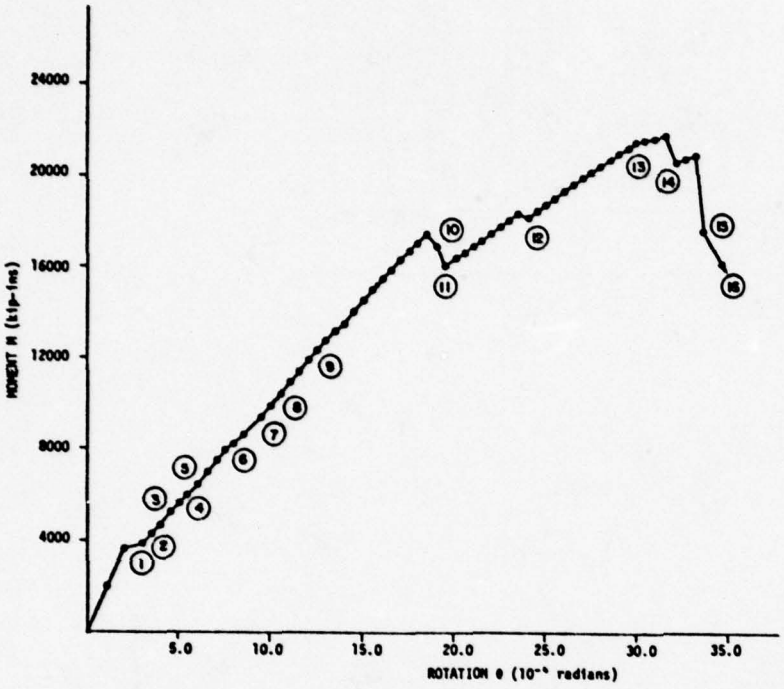

NOTE NO.	EVENT
1	Cracking of Elem #7, 8.
2	Cracking of Elem #6 (4 nodes).
3	Cracking of Elem #6 (8 nodes).
4	Cracking of Elem #5 (6 nodes).
5	Cracking of Elem #5 (8 nodes).
6	Cracking of Elem #4 (6 nodes).
7	Yield of Elem #1 (4 nodes in compression).
8	Yield of Elem #1 (8 nodes in compression).
9	Yield of Elem #2 and 3 (8 nodes in compression).
10	Crushing of Elem #3 (3 nodes in tension-compression.
11	Crushing of Elem #3 (4 nodes in tension-compression, Elem #2 (2 nodes in tension-compression).
12	Crushing of Elem #2 (3 nodes in tension-compression).
13	Yield of longitudinal re-bars in tension and in compression
14	Crushing of Elem #7 (1 node in compression).
15	Crushing of Elem #1 (4 nodes in compression).
16	Failure of section.

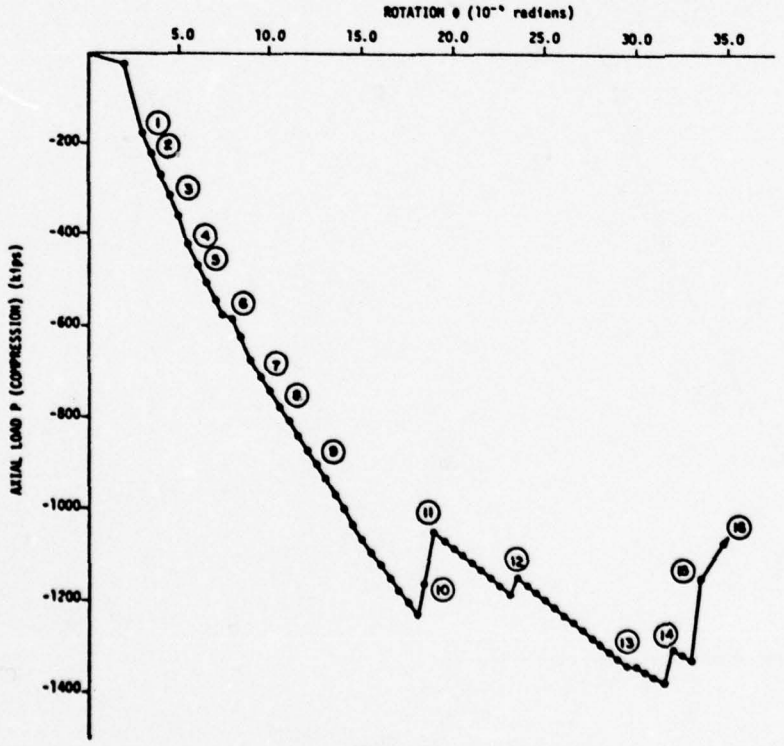

Figure 44.3 CRS#4.2 Pure Rotation

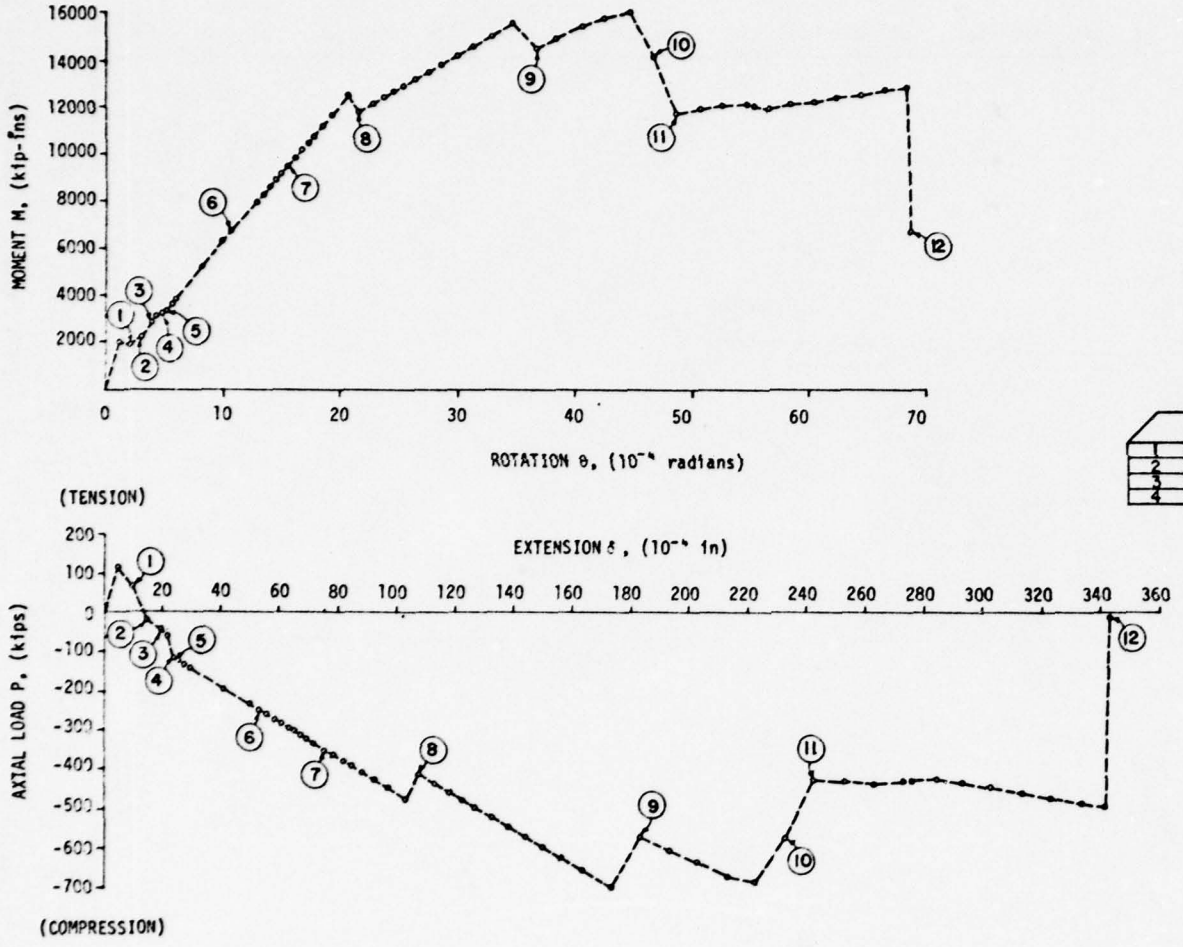

NOTE NO.	EVENT
1	Element #4 cracks completely.
2	Element #3 cracks 6 nodes. Solution does not converge.
3	Element #3 cracks completely.
4	Element #2 cracks 6 nodes. Solution does not converge.
5	Element #2 cracks completely.
6	Element #1 yields 4 nodes in tension-compression.
7	Element #1 yields completely.
8	Element #1 crushes 2 nodes. Bottom re-bar yields in tension.
9	Element #1 crushes 4 nodes.
10	Element #1 crushes 5 nodes. Top re-bar yields in compression.
11	Element #1 crushes 6 nodes.
12	Element #1 crushes 7 nodes.

Figure 44.4 CRS #4.2 - Extension/Rotation = 5.0

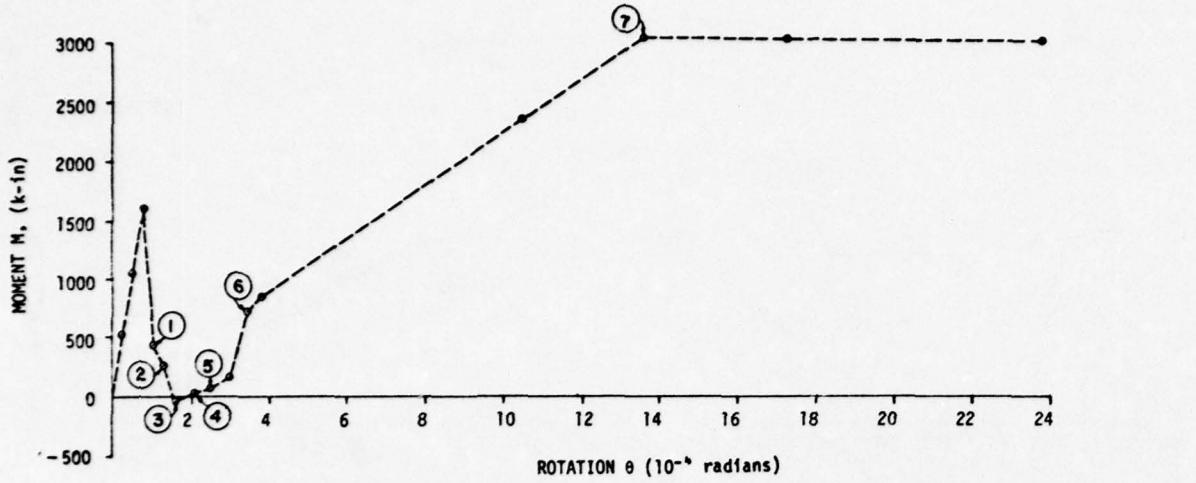

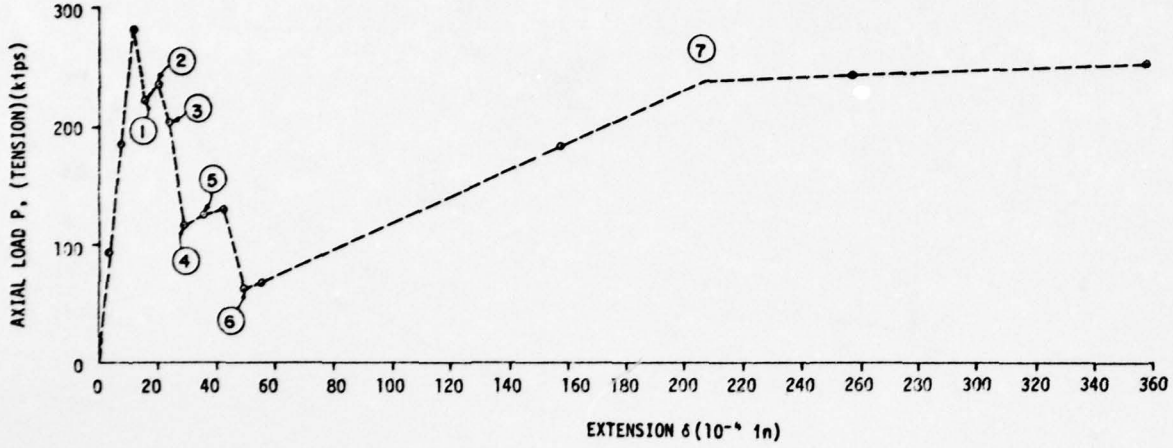

NOTE NO.	EVENT
(1)	Element #4 cracks completely.
(2)	Element #3 cracks 4 nodes.
(3)	Element #3 cracks completely.
(4)	Element #2 cracks 6 nodes.
(5)	Element #2 cracks completely.
(6)	Element #1 cracks completely. Solution does not converge.
(7)	Bottom longitudinal steel yields in tension.

Figure 44.5 CRS #4.2 - Extension/Rotation = 5.0

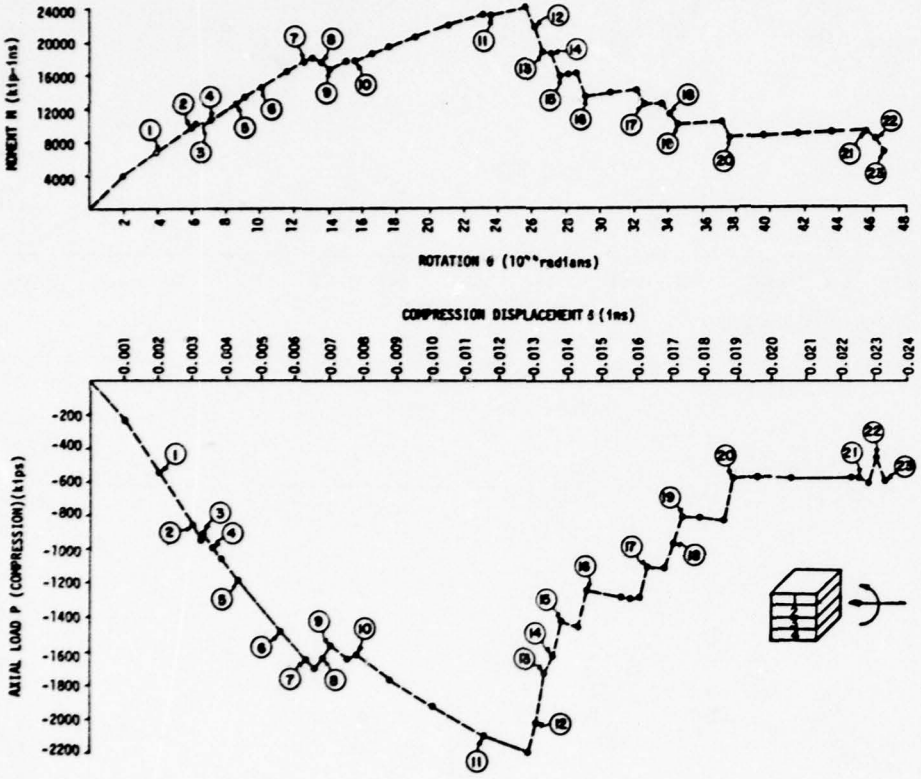

NOTE NO.	EVENT
(1)	Cracking of Element #4 (4 nodes).
(2)	Cracking of Element #4 complete.
(3)	Cracking of Element #3 (5 nodes). Crushing of Element #3 (2 nodes) in tension-compression.
(4)	Yield of Element #1 in compression (4 nodes).
(5)	Complete yield of Element #1 (4 nodes in tension-compression).
(6)	Complete yield of Element #2.
(7)	Failure of Element #3.
(8)	Crushing of Element #1 (1 node in tension compression).
(9)	Crushing of Element #1 (2 nodes in tension-compression).
(10)	Crushing of Element #2 (1 node in tension-compression).
(11)	Yield of re-bars in compression.
(12)	Crushing of Element #1 (1 node in compression, 2 nodes in tension-compression).
(13)	Crushing of Element #1 (2 nodes in compression, 2 nodes in t-c). Crushing of Element #2 (2 nodes in t-c).

NOTE NO.	EVENT
(14)	Crushing of Element #2 (3 nodes in t-c).
(15)	Crushing of Element #1 (3 nodes in compression, 2 nodes in t-c).
(16)	Crushing of Element #1 (4 nodes in compression, 2 nodes in t-c).
(17)	Crushing of Element #1 (5 nodes in compression, 2 nodes in t-c).
(18)	Crushing of Element #1 (1 node in compression, 3 nodes in t-c).
(19)	Crushing of Element #2 (2 nodes in compression, 3 nodes in t-c).
(20)	Failure of Element #1 (6 nodes in compression, 2 nodes in t-c).
(21)	Yield of re-bars in tension.
(22)	Crushing of Element #2 (3 nodes in compression, 3 nodes in t-c).
(23)	Crushing of Element #2, (4 nodes in compression, 3 nodes in t-c). Failure of section.

Figure 44.6 CRS #4.2 - Compression/Rotation = 5.0

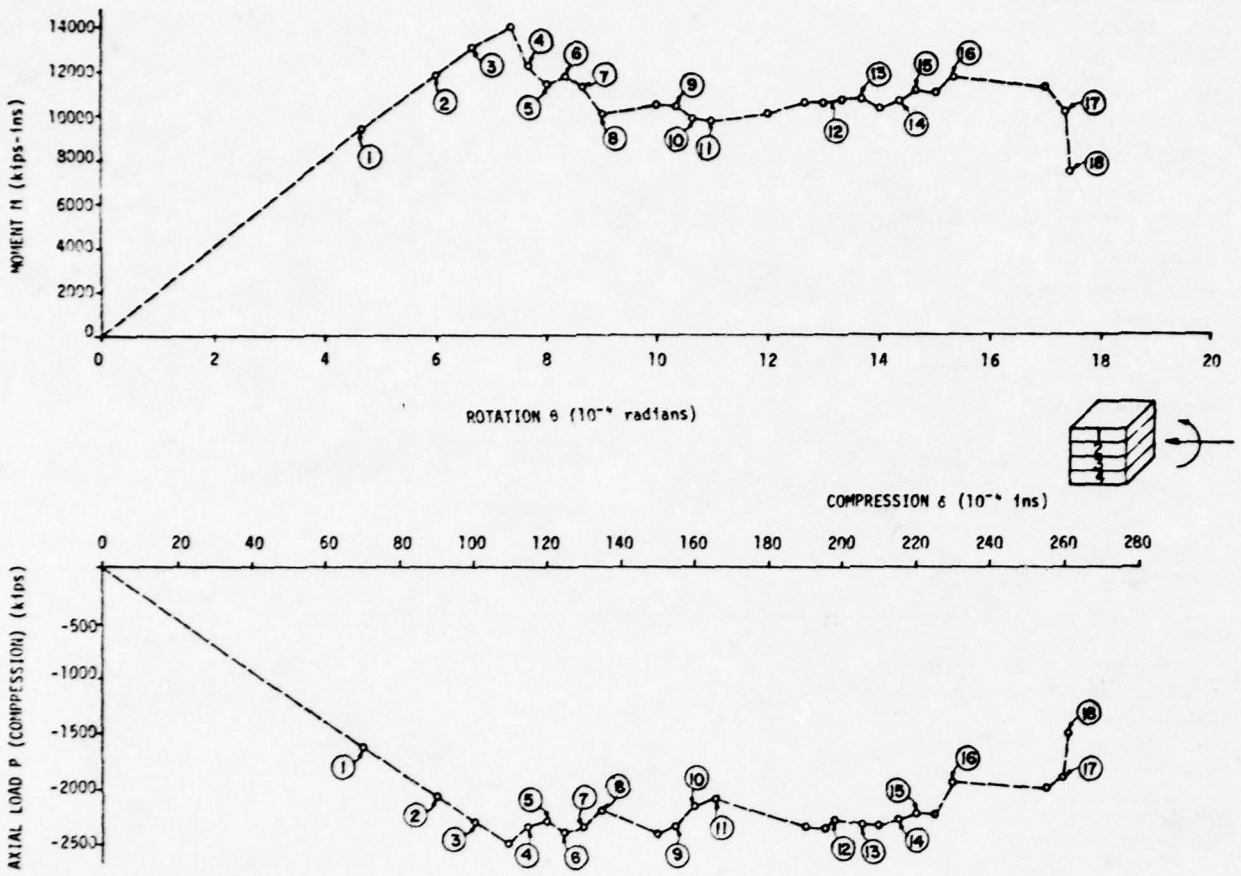

NOTE NO.	EVENT
(1)	Elem #1 yields 4 nodes.
(2)	Elem #1 yields 5 nodes.
(3)	Elem #1 yields 7 nodes. Elem #3 yields 4 nodes.
(4)	Elem #1 crushes 2 nodes.
(5)	Elem #1 crushes 3 nodes.
(6)	Elem #2 yields 3 nodes Elem #4 yields 2 nodes.
(7)	Elem #2 yields 7 nodes. Elem #2 crushes 1 node. Elem #2 yields completely. Elem #4 yields 8 nodes.
(8)	Elem #2 crushes 3 nodes.
(9)	Elem #2 crushes 4 nodes.
(10)	Elem #2 crushes 6 nodes.
(11)	Elem #2 crushes 7 nodes.
(12)	Elem #3 crushes 1 node.
(13)	Top rebar yields in compre compression.
(14)	Elem #3 crushes 2 nodes.
(15)	Elem #3 crushes 3 nodes.
(16)	Elem #3 crushes 6 nodes.
(17)	Elem #1 crushes 5 nodes.
(18)	Elem #4 crushes 3 nodes.

Figure 44.7 CRS #4.2 - Compression/Rotation = 15.0

3. SUMMARY OF RECTANGULAR SECTION RESULTS

The response of various sections subjected to different types of loading patterns has been presented in detail in the preceeding paragraphs. Some generalized observations are now summarized.

(1) The shape of the failure envelopes was similar for all the rectangular sections analyzed.

(2) The numerical solution was quite sensitive for pure rotation cases and lightly reinforced sections with transverse steel. Step sizes had to be reduced and finer meshes employed. In spite of the extra cost we would recommend for future studies that finer meshes be employed for all cases. More consistent and smoother curves would result.

(3) When the strength of concrete in uniaxial compression was increased from 5.0 ksi to 6.0 ksi, while the longitudinal and transverse reinforcement was kept constant, the deformation strength of the section reduced with an increase of concrete strength. (CRS #3, CRS #7)

(4) The deformation strength of the section reduced when the percentage of longitudinal steel was reduced from 2 percent to 1/4 percent. Both sections had the same strength concrete. (CRS #3, CRS #4.1)

(5) An increase in the amount of transverse reinforcement increased the deformation capacity and the ductility of the section. (CRS #4.1, CRS #4.2) Note that the percentage of longitudinal reinforcement, and the strength of concrete in uniaxial compression was the same for both these sections.

4. CYLINDRICAL SECTION RESULTS

Development of failure envelopes for cylindrical sections similar to those of the rectangular sections formed the second major phase of the study

of failure criteria for reinforced concrete structures. Only confined sections were analyzed. The main parameter of interest was the r/t ratio of the cylindrical section and its effect on the failure envelope. Two r/t ratios were analyzed: one r/t of 4 and the other r/t of 8. (Note r = inside radius of the cylinder and t = thickness of the cylinder). The percentage of total longitudinal reinforcement at any section was 2 percent. Ultimate uniaxial compressive stress of concrete used was 5.0 ksi (Figure 17) while the properties of steel were idealized as shown in Figure 18. Both cylindrical sections were analyzed for seven deformation ratios, similar to the rectangular sections. A third cylindrical section was also analyzed where the section with r/t ratio of 4 was subjected to a pressure load of 3-4-5. The cases analyzed are shown in Table 2.

a. Analytical Modeling For Concrete

The dimensions of the cylindrical section analyzed are shown in Figure 45.1. The thickness of the section was constant (1 meter or 39.37 inches) while the radius of section was changed depending on the r/t ratio. Thus section CCS-1 had a radius of 157.48 inches (4 meters) while section CCS-2 had a radius of 314.96 inches (8 meters). Since the section was cylindrical, and the loading was symmetric about its diameter, for the purposes of analysis, half of the section was considered. The finite element model used in the analysis is shown in Figure 45.2. The left face of the section was fixed while deformations were imposed on the right face (face 24-28-32-36-40-37-33-29-25-21) in Figure 40.

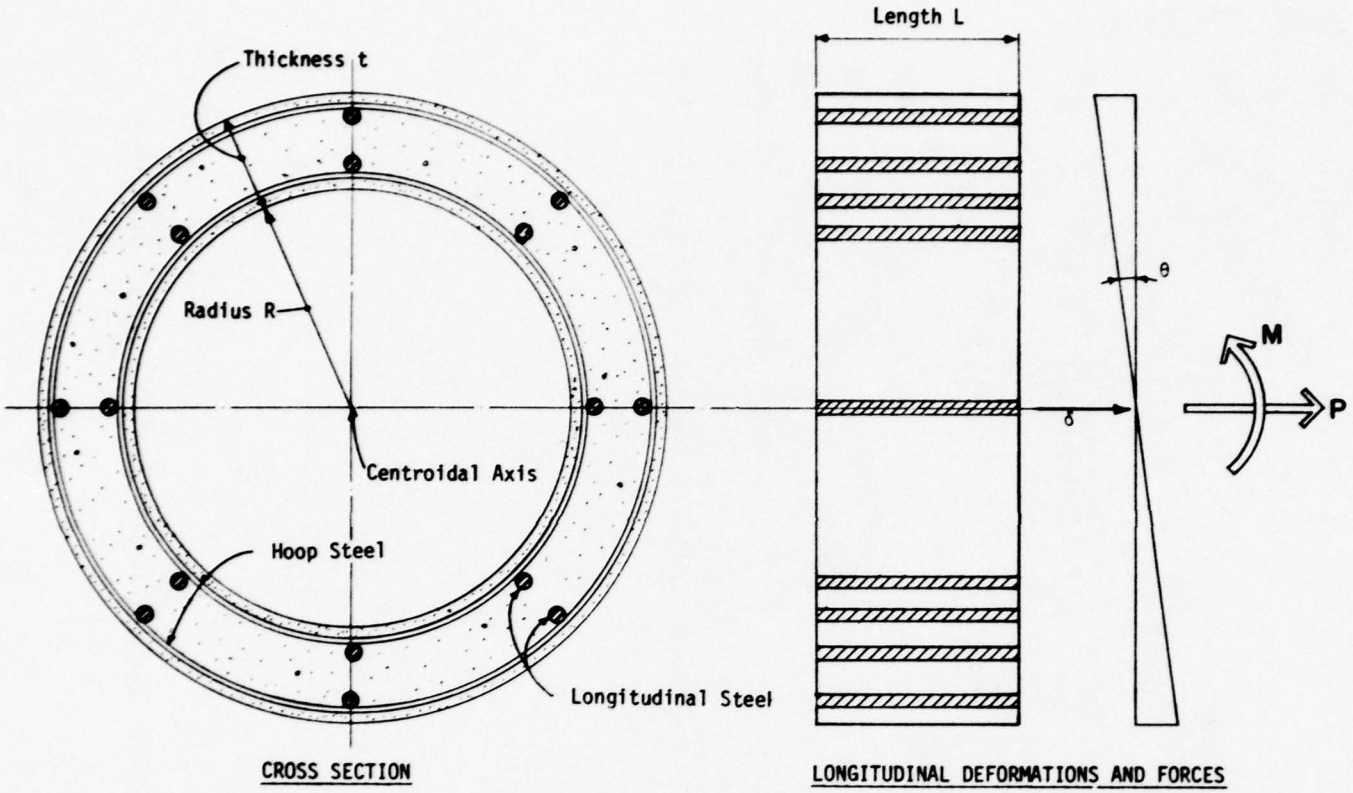

CCS-1: r = 157.48" (4m) t = 39.37" (1m) r/t = 4 L = 39.37"

CCS-2: r = 314.96" (8m) t = 39.37" (1m) r/t = 8 L = 39.37"

Figure 45.1 Cylindrical Section. Dimensions, Layout of Reinforcement, and Definition of Longitudinal Deformations and Forces

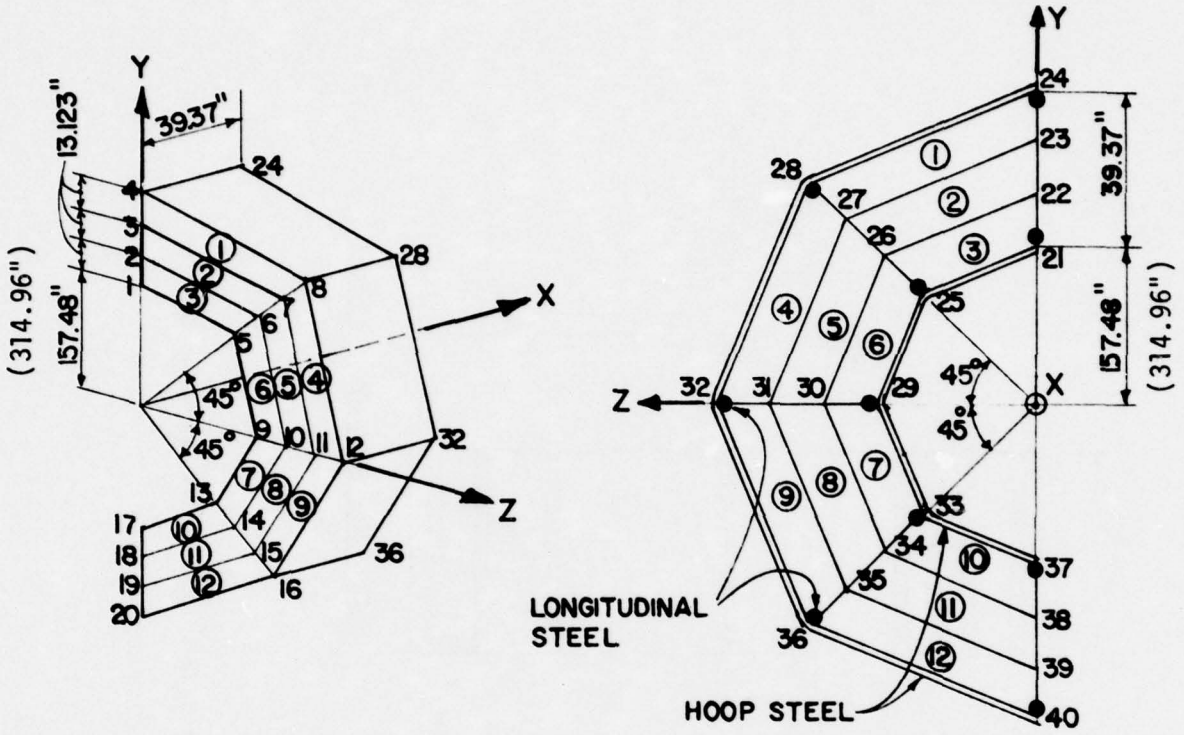

Note: Figures in Parentheses indicate dimension changes for CCS-2.

Figure 45.2 Finite Element Model for Cylindrical Section

Table 2
CONFINED CYLINDRICAL SECTION (CCS)
PARAMETRIC STUDY LAYOUT

DEFORMATION RATIOS[a] $\delta/\theta = \pm \infty, 0, \pm 5, \pm 15$

Identification Number	Ultimate Compressive Stress f'c (ksi)		Reinforcement Ratio[b] %				Radius to Thickness Ratio (r/t)	
	5	9	1/4	1/2	1	2	4	8
CCS-1	X					X	X	
CCS-2	X					X		X
CCS-3[c]	X					X	X	

a) Positive value of δ/θ ratio indicates extension combined with rotation.

b) Longitudinal reinforcement ratio expressed as a percentage (total) at any section.

c) This section was subjected to a pressure load of 3-4-5.

(1) Response Of CCS-1

Figure 46 shows the failure envelope of confined cylindrical section CCS-1. As can be seen from the figure, the failure points for deformation ratios of extension/rotation of 5 and 15 and compression/rotation of 5 and 15 are all clustered in a single area. This is because the neutral axis of imposed deformation always lies within the section and within the first set of elements close to the geometric neutral axis. Again, the failure strength of the section is less when subjected to pure rotation than when subjected to deformation ratios of displacement/rotation of 5.0.

Figures 47.1 through 47.6 indicate the response in terms of M-θ and P-δ curves for various deformation ratios. A complete history of events is also indicated throughout the loading history for each deformation ratio.

(2) Response Of CCS-2

The failure envelope for CCS-2 with r/t ratio of 8 is indicated in Figure 48. Comparing this envelope to that of CCS-1 (Figure 46) reveals that the strength of the section is reduced further when subjected to pure rotation with an increase in the r/t ratio. Also, an interesting point to note is that the strength of Section CCS-2 is less when subjected to displacement/rotation ratio 5.0 compared to an imposed pure rotation case, while the strength is higher for imposed displacement/rotation ratio of 15 compared to the imposed rotation case. A reverse phenomenon is observed in the case of CCS-1 (Figure 46). Figures 49.1 through 49.6 indicate the M-θ and P-δ curves for various deformation ratios.

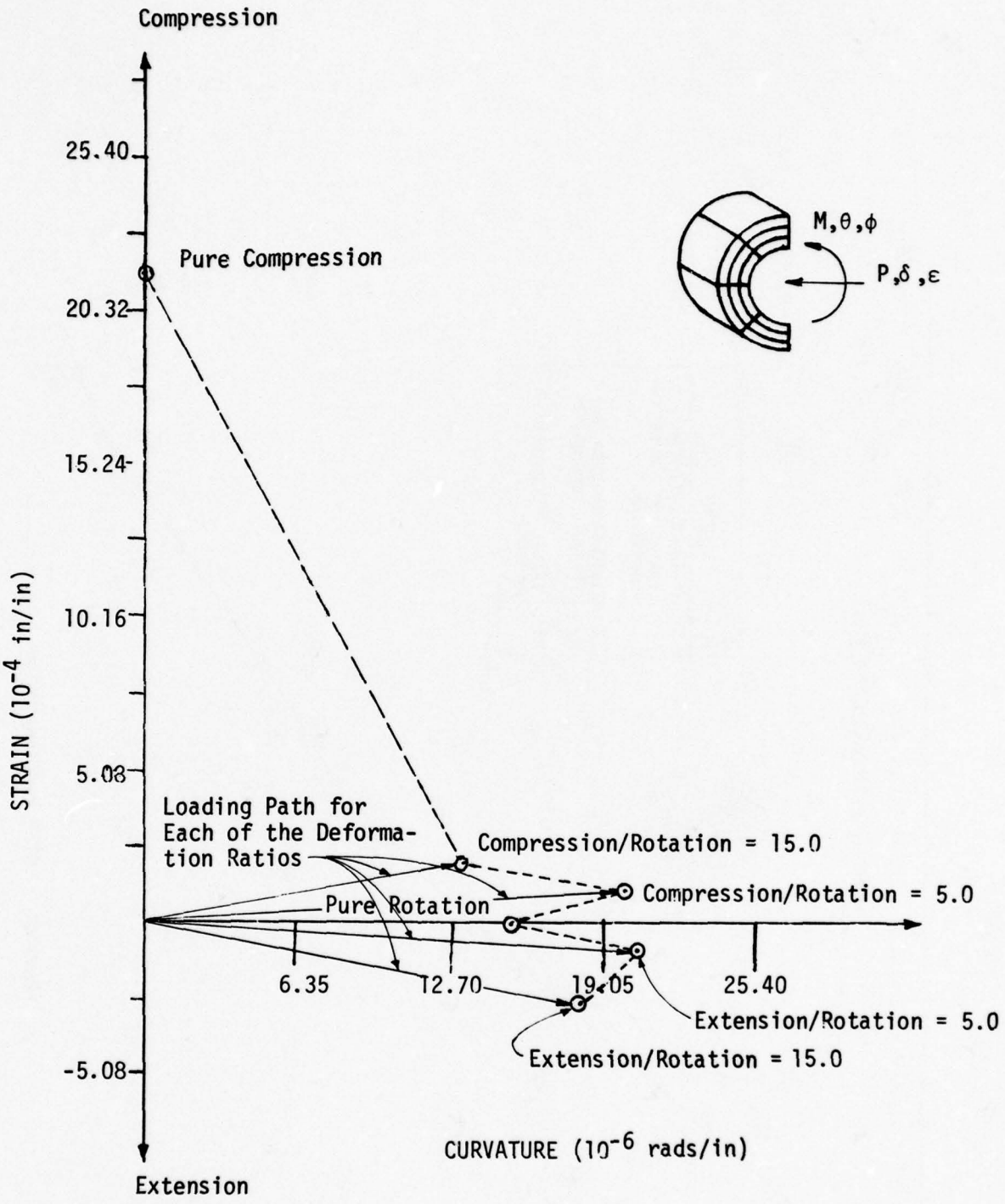

Figure 46 CCS-1 Failure Envelope

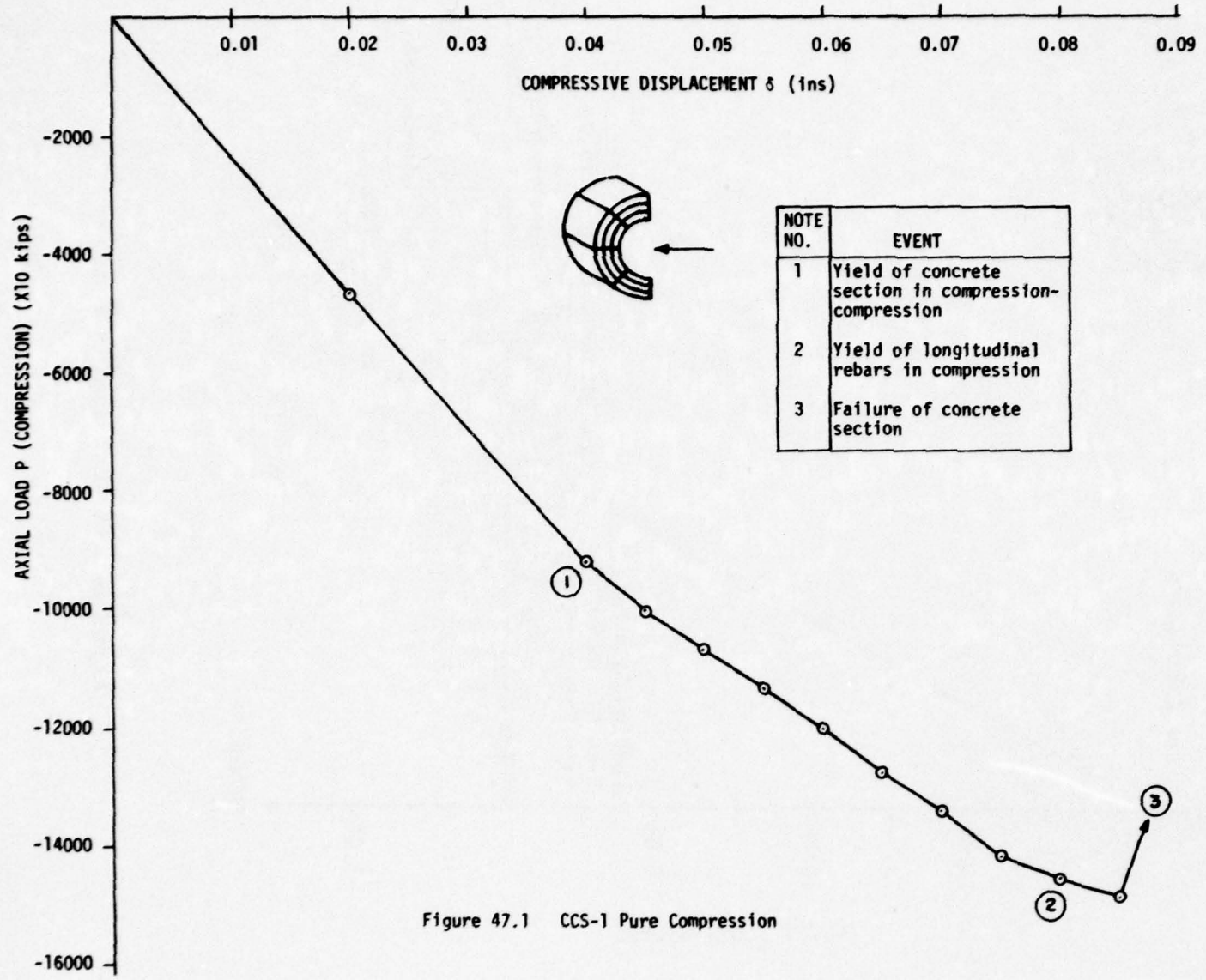

Figure 47.1 CCS-1 Pure Compression

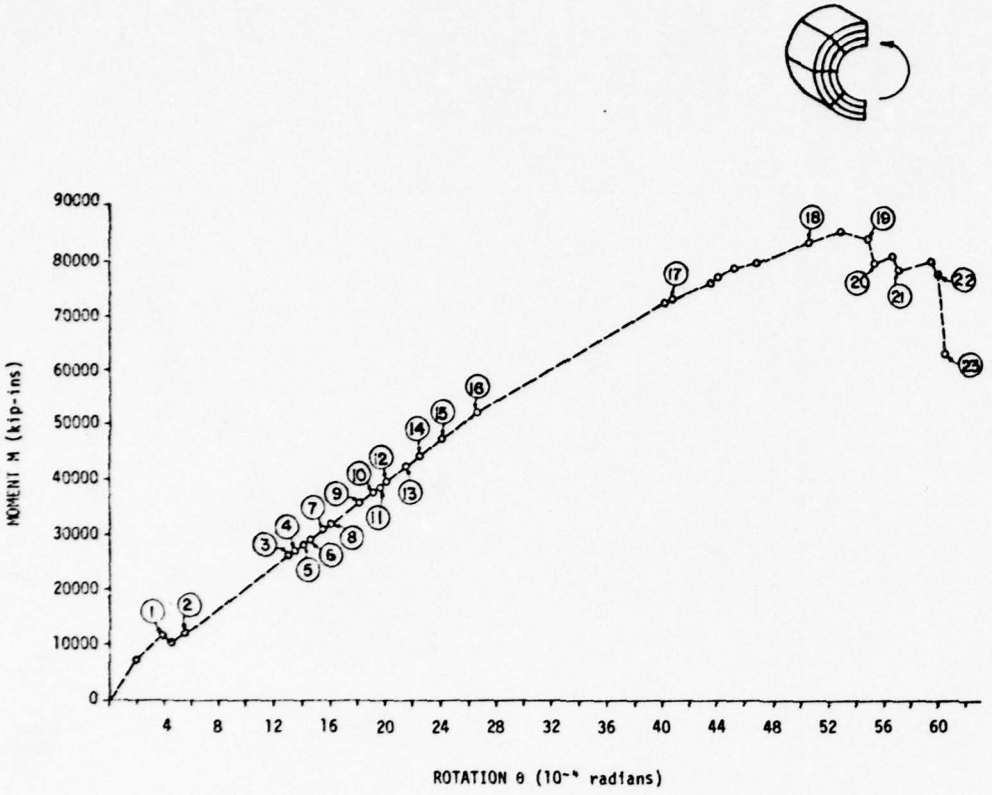

NOTE NO.	EVENT
(1)	Cracking of Elems #10, 11, 12.
(2)	Cracking of Elem #7 (4 nodes) Elem #8 (4 nodes) Elem #9 (4 nodes).
(3)	Yield of Elem #1 (2 nodes).
(4)	Yield of Elem #1 (2 nodes).
(5)	Yield of Elem #2 (2 nodes).
(6)	Yield of Elem #2 (2 nodes).
(7)	Yield of Elem #3 (2 nodes).
(8)	Yield of Elem #1 (1 node), Elem #3 (2 nodes).
(9)	Yield of Elem #1 (total).
(10)	Yield of Elems #2, 3 (total, cracking of Elem #8 (total), #7 (2 nodes).
(11)	Cracking of Elem #7 (1 node).

NOTE NO.	EVENT
(12)	Cracking of Elem #7 (1 node).
(13)	Cracking of Elem #4 (2 nodes).
(14)	Yield of Elem #4 (2 nodes), Elem #5 (1 node).
(15)	Yield of Elem #5 (3 nodes).
(16)	Yield of Elem #6 (4 nodes).
(17)	Yield of rebar in tension and compression.
(18)	Yield of rebar in tension and compression.
(19)	Crushing of Elem #1 (1 node).
(20)	Crushing of Elem #1 (2 nodes).
(21)	Crushing of Elem #1 (1 node). Yield of rebars in tension and compression.
(22)	Crushing of Elem #2 (1 node).
(23)	Failure of concrete section.

Figure 47.2 CCS-1 Pure Rotation

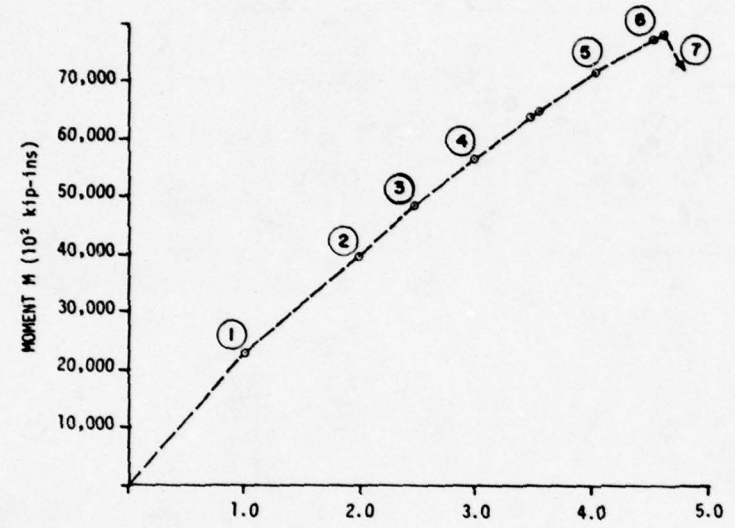

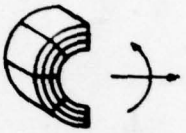

NOTE NO.	EVENT
1	Cracking of Elem. #10, 11, 12.
2	Cracking of Elem. #7, 8, 9.
3	Yield of Elem #1, 2, 3 (complete in compression-compression), Elem #4 (4 nodes), Elem #3 (3 nodes).
4	Yield of Elem #6 (4 nodes).
5	Yield of re-bars in tension.
6	Yield of re-bar in compression.
7	Failure of concrete section.

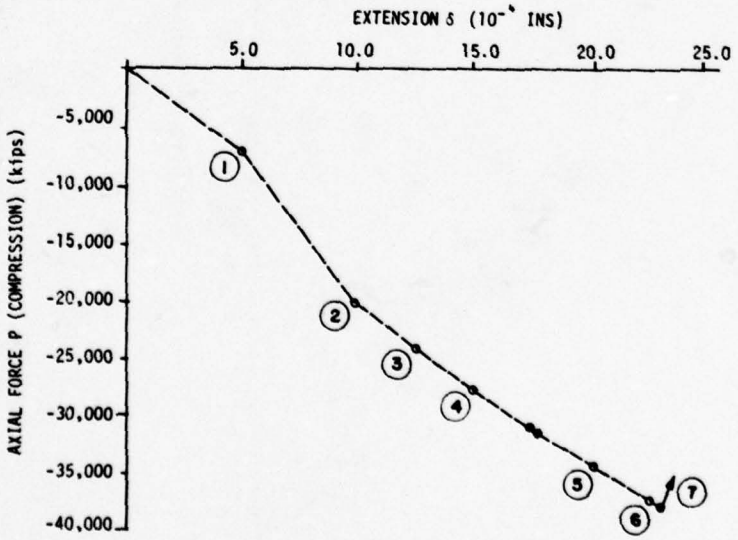

Figure 47.3 CCS-1 Extension/Rotation = 5.0

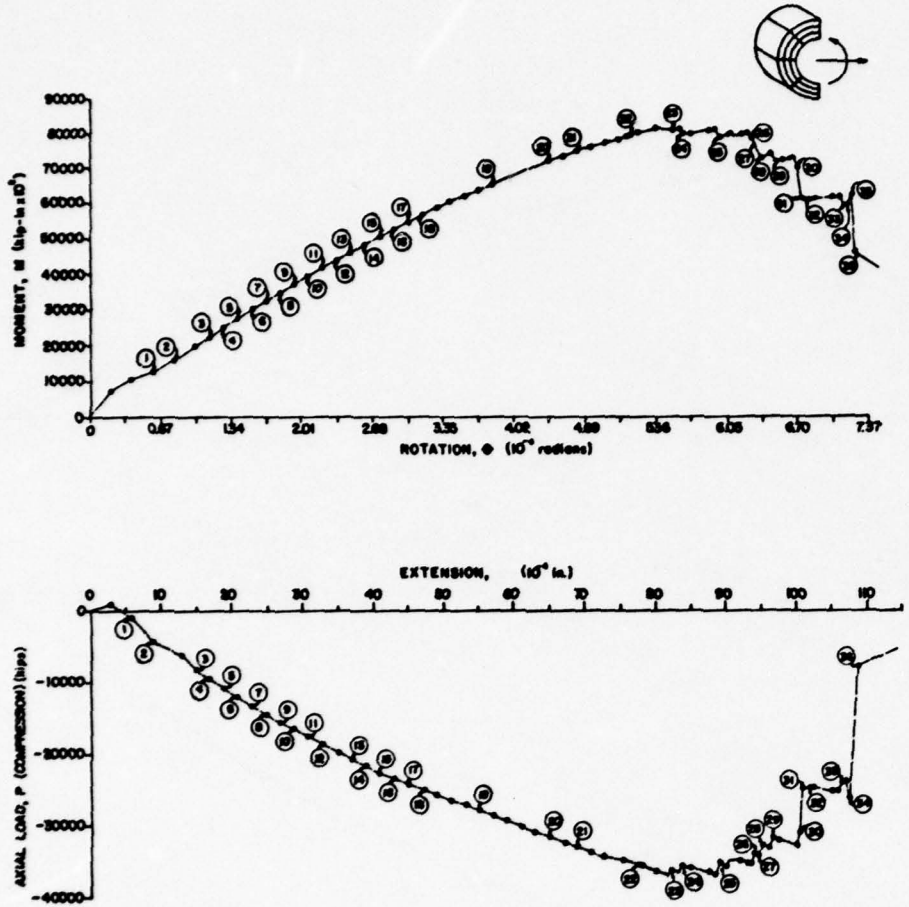

NOTE NO.	EVENT
①	Cracking of elements 10, 11, 12.
②	Cracking of Elem #7 (4 nodes), Elem #8 (4 nodes), Elem #9 (4 nodes).
③	Cracking of Elem #7 (6 nodes), Elem #8 (6 nodes), Elem #9 (6 nodes).
④	Cracking of Elem #9 (7 nodes).
⑤	Cracking of Elems. 7, 8, 9 complete.
⑥	Yield of Elem #1 (2 nodes).
⑦	Yield of Elem #1 (4 nodes), Elem #2 (2 nodes).
⑧	Yield of Elem #2 (4 nodes).
⑨	Yield of Elem #1 (total), Elem #3 (4 nodes).
⑩	Yield of Elem #2 (6 nodes).
⑪	Yield of Elem #2 (total), Elem #3 (7 nodes).
⑫	Yield of Elem #3 (total).
⑬	Yield of Elem #4 (2 nodes).
⑭	Yield of Elem #4 (4 nodes).
⑮	Yield of Elem #5 (3 nodes).
⑯	Yield of Elem #5 (5 nodes), Elem #6 (1 node).
⑰	Yield of Elem #5 (7 nodes).
⑱	Yield of Elem #5 (8 nodes).
⑲	Yield of bottom re-bar in tension.
⑳	Yield of re-bar in compression.
㉑	Yield of re-bar in tension.
㉒	Yield of re-bar in tension.
㉓	Crushing of Elem #1 (1 node), yield of re-bar in compression.
㉔	Crushing of 2 nodes of Elem #1.
㉕	Crushing of Elem #1 (3 nodes).
㉖	Yield of re-bar in tension.
㉗	Crushing of Elem #1 (4 nodes), yield of Elem #4 (5 nodes).
㉘	Crushing of Elem #2 (2 nodes), yield of re-bar in compression.
㉙	Crushing of Elem #2 (3 nodes).
㉚	Crushing of 2 nodes of Elem #3, Elem #2 (4 nodes).
㉛	Crushing of 5 nodes of Elem #3.
㉜	Yield of Elem #4 (6 nodes).
㉝	Crushing of Elem #1 (1 node).
㉞	Crushing of Elem #1 (5 nodes).
㉟	Cracking and crushing of Elems #5, 6 (4 nodes).
㊱	Failure of section.

Figure 47.4 CCS-1 Extension/Rotation = 15.0

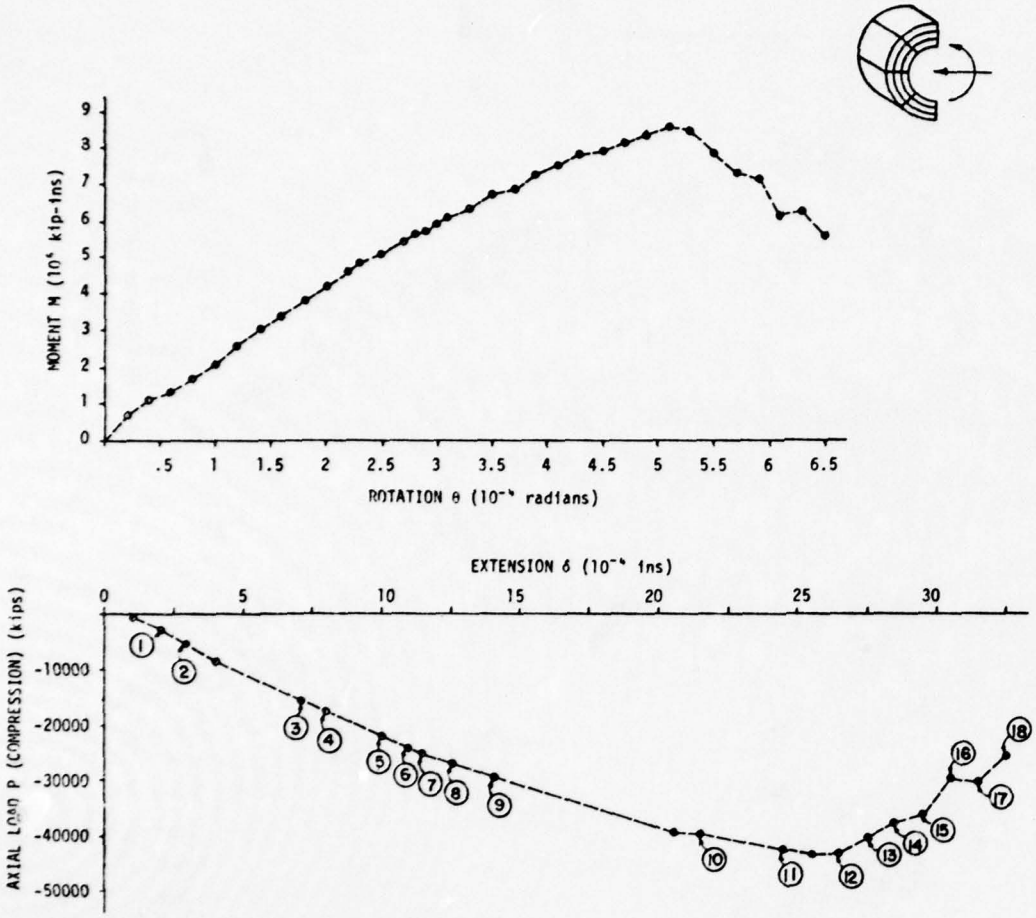

NOTE NO.	EVENT
(1)	Elems #11 & 12 crack completely. Elem #10 cracks 6 nodes.
(2)	Elems #10 & 11 crack completely. Elems #7, 8, & 9 crack 4 nodes.
(3)	Elems #1 & 2 yield 4 nodes.
(4)	Elem #1 yields completely. Elem #2 yields 5 nodes. Elem #3 yields 4 nodes.
(5)	Elems #2 & 3 yield completely. Elem #9 cracks 7 nodes.
(6)	Elem #4 yields 1 node. Elems 8 & 9 crack completely.
(7)	Elem #4 yields 4 nodes. Elem #5 yields 4 nodes. Elem #7 cracks 5 nodes.
(8)	Elem #6 yields 2 nodes. Elem #7 cracks completely.
(9)	Elem #6 yields 4 nodes.

NOTE NO.	EVENT
(10)	Steel yields in compression. Steel yields in tension.
(11)	Steel yields in compression. Elem #4 yields 5 nodes. Elem #1 crushes 1 node.
(12)	Steel yields in tension.
(13)	Elem #1 crushes 4 nodes. Steel yields in compression.
(14)	Elem #2 crushes 3 nodes.
(15)	Steel yields in tension. Elem #4 yields 6 nodes. Elem #2 crushes 4 nodes.
(16)	Elem #2 crushes 6 nodes. Elem #3 crushes 5 nodes. Elem #6 yields 5 nodes. Elem #4 yields completely.
(17)	Elem #6 yields 6 nodes. Elem #5 yields 6 nodes.
(18)	Elem #1 crushes 7 nodes.

Figure 47.5 CCS-1 Compression/Rotation = 5.0

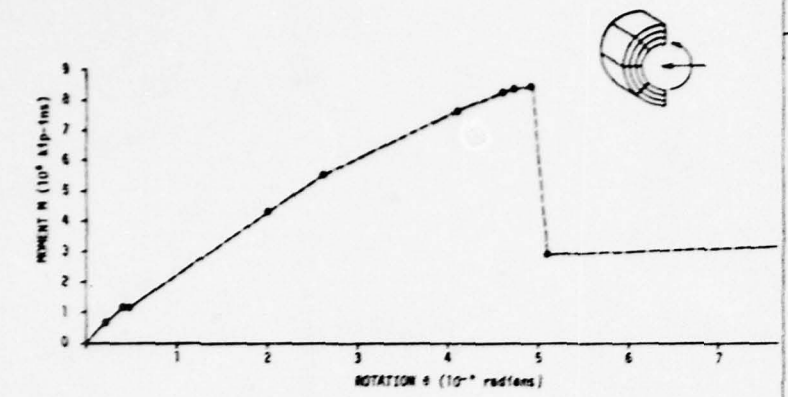

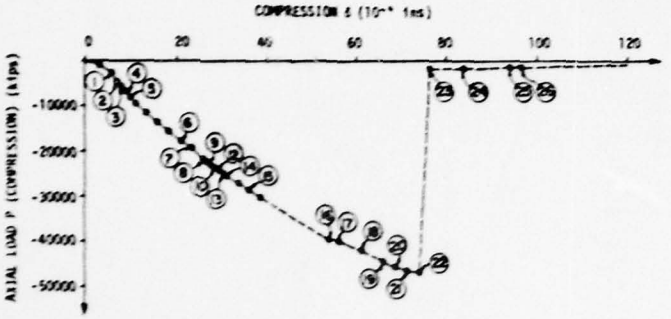

NOTE NO.	EVENT
1	Elem #12 cracks completely. Elem #11 cracks 6 nodes. Elem #10 cracks 4 nodes.
2	Elem #11 cracks completely. Elem #10 cracks completely.
3	Elem #9 cracks 2 nodes.
4	Elem #9 cracks 4 nodes. Elem #8 cracks 4 nodes.
5	Elem #7 cracks 4 nodes.
6	Elem #9 cracks 6 nodes. Elem #8 cracks 6 nodes. Elem #7 cracks 6 nodes. Elem #3 yields 3 nodes. Elem #2 yields 5 nodes. Elem #1 yields 4 nodes.
7	Elem #3 yields 4 nodes. Elem #2 yields completely. Elem #1 yields completely.
8	Elem #3 yields completely.
9	Elem #4 yields 1 node.
10	Elem #4 yields 2 nodes.
11	Elem #4 yields 3 nodes.
12	Elem #4 yields 4 nodes.
13	Elem #5 yields 4 nodes.
14	Elem #5 yields 1 node.
15	Elem #5 yields 4 nodes.
16	Elem #9 cracks 7 nodes.
17	Elem #9 cracks completely. Steel yields in compression.
18	Elem #4 yields 5 nodes. Elem #3 cracks 7 nodes.
19	Steel yields in tension. Elem #8 cracks completely. Elem #4 yields 6 nodes.
20	Elem #7 cracks 7 nodes. Steel yields in compression.
21	Elem #7 cracks completely. Elem #2 crushes 1 node.
22	Elem #5 yields 5 nodes. Elem #4 yields 6 nodes. Elem #1 crushes 2 nodes.
23	Entire concrete section is either cracked or crushed. Steel yields in compression.
24	Steel yields in tension.
25	Steel yields in compression.
26	Steel yields in tension.

Figure 47.6 CCS-1 Compression/Rotation = 15.0

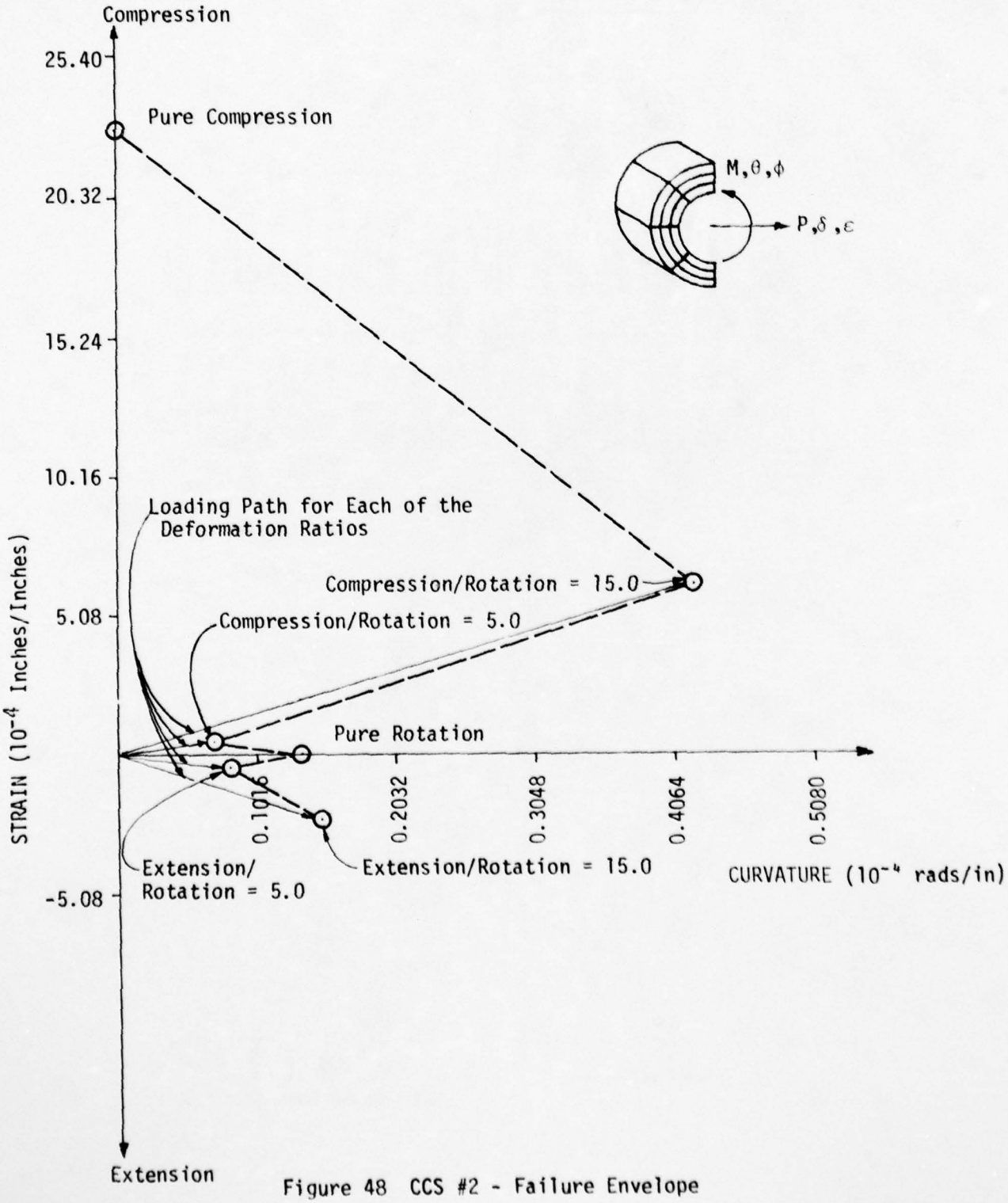

Figure 48 CCS #2 - Failure Envelope

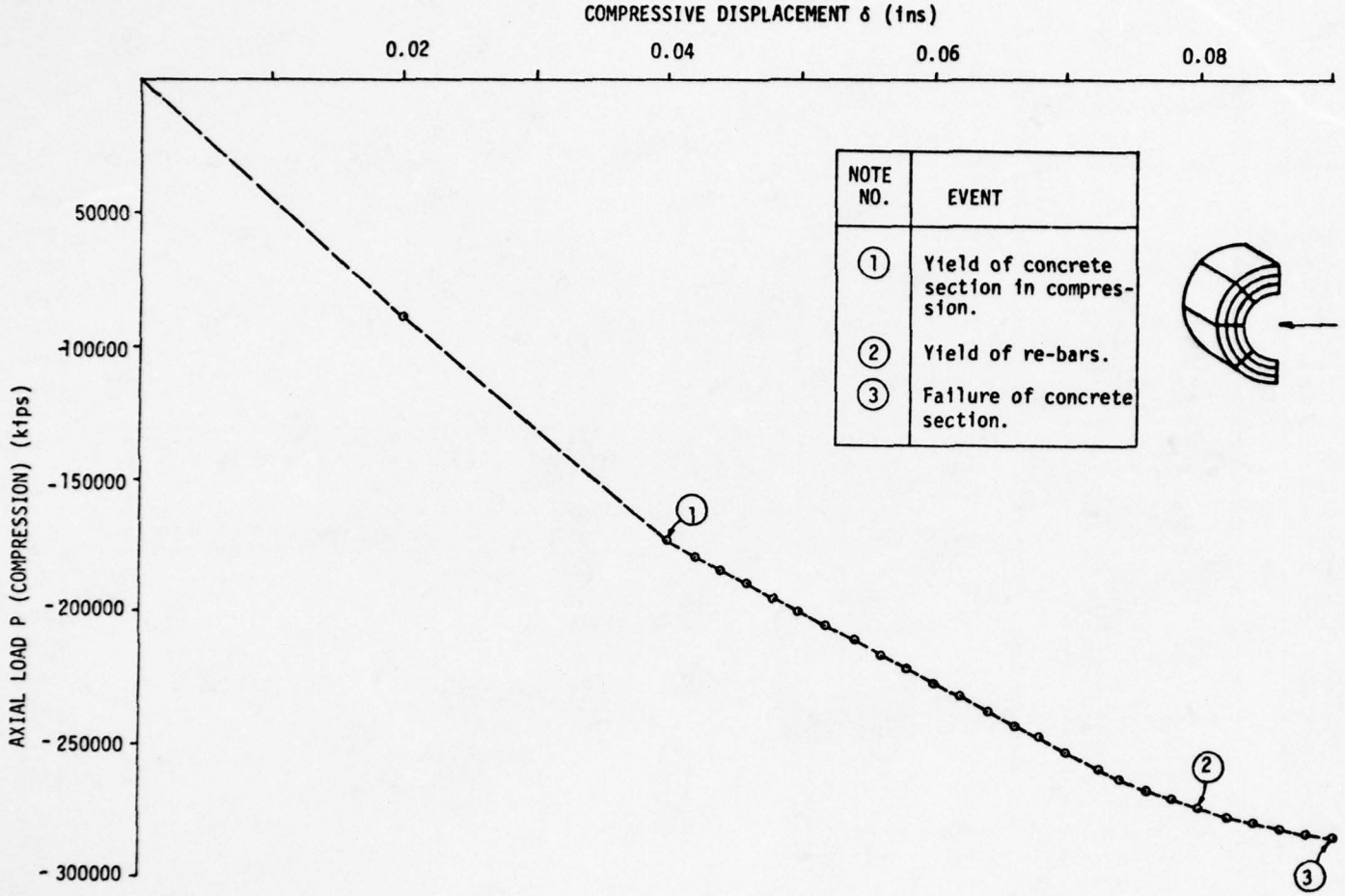

Figure 49.1 CCS-2 Pure Compression

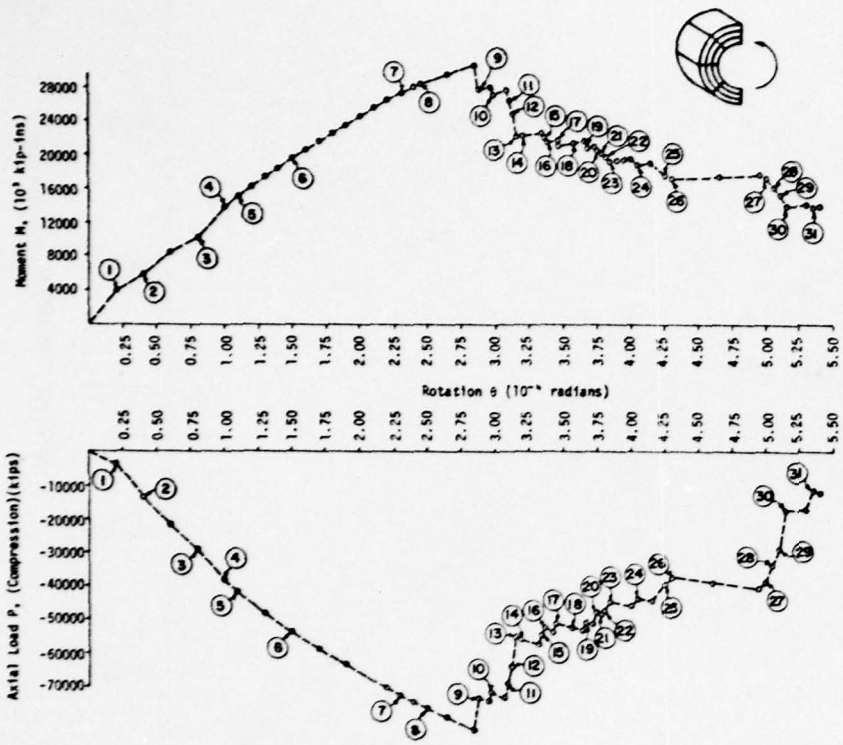

NOTE NO.	EVENT
1	Cracking of Elements #10, 11, 12.
2	Cracking of Elements #7,8,9 (4 nodes each).
3	Yield of Element #1, 2 (4 nodes each in compression) Yield of Element #3 (2 nodes in compression).
4	Complete yield of Elements #1, 2, 3 in compression. Cracking of elements #8, 9 (complete).
5	Cracking of Element #7 (complete).
6	Yield of Elements #7, 5, 6 (4 nodes each in compression).
7	Yield of re-bars in compression and tension.
8	Yield of re-bars in tension and compression.
9	Crushing of Element #1 (3 nodes in compression, 1 node in tension-compression).
10	Crushing of Element #1 (4 nodes in compression, 1 node in t-c).
11	Crushing of Element #2 (2 nodes in compression).
12	Crushing of Element #2 (3 nodes in compression). Crushing of Element #3 (2 nodes in compression.)

NOTE NO.	EVENT
13	Crushing of Element #2, 3 (4 nodes each in compression).
14	Yield of re-bars in tension and compression.
15	Crushing of Element #2 (5 nodes in compression).
16	Crushing of Element #2 (6 nodes in compression).
17	Crushing of Element #1 (5 nodes in compression, 1 node in t-c).
18	Yield of re-bars in compression and tension.
19	Crushing of Element #1 (6 nodes in compression, 1 node in t-c).
20	Crushing of Element #3 (5 nodes in compression).
21	Crushing of Element #3 (6 nodes in compression).
22	Yield of Element #4 (4 nodes in compression, 2 nodes in t-c).
23	Failure of Element #1.
24	Crushing of Element #2 (7 nodes in compression).
25	Failure of Elements #2, 3.

NOTE NO.	EVENT
26	Complete yield of Element #4, 4 nodes in compression, 4 nodes in t-c. Yield of Element #5 (4 nodes in compression, 3 nodes in t-c). Yield of Element #6 (4 nodes in compression, 2 nodes in t-c).
27	Crushing of Element #4 (1 node in compression).
28	Crushing of Element #4 (3 nodes in compression).
29	Crushing of Element #5 (1 node in compression). Cracking of Element #5 (1 node). Crushing of Element #6 (1 node in compression).
30	Crushing of Element #4 (3 nodes in compression, 2 nodes in t-c). Cracking of Element #5 (3 nodes). Cracking of Element #6 (3 nodes). Crushing of Element #6 (3 nodes in compression).
31	Crushing of Element #4 (3 nodes in compression, 4 nodes in t-c). Crushing of Element #5 (1 node in compression, 2 nodes in t-c). Cracking of Element #5 (3 nodes). Failure of Element #6.

Figure 49.2 CCS-2 Pure Rotation

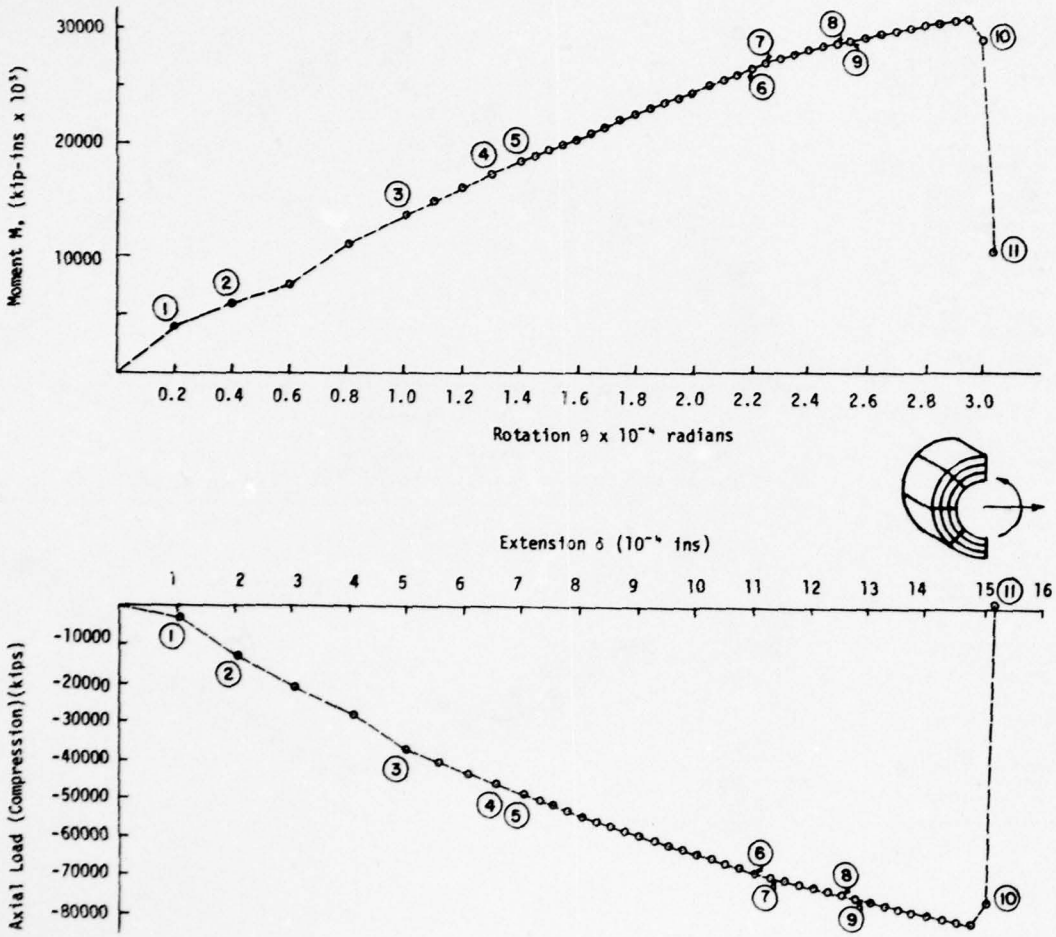

NOTE NO.	EVENT
1	Cracking of elements #10, 11, 12.
2	Cracking of element #7, 8, 9 (4 nodes each.
3	Complete cracking of element #7, 8, 9. Complete yield of element #1, 2, 3 in compression.
4	Yield of element #4, 5 (4 nodes each) element #6 (1 node).
5	Yield of element #6 (3 nodes).
6	Yield of re-bar in tension.
7	Yield of re-bar in compression.
8	Yield of re-bar in tension.
9	Yield of re-bar in compression.
10	Crushing of element #1 (5 nodes).
11	Crushing of whole section.

Figure 49.3 CCS-2 Extension/Rotation = 5.0

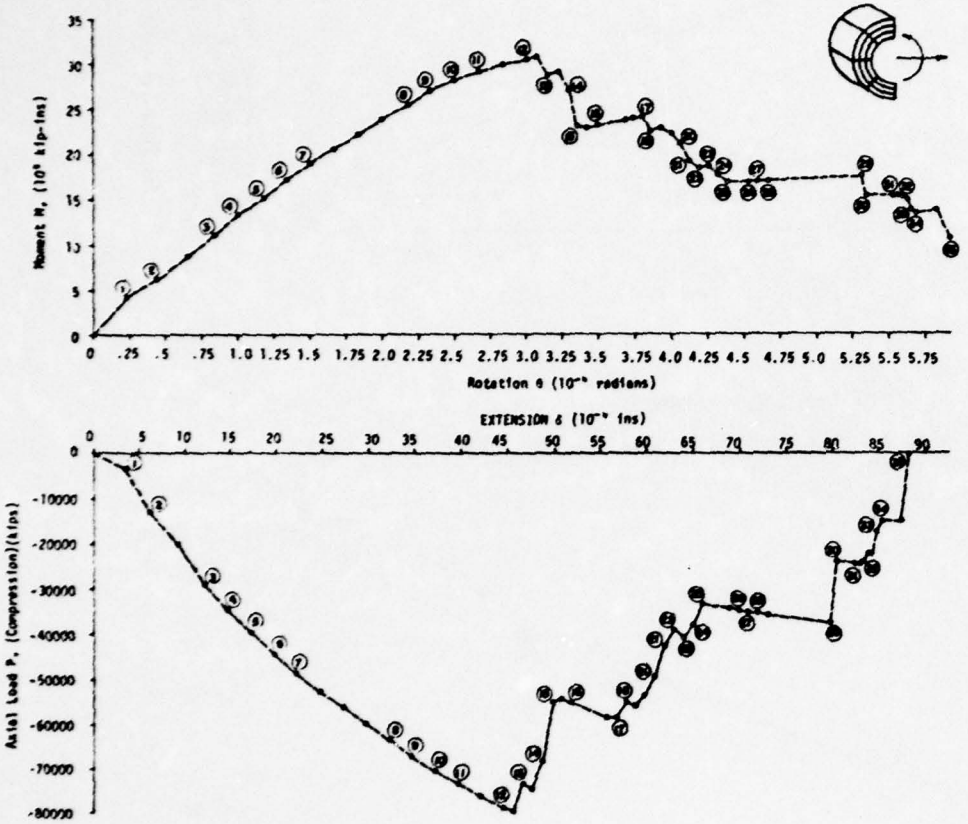

NOTE NO.	EVENT
(1)	Elements #10, 11, 12 crack 8 nodes. Element #9 cracks 2 nodes.
(2)	Elements #7, 8, 9 crack 4 nodes.
(3)	Elements #7, 8, 9 crack 8 nodes. Elements #1, 2, 3 yield 4 nodes.
(4)	Elements #1, 2 yield 8 nodes. Element #3 yields 7 nodes.
(5)	Element #3 yields 8 nodes.
(6)	Element #4 yields 2 nodes. Element #5 yields 1 node.
(7)	Elements #4, 5, 6 yield 4 nodes.
(8)	Steel element #10 yields in tension.
(9)	Steel element #2 yields in compression.
(10)	Steel element #9 yields in tension.
(11)	Steel element #1 yields in compression.
(12)	Steel element #8 yields in tension.
(13)	Element #1 crushes 3 nodes (c).
(14)	Element #1 crushes 4 nodes (c). Element #2 crushes 3 nodes (2c, 1t-c). Element #3 crushes 1 node (t-c).
(15)	Element #2 crushes 4 nodes (3c, 1t-c). Element #3 crushes 5 nodes (4c, 1t-c). Steel element #4 yields in compression. Steel element #7 yields in tension. Solution does not converge.
(16)	Element #1 crushes 5 nodes (4c, 1t-c).
(17)	Steel element #3 yields in compression. Element #2 crushes 5 nodes (4c, 1t-c).
(18)	Element #1 crushes 6 nodes.
(19)	Element #1 crushes 7 nodes.
(20)	Element #2 crushes 6 nodes.
(21)	Element #1 crushes 8 nodes. Element #3 crushes 6 nodes (5c, 1t-c). Solution does not converge.
(22)	Element #2 crushes 7 nodes.
(23)	Element #4 yields 5 nodes.
(24)	Element #2 crushes 8 nodes. Element #3 crushes 7 nodes. (6c, 1t-c).
(25)	Element #3 crushes 8 nodes (7c, 1t-c). Element #4 yields 6 nodes. Element #5 yields 5 nodes.
(26)	Element #6 yields 5 nodes.
(27)	Element #5 yields 6 nodes.
(28)	Element #6 yields 6 nodes.
(29)	Element #4 yields 7 nodes.
(30)	Element #4 crushes 8 nodes.
(31)	Element #5 yields 7 nodes.
(32)	Element #5 crushes 1 node (c).
(33)	Element #5 crushes 3 nodes (c). Solution does not converge.
(34)	Element #5 crushes 4 nodes (c).
(35)	Element #5 crushes 7 nodes (4c, 3t-c). Element #6 crushes 8 nodes.

Figure 49.4 CCS-2 Extension/Rotation = 15.0

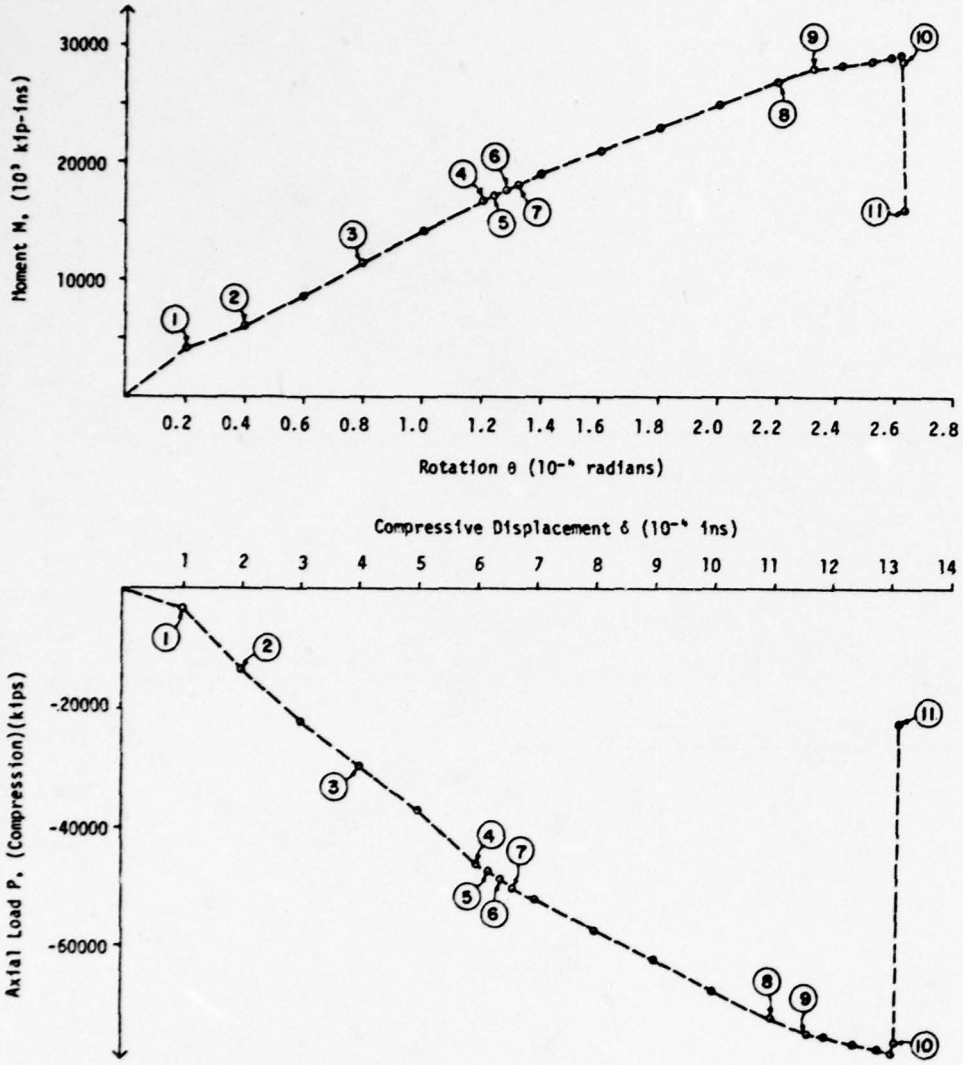

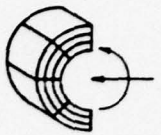

NOTE NO.	EVENT
(1)	Cracking of Elements #11, 12 (total). Element #10 (7 nodes).
(2)	Cracking of Element #10 (1 node). Cracking of Elements #7, 8, 9 (4 nodes each).
(3)	Yield of Elements #1, 2 (in compression, 4 nodes each). Yield of Element #3 (3 nodes).
(4)	Yield of Elements #1, 2, 3 complete. Failure of Elements #7, 8, 9.
(5)	Yield of Elements #4, 5 (4 nodes each). Yield of Element #6 (1 node).
(6)	Yield of Element #6 (2 nodes).
(7)	Yield of Element #6 (1 node).
(8)	Yield of re-bar in compression.
(9)	Yield of re-bar in tension.
(10)	Crushing of Element #1 in tension-compression (1 node).
(11)	Failure of concrete section.

Figure 49.5 CCS-2 Compression/Rotation = 5.0

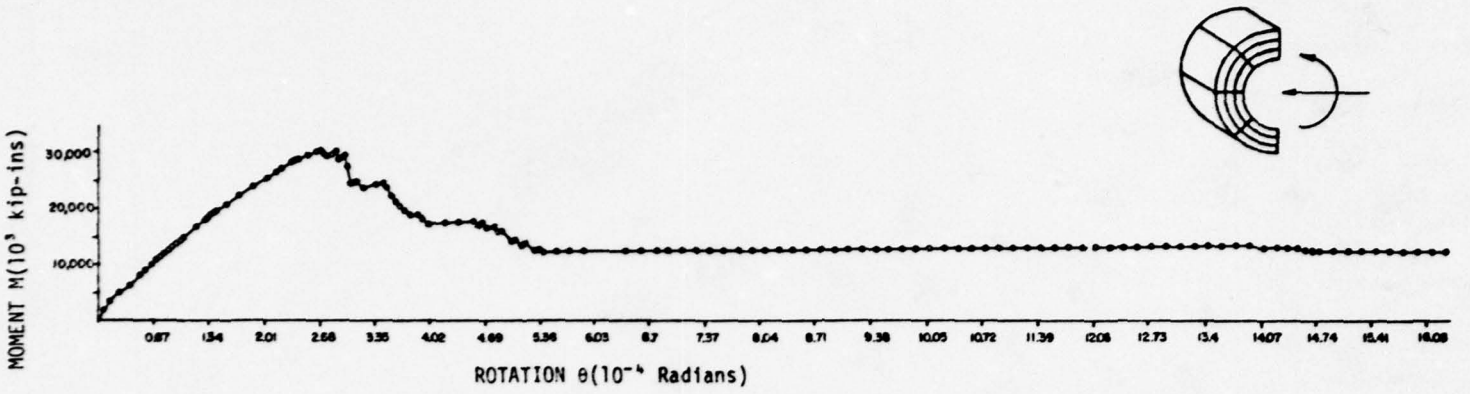

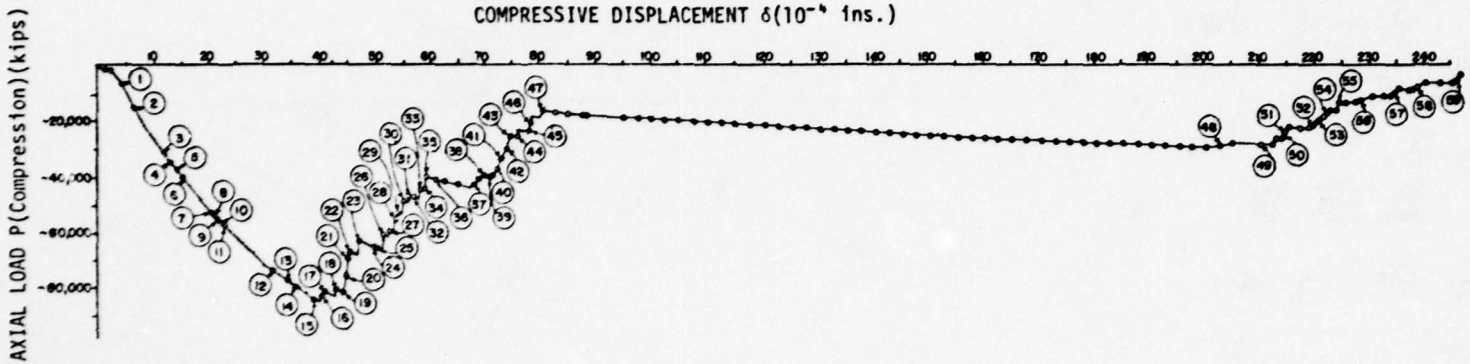

Figure 49.6a CCS-2 Compression/Rotation = 15.0

NOTE NO.	EVENT
(1)	Cracking of Elements #10, 11, 12 (total).
(2)	Cracking of Elements #7, 8, 9 (4 nodes each).
(3)	Yield of Elements #1, 2, 3 (4 nodes each in compression).
(4)	Complete yield of Element #1 in compression.
(5)	Complete yield of Element #2 in compression. Cracking of Element #8, 9 (6 nodes each).
(6)	Complete yield of Element #3 in compression.
(7)	Failure of Element #9; Cracking of Element #7 (5 nodes).
(8)	Cracking of Element #8 (7 nodes).
(9)	Failure of Element #8; cracking of Element #7 (6 nodes).
(10)	Cracking of Element #7 (7 nodes).
(11)	Failure of Element #7.
(12)	Yield of re-bar in compression.
(13)	Yield of re-bar in tension.
(14)	Yield of re-bar in compression.
(15)	Yield of re-bar in tension.

NOTE NO.	EVENT
(16)	Crushing of Element #1 (1 node in compression).
(17)	Crushing of Element #1 (2 nodes in compression).
(18)	Crushing of Element #1 (3 nodes in compression).
(19)	Yield of re-bar in compression.
(20)	Crushing of Element #2 (1 node in compression). Crushing of Element #2 (2 nodes in compression).
(21)	Crushing of Element #1 (4 nodes in compression). Crushing of Element #2 (3 nodes in compression).
(22)	Crushing of Element #2 (4 nodes in compression).
(23)	Crushing of Element #3 (4 nodes in compression).
(24)	Yield of re-bar in tension.
(25)	Yield of re-bar in compression.
(26)	Crushing of Element #1 (6 nodes in compression).
(27)	Crushing of Element #1 (7 nodes in compression).
(28)	Crushing of Element #2 (6 nodes).
(29)	Failure of Element #1 in compression.

NOTE NO.	EVENT
(30)	Crushing of Element #3 (6 nodes in compression).
(31)	Crushing of Element #2 (7 nodes in compression).
(32)	Yield of re-bar in tension.
(33)	Failure of Element #2 in compression.
(34)	Crushing of Element #3 (7 nodes in compression).
(35)	Failure of Element #3 in compression.
(36)	Complete yield of Elements #4, 5, and 6.
(37)	Crushing of Element #4 (1 nodes in compression).
(38)	Crushing of Element #4 (2 nodes in compression).
(39)	Crushing of Element #4 (3 nodes in compression.)
(40)	Crushing of Element #5 (1 node in compression).
(41)	Crushing of Element #5 (2 nodes in compression).
(42)	Crushing of Element #6 (2 nodes in compression).
(43)	Crushing of Element #4 (4 nodes in compression).
(44)	Crushing of Element #5 (3 nodes in compression).

NOTE NO.	EVENT
(45)	Crushing of Element #5 (4 nodes in compression).
(46)	Crushing of Element #6 (3 nodes in compression).
(47)	Crushing of Element #6 (4 nodes in compression).
(48)	Crushing of Element #5 (4 nodes in compression, 1 node in tension-compression).
(49)	Crushing of Element #4 (5 nodes in compression).
(50)	Crushing of Element #4 (6 nodes in compression).
(51)	Crushing of Element #5 (5 nodes in compression, 1 node in t-c).
(52)	Crushing of Element #4 (7 nodes in compression).
(53)	Crushing of Element #6 (5 nodes in compression).
(54)	Crushing of Element #6 (6 nodes in compression).
(55)	Failure of Element #4.
(56)	Crushing of Element #5 (6 nodes in compression, 1 node in t-c).
(57)	Failure of Element #5.

NOTE NO.	EVENT
(58)	Crushing of Element #6 (7 nodes in compression).
(59)	Failure of entire concrete section.

Figure 49.6b CCS-2 Compression/Rotation = 15.0

(3) Response Of CCS-3

The cylindrical sections analyzed CCS-1, CCS-2 seemed to indicate that a change in the r/t ratio changed the form of the failure envelope. Both these sections were subjected to imposed deformation of displacements and rotations. The response of a cylindrical section was now analyzed when subjected to a pressure load of "3-4-5" (Figure 50). This pressure loading was idealized as shown in Figure 50. The cylinder was symmetrically loaded with respect to vertical and horizontal planes through the longitudinal axis. Such a symmetric loading pattern causes symmetric cracking and yield patterns. Thus only a quarter of the cylinder was modeled with appropriate boundary conditions. The boundary conditions imposed on the section were as follows: symmetry boundary condition in X-direction on face (1-4-12-9), symmetry boundary condition on face (9-12-24-21) in the Y-direction while the face (1-4-16-13) was restrained in the Z-direction. The finite element model is shown in Figure 51. As before, concrete was modeled using three-dimensional brick elements while steel was modeled as 3-D truss elements. The uniaxial stress-strain relations for concrete and steel are shown in Figure 17 and Figure 18. The ratio r/t was assumed to be 4.

Figure 52 shows a plot of load vs. displacement at the crown of the cylinder (node 4) when subjected to a monotonically increasing distributed load of "3-4-5". As can be seen from this figure, the section yields completely in isotropic compression at point 2, while failure of the section occurs at point 3 at a displacement of

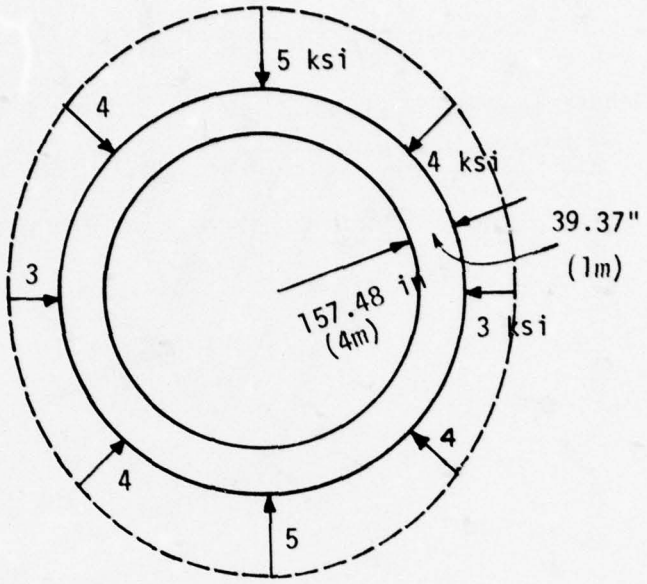

Actual cylindrical section with actual "3-4-5" pressure load distribution

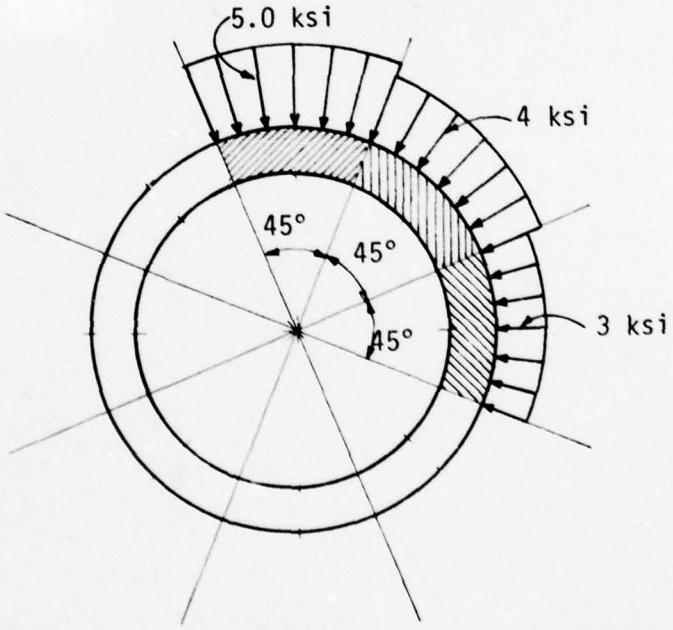

Actual cylindrical section with idealized pressure loading

Figure 50. Actual and Idealized Loading. Cylindrical Section with a Pressure Load of "3-4-5"

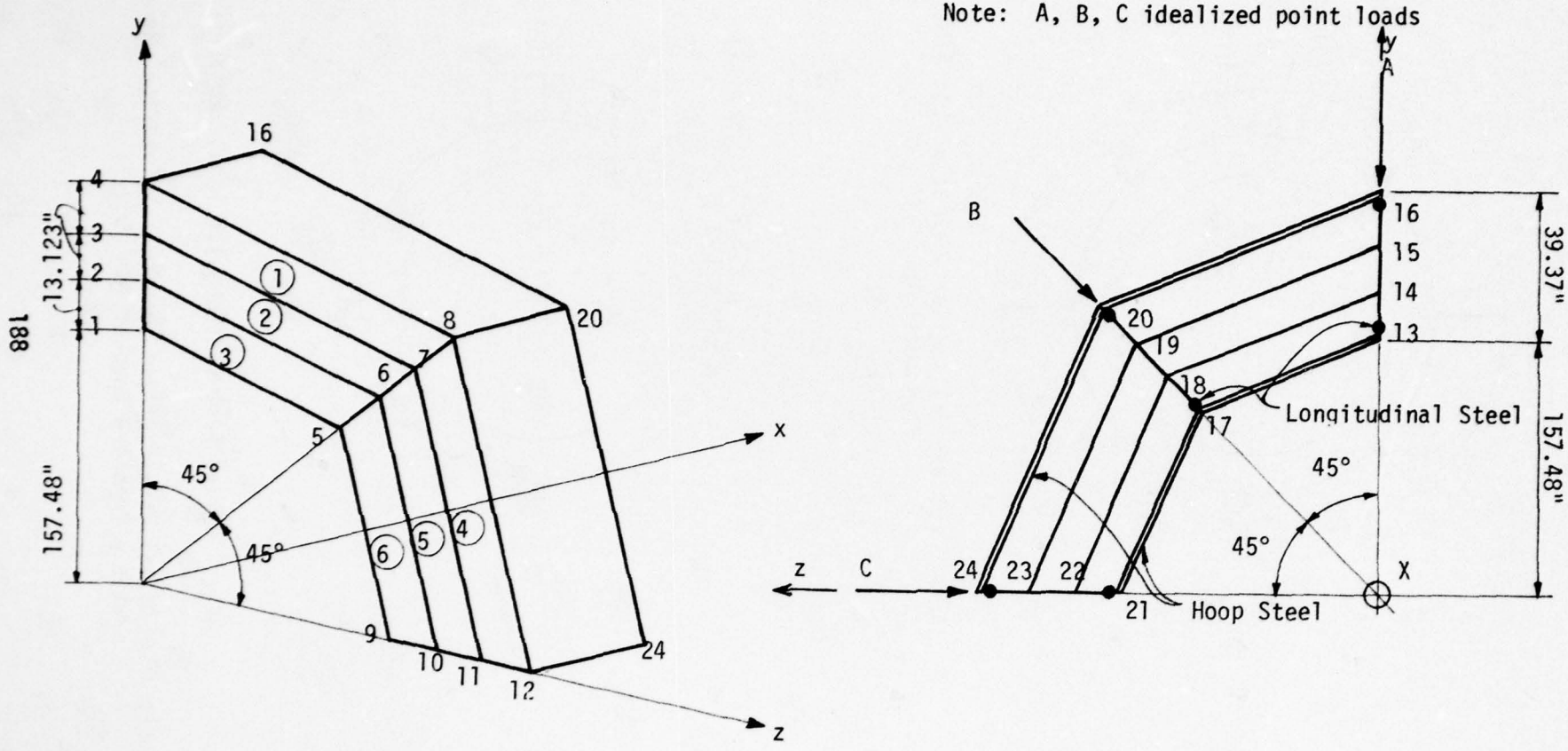

Figure 51. Finite Element Model for Cylindrical Section with a Pressure Load of "3-4-5"

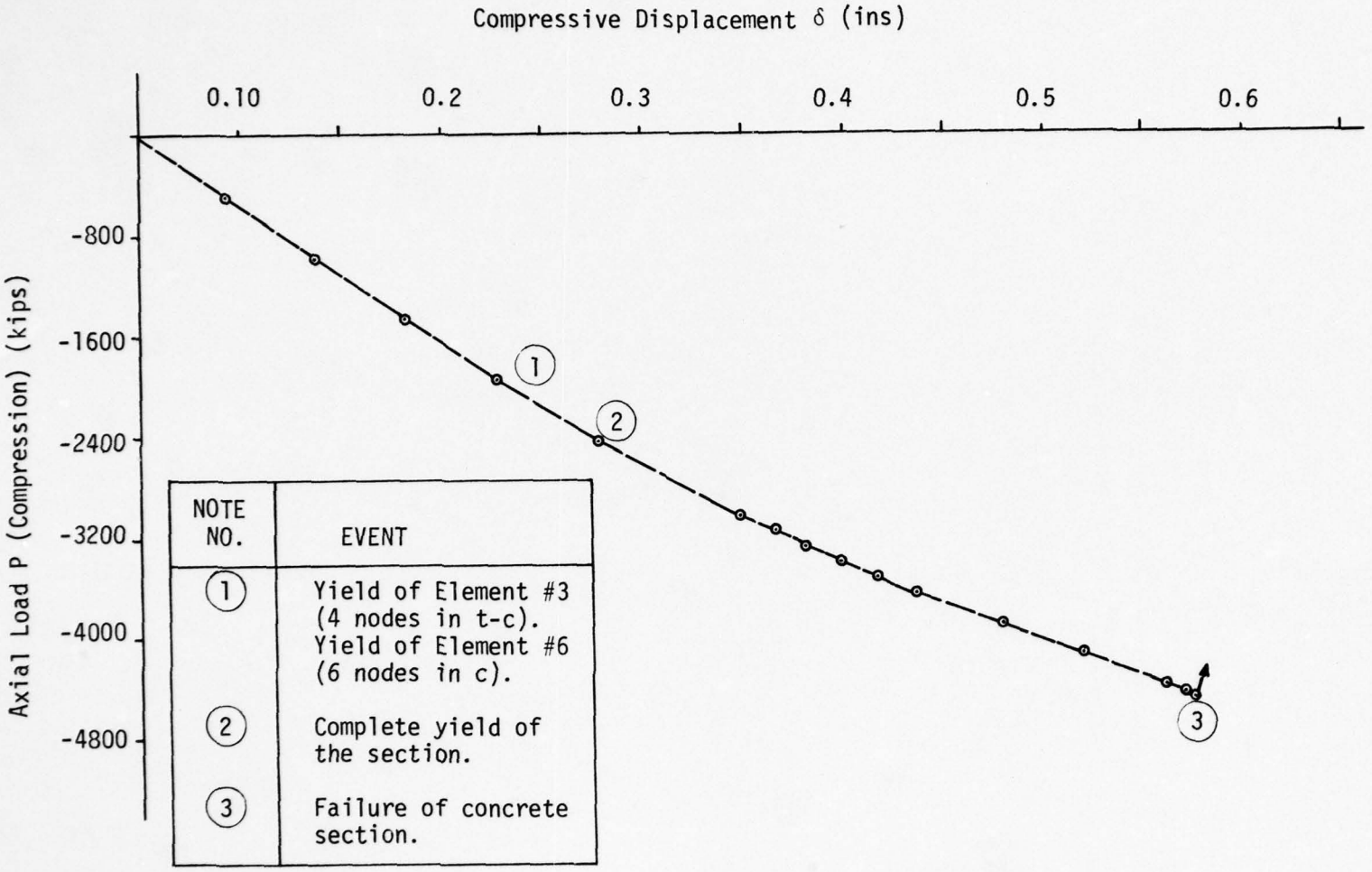

Fig. 52 CCS-3 - Load vs. Deformation Nodes 4, 16

0.58 ins. Failure of the section is defined when the concrete section completely crushes.

AD-A070 644 PMB SYSTEMS ENGINEERING INC SAN FRANCISCO CA F/G 11/2
FAILURE CRITERIA FOR REINFORCED CONCRETE STRUCTURES. VOLUME II.--ETC(U)
MAY 79 R W LITTON, J M GIDWANI F29601-76-C-0135
UNCLASSIFIED AFWL-TR-77-239-VOL-2 NL

3 OF 3
AD A070644

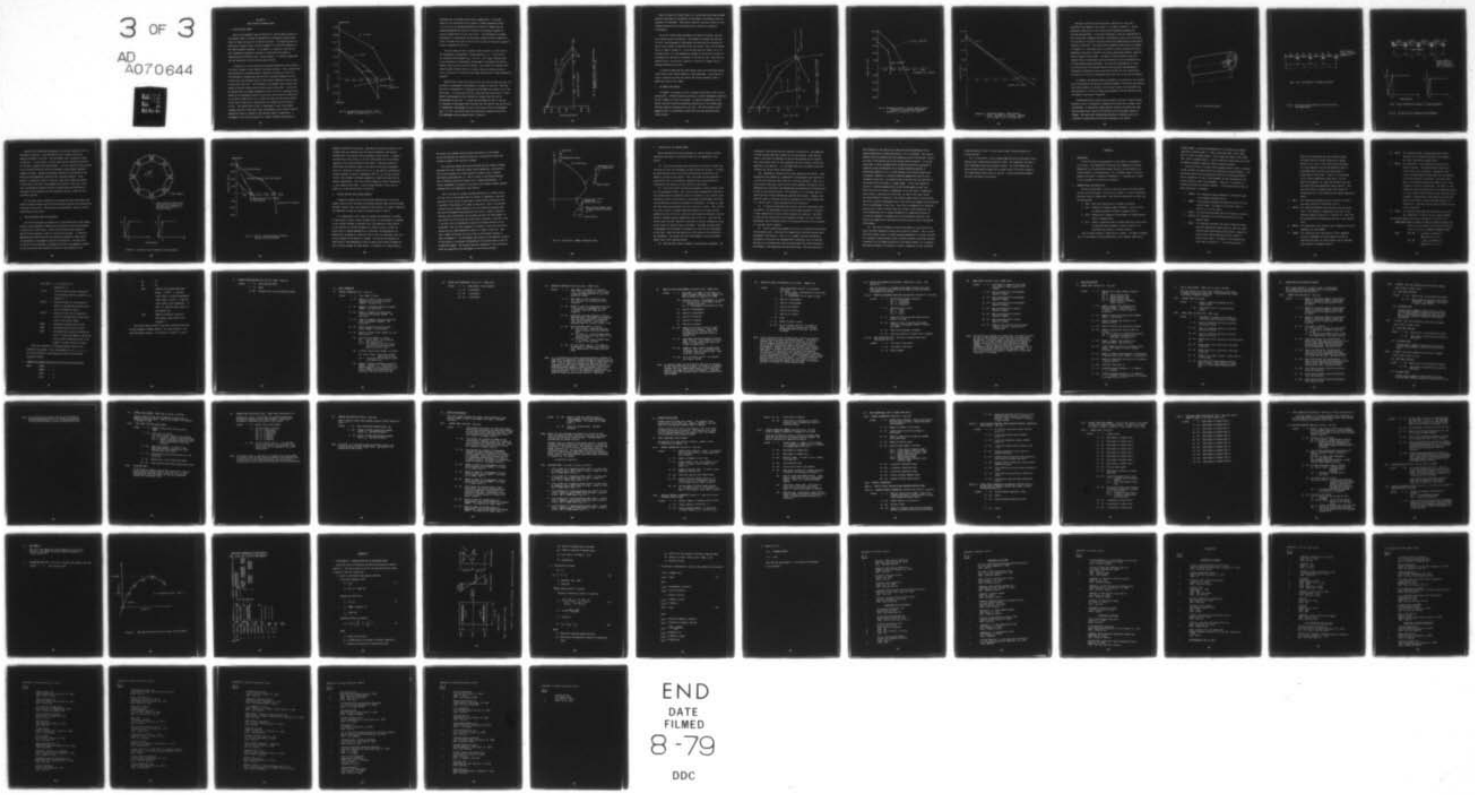

END
DATE FILMED
8-79
DDC

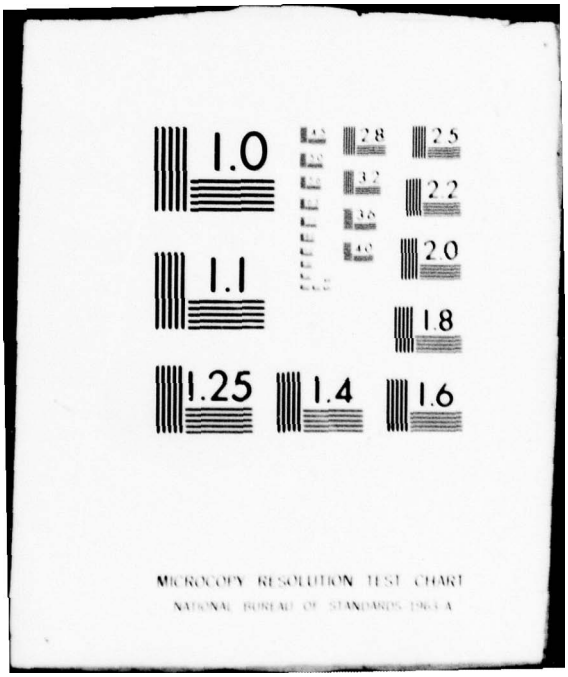
1.0
1.1
1.25
1.4
1.6
2.8
3.2
3.6
4.0
2.5
2.2
2.0
1.8
MICROCOPY RESOLUTION TEST CHART
NATIONAL BUREAU OF STANDARDS 1963 A

SECTION IV

APPLICATIONS OF PROPOSED MODEL

1. FAILURE DESIGN CURVES

Based on the parametric data of Section III, failure design curves are now proposed shown in Figures 53 through 56 for rectangular sections while Figure 57 shows the curve for cylindrical sections. In formulating each of these sets of design curves, only one parameter is varied while keeping all the other parameters constant. As an example, in Figure 53, only the uniaxial compressive strength of concrete is varied while the amount of longitudinal and transverse steel is kept constant. It should be emphasized that the dimensions of the section are kept constant.

In Figure 53 it can be seen that the maximum deformation of the section, at failure, reduces as the strength of concrete increases. Thus a section with concrete having an ultimate uniaxial compressive strength of 6.0 ksi has less deformation strength than the one with a concrete strength of 5.0 ksi. In both cases, the ultimate strain of the uniaxial compressive stress-strain relation was 0.003 in/in. This difference in strengths could be due to the nature of uniaxial stress-strain relations used in both cases. In the case of concrete with an ultimate compressive stress of 6.0 ksi, unloading corresponding to the descending portion of the curve, from a strain of 0.002 in/in to a strain of 0.003 in/in is at a faster rate than for the similar portion of the curve in the case of concrete with an ultimate uniaxial stress of 5.0 ksi. This imples that failure is accelerated in case of the higher strength concrete as the stress state corresponding to the ultimate uniaxial compressive stress is reached in the concrete loaded in compression. A refinement of the failure envelope for a higher strength concrete may be

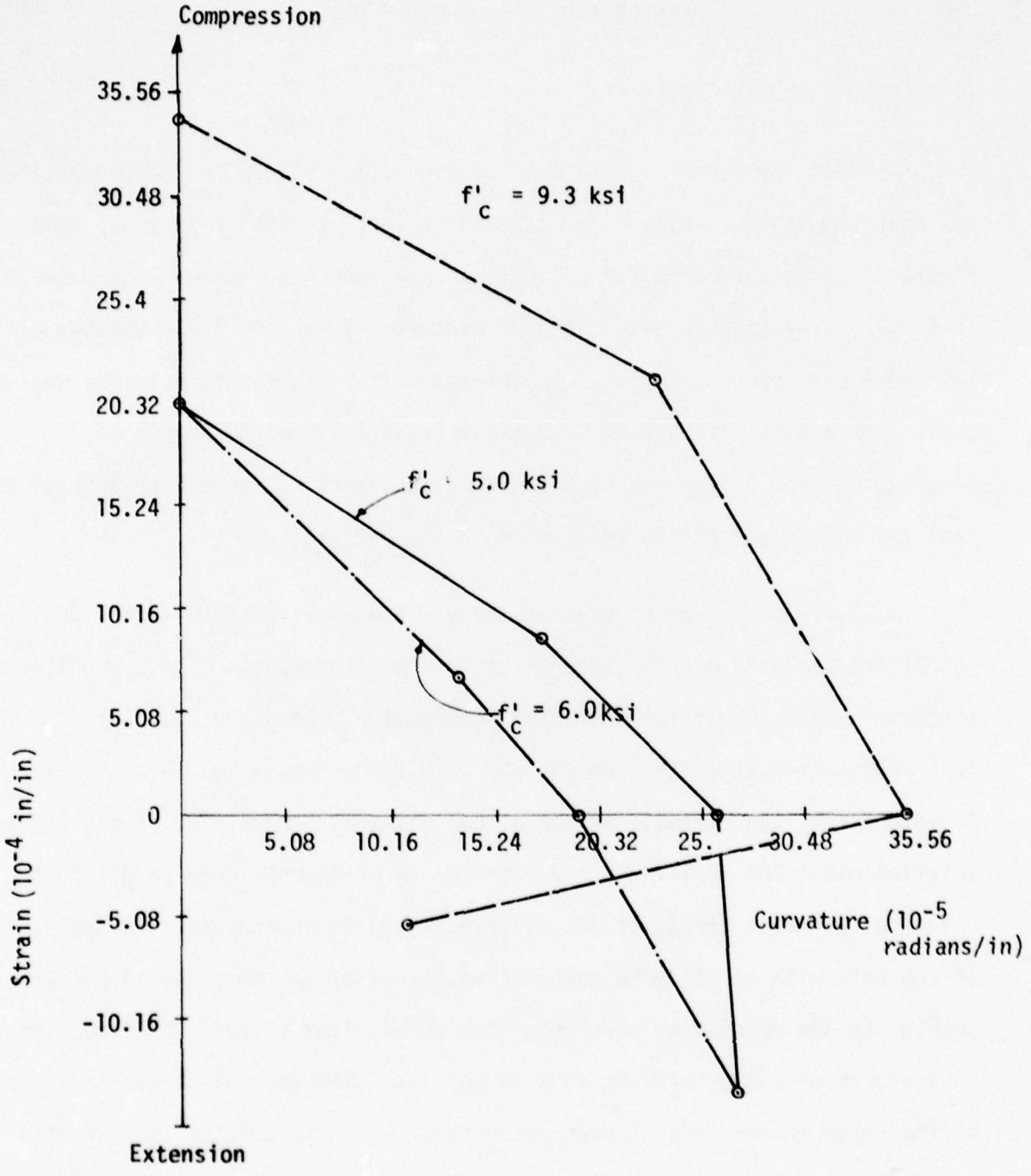

Fig. 53 Rectangular Section, "Design" Failure Curves. Variation of f'_c, $p = p' = 2\%$

obtained with a refinement of the finite element mesh. In the same Figure 53, for the section with a uniaxial ultimate compressive stress f'_c of 9.3 ksi, the maximum deformation at failure is higher than the maximum deformation at failure of sections with concrete strengths in uniaxial compression of 5.0 ksi and 6.0 ksi. This difference in maximum deformations is exhibited due to the higher ultimate uniaxial compressive strain of 0.0045 in/in used in the case of sections with concrete strength in uniaxial compression of 9.3 ksi.

Figure 54 shows the failure design curves varying f'_c of the section. The longitudinal reinforcement is kept constant ($p = p' = 1/4\%$) as also the transverse reinforcement ($A_{sh} = 0.6$ in^2). This figure indicates that as the percentage of longitudinal reinforcement is decreased, the section behaves close to a plain concrete section. This figure also indicates that given the same ultimate strain for concrete having an ultimate stress of 5.0 ksi and 6.0 ksi, the section with higher concrete has a higher deformation strength.

Design failure curves for sections having the same strength concrete, but variation in longitudinal reinforcement, are shown in Figure 55. Note that the ratio of longitudinal to transverse reinforcement was constant in all the three cases. It can be seen from this figure that the section with 1% longitudinal reinforcement has more deformation strength than one with 2% reinforcement at each face. It should be mentioned here that if the area of transverse reinforcement would have been kept the same for the section with 1% longitudinal reinforcement as that of the section with 2% reinforcement ($A_{sh} = 3.5$ in^2), the section would gain additional strength and ductility. This phenomenon has been demonstrated in Figure 56.

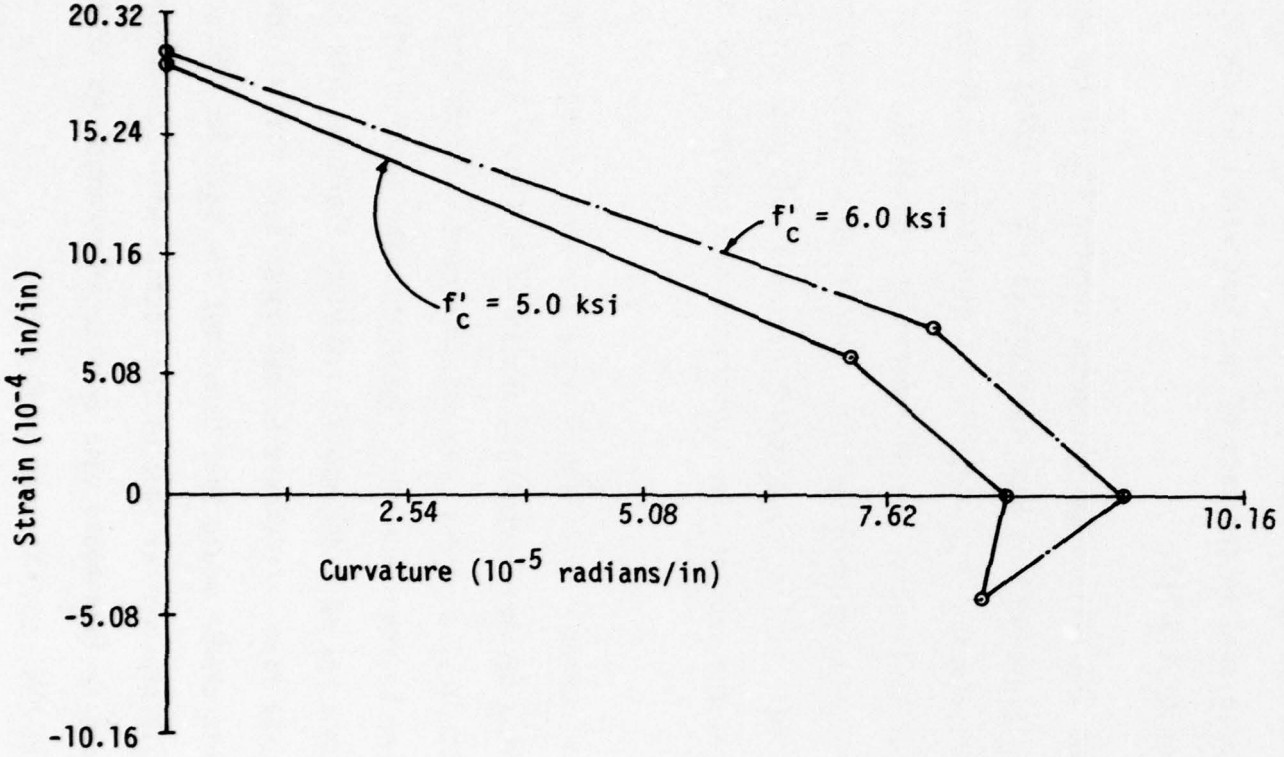

Fig. 54 Rectangular Section. Design Failure Curves. Variation of f'_c, $p = p' = 1/4\%$.

Figure 56 shows the failure curves of a section having the same strength concrete, percentage of longitudinal reinforcement, but different areas of transverse reinforcement. These curves indicate a definite increase in the strength and ductility of the section with an increase in transverse reinforcement.

Due to the limited study performed on cylindrical sections, only one set of design curves is presented. The strength of concrete was the same (5.0 ksi), the percentage of longitudinal and hoop steel was constant but the r/t ratio (radius to thickness ratio) was varied. Such a set of design curves is shown in Figure 57. As can be seen from this figure, as r/t is increased from 4 to 8, the deformation strength of the section increases in the compression zone while it decreases in the tension zone. Near the pure rotation zone, a section with a smaller r/t ratio has a higher value of maximum deformation at failure.

It should be mentioned that these design curves are preliminary design curves based on the limited parametric study undertaken. A more extensive study is required to verify and confirm the results presented, which is beyond the scope of this report.

2. AN EXAMPLE APPLICATION

An attempt is now made to define an example application of the failure design curves. Different modeling techniques to obtain deformation quantities for this example will also be reviewed. It should be emphasized, at the outset, that while obtaining deformation quantities for this example only nonlinear analysis techniques are to be used. The failure design curves cannot be used if the deformation quantities have been obtained using a linear analysis.

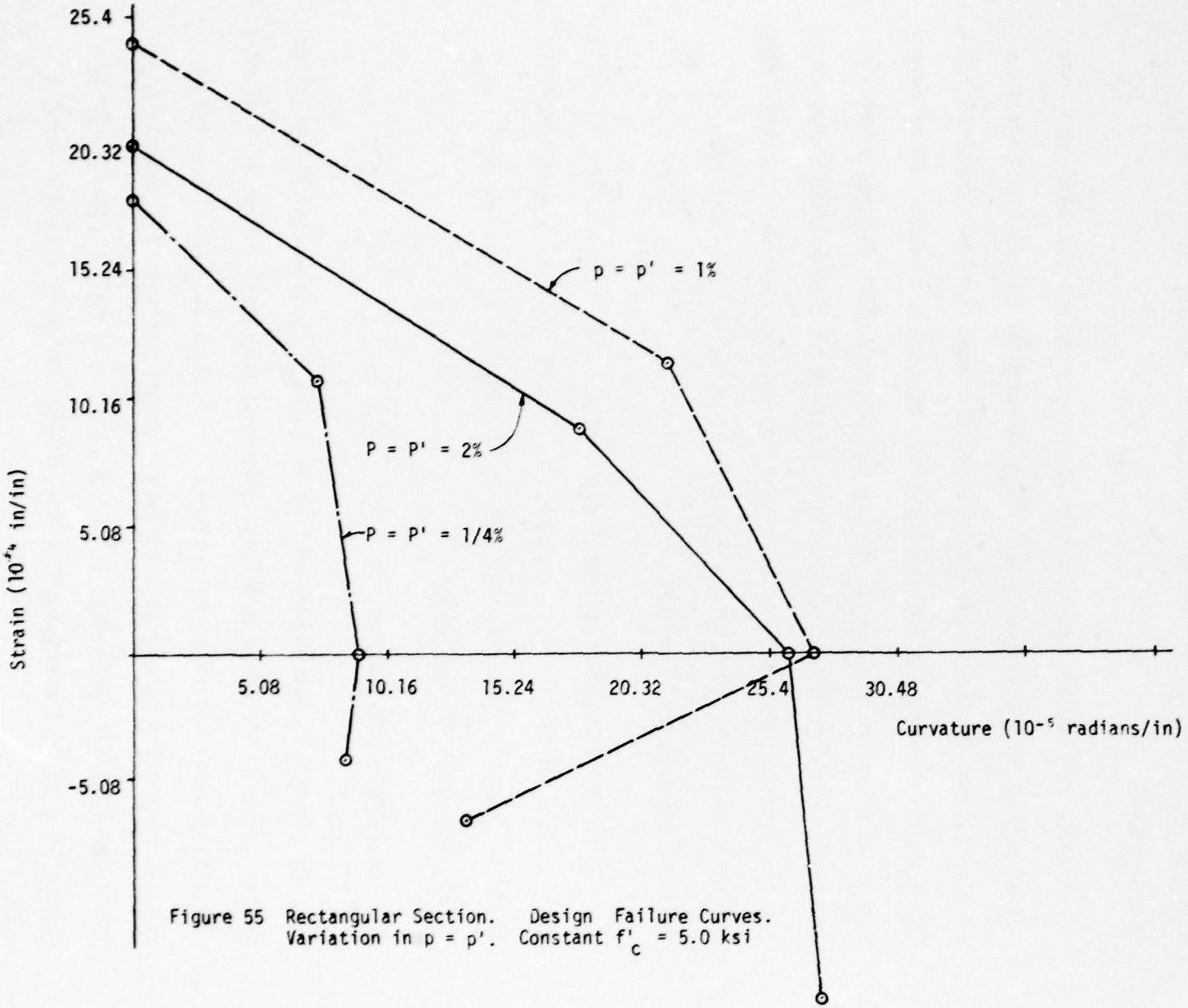

Figure 55 Rectangular Section. Design Failure Curves. Variation in p = p'. Constant f'_c = 5.0 ksi

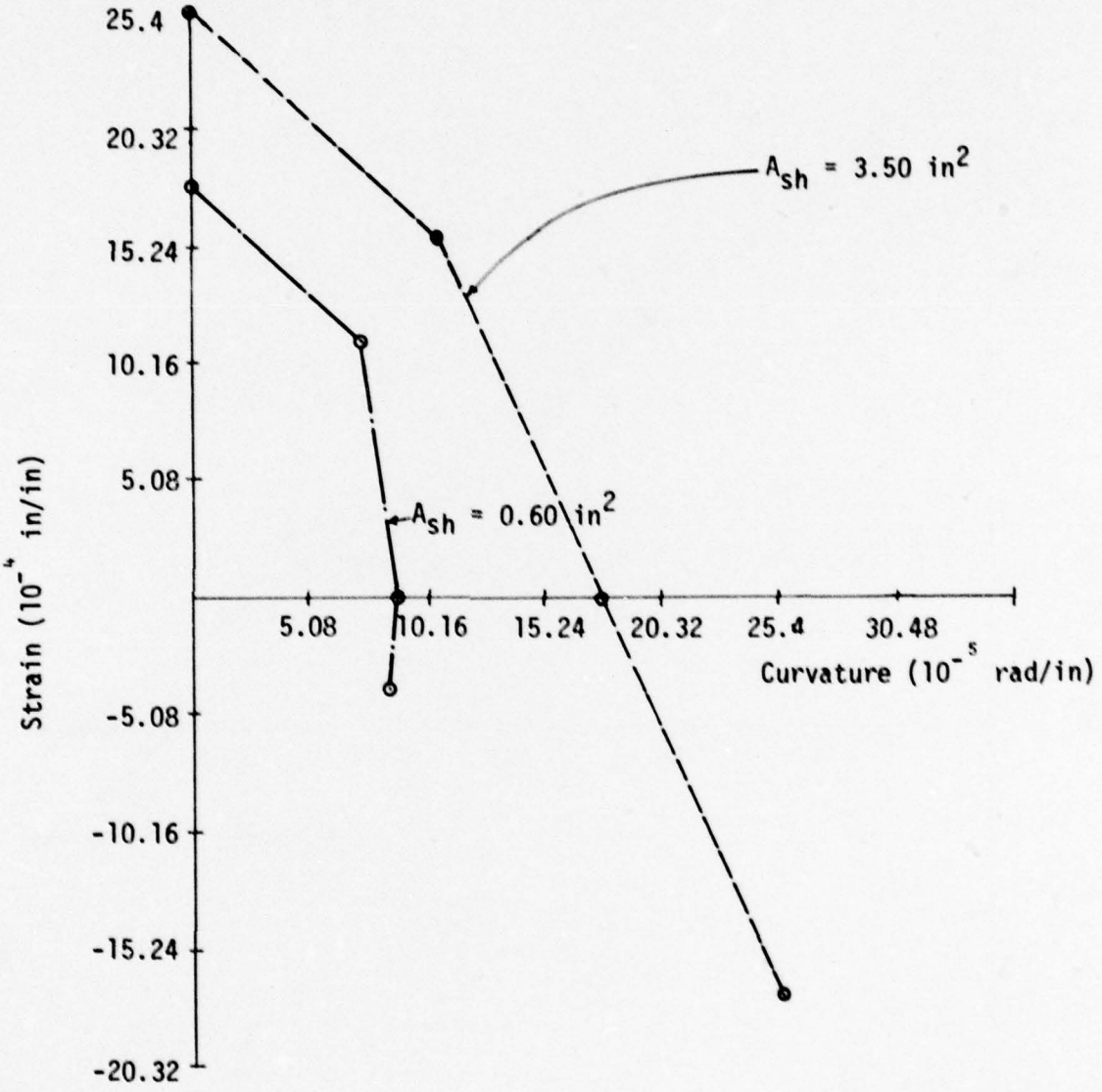

Fig. 56 Rectangular Section. Design Failure Curves. Variation of Transverse Reinforcement. Constant f'_c = 5.0 ksi, p = p' = 1/4%

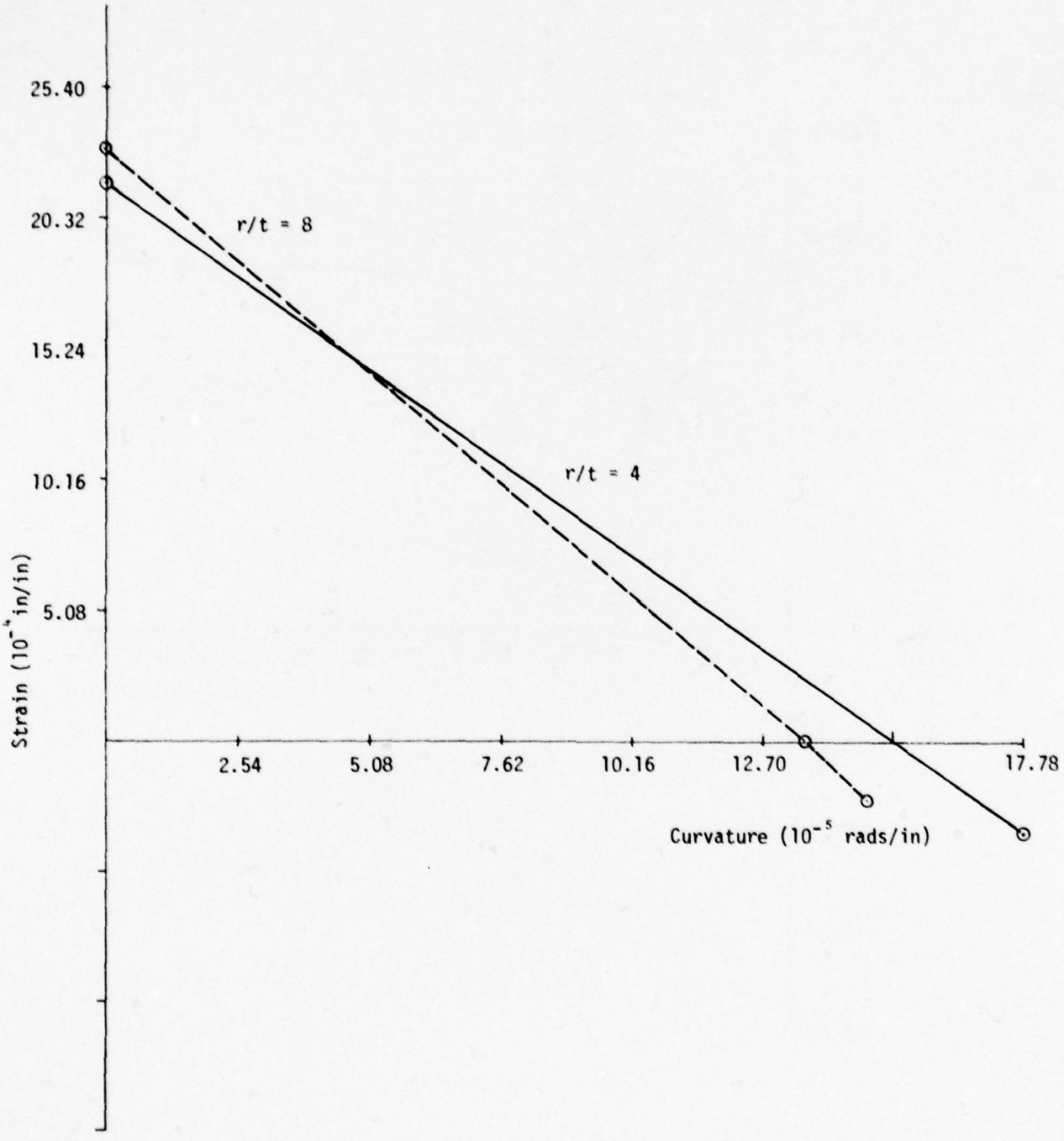

Figure 57. Cylindrical Section. Design Failure Curves. Variation of r/t ratio. Constant f'_c = 5.0 ksi, p = p' = 2%, hoop steel.

Consider a cylindrical section having a specified r/t ratio and a specified finite length of the section, L, as shown in Figure 58. Various deformation quantities for this section can be obtained by modeling the structure appropriately. If one were interested in the axial deformations of the cylinder when subjected to forces or deformations axially, one could model the structure as a series of discrete springs with lumped masses at appropriate intervals (Figure 59). The system could be modeled to have only axial degrees of freedom; i.e., the masses have no rotational inertia associated with them. Depending on the type of problem to be solved, appropriate boundary conditions could be imposed on this model. The model is then analyzed for the axial imposed forces or deformations and the distribution of axial deformation due to these imposed forces calculated. Once the axial deformations are known one could go back to the design failure curves and check the deformations (converted to appropriate strain quantities) against the axial deformations the section can resist as indicated by the strain axis of the failure envelope.

If, however, the maximum rotation attainable at any section of the cylinder was to be checked at various points along the length of the section when imposed with certain moments or rotations, with no axial forces, one could model the same structure as a series of beams interconnected at various intervals along the length of the section (Figure 60).

Concentrated plastic hinges could be formed at the end of these sections. Rotation, as well as extension or compression of these plastic hinges, could be permitted. If the plastic hinges had only rotation associated with them; then one would have a case of pure rotation at the displacement degrees of freedom. One could check these maximum rotations so obtained against the rotational strength given by the failure envelope of the section.

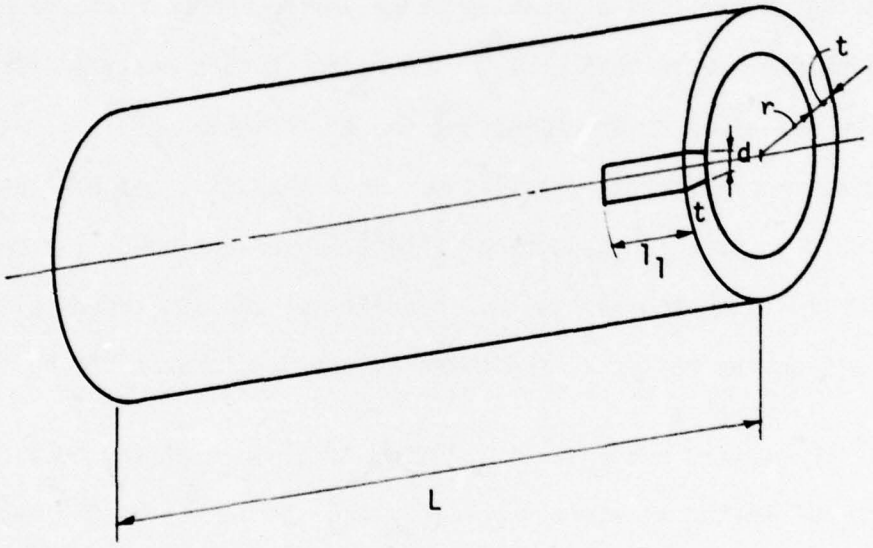

Fig. 58 Cylindrical Section

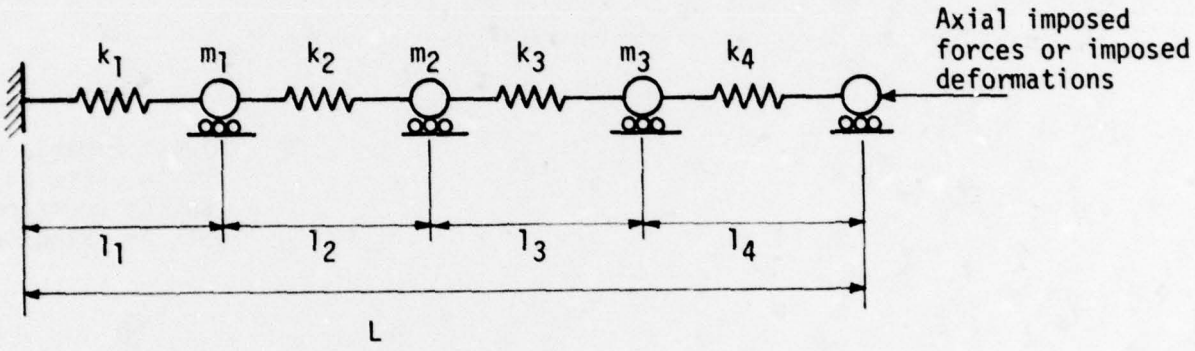

Note: Only axial degrees of freedom considered

Fig. 59 Cylindrical Section Modeled as Discrete Springs and Lumped Masses

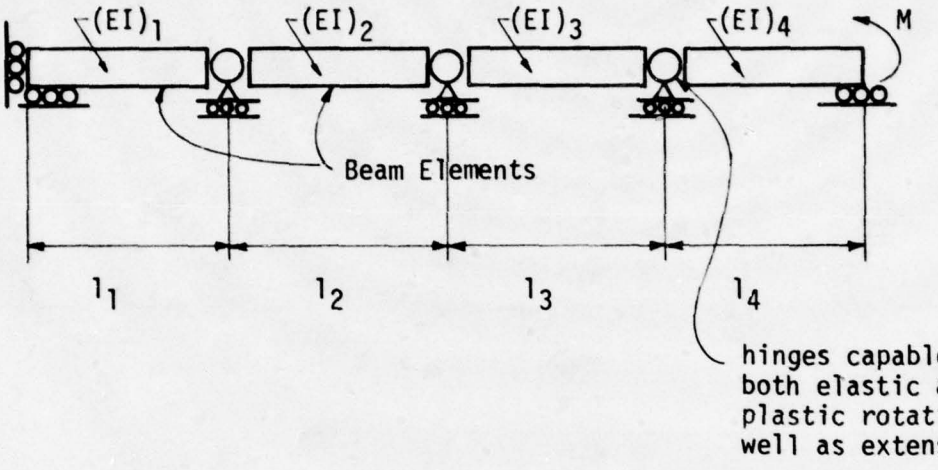

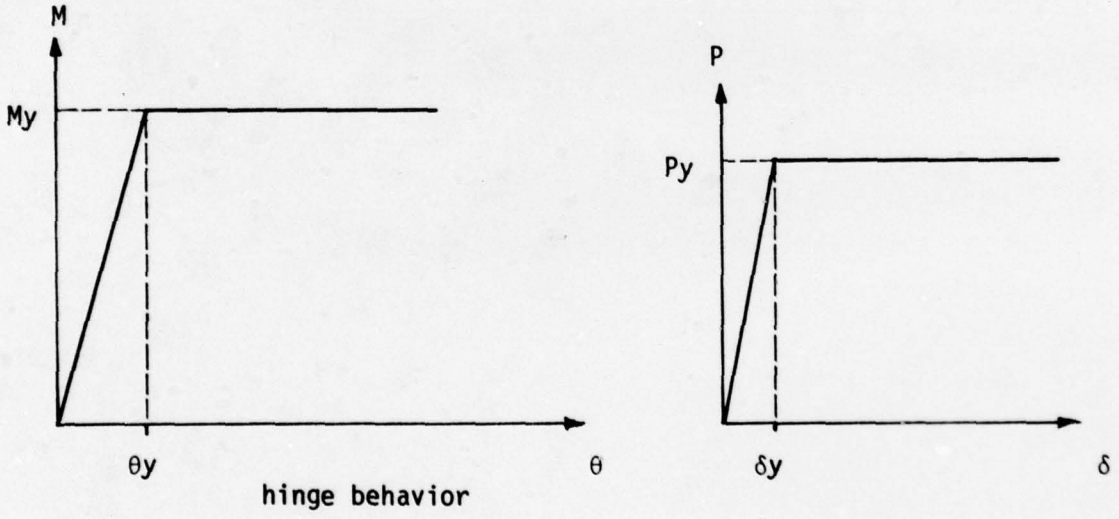

Note: Axial and Rotational Degrees of Freedom Considered

Fig. 60 Cylindrical Section Modeled As Beam Elements

Consider the cylinder being subjected to a pressure loading of 3-4-5 as indicated in Figure 61. Local buckling of such a section could be an important mechanism of failure. One could model such a structure as shown in Figure 61. In this figure, it can be seen that the transverse section of the cylinder is modeled with beam elements. A critical portion of the cylinder can be isolated (Figure 61) and can be modeled as beam elements connected together by hinges. Appropriate boundary conditions can be applied at the hinges and the deformations obtained from a nonlinear analysis. Hinge behavior is graphically shown in Figure 61, where these hinges are capable of both elastic and plastic displacements and rotation. Note that in this case, the deformation capacity would be checked against the deformation of the design failure envelopes for the rectangular section, rather than the cylindrical section.

All the above cases of modeling of structures and their application with respect to design failure curves form the analytical portion of the application of design failure curves. One could also use experimental results to verify these design failure curves.

3. FAILURE ENVELOPES AND YIELD ENVELOPES

The failure envelopes as obtained from a three-dimensional finite element analysis, were presented in dimensionless quantities of strain and curvature in Section III of this report. These failure envelopes were reduced to design failure envelopes in terms of strains and curvatures. It should be emphasized here that the strains and curvatures presented in these curves are referenced at the geometric centroid of the section. Thus the strain at failure is the extensional or compression strain at the geometric centroid of the section while the curvature at failure is the curvature at the

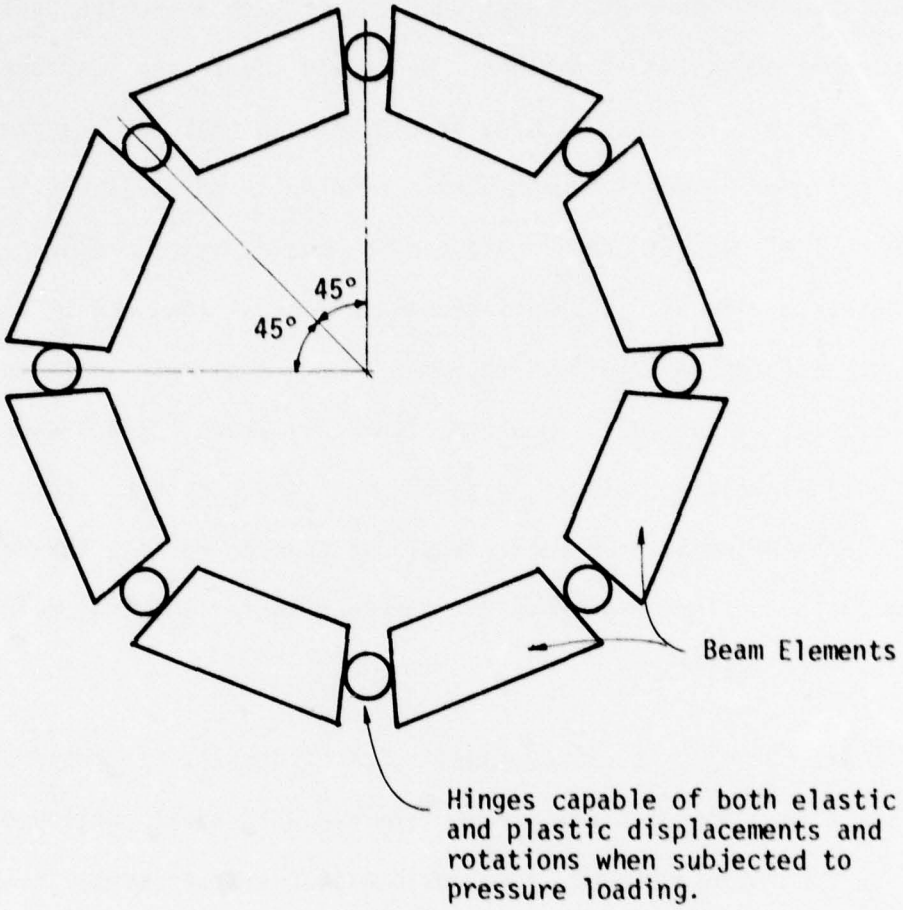

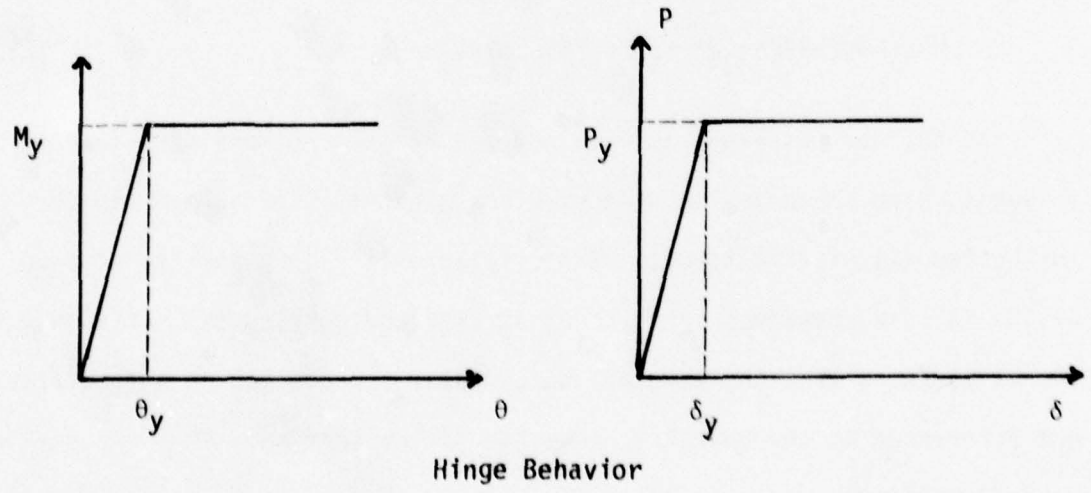

Figure 61. Cylindrical Section Modelled as Beam Elements.

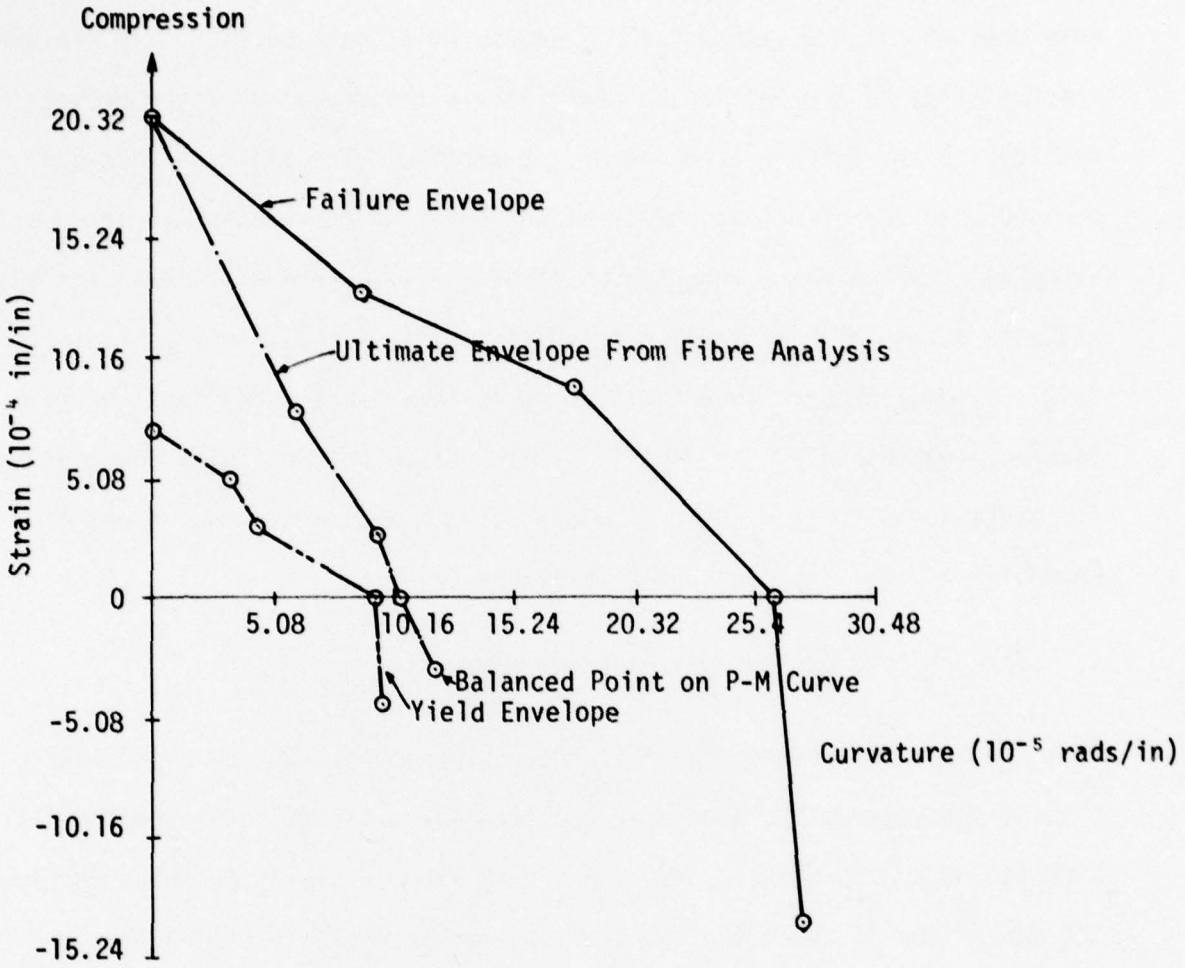

Fig. 62 CRS #3. Failure Envelope, Ultimate, Envelope and Yield Envelope

geometric centroid of the section. Note that at failure the strains in the extreme fibers are different from the strains presented in the failure envelopes and in the design failure envelopes of each section. To measure the ductility of the section, an initial yield surface has to be defined compared to the failure envelope of the section. The yield surface was defined when the effective stress at any point in the section exceeded a value of τ_o which was a function of f'_c, f_c, f_t, f_{bc} where f'_c indicates the ultimate strength in uniaxial compression, while f_c, f_t, and f_{bc} indicate initial yield strength in uniaxial compression, tension and equal biaxial loading, respectively. The initial yield strength in uniaxial compression, f_c, was assumed to be $0.65f'_c$. A yield surface defined in such a way is shown for a single section CRS-3 in Figure 62.

4. FAILURE ENVELOPE AND ULTIMATE ENVELOPE

A comparison between the failure envelope obtained from a 3-D finite element analysis with a nonlinear constitutive material model and the ultimate strength envelope using a one dimensional fiber analysis is shown in Figure 62. The comparison of these two types of envelopes refers to CRS #3.

It is appropriate at this stage to reiterate the difference in loading of the section to obtain failure strength using a 3-D FEA analysis as compared to the ultimate strength as obtained from a one dimensional fiber analysis. In the analysis of a failure strength of a section, using a 3-D FEA, the neutral axis of imposed deformations is fixed while the deformations are monotonically increased in a specific ratio of axial to rotational, until the failure strength of the section is reached. The section was subjected to seven specific fixed deformation ratios to obtain seven failure strengths to give a failure envelope for that section. In contrast, in a fiber analysis,

the neutral axis changes position within the section, as the imposed strain distributions are varied from zero to a distribution at which the ultimate strength of the section is reached.

The similarity between the failure envelope and the ultimate strength envelope (P-M curve, Figure 63) should also be emphasized. Each point on the failure envelope has a unique position of neutral axis of imposed deformation associated with it. Thus all points in the failure envelope have a different position of neutral axis of imposed deformations. A similar phenomenon is observed in the case of the ultimate strength envelope obtained from a one dimensional fiber analysis.

Thus, if we have an ultimate envelope defined for an ultimate strain of 0.002 in/in in the extreme fiber of concrete in compression, then with each point on this curve is associated a certain strain distribution with a location of the neutral axis unique to that point. Thus, if we consider a point A on this ultimate envelope of the P-M interaction diagram, then the strain distribution associated with this point is shown in Figure 63. From the strain distribution, the curvature and hence the displacement (δ) and rotation (θ) for the section can be easily calculated. Given this δ and θ, the ratio (δ/θ) of deformations causing the ultimate condition can be calculated. This δ/θ ratio compared to a similar δ/θ ratio for the failure envelope using a three-dimensional analysis is shown in Figure 62. Note that a sample calculation for such a point on the ultimate envelope is shown in Appendix B. The displacement and rotation at the geometric centroid of the section is calculated corresponding to the balanced point on the P-M interaction diagram. The concrete cover was considered in the calculations which was neglected in the development of the failure envelopes.

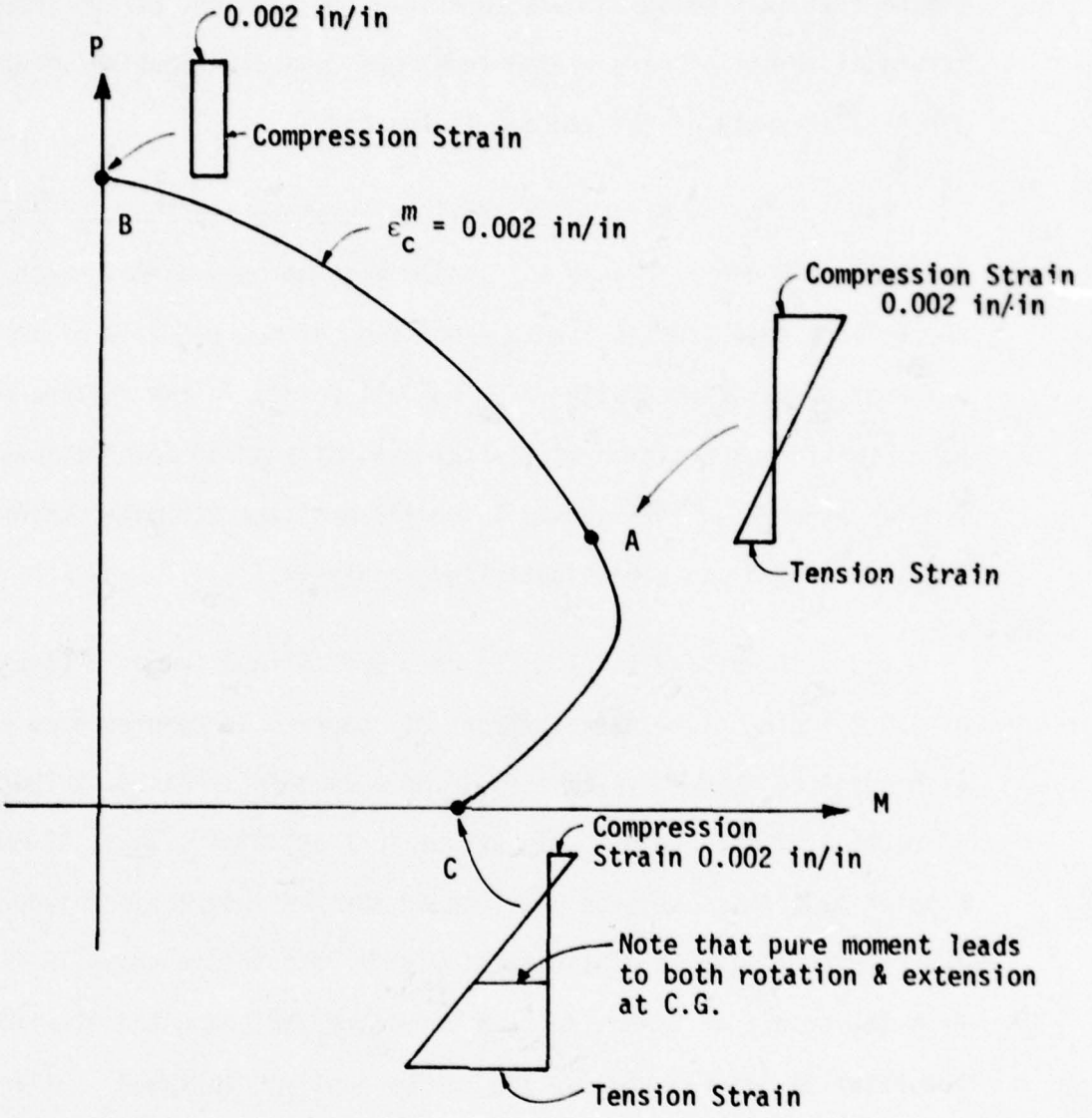

Fig. 63 Axial Force - Moment Interaction Curve

5. LIMITATIONS OF THE PROPOSED MODEL

While developing the failure envelopes for various sections, certain assumptions were made in the analysis which will be summarized in this section.

(1) The failure envelopes were presented in the terms of strains and curvatures for both the rectangular and the cylindrical sections. It should be emphasized that these strains and curvatures were referenced to the geometric centroid of the section. Thus, the strain was the extension or compressive strain at the geometric centroid of the section while the curvature was the curvature at the centroid of the section.

(2) The design failure curves were presented in three different forms for the rectangular section: One, failure curves obtained with variation of the ultimate uniaxial compressive stress of concrete f'_c; two, failure curves obtained by varying the percentage of longitudinal reinforcement; and three, curves obtained by varying the transverse reinforcement. By doing so, upper and lower bounds were obtained for each of the set of curves. Thus, for the first set of curves, the upper bound was defined by an ultimate uniaxial compressive stress of 9.0 ksi, while the lower bound was defined by concrete having an ultimate uniaxial compressive stress of 5.0 ksi. Note that the failure curves are very sensitive to the type of uniaxial compressive stress strain curves for concrete input to the model. The upper and lower bound of percentage of reinforcement is defined as 2% and 1/4% of reinforcement at each face. Note also the sensitivity of the curves to the variation of this parameter. The section with 1/4% reinforcement on each face behaves almost like a plain concrete section.

(3) Only two basic types of geometric sections were considered: the

rectangular cross-section and the cylindrical cross-section. The dimensions of these sections were kept constant for all the analyses. Note that the effect of variation in dimensions on the failure envelope was not studied. Also, the concrete cover for the rectangular and the cylindrical section was neglected in the analysis. It is believed that such an assumption would not influence the failure curves significantly.

(4) Deformations instead of forces were imposed on the section. These deformations were imposed as a combination of displacements and rotations in a certain ratio which was kept fixed for a particular analysis. Thus, for a given analysis that gave a point on the failure envelope, the neutral axis of deformation was fixed while the deformations were monotonically increased until failure of the section occurred. This assumption, it is believed, does not affect the final failure deformations obtained from analyses. However, care should be taken to interpret the results obtained up to failure deformations; i.e., the M-θ and P-δ curves obtained from such an analysis.

(5) It should be noted that only flexural and axial deformations were considered in the development of these failure design envelopes. The effect of shear deformations on these failure envelopes was neglected. The effect of shear and the interaction failure envelopes of shear, axial and flexural deformations form a different aspect of the problem which has to be considered as a separate item of research.

(6) Certain engineering judgments will have to be made while using these failure design curves. Note that only symmetrically reinforced sections were considered in the analysis. Thus, if, for example, one were considering a rectangular section which was unsymmetrically reinforced, say 1% on the top face and 2% at the bottom face, then one would expect the failure envelope to be different in the compression and the tension zone. The curve may not be

very different in the tension zone, where the failure deformation for an imposed deformation of extension/rotation = 5.0 is considered. This type of behavior would be expected since the compressive zone of the section is small, and steel in the tension zone of the section controls behavior. If, on the other hand, a similar unsymmetrically reinforced section was considered to establish failure deformations for an imposed deformation pattern of compression/rotation of 5.0, a slight increase in the section capacity may be expected, compared to a section reinforced symmetrically with 2% reinforcement on each face. This would be due to the fact that the ductility of the section can be utilized to a larger extent. In this case, where the section is reinforced symmetrically with 2% reinforcement on each face, before the yield of re-bars in compression, it is this steel in compression which resists a large portion of the load. As soon as this steel yields, the redistribution of stresses in the concrete causes failure of the concrete section at a smaller displacement than if the section was symmetrically reinforced with 1% reinforcement in each face. Thus, with an unsymmetrically reinforced section with 1% steel on the top face and 2% steel on the bottom face, the failure deformation for an imposed deformation of compression/rotation of 5.0 would be somewhere in between the failure deformation obtained if the section was symmetrically reinforced on each face with 1% and 2% longitudinal reinforcement.

(7) The failure strengths and failure envelopes are very sensitive to type of uniaxial compressive stress-strain curve for concrete. Thus, in using the failure design curves, to compare maximum deformations of critical sections of a structural system obtained using a nonlinear analysis (technique outlined in Section IV as an example application of the design curves), it is essential that material behavior of concrete in uniaxial compression of this structural

system be similar to the σ-ε curves used to obtain failure envelopes for various sections.

(8) In conclusion, it must be emphasized that while using these failure design curves, extreme caution should be taken. The assumptions involved in their development should be thoroughly studied. Any given problem that is being analyzed should be reduced to a problem similar to the ones studied in this report before these curves are applied. Certain engineering judgments may have to be made in the process.

APPENDIX A

1. INTRODUCTION

A brief discussion and explanation of the program is presented in this section. The organization of the auxiliary subprogram, the three-dimensional 8 to 20 node finite element solution, and the material constitutive model is discussed herein. For a complete summary of the base program, the reader is referred to Reference 4. A complete user's guide is also presented at the end of this appendix.

2. PROGRAM LAYOUT AND CAPABILITIES

The main program ANSR is set up in two basic parts; the base program and the auxiliary programs. Each auxiliary program is a set of subroutines defining a specific element type. Each auxiliary program has at least four main subroutines.

1. INEL: Input and initialization of element information.
2. STIF: Formation of element tangent stiffness in static analysis, or effective element stiffness in dynamic analysis.
3. RESP: Computation of response of the elements to imposed deformations or imposed forces.
4. OUT: Output of envelope values of element deformation and actions at specified load increments in static analysis or at specified time intervals in dynamic analysis.

Each of these routines is identified by a number. Two types of elements exist in the program, the three-dimensional truss elements identified as

element number 1, and the three-dimensional 8 to 20 node finite element, specified as element number 4. Hence, subroutines INEL1, STIF1, RESP1, OUT1 all refer to element number 1, while subroutines INEL4, STIF4, RESP4, OUT4 refer to element number 4. Each of these main subroutines could refer to numerous secondary subroutines defining material behavior.

The elastic plastic fracture strain hardening material model as proposed by Chen and Chen with modifications was identified as material Model 5. The subroutines describing the constitutive relations are discussed herewith with an explanation of some of the parameters and the significance of the values assigned to some of the parameters. There are 12 secondary subroutines that define the material behavior. A brief description of each of these subroutines is presented.

1. ADRS45: This subroutine assigns addresses to the material data in the element information array.
2. CMAT45: This subroutine evaluates the elasticity matrix for the material model. For details of the matrix refer to Section II.2 of this report.
3. EPSLOP: This subroutine evaluates the strain hardening function H.
4. CMAT45A: This subroutine forms the elasticity matrix for the material model.
5. YVALUE: This subroutine evaluates the value of effective stress using the appropriate loading function, after the stress state has been established as being either a compressive stress state, tension-compression stress state or a tensile stress state. For details of the loading function, refer to Section II.2. The loading function is

found to be inconsistent with the criteria to check the stress state for certain conditions of loading (Section II.2). Thus, if the stress-state established is a pure compressive one and the effective stress so calculated found to be zero, the stress state so established is inconsistent. Hence, it is now assumed to be a tension compression stress state. All the requisite parameters are reset and the effective stress calculated using the appropriate loading function. Note that the criteria to establish the stress-states are inconsistent only in the compression and tension-compression region.

6. TWXIJ: This subroutine evaluates the first invariant of stress I_1 and second invariant of deviatoric stress J_2.

7. OSHT45: This subroutine determines the overshoot into the plastic state. The overshoot is determined by the roots of the quadratic equation (Section II.2, Equation 18). Both roots are evaluated and the minimum positive root is the required value.

8. MANV45: This subroutine prints the peak stress components and strain components for each element.

9. PRIN45: This subroutine prints the values of stress components and strain components for each element at the end of specified load steps for static analysis and at specified time intervals for dynamic analysis.

10. MATP45: This subroutine reads in appropriate material data, evaluates all the material properties and parameters, and prints the material property table.

11. MRES45: This subroutine is the routine which evaluates the material response. State determination phase occurs at this level in this subroutine. Appropriate stress states are established following which the crack behavior or the yield behavior is evaluated. The stress increment is calculated assuming elastic behavior for a given increment of loading or deformation. The stress is then checked for being outside the initial discontinuous surface. If it has overshot into the plastic range, then the elastic increment is appropriately scaled down and the remaining portion of the plastic strains evaluated (Section II.2, Equation 22). The codes for each type of behavior are set in this subroutine.

12. STRAIN This subroutine evaluates the equivalent plastic strain. This subroutine is called at various stages by MRES45.

The labelled common blocks used in the above 12 subroutines are:

1. COMMON/CONCRT/AAU(2,10),AAO(2,10),TAU(2,10),TAO(2,10),ALFA(2,10), BETA(2,10),XK(2,10),XN(2,10),PHC(10,10),PHT(10,10), PFC(10,10),PFT(10,10),STRNO(10),STRNF(10),COEFF.

where AAU, AAO $\equiv$ A_u and A_o of Section II.2 Equations 5, 6, 9, 10.

TAU, TAO $\equiv$ τ_u and τ_o of Section II.2 Equations 7, 8, 11, 12.

ALFA, BETA ≡ α, β of Section II.2 Equations 3, 4.

XK, XN ≡ The first and the section coefficient in the loading functions in Section II.2, Equations 1, 2.

PHC,PFC ≡ Strain and stress for the nonelastic portion of the equivalent stress strain curve in compression region.

PHT,PFT ≡ Strain and stress for the nonelastic portion of the equivalent stress-strain curve in the tension region.

STRNU ≡ Equivalent ultimate plastic strain.

STRNF ≡ Equivalent fracture plastic strain

COEFF ≡ The coefficient by which the elasticity matrix in subroutine CMAT45 is multiplied once the gauss integration point in the element is either cracked or crushed.

Note that a maximum of 10 different material types can be handled by the program. Also, the parameters A_u, A_o, τ_u, τ_o, α, β, XK, XN are different in the compression region and the tension compression region.

2. COMMON/CRITER/CONSTA,CONSTB,YLDST,ULTST,GK,GN,IDTC,QFC(10),KKCC.

where CONSTA ≡ α

CONSTB ≡ β

YLDST ≡ τ_o

ULTST ≡ τ_u

GK ≡ XK

GN ≡ XN

IDTC ≡ Indicator for establishing stress states. If IDTC = -1, then the stress state is a tension-compression stress state; If IDTC = 1, then the stress state is pure compression. If IDTC = -6, then the stress state is a pure tension one.

KKCC ≡ Number of nonelastic portions of the uniaxial stress-strain curve (Figure A.1).

The possible codes printed at the end of specified load steps for each element of element number 4, for static analysis, or at specified dynamic analysis, are indicated in Figures 3, 4 and 5.

A. PROBLEM INITIATION AND TITLE (A5, 3X, 18A4) - One card

Columns	1 - 5:	Punch the word START
	6 - 8:	Blank
	9 - 80:	Problem title, to be printed with output.

B. NODE INFORMATION

B1. CONTROL INFORMATION (9I5) - One card

Columns 1 - 5: Total number of nodes.

6 - 10: Number of "control" nodes, for which coordinates are specified directly (NCNOD). See section B2.

11 - 15: Number of coordinate generation commands (NODGC). See section B3.

16 - 20: Number of commands specifying nodes with zero displacements (NDCON). See section B4.

21 - 25: Number of commands specifying nodes with equal displacements (NIDDOF). See section B5.

26 - 30: Number of commands specifying nodal masses (NMSGC). See section B6.

31 - 35: Number of element groups (NELGR, max. 20). See section E.

40: Execution code (KEXEC) as follows:
(a) zero or blank: full execution.
(b) 1: data checking only.
(c) -1: full execution, but only if the structure stiffness and element data can be held in core.

45: Stiffness storage code (KSCHM), as follows.

(a) zero or blank: duplicate stiffness matrix held in core.
(b) 1: duplicate stiffness matrix stored on scratch file.

50: Number of imposed displacement directions (NCORD). Maximum = 3. If specified as a negative quantity, then a printout of axial force P, Moment M and unbalanced load is obtained at the end of each load step.

B2. CONTROL NODE COORDINATES (I5,3F10.0) - NCNOD cards

Columns	1 - 5:	Node number, in any sequence.
	6 - 15:	X coordinate.
	16 - 25	Y coordinate.
	26 - 35:	Z coordinate.

B3. COORDINATE GENERATION (4I5,F10.0,10I5) - NODGC cards.

Columns 1 - 5: Node number at beginning of generation line. This must either be a control node, or must have been generated by a previous generation command.

6 - 10: Node number at end of generation line. This node must also have been specified previously.

11 - 15: Number of nodes to be generated along line. If the nodes to be generated are listed in Columns 31-80, this number may not exceed 10.

16 - 20: Node number difference between successive generated nodes, and between first generated node and node at beginning of generation line. May be negative. Leave blank if generated nodes are listed in Columns 31-80.

21 - 30: Spacing between nodes, as follows:
(a) zero or blank: generated nodes are spaced uniformly along the generation line.
(b) less than 1.0: spacing between nodes is this proportion of the length of the generation line.
(c) 1.0 or larger: spacing between nodes is equal to this distance.

31 - 80: Up to 10 fields, each I5. List nodes to be generated, in sequence along generation line. Required only if Columns 16-20 are blank.

Note: It is not necessary to provide coordinate generation commands for nodes which are sequentially numbered between the beginning and end nodes of any straight line, and which are equally spaced along that line. After all generation commands have been executed, the coordinates for each group of unspecified nodes are automatically generated assuming sequential numbering and equal spacing along a line joining the specified nodes immediately preceding and following the group. That is, any generation command with a node number difference of one and equal spacing is superfluous.

B4. NODES WITH ZERO DISPLACEMENTS (I5,4X,6I1,13I5) - NDCON cards

Columns 1 - 5: Node number, or number of first node in a series of nodes covered by this command. See Note following for repetition of nodes.

10: Constraint code for X displacement, as follows.
(a) zero or blank: displacement, not constrained to be zero.
(b) 1: displacement constrained to be zero.

11: Code for Y displacement.

12: Code for Z displacement.

13: Code for XX rotation.

14: Code for YY rotation.

15: Code for ZZ rotation.

16 - 20: Number of last node in series of nodes covered by this command. Leave blank or punch zero for a single code, or if the nodes in the series are listed in columns 31-80.

21 - 25: Node number difference between successive nodes in series. Leave blank for a single node, or if the nodes in the series are listed in Columns 31-80.

29 - 30: Number of nodes listed in Columns 31-80, following. This list is considered only if Columns 16-20 are blank or zero. Leave blank for a single node.

31 - 80: Up to 10 fields, each I5. List second, etc. node of series.

Note: If constraint codes are specified more than once for any node, the last specified value is assumed. For plane or axisymmetric problems, the first command should cover all nodes and should constrain all except the relevant displacements. Additional cards to modify the constraint codes at particular nodes should then be added.

B5. NODES WITH EQUAL DISPLACEMENTS (6I1,4X,14I5) - NIDDOF cards

Columns		
	1:	Equal displacement code for X displacement, as follows. (a) zero or blank: displacement not constrained to be identical. (b) 1: displacement for all nodes in group.
	2:	Code for Y displacement.
	3:	Code for Z displacement.
	4:	Code for XX rotation.
	5:	Code for YY rotation.
	6:	Code for ZZ rotation.
7 -	10:	Blank
11 -	15:	Number of nodes in group.
16 -	80:	Up to 13 fields, each I5. List nodes in group. The first node must be the smallest numbered node in the group. See Note following.

Note: If the group has more than thirteen nodes, specify the remaining nodes on additional equal displacement commands. The smallest numbered node in the group must be the first node in the list for all commands defining the group. Greater computational efficiency may be obtained by constraining nodes to have equal displacements. However, the effect of specifying equal displacements may be to increase the band width of the structure stiffness matrix. This may result in an increase in the required stiffness matrix storage and/or the computational effort required to solve the equations of motion. Equal displacements specifications should therefore be used with caution. It should be noted that the equation solver used in the program is less sensitive to local increases in the stiffness matrix band width than a conventional equation solver based on a banded storage scheme.

B5.1 IMPOSED DISPLACEMENT SPECIFICATION - NCORD sets of cards. (See Section b1).

Each set consists of an imposed displacement direction card and a node specification card specifying the nodes at which the imposed displacements are applied.

B5.1(a) IMPOSED DISPLACEMENT DIRECTION SPECIFICATION (4I5,2F10.0) - One card.

Columns 1 - 5: Specified displacement directions.
(a) 1: X-direction.
(b) 2: Y-direction.
(c) 3: Z-direction.

6 - 10: Specified lever arm axis.
(a) 1: X-axis.
(b) 2: Y-axis.
(c) 3: Z-axis.

11 - 15: Number of cards to describe nodes defining neutral axis (NDC).

16 - 20: Number of cards to describe other nodes (rotation + displacement nodes) off neutral axis (NRC).

21 - 30: Specified displacement increment.

31 - 40: Specified rotation (of neutral axis) increment.

B5.1(b) NODE DESCRIPTION (3I5) - NDC cards followed by NRC cards. (See Section B5.1(a))

Columns 1 - 5: First node in the series.

6 - 10: Last node in the series.

11 - 15: Node increment.

B6. NODAL MASSES (I5,6F10.0,2I5) - NMSGC cards

Columns	1 - 5:	Node number, or number of first node in a series of nodes covered by this command.
	6 - 15:	Mass associated with X-displacement degree of freedom.
	16 - 25:	Mass associated with Y-displacement degree of freedom.
	26 - 35:	Mass associated with Z-displacement degree of freedom.
	36 - 45:	Mass associated with X-rotation degree of freedom.
	46 - 55:	Mass associated with Y-rotation degree of freedom.
	56 - 65:	Mass associated with Z-rotation degree of freedom.
	66 - 70:	Number of last node in series of nodes covered in series. Leave blank for a single node.

Note: The specification commands for lumped masses will generally permit the user to input the nodal masses with only a few data cards. Any node may, if desired, appear in more than one specification command. In such cases the mass associated with any degree of freedom will be the sum of the masses specified in separate commands. If certain nodes are constrained to have an equal displacement, the mass associated with this displacement will be the sum of the masses specified for the individual nodes. If a mass is specified for any degree of freedom that is constrained to be zero, it is ignored.

C. LOAD SPECIFICATION

C1. CONTROL CARD (10I5,3F10.0) - One card

Columns 1 - 5: Code for static and/or dynamic analysis, (KSTAT).
(a) 1: static analysis only.
(b) 2: thermal analysis only.
(c) 3: dynamic analysis only.
(d) 6: static analysis followed by dynamic analysis.

6 - 10: Number of static force patterns to be specified (NSPAT). See section C2. If blank or zero, no static loads will be applied.

11 - 15: Number of static force application commands (NSLGC). See Section F.

16 - 20: Number of thermal load patterns to be specified (NTPAT).

21 - 25: Number of thermal load application commands.

26 - 30: Code for ground motion records (IGM), as follows:
(a) zero or blank: no ground motion records.
(b) 1: ground motion records will be specified. See Section C3.

31 - 35: Number of dynamic force records to be specified (NDLR). See Section C4.

36 - 40: Largest number of points on any dynamic force record. This number is used for storage allocation.

41 - 45: Number of commands defining points of application of dynamic force records (NDLGC). See Section C5.

46 - 50: Number of integration time steps to be considered in dynamic analysis.

51 - 60: Integration time step, Δt.

61 - 70: Integration method parameter, δ, in Newmark's $\beta - \gamma - \delta$ method.

71 - 80: Integration method parameter, β, in Newmark's $\beta - \gamma - \delta$ method. If zero or blank, β is assumed to be equal to $0.25\ (1 + \delta)^2$.

C2. STATIC LOAD PATTERNS - NSPAT sets of cards as follows.

Each set consists of a control card followed by as many cards as needed to define the nodal loads. Load patterns are assumed to be input in numerical sequence.

C2(a) CONTROL CARD (I5,3X,18A4)

Columns	1 - 5:	Number of nodal load commands for this pattern (NSLC).
	9 - 80:	Load pattern title, to be printed with output.

C2(b) NODAL LOADS (I5,6F10.0,2I5) - NSLC cards

Columns	1 - 5:	Node number, or number of first node in a series of nodes covered by this command.
	6 - 15:	Load in X-direction, positive in positive direction of X-axis.
	16 - 25:	Load in Y-direction, positive in positive direction of Y-axis.
	26 - 35:	Load in Z-direction, positive in positive direction of Z-axis.
	36 - 45:	Moment about X-axis, positive by right hand screw rule.
	46 - 55:	Moment about Y-axis, positive by right hand screw rule.
	56 - 65:	Moment about Z-axis, positive by right hand screw rule.
	66 - 70:	Number of last node in series. Leave blank for a single node.
	71 - 75:	Node number difference between successive nodes in series. Leave blank for a single node, or if node number difference equals one.

C3. GROUND MOTION (ACCELERATION) RECORDS

Omit if IGM, Section C1, is zero or blank. Accelerations are assumed to be in acceleration units, not as multiples of the acceleration due to gravity.

C3(a) CONTROL CARD (4I5,6F10.0) - One card

Columns 1 - 5: Number of time points defining ground motion record in X-direction (NIPX). Leave blank or punch zero for no ground motion in this direction.

6 - 10: Number of time points defining ground motion record in Y-direction (NIPY). Leave blank or punch zero for no ground motion in this direction.

11 - 15: Number of time points defining ground motion record in Z-direction (NIPZ). Leave blank or punch zero for no ground motion in this direction.

16 - 20: Print code, as follows
(a) zero or blank: records are not printed.
(b) 1: records are printed as input and scaled.
(c) -1: records are printed as input, scaled and interpolated at time step intervals.

21 - 30: Input time interval for X-ground motion. If blank or zero, both time and acceleration values must be input; otherwise only acceleration values must be input, the times being automatically determined. See Section C3(b).

31 - 40: Input time interval for Y-ground motion. If blank or zero, both time and acceleration values must be input; otherwise only acceleration values must be input. See Section C3(c).

41 - 50: Input time interval for Z-ground motion. If blank or zero, both time and acceleration values must be input; otherwise only acceleration values must be input. See Section C3(d).

51 - 60: Scale factor by which X-ground accelerations are to be multiplied.

61 - 70: Scale factor by which Y-ground accelerations are to be multiplied.

71 - 80: Scale factor by which Z-ground accelerations are to be multiplied.

C3(b) X RECORD - One card followed by as many cards as needed.

Omit if NIPX is blank or zero.

(i) FIRST CARD (15A4,5A4)

Columns 1 - 60: Record title, to be printed with output.

61 - 80: Input format to read NIPX points defining the record. For example, if the format is 12F6.0, punch (12F6.0).

(ii) FOLLOWING CARDS

As many cards as needed to specify NIPX input points, with the format defined in columns 61-80 of the first card. If both time and acceleration values are input, the time must immediately precede the corresponding acceleration.

C3(c) Y RECORD - One card followed by as many cards as needed.

Omit if NIPY is blank or zero.

(i) FIRST CARD (15A4,5A4)

Columns 1 - 60: Record title, to be printed with output.

61 - 80: Input format to read NIPY points defining the record.

(ii) FOLLOWING CARDS

As many cards as needed to specify NIPY input points, with the format defined in columns 61-80 of the first card.

C3(d) Z RECORD - One card followed by as many cards as needed.

Omit of NIPZ is blank or zero.

(i) FIRST CARD (15A4,5A4)

Columns 1 - 60: Record title, to be printed with output.

61 - 80: Input format to read NIPZ points defining the record.

(ii) FOLLOWING CARDS

As many cards as needed to specify NIPZ input points, with the format defined in columns 61-80 of the first card.

Note: The acceleration scale factor may be used to increase or decrease the accelerations, or to convert from multiples of the acceleration due to gravity to acceleration units.

C4. DYNAMIC FORCE RECORDS - NDLGC sets of cards, as follows.

Each set consists of one card followed by as many cards as needed to define the record. Records are assumed to be numbered in sequence as input.

C4(a) FIRST CARD (2I5,2F10.0,8A4,2X,4A4)

Columns 1 - 5: Number of time points defining record (NIPT).

6 - 10: Print code, as follows.
(a) zero or blank: record is not printed.
(b) 1: record is printed as input and scaled.
(c) -1: record is printed as input and scaled and as interpolated at time step intervals.

11 - 20: Input time interval. If blank or zero, both time and force values must be input; otherwise only force values.

21 - 30: Scale factor by which force values are to be multiplied.

31 - 62: Record title, to be printed with output.

65 - 80: Input format to read points defining the record.

C4(b) FOLLOWING CARDS

As many cards as needed to specify NIPT input points, with the format defined in columns 65-80 of the first card. If both time and force values are input, the time must immediately precede the corresponding force.

C5. DYNAMIC FORCE APPLICATION (16I5) - NDLGC Cards (See Section C1)

Acceleration records, if specified, are applied automatically, assuming all support points to move in phase. Force records are applied as defined by the cards of this section.

Columns 1 - 5: Dynamic force record number.

10: Direction code, as follows.
(a) 1: X translation.
(b) 2: Y translation.
(c) 3: Z translation.
(d) 4: X rotation.
(e) 5: Y rotation.
(f) 6: Z rotation.

11 - 80: Up to 14 fields, each I5. List the nodes at which the record is to be applied. Each node in the list is subjected to the scaled force record.

Note: The dynamic forces as specified by the dynamic force record number are applied in the positive direction defined by the direction code. To apply forces in the negative direction, the scale factor by which the force values are multiplied (Section C4) should be negative.

C6. DAMPING SPECIFICATION (3F10.0) - One card.

Omit if code for static and/or dynamic analysis, KSTAT (Section C1) equals -1.

Columns	1 - 10:	Mass proportional damping factor, β_M.
	11 - 20:	Tangent stiffness proportional damping factor, β_T. See Note following.
	21 - 30:	Initial stiffness proportional damping factor, β_0. See Note following.

Note: If desired, it is possible to specify different values of the factors β_T and β_0 for each element group. See Section E for explanation of this option.

D. OUTPUT SPECIFICATION

This set of cards consists of a control card followed by as many cards as needed to specify node numbers for output. See Note following.

D(a) CONTROL CARD (10I5,7A4) - One card.

Columns		
	1 - 5	Time interval for printout of nodal displacement, velocity and acceleration time histories, expressed as a multiple of the integration time step. Leave blank or punch zero for no time history output or if there is no dynamic analysis.
	6 - 10:	Time interval for printout of element action time histories (stresses, forces, etc.) expressed as a multiple of the integration time step. Leave blank or punch zero for no time history output or if there is no dynamic analysis.
	11 - 15:	Time interval for printout of intermediate envelopes of nodal displacements and element actions, expressed as a multiple of the integration time step. Leave blank of punch zero for no intermediate envelope output or if there is no dynamic analysis. Envelopes are automatically output at the end of the dynamic analysis.
	16 - 20:	Number of nodes for X-displacement, velocity and acceleration output (NODSC). For output at all nodes, punch -1.
	21 - 25:	Number of nodes for Y-displacement, velocity and acceleration output (NODSY). For output at all nodes, punch -1.
	26 - 30:	Number of nodes for Z-displacement, velocity and acceleration output (NODSZ). For output at all nodes, punch -1.
	31 - 35:	Time interval for punched output of nodal displacement, velocity and acceleration time histories, expressed as a multiple of the integration time step. Leave blank or punch zero for no punched output or if there is no dynamic analysis.
	36 - 40:	Number of nodes for punched output of X-displacement, velocity and acceleration response (NODXP). For output at all nodes, punch -1.
	41 - 45:	Number of nodes for punched output of Y-displacement, velocity and acceleration response (NODYP). For output at all nodes, punch -1.

Column 46 - 50: Number of nodes for punched output of Z-displacement, velocity and acceleration response (NODZP). For output at all nodes, punch -1.

51 - 78: Format for punched output. See Note following.

Note: Results for the same nodes and elements are printed for both static and dynamic analyses, except that velocities and accelerations are not printed for static analyses. Punched output is provided only for dynamic analyses.

Envelope values are printed for the dynamic analysis, and may be printed at the end of each static load increment if so specified on Card F(a). For punched output, the quantities output are node number, direction (i.e., X, Y or Z), displacement, velocity, acceleration and time. The node number and direction must be output in I5 and A5 format respectively; whereas other quantities may be output in any desired format, specified between parentheses in column 51-78. For example

(I5,A5,3E15.5,15X,E10.4)

D(b) FOLLOWING CARDS - Six sets of cards, as follows.

1. List of nodes for X response printout (16I5) - As many cards as needed to specify NODSX number of nodes, sixteen to a card. Omit if NODSX equals zero or -1.

2. List of nodes for Y response printout (16I5) - As many cards as needed to specify NODSY number of nodes, sixteen to a card. Omit if NODSY equals zero, or -1.

3. List of nodes for Z response printout (16I5) - As many cards as needed to specify NODSZ number of nodes, sixteen to a card. Omit if NODSZ equals zero, or -1.

4. List of nodes for X response punched output (16I5) - As many cards as needed to specify NODXP number of nodes, sixteen to a card. Omit if NODXP equals zero, or -1.

5. List of nodes for Y response punched output (16I5) - As many cards as needed to specify NODYP number of nodes, sixteen to a card. Omit if NODYP equals zero, or -1.

6. List of nodes for Z response punched output (16I5) - As many cards as needed to specify NODZP number of nodes, sixteen to a card. Omit if NODZP equals zero, or -1.

E. ELEMENT SPECIFICATION

Elements must be divided into "groups." All elements in any groups must be of the same type. However, elements of the same type may be divided into separate groups if desired.

Elements groups may be input in any sequence. The total number of element groups may not exceed 20. The elements in any group must be numbered sequentially, the number of the first element in the group being any convenient number.

E1. THREE DIMENSIONAL TRUSS ELEMENTS

See Appendix B1 for description of element. Number of words of information per element = 96.

E1(a) CONTROL INFORMATION (12I5,4F5.0) - One card.

Columns		
	5:	Element group indicator. Punch 1 (to indicate that the group consists of three dimensional truss elements).
	6 - 10:	Number of elements in this group.
	11 - 15:	Element number of the first element in this group. If blank or zero, assumed to be equal to 1.
	16 - 20:	Number of material types. If blank or zero, assumed to be equal to 1.
	21 - 60:	Blank (not used for this element type).
	61 - 65:	Initial stiffness damping factor βo. If blank or zero, βo is assumed to be equal to the system βo value input in card C6.
	66 - 70:	Current tangent stiffness damping factor, β_T. If blank or zero, β_T is assumed to be equal to the system β_T value input in card C6.

E1(b) MATERIAL PROPERTY INFORMATION (I5,4F10.0) - One card for each different material type.

Columns		
	1 - 5:	Material number, in sequence starting with 1.
	6 - 15:	Young's modulus of elasticity, E.
	16 - 25:	Strain hardening modulus as a proportion of Young's modulus (i.e., the ratio E_h/E).

Column 26 - 35: Yield stress in tension.

36 - 45: Yield stress in compression, or elastic buckling stress in compression (input as a positive value).

El(c) ELEMENT GENERATION COMMANDS (4I5,2F10.0,4I5) - As many cards as needed to generate all elements in this group.

Cards must be entered in order of increasing element number. Cards for the first and last element must be included. See Note for explanation of generation procedure.

Columns 1 - 5: Element number, or number of first element in a sequentially numbered series of elements to be generated by this card.

6 - 10: Node number at element end i.

11 - 15: Node number at element end j.

16 - 20: Material number. If blank or zero, assumed to be equal to 1.

21 - 30: Cross-sectional area.

31 - 40: Initial axial force on the element.

41 - 45: Node number increment for element generation. If blank or zero assumed to be equal to 1.

50: Code for large displacement effects. Leave blank or punch zero, for small displacement effects. Punch 1 for large displacement effects.

55: Time history output code. Leave blank or punch zero for no time history output. Punch 1 if time history output is required.

60: Buckling code. Leave blank or punch zero if element yields in compression without buckling. Punch 1 if element buckles elastically in compression.

E4. THREE DIMENSIONAL EIGHT TO TWENTY NODE SOLIDS

E4(a) CONTROL INFORMATION (12I5,4F5.0) - One card.

Columns 1 - 5: Element group indicator. Punch 4 (to indicate that the group consists of three-dimensional solid elements).

6 - 10: Number of elements in this group.

11 - 15: Element number of the first element in this group.

16 - 20: Number of nodes (8 to 20 nodes per element can be specified).

21 - 25: Number of material types.

26 - 30: Material model number as follows:

(a) 1: Linear elastic isotropic model.
(b) 2: Linear elastic orthotropic model.
(c) 3: Elastic perfectly plastic. Von Misces yield criteria.
(d) 4: Ramberg-Osgood model.
(e) 5: Elastic Plastic Fracture strain-hardening model.

31 - 35: r-direction integration order.

36 - 40: s-direction integration order.

41 - 45: t-direction integration order.

61 - 65: Initial stiffness damping factor.

66 - 70: Tangent stiffness damping factor.

E4(b) MATERIAL INFORMATION

E4(b).5 ELASTIC PLASTIC FRACTURE STRAIN HARDENING MATERIAL MODEL

E4(b).5.1 GENERAL MATERIAL INFORMATION (I5,2F10.0,F5.0,2F10.0) - One card.

Columns 1 - 5: Material identification number. Punch 5 (to indicate that model is elastic plastic fracture strain hardening material model).

6 - 15: Young's Modulus of Elasticity E.

16 - 25: Poisson's ratio.

26 - 30: Number of increments describing the nonelastic portion of uniaxial stress-strain curve (KKCC).

31 - 40: Coefficient by which the C^e matrix is to be multiplied after cracking or crushing of concrete. Punch 1 in column 40 if material is not concrete.

E4(b).5.2 ELASTIC PLASTIC FRACTURE STRAIN HARDENING MATERIAL INFORMATION (4F5.0,6F10.0) - One card.

Columns 1 - 5: K^2- value for compression region (default value = 3).

6 - 10: K^2-value for tension region (default value = 3).

11 - 15: X-value for compression region (default value = 3).

16 - 20: X-value for tension region (default value = -3).

21 - 30: Ultimate compressive stress (must be greater than zero).

31 - 40: Ultimate tensile stress/ultimate compressive stress (must be greater than zero).

41 - 50: Ultimate biaxial compressive stress/ultimate compressive stress.

51 - 60: Yield compressive stress/ultimate compressive stress.

61 - 70: Yield tensile stress/utlimate compressive stress.

71 - 80: Yield biaxial stress/ultimate compressive stress.

E4(b).5.3 STRESS-STRAIN INFORMATION FOR NONELASTIC PORTION (8F10.0) - As many cards as needed to specify KKCC number of points. (See Section E4(b).5.1).

Columns 1 - 10: Stress/ultimate compressive stress.

11 - 20: Strain

21 - 30: Stress/ultimate compressive stress.

'
'
'

71 - 80 Strain

E4(c) ELEMENT GENERATION COMMANDS - Two cards per element if the number of nodes per element is greater than 8. As many sets of these two cards as needed to generate all the elements in this group.

E4(c).1 ELEMENT CARD (13I5,3F5.0)

Columns		
	1 - 5:	Element number.
	6 - 10:	Node number at element node 1.
	11 - 15:	Node number at element node 2.
	16 - 20:	Node number at element node 3.
	21 - 25:	Node number at element node 4.
	26 - 30:	Node number at element node 5.
	31 - 35:	Node number at element node 6.
	36 - 40:	Node number at element node 7.
	41 - 45:	Node number at element node 8.
	46 - 50:	Material model number.
	51 - 55:	Node number increment for element generation.
	56 - 60:	Large displacement effects code. (a) 1: include large displacement effects. (b) 0: small displacement effects only.
	61 - 65:	Time history output code, printout of stresses and strains as follows: (a) 0: no printout. (b) 1: printout at output point. (c) 2: printout at gauss points and output point.
	66 - 70:	r-coordinate of output point.
	71 - 75:	s-coordinate of output point.
	76 - 80:	t-coordinate of output point.

E4(c).2 ADDITIONAL NODES SPECIFICATION (12I5) - Omit this card if number of nodes is less than or equal to 8.

Columns	1 - 5:	Node number at element node 9.
	6 - 10:	Node number at element node 10.
	11 - 15:	Node number at element node 11.
	16 - 20:	Node number at element node 12.
	21 - 25:	Node number at element node 13.
	26 - 30:	Node number at element node 14.
	31 - 35:	Node number at element node 15.
	36 - 40:	Node number at element node 16.
	41 - 45:	Node number at element node 17.
	46 - 50:	Node number at element node 18.
	51 - 55:	Node number at element node 19.
	56 - 60:	Node number at element node 20.

F. STATIC ANALYSIS SPECIFICATION - NSLGC sets of cards (see Section C1).

Each set consists of a solution procedure card followed by one or more cards defining a linear combination of static force patterns. Each set defines an increment of static load.

F(s). SOLUTION PROCEDURE CARD (8I5, 4F10.0) - One Card

Columns 1 - 5: Number of equal steps in which load increment is to be applied, positive if results envelopes are not to be printed at the end of the increment, otherwise negative.

6 - 10: Iteration type, as follows:
(a) zero or blank: Newton-Raphson iteration
(b) n: Constant stiffness iteration with alpha-constant over-relaxation, the alpha matrix being reinitialized every n iterations.

15: Type of state determination calculation to be used for constant stiffness iteration as follows:
(a) zero or blank: path independent.
(b) 1: path dependent.
Path dependent state determination is always used for Newton-Raphson iteration.

16 - 20: Stiffness reformation code, as follows.
(a) zero or blank: stiffness used in preceding step is retained.
(b) n: stiffness is reformed every n load steps.

25: Termination code, as follows.
(a) zero or blank: If the solution does not converge within the maximum number of iterations for any load step, the next load step will be applied.
(b) 1: If the solution does not converge, the execution will terminate.

26 - 30: Print code, as follows.
(a) -1: results are not printed for this increment.
(b) zero or blank: results are printed at the end of the increment only.
(c) 1: results are printed after each load step.
(d) 2: results are printed every iteration. This option should be used for debugging purposes only.

Columns 31 - 35: Maximum number of cycles of iteration within any load step. If set to -1, the unbalanced load will be set to zero at a new load step--works only for imposed displacements option.

36 - 40: Maximum number of iterations within any cycle.

41 - 50: Nodal force convergence tolerance to be used in last step of load increment.

51 - 60: Nodal force convergence tolerance to be used in all except last step of load increment.

61 - 70: Nodal force tolerance for change of stiffness in Newton-Raphson iteration. If the unbalanced force reduces below this tolerance, the stiffness will not be reformed for the next iteration.

71 - 80: Maximum nodal displacement (translation or rotation) increment permitted in any iteration step. Leave blank for unlimited displacement. Displacement limits should be specified only with Newton-Raphson iteration.

F(b). FOLLOWING CARDS (8F10.0) - As many cards as needed.

Columns 1 - 80: Up to eight fields, each F10.0. For each static force pattern in turn, specify a scale factor by which the pattern is to be multiplied. The scaled patterns are added together to produce the load increment.

Scale factors may be positive or negative. Leave the corresponding field blank or punch zero to ignore any force pattern.

F(c) IMPOSED DISPLACEMENT CONTROL (I5,F10.0) - Omit this card if NCORD = 0 (See section B1) - One card.

Columns 1 - 5: Imposed displacements identification as follows:
(a) 0: no displacements imposed.
(b) 1: imposed displacements.

6 - 15: Scale factor by which the imposed displacement pattern is to be multiplied. The scale factor multiplied to the imposed displacement pattern is the net value of imposed displacements in a single load step.

H. NEW PROBLEM

Data for a new problem may follow immediately starting with Section A. Any number of structures may be analyzed in a single computer run.

I. TERMINATION CARD (A4) - One card to terminate the complete data deck.

Columns 1 - 4: Punch the word STOP.

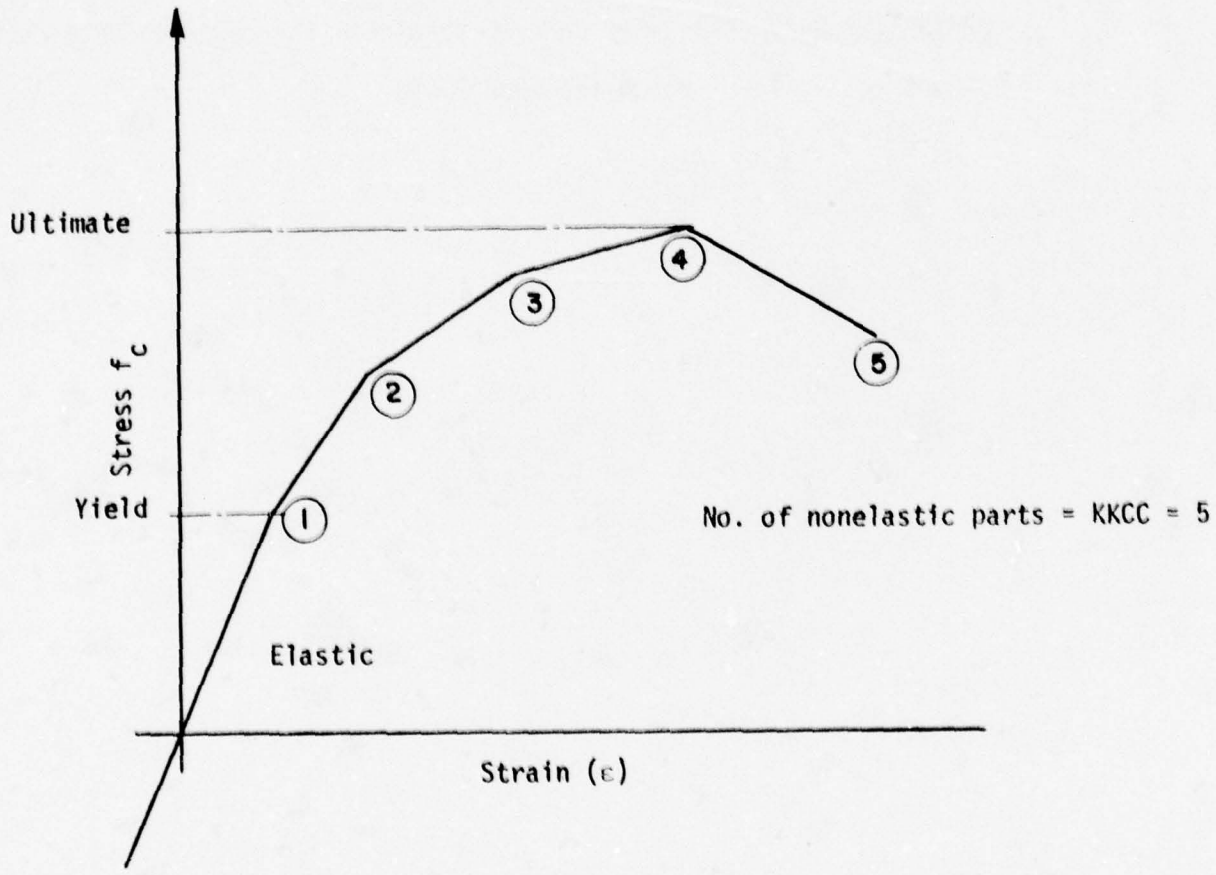

Figure A.1. Idealized Stress-Strain Curve as Input into the Program

SAMPLE INPUT TO PROGRAM FOR CCS-2 (REFER FIGURE 45)

```
START   * CCS-2 * RHO = 2 PER CENT * PURE COMPRESSION *
  40   20    0    2    0    0    2    0    0   -1
   1            314.96
   4            354.33
   5            222.71    222.71
   8            250.55    250.55
   9                      314.96
  12                      354.33
  13           -222.71    222.71
  16           -250.55    250.55
  17           -314.96
  20           -354.33
  21  39.37     314.96
  24  39.37     354.33
  25  39.37     222.71    222.71
  28  39.37     250.55    250.55
  29  39.37               314.96
  32  39.37               354.33
  33  39.37    -222.71    222.71
  36  39.37    -250.55    250.55
  37  39.37    -314.96
  40  39.37    -354.33
   1    000111   40
   1    111111   20
   1    2    1    4 -1.0     0.0
  29   32    1
  21   24    1
  25   28    1
  33   36    1
  37   40    1
   1    1    2
   1      CCS-2  PURE COMPRESSION
   1
                 -1   -1   -1
   1   26    1    1
   1  30000.     0.02      60.0          60.0
   1    1   21    1   82.78                3    0    1    0
   3    5   25    1   82.78                3    0    1    0
   5    9   29    1   82.78                3    0    1    0
   7   13   33    1   82.78                3    0    1    0
   9   17   37    1   82.78                3    0    1    0
  11    1    5    1   15.50                4    0    1    0
  15    4    8    1   15.50                4    0    1    0
  19   21   25    1   15.50                4    0    1    0
  23   24   28    1   15.50                4    0    1    0
  26   36   40    1   15.50                4    0    1    0
   4   12    1    8    1    5    2    2    2
   1  4000.    .000000001    4    0.10     4.0
                      5.0        0.12        1.15        0.48        0.10     0.552
 0.48      0.0006      0.717      0.001       1.0        0.002       0.65      0.003
   1    4    8   28   24    3    7   27   23    1   -1          2
   4    8   12   32   28    7   11   31   27    1   -1    0     2
   7   13    9   29   33   14   10   30   34    1    1    0     2
  10   17   13   33   37   18   14   34   38    1    1    0     2
  12   19   15   35   39   20   16   36   40    1    1    0     2
   2    1    0    1    0    1    5    2    1.0      1.0      1.0

   1 0.02

   5    1    0    1    0    1    5    2    1.0      1.0      1.0

   1 0.002
STOP
```

APPENDIX B

1. FIBER ANALYSIS: BALANCED POINT ON P-M INTERACTION CURVE

Assume the strain distribution and stress distribution as shown in Figure B.1. The stress-strain curves for concrete and steel are shown in Figures 17 and 18, respectively.

a. Forces in the Tension and Compression Blocks

Since steel undergoes yield

$$T_s = f_y A_s \tag{1}$$

$$T_s = 60 \times 31 = 1860 \text{ kips}$$

Compressive steel force:

$$C_s = E_s \varepsilon'_s A_s \tag{2}$$

$$C_s = 30000 \times 0.00129 \times 31$$

$$C_s = 1203 \text{ kips}$$

Compressive block of concrete:

$$C_c = f'_c \, bc \left[\frac{\varepsilon_c^m}{\varepsilon_{co}} - \frac{1}{3} \left(\frac{\varepsilon_c^m}{\varepsilon_{co}} \right)^2 \right] \tag{3}$$

where

b = width of the section

f'_c = ultimate stress of concrete in uniaxial compression

c = depth of the neutral axis from the top fiber

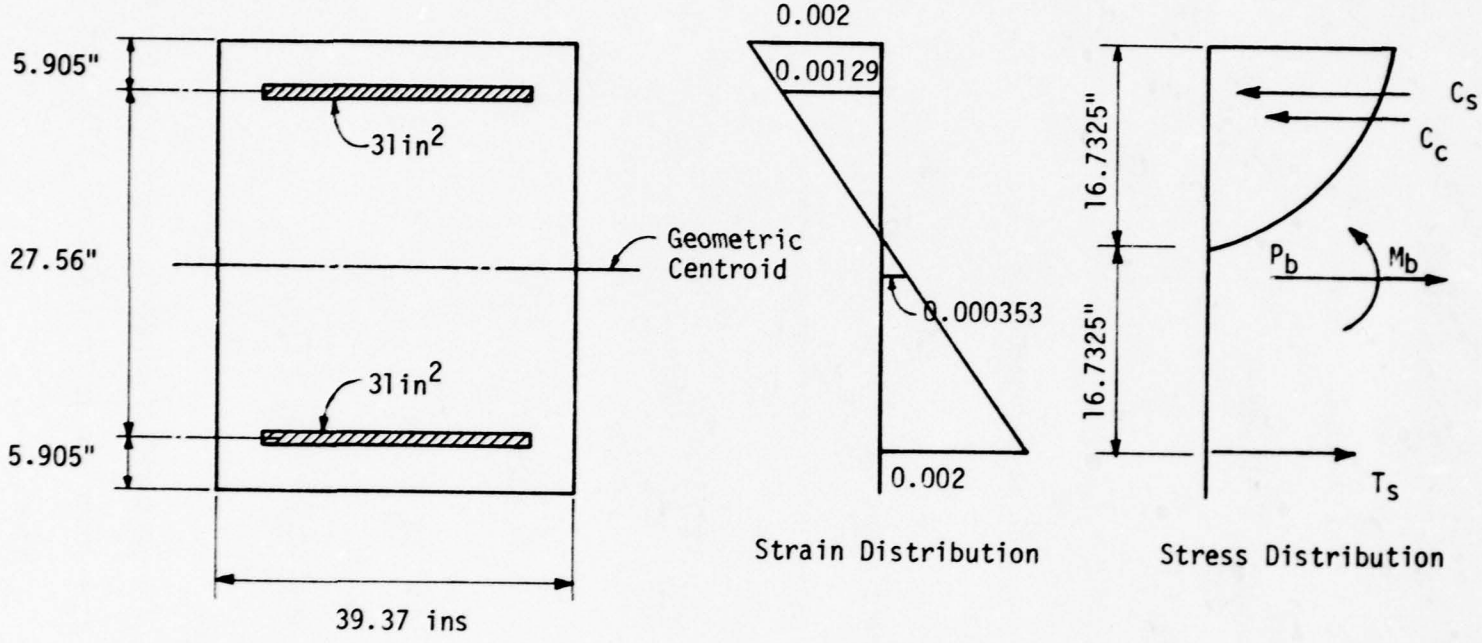

Note: Length of Section = 19.685"

Figure B-1 Strain and Stress Distribution. Balanced Point on P-M Interaction Curve

ε_c^m = strain in extreme fiber of concrete

ε_{co} = strain in concrete at maximum stress

$C_c = 5.0 \times 39.37 \times 16.7325 \left[1 - 1/3\right]$

$C_c = 2195.86$ kips

b. Calculation of P and M:

$$\Sigma F_x = 0$$

$$C_c + C_s = P + T_s \tag{4}$$

$P = 2195.86 + 1203 - 1860$

$P = 1538$ kips

Moments about centroid of section:

Centroid of compression center $\bar{y}$ is given by

$$\bar{y} = \frac{c\left[2/3\ (\varepsilon_c^m/\varepsilon_{co}) - 1/4\ (\varepsilon_c^m/\varepsilon_{co})^2\right]}{(\varepsilon_c^m/\varepsilon_{co}) - 1/3\ (\varepsilon_c^m/\varepsilon_{co})^2} \tag{5}$$

$$\bar{y} = 16.7325\ \frac{[2/3 - 1/4]}{[1-1/3]}$$

$\bar{y} = 10.46$ ins.

$$M = C_c\bar{y} + C_s y_s' + T_s y_s \tag{6}$$

where

$\bar{y}$ = centroid of concrete compressive block

y_s' = lever arm to the centroid of section of compression steel

y_s = lever arm to the centroid of section of tension steel

M = 2195.86 x 13.4125 + 1538 x 13.78 + 1860 x 13.78

M = 76.276.41 kip-ins

c. Calculation of deformations δ and θ at the centroid of the section:

ε_{cent} = 0.000353 in/in

$$\delta_{cent} = \varepsilon_{cent} L \qquad (7)$$

where

δ_{cent} = displacement at centroid

ε_{cent} = strain at centroid

L = length of section

δ_{cent} = 0.000353 x 19.685

δ_{cent} = 0.00695 ins

$$\theta_{cent} = \phi_{cent} L \qquad (8)$$

where

θ_{cent} = rotation at geometric centroid

ϕ_{cent} = curvature at geometric centroid

$$\phi_{cent} = \frac{0.002 - 0.000353}{13.78}$$

ϕ_{cent} = 0.0001195 1/in

θ_{cent} = 0.0001195 x 19.685

θ_{cent} = 0.002353 rad.

d. Ratio of δ to θ

$\delta/\theta = 0.00695/0.002353$

$\delta/\theta = 2.95$

Note that the displacement δ is an extension displacement at the centroid.

Department of the Navy, Cont'd.

No. of
Copies

Commander, Naval Surface Weapons Ctr
White Oak, Silver Spring, MD 20910
1 ATTN: Code WX21 Tech Lib

Commander, Naval Surface Weapons Ctr
Dahlgren Laboratory, Dahlgren, VA 22448
1 ATTN: Tech lib

President, Naval War College
Newport, RI 02840
1 ATTN: Tech Lib

Commander, Naval Weapons Ctr
China Lake, CA 93555
1 ATTN: Code 533 Tech Lib

Commanding Officer, Naval Weapons Evaluation Facility
Kirtland Air Force Base, Albuq, NM 87117
1 ATTN: Tech Lib

Director, Strategic Systems Project Office
Navy Dept, Washington, DC 20376
1 ATTN: NSP-43 Tech Lib

Department of the Air Force

AF Geophysics Laboratory, AFSC
Hanscom AFB, MA 91731
1 ATTN: SUOL AFCRL Rsch Lib

AF Institute of Technology, AU
Wright-Patterson AFB OH 45433
1 ATTN: Library AFIT Bldg 640 Area B

AF Weapons Laboratory, AFSC
Kirtland AFB, NM 87117
1 ATTN: DE, M. A. Plamondon
2 ATTN: SUL
30 ATTN: DES, Mr Rodney G. Galloway
1 ATTN: HO

HQ, Air Force Systems Command
Andrews AFB, Washington DC 20331
1 ATTN: Tech Lib
1 ATTN: DLWM

Department of Defesne, cont'd.

No. of
copies

Department of the Army

Director, Construction Engineering Research Laboratory
P.O. Box 4005, Champaign IL 61820
1 ATTN: CERL-SL

Dep Chief of Staff or Rsch Dev & Acq
Dept of the Army, Washington DC 20310
1 ATTN: Technical Library

Deputy, Chief of Staff for Ops & Plans
DOA, Washington, DC 20310
1 ATTN: Technical Library

Commander, Harry Diamond Laboratories
2800 Powder Mill Rd., Adelphi, MD 20783
1 ATTN: DRXDO-TI Tech Lib

Commander, Picatinny Arsenal
Dover, NJ 07801
1 ATTN: Technical Library

Commander, Redstone Scientific Information Center
U.S. Army Missile Command
Redstone Arsenal, AL 35809
1 ATTN: Chief, Documents

Commander, U. S. Army Armament Command
Rock Island, IL 61202
1 ATTN: Technical Library

Director, US Army Ballistic Research Labs
Aberdeen Proving Ground, MD 21005
1 ATTN: Tech Lib

Commander, U. S. Army Communications CMD
Fort Huachuca, AZ 85613
1 ATTN: Technical Library

Commander, U. S. Army Engineer Center
Fort Belvoir, VA 22060
1 ATTN: ATSEN-SY-L

Division Engineer, U.S. Army Engineer Div Huntsville
P.O. Box 1600, West Station, Huntsville, AL 35807
1 ATTN: HNDED-SR

Department of the Army, Cont'd.

No. of
Copies

Division Engineer, U.S. Army Engineer Div Ohio River
P.O. Box 1159, Cincinnati, OH 45201
1 ATTN: Technical Library

Director, US Army Engr Waterways Exper Sta
P.O. Bx631, Vicksburg, MS 39180
1 ATTN: Tech Lib
1 ATTN: William Flathau
1 ATTN: James Ballard

Commander, US Army Mat & Mechanics Rsch Ctr
Watertown, MA 02172
1 ATTN: Technical Library

Commander, US Army Material Dev & Readiness Cmd
5001 Eisenhower Ave., Alexandria, VA 22333
1 ATTN: Technical Library

Commander, US Army Mobility Equip R&D Ctr
Fort Belvoir, VA 22060
1 ATTN: Technical Library

Commander, US Army Nuclear Agency
Ft. Bliss, TX 79916
1 ATTN: Tech Lib

Commandant, US Army War College
Carlisle Barracks, PA 17013
1 ATTN: Library

Department of the Navy

Chief, Naval Research, Navy Dept.
Arlington, VA 22217
1 ATTN: Tech Lib

Civil Engineering Laboratory
Naval Construction Battalion Ctr, port Hueneme, CA 93041
1 ATTN: Technical Lib

Commander, Naval Facilities Engineering Command Hqs
Washington DC 20390
1 ATTN: Technical Library

Superintendent (Code 1424), Naval Postgraduate School
Monterey, CA 93940
1 ATTN: Code 2124 Tech Rpts Librarian

DISTRIBUTION

No. of
Copies

Department of Defense

Director, Defense Advanced Rsch Proj Agency
Architect Bldg, 1400 Wilson Blvd., Arlington, VA 22209
1 ATTN: Technical Library

Defense Documentation Center
Cameron Station, Alexandria, VA 22314
12 ATTN: TC

Director, Defense Intelligence Agency
Washington, DC 20301
1 ATTN: Technical Library

Director, DNA
Washington, DC 20305
2 ATTN: SPSS
3 ATTN: TITL Tech Library
1 ATTN: TISI Archives

Director, Defense Rsch & Engineering
DOD, Washington, DC 20301
1 ATTN: S&SS (OS)

Commander, Field Command
DNA, Kirtland AFB, NM 87115
1 ATTN: FCPR
1 ATTN: FCTMOF

Director, Interservice Nuclear Weapons School
Kirtland AFB, NM 87115
1 ATTN: Tech Lib

Director, Joint Strat Tgt Planning Staff JCS
Offutt AFB, Omaha, NB 68113
1 ATTN: STINFO Library

Chief, Livermore Div, Fld Command DNA
Lawrence Livermore Laboratory, P.O. Box 808, Livermore CA
94550
1 ATTN: FCPRL

1 AUL/LDE/Maxwell AFB, AL 36112

Department of the Air Force, Cont'd.

No. of
Copies

Commander, Armament Dev & Test Center
Eglin AFB, FA 32542
1 ATTN: Tech Lib

Commander, ASD
WPAFB, OH 45433
1 ATTN: Tech Lib

Commander, Foreign Technology Div, AFSC
1 Wright-Patterson AFB, OH 45433
1 ATTN: TD-BTA Lib

Hq USAF/RD
Washington, DC 20330
1 ATTN: RDQRM, Col S.C. Green
1 ATTN: RDPM
1 ATTN: RDPS, LTC A. Chiota
1 ATTN: RDQPN, Maj F. Vajda

Commander, Rome Air Dev Ctr, AFSC
Griffiss AFB, NY 13440
1 ATTN: EMTLD Doc Library

SAMSO/DE
Norton AFB, CA 92409
1 ATTN: DEB

SAMSO/MN
NORTON AFB, CA 92409
1 ATTN: MNNH
1 ATTN: MMH

Commander in Chief, Strategic Air Command
Offutt AFB, NB 68113
1 ATTN: NRI-Stinfo Lib

U. S. Energy Rsch and Dev Admin

Division of Military Application
U.S. Energy Rsch & Dev Admin, Washington, DC 20545
1 ATTN: Doc Control for Test Office

University of California, Lawrence Livermore Laboratory
P.O. Box 808, Livermore, CA 94550
1 ATTN: Tech Info Dept L-3

U.S. Energy Rsch and Dev Admin, Cont'd.

No. of
Copies

Los Alamos Scientific Laboratory
P.O. Box 1663, Los Alamos, NM 87545
1 ATTN: Doc Control for Reports Lib

Sandia Laboratories
Livermore Laboratory, P.O. Box 969, Livermore, CA 94550
1 ATTN: Doc Control for Tech Lib

Sandia Laboratories
P.O. Box 5800, Albuquerque, NM 87115
1 ATTN: Doc Con for 3141 Sandia Rpt Coll

U.S. Energy Rsch & Dev Admin, Div of Hq Services
Library Branch G-043
Washington, DC 20545
1 ATTN: Doc Con for class Tech Lib

U.S. Energy Rsch & Dev Admin
Nevada Operations Office, P.O. Box 5400, Albuq, NM 87115
1 ATTN: Doc for Tech Lib

U.S. Energy Rsch & Dev Admin, Div of Hq Services
Library Branch G-043
Washington, DC 20545
1 ATTN: Doc Con for Class Tech Lib

US Energy Rsch & Dev Admin
Nevada Operations Office
P.O. Box 14100, Las Vegas, NV 89114
1 ATTN: Doc Con for Tech Lib

Dept of the Interior
Bureau of Mines
Bldg 20, Denver Federal Center, Denver, CO 80225
1 ATTN: Tech Lib

Department of Defense Contractors

Aerospace Corporation
P.O. Box 92957, Los Angeles, CA 90009
1 ATTN: Tech Info Services

Agbabian Associates
250 N. Nash St., El Segundo, CA 90245
1 ATTN: M. Agbabian

Analytic Services, Inc.
5613 Leesburg Pike, Falls Church, VA 22041
1 ATTN: George Hesselbacher

Department of Defense Contractors , Cont'd.

No. of
Copies

Applied Theory, Inc.
1010 Westwood Blvd, Los Angeles, CA 90024
1 ATTN: John G. Trulio

Artec Associates, Inc.
26046 Eden Landing Road, Hayward CA 94545
1 ATTN: Steven Gill

Avco Research & Systems Group
201 Lowell Street, Wilmington MA 01887
1 ATTN: Research Lib A830 Rm 7201

Battelle Memorial Institute
505 King Ave., Columbus OH 43201
1 ATTN: Tech Lib

BDM Corporation
1920 Aline Ave,. Vienna VA 22180
1 ATTN: Tech Lib

Ted Belytschko
6304 No. Hiawatha Ave., Vienna VA 22180
1 ATTN: Ted Belytschko

Boeing Company
P.O. Box 3607, Seattle, WA 98124
1 ATTN: Aerospace Lib

Brown Engineering Co., Inc
Cummings Research Park, Huntsville AL 35807
1 ATTN: Manu Patel

California Institute of Technology
1201 E. California Blvd, Pasadena CA 91109
1 ATTN: Thomas J. Ahrens

California Research & Technology, Inc.
6269 Variel Ave., Woodland Hills CA 91364
1 ATTN: Tech Lib

Calspan Corporation
P.O. Box 235, Buffalo NY 14221
1 ATTN: Tech Lib

Department of Defense Contractors, Cont'd.

No. of
Copies

Civil/Nuclear Systems Corp.
1200 University Blvd., NE., Albuquerque NM 87102
1 ATTN: Tech Lib

Dayton, University of
Industrial Security Super KL-505
300 College Park Ave., Dayton, OH 45409
1 ATTN: Hallock F. Swift

University of Denver
Colorado Seminary
Denver Research Institute
p.O. Box 10127, Denver, CO 80210
1 ATTN: Sec Officer for Tech Lib

EG&G, Inc.
Albuquerque Division
P.O. Box 10218, Albuquerque, NM 87114
1 ATTN: Tech Lib

Electric Power Research Institute
3412 Hillview Ave., Palo Alto, CA 94303
1 ATTN: George Sliter

Engrg Decision Analysis Co., Inc.
2400 Michelson Dr., Irvine, CA 92715
1 ATTN: R. P. Kennedy

Franklin Institute
20th Street and Parkway, Philadelphia, PA 19103
1 ATTN: Zenons Zudans

General Electric Co., TEMPO-Center for Advanced Studies
816 State St., (P.O. Drawer QQ), Santa Barbara, CA 93102
1 ATTN: DASIAC

General Research Corporation
P.O. Box 3587, Santa Barbara, CA 93105
1 ATTN: Benjamin Alexander

H-Tech Laboratories, Ind.
P.O. Box 1686, Santa Monica, CA 90406
1 ATTN: B. Hartenbaum

Department of Defense Contractors, Cont'd.

No. of Copies	
	IIT Research Institute 10 West 35th St., Chicago, IL 60616
1	ATTN: Tech Lib
	Institute for Defense Analyses 400 Army-Navy Dr., Arlington, VA 22202
1	ATTN: IDA Librarian Ruth S. Smith
	J. H. Wiggins, co., Inc. 1650 S. Pacific Coast Highway, Redondo Beach, CA 90277
1	ATTN: John Collins
	Kaman Avidyne, Division of Kaman Sciences Corp. 83 Second Ave., Northwest Industrial park, Burlington, MA 01803
1	ATTN: Tech Lib
	Kaman Sciences Corporation P.O. Box 7463, Colorado Springs, CO 80933
1	ATTN: Library
	Karagozian and Case 6330 N. Figueroa St., Los Angeles, CA 90042
1	ATTN: John Karagozian
	Lockheed Missiles & Space Co., Inc. P.O. Box 504, Sunnyvale, CA 94088
1	ATTN: Tech Lib
	Martin Marietta Aerospace, Orlando Div P.O. Box 5836, Orlando, FL 32805
1	ATTN: G. Fotieo
	McDonnell Douglas Corp. 5301 Bolsa Ave., Huntington Beach, CA 92647
1	ATTN: Robert W. Halprin
	Merritt Cases, Inc. P.O. Box 1206, Redlands, CA 92373
1	ATTN: Tech Lib
	Newmark, Nathan M., Consulting Engineering Services 1211 Civil Engineering Bldg., Rm B106A, Univ of Illinois
1	ATTN: Nathan M. Newmark

Department of Defense Contractors, Cont'd.

No. of Copies

TRW Systems Group
One Space Park, Redondo Beach, CA 90268
1 ATTN: Tech Info Center/S-1930
1 ATTN: Peter K. Dai, R1/2170
1 ATTN: Norm Lipner

TRW Systems Group, San Bernardino Operations
P.O. Box 1310, San Bernardino, CA 92402
1 ATTN: E. Y. Wong, 527/712

TRW Systems Group
Room 712, Bldg 572,Norton AFB, CA 92409
1 ATTN: Gregory D. Hulcher

Universal Analytics, Inc.
7740 W. Manchester Bld., Playa Del Rey, CA 90291
1 ATTN: E. I. Field

URS Research Co.
155 Bovet Rd., San Mateo, CA 94402
1 ATTN: Tech Lib

Eric H. Wang Civil Engineering Rsch Fa, University Station
Box 188, University of NM, Albuquerque, NM 87121
2 ATTN: Jerry Berglund

Weidlinger Assoc. Consulting Engineers
110 East 59th St., New York, NY 10022
1 ATTN: Melvin L. Baron

Weidlinger Associates Consulting Engineers
Suite 245, 3000 Sand Hill Road, Menlo Park, CA 94025
1 ATTN: F. S. Wong
1 ATTN: J. Isenberg

Dept of Civil Engineering
University of California
1 ATTN: Prof Alex. C. Scordelis
729 Davis Hall
Berkeley, CA 94720

Purdue University
School of Civil Engineering
West Lafayette, IN 47907
1 ATTN: Prof W. F. Chen

Department of Defense Contractors, Cont'd.

No. of Copies	
	Pacifica Technology P.O. Box 148, Del Mar, CA 92014
1	ATTN: G. Kent
4	ATTN: Prof. Robert Dunham
	Physics International Co. 2700 Merced St., San Leandro, CA 94577
1	ATTN: Doc Con for Tech Lib
	R & D Associates P.O. Box 9695, Marine Del Rey, CA 90291
1	ATTN: Tech Lib
	Rand Corporation 1700 Main St., Santa Monica, CA 90406
1	ATTN: Tech Lib
	Science Applications, Inc. 2201 San Pedro NE, Albuquerque, NM 87110
1	ATTN: J. L. Bratton
	Science Applications, Inc. P. O. Box 2351, La Jolla, CA 92038
1	ATTN: Tech Lib
	Southwest Research Institute P.O. Box Drawer 28510, San Antonio, TX 78284
1	ATTN: Wilfred E. Baker
	Stanford Research Institute 333 Ravenswood Ave., Menlo Park, CA 94026
1	ATTN: Carl Peterson
	Systems, Science and Software, Inc. p.O. Box 1620, La Jolla, CA 92038
1	ATTN: Tech Lib
1	ATTN: G. Hegemeir, Room 2091
	Terra Tek, Inc. 420 Wakara Way, Salt Lake City, UT 87108
1	ATTN: Tech Lib
	Tetra Tech, Inc 630 North Rosemead Blvd., Pasadena, CA 91107
1	ATTN: Tech Lib

Department of Defense Contractors Cont'd.

No. of
Copies

PMB Systems Eng
500 Sansome Street
San Francisco 94111
15 ATTN: Dr. R. Litton